

# **Stony Brook University**



OFFICIAL COPY

**The official electronic file of this thesis or dissertation is maintained by the University Libraries on behalf of The Graduate School at Stony Brook University.**

**© All Rights Reserved by Author.**

**Mechanism and Inhibition Studies of Enoyl-ACP Reductases and  
Dihydroxynaphthoyl-CoA Synthase in Pathogenic Bacteria**

A Dissertation Presented

by

**Nina Liu**

to

The Graduate School  
in Partial Fulfillment of the  
Requirements  
for the Degree of  
**Doctor of Philosophy**  
in  
**Chemistry**

Stony Brook University

**August 2011**

**Stony Brook University**

The Graduate School

**Nina Liu**

We, the dissertation committee for the above candidate for the  
Doctor of Philosophy degree, hereby recommend  
acceptance of this dissertation.

**Peter J. Tonge – Dissertation Advisor  
Professor of Chemistry Department**

**Elizabeth M. Boon - Chairperson of Defense  
Assistant Professor of Chemistry Department**

**Jin Wang – Committee Member of Defense  
Associate Professor of Chemistry Department**

**Stephen G. Walker – External Committee Member of Defense  
Associate Professor of School of Dental Medicines, Stony Brook University**

This dissertation is accepted by the Graduate School

Lawrence Martin

Dean of the Graduate School

Abstract of the Dissertation

**Mechanism and Inhibition Studies of Enoyl-ACP Reductases and  
Dihydroxynaphthoyl-CoA Synthase in Pathogenic Bacteria**

by

**Nina Liu**

**Doctor of Philosophy**

in

**Chemistry**

Stony Brook University

**2011**

Resistance to existing antimicrobial agents is a global threat to human health care, and new drugs with novel mechanisms of action are required in order to keep pace with the emergence of drug resistant pathogens. The bacterial fatty acid biosynthesis (FAS-II) and menaquinone pathways represent attractive yet relatively unexploited targets for new antibiotic development and consequently there is significant interest in developing potent inhibitors of enzymes in these two pathways. My research is mainly focused on the mechanism and inhibition of the enoyl-ACP reductases from the FAS-II pathway and dihydroxynaphthoyl-CoA synthase from the menaquinone pathway.

The mechanism and inhibition of the enoyl-ACP reductase from *Mycobacterium tuberculosis* (InhA) was studied. A series of compounds with nanomolar affinity for the enzyme and reduced lipophilicity were identified. In addition, a slow-onset inhibitor of

InhA that has a  $K_1$  value of 22 pM and a residence time of 23 min on the enzyme was identified and characterized. Site-directed mutagenesis and X-ray structural studies demonstrated that slow onset inhibition of InhA results in ordering of a substrate-binding loop that covers the entrance to the binding pocket and thereby locks the inhibitor in the substrate binding cavity and increases its residence time. This is significant since long drug-target residence time is thought to be an important factor for *in vivo* drug activity.

Studies of enoyl-ACP reductases have also been extended to *Burkholderia pseudomallei* (bpmFabIs) and *Yersinia pestis* (ypFabV). Mechanistic studies were performed on two FabI homologues in *B. pseudomallei*, which demonstrated that only one (bpmFabI-1) has enoyl-ACP reductase activity. As a prelude to rational inhibitor development, the sensitivity of bpmFabI to four diphenyl ethers has been evaluated. In each case the compounds are nanomolar slow onset inhibitors. Reduction in MIC values is observed for the *Burkholderia sp.* efflux pump mutant with all diphenyl ethers suggesting that bpmFabI-1 is a suitable target for drug discovery provided that efflux can be circumvented. Mechanistic studies are also performed on the enoyl ACP reductase FabV homologue in *Y. pestis*. Steady-state kinetics has been used to study the reaction mechanism of ypFabV. Preliminary inhibition studies indicate that diphenyl ethers are not promising leads for developing potent FabV inhibitors.

Interestingly, during the study of the FabI in *B. pseudomallei*, we found this organism has a high level of unsaturated fatty acids (UFAs), but lacks *fabA* and *fabB* homologues that normally found in the UFA biosynthesis pathway. We attempted to identify the putative *trans*-2, *cis*-3-enoyl-ACP isomerase (FabM), which is a key enzyme in alternative UFA biosynthesis pathway. However, the candidate was characterized

and found as a *trans*-2, *cis*-3-enoyl-CoA isomerase. Through sequence alignment with other members of the crotonase superfamily, conserved catalytic residues were recognized and enzymatic mechanism for this candidate was proposed.

Finally, the mechanism and inhibition of the dihydroxynaphthoyl-CoA synthase (MenB) from *Mycobacterium tuberculosis* was studied. In the menaquinone pathway, MenB catalyzes the formation of a carbon-carbon bond through a Dieckmann condensation. We compared the mechanism of the *M. tuberculosis* MenB enzyme with that of MenB from *E. coli*. Kinetic data and X-ray crystallography suggest that MenBs from *M. tuberculosis* and *E. coli* utilize the same substrate for catalysis and share the same reaction mechanism. In addition, we performed an structure activity relationship study on MenB inhibitors, based on two studied leads: the 2-amino-4-oxo-phenylbutanoic acids and the benzoxazinones from high throughput screen. The most potent compound against MenB exhibits excellent inhibition *in vitro* with the  $K_1$  value of 18 nM. These studies will help us to validate MenB as a target for the development of novel microbial chemotherapeutics.

## Table of Contents

List of Figures.....	xi
List of Tables.....	xvi
List of Abbreviations.....	xviii
Acknowledgments.....	xxiv
List of Publications.....	xxv
Chapter 1 : Fatty acid and Menaquinone biosynthesis pathway as novel target for drug discovery.....	1
The History of Antibiotics.....	1
Fatty Acid Biosynthesis (FAS-II) Pathway.....	3
Enoyl-ACP Reductase.....	6
Inhibitor of FabI.....	9
Menaquinone Biosynthesis Pathway.....	18
Inhibitors of Menaquinone Biosynthesis Pathway.....	22
Research Project Overview.....	26
Chapter 2 : Slow Onset Inhibition of Enoyl-ACP Reductase (InhA) from <i>Mycobacterium tuberculosis</i> .....	27
Background.....	27
Tuberculosis and <i>Mycobacterium tuberculosis</i> .....	27
Isoniazid Resistance.....	28
Diphenyl Ether Inhibition Activity against InhA Mutant from Isoniazid and Triclosan Resistant Strains.....	29
Diphenyl Ether Scaffold Optimization.....	30
Project Goal.....	31
Materials and Methods.....	32
Expression and Purification of InhA.....	32
Site-Directed Mutagenesis, Expression and Purification of InhA Mutants.....	33
Synthesis of Trans-2-Dodecenoyl-CoA.....	35
Synthesis of Diphenyl Ethers.....	36

Steady-state Kinetic Assay.....	36
Progress Curve Analysis.....	38
Preincubation Inhibition Assay for Slow Binding Inhibitors.....	39
Direct Determination of $k_{off}$ .....	40
Whole Cell Antibacterial Assay.....	41
X-Ray Crystallography of InhA with 2-(o-Tolyloxy)-5-hexylphenol.....	42
Results and Discussion.....	43
Characterization of the Inhibition of Triclosan-Resistant Mutants by B ring Diphenyl Ethers.....	43
<i>In vitro</i> Antimycobacterial Activity of B ring Modified Diphenyl Ethers.....	45
Kinetic Characterization of PT70.....	50
Basis of the PT70 Slow-onset Inhibition.....	61
Mechanism of InhA Slow-onset Inhibition.....	65
Conclusions.....	70
Chapter 3 : Mechanism and Inhibition of FabI Enoyl-ACP Reductases from <i>Burkholderia pseudomallei</i> (bpmFabI-1 and bpmFabI-2).....	71
Background.....	71
Meliodosis and <i>Burkholderia pseudomallei</i> .....	71
Multidrug Resistant Efflux Pump.....	73
Targeting on Enoyl ACP Reductase.....	73
Project Goals.....	75
Materials and Methods.....	76
Cloning, Expression and Purification of bmaFabI-1 and bmaFabI-2.....	76
Circular Dichroism (CD) Spectroscopy.....	78
Fluorescence Titration Experiments.....	78
Expression and Purification of ftuACP.....	79
Preparation of Crotonyl-ACP (Cro-ACP).....	80
Preparation of CoA Substrate Analogues.....	80
Steady-state Kinetic Assays.....	82
Progress Curve Analysis.....	83



Inhibition of bpmFabI-1 by Triclosan and Select Diphenyl Ether Inhibitors. .	84
Results and Discussion.....	87
Cloning, Overexpression and Purification of bpmFabI-1 and bpmFabI-2. ...	87
Catalytic Activity of bpmFabI-1 and bpmFabI-2. ....	90
Antimicrobial Activity of the Diphenyl Ether bpmFabI-1 Inhibitors.....	96
Conclusions .....	104
Chapter 4 : Mechanism and Inhibition of the FabV enoyl-ACP Reductase from <i>Yersinia pestis</i> .....	105
Background.....	105
Plague .....	105
<i>Yersinia pestis</i> .....	106
FabV, the fourth Enoyl-ACP Reductase .....	107
Project Goal.....	107
Materials and Methods.....	108
Cloning, Expression, and Purification of ypFabV.....	108
Synthesis of Trans-2-dodecenoyl-CoA, Cis-5-trans-2-dienoyl-CoA and Lauryl-CoA .....	109
Steady-State Kinetics Analysis .....	110
Inhibition by Diphenyl Ether Compounds.....	110
Results and Discussion.....	111
Bioinformatic Analysis.....	111
Kinetic Mechanism.....	113
Preference toward Saturated Acyl Chain Substrate and Unsaturated Acyl Chain Substrate. ....	115
Inhibition of ypFabV by diphenyl ethers.....	118
Conclusion .....	128
Chapter 5 : Identification of putative trans-2, cis-3-decenoyl-CoA isomerase in <i>Burkholderia mallei</i> .....	129
Introduction .....	129

Bacterial Unsaturated Fatty Acid (UFA) Biosynthesis.....	129
Putative trans-2, cis-3-Decenoyl-CoA Isomerase (FabM) in <i>B. mallei</i> .....	134
Crotonase Superfamily .....	134
Project Goals .....	135
Materials and Methods.....	136
Cloning, Expression, and Purification of the bmaa0541 .....	136
Cloning, Expression and Purification of the bmaa0541 Mutants.....	137
Synthesis of trans-2-Decenoyl-CoA and cis-3-Decenoyl-CoA. ....	138
Preparation of trans-2-Decenoyl-ecACP and cis-3-Decenoyl-ecACP .....	139
Enzymatic Activity of the bmaa0541 .....	140
Results and Discussion.....	141
Putative UFAs Biosynthesis Pathways in <i>B. mallei</i> .....	141
<i>In vitro</i> Activity of the Putative trans-2, cis-3-enoyl-ACP Isomerase (FabM).....	147
Crystal Structure of the bmaa0541. ....	150
Catalytic Mechanism.....	155
Conclusions .....	158
Chapter 6 : Mechanism and Inhibition of the Dihydroxynaphthoyl-CoA Synthase (MenB) from <i>Mycobacterium tuberculosis</i> .....	159
Background.....	159
Crotonase Superfamily. ....	159
Mechanism of MenB Catalyzed Reaction. ....	162
High throughput screen of potent inhibitors of mtMenB .....	165
Project Goals. ....	168
Materials and Methods.....	170
Expression and purification of mtMenB and ecMenB. ....	170
Site-Directed Mutagenesis, Expression and Purification of MenB Mutants.....	171
Expression and purification of ecMenE.....	173
Coupled kinetic assay of MenB reaction.....	174
Preincubation assay. ....	176
Pyrophosphate release assay. ....	176

Synthesis of o-(3-carboxypropyl)-benzoyl CoA (OCPB-CoA) .....	177
Determination of <i>M. tuberculosis</i> antimicrobial activity. ....	177
Results and Discussion.....	178
Role of D185 in mtMenB and G156 in ecMenB .....	178
Discovery of “substrate-like” inhibitors. ....	190
Discovery of “product-like” inhibitors.....	203
<i>In vitro</i> enzymatic inhibition assay of other inhibitors.....	208
Conclusions .....	211
Bibliography .....	212

## List of Figures

Figure 1.1: The history of antibiotics development (4).....	2
Figure 1.2: Key steps in the genomics-driven antibiotic drug discovery process (8). ....	3
Figure 1.3: Fatty acid synthesis pathway in <i>E. coli</i> .....	5
Figure 1.4: The <i>E. coli</i> enoyl-ACP reductase (FabI) catalytic mechanism (29). ....	7
Figure 1.5: The <i>Burkholderia mallei</i> enoyl-ACP reductase (FabV) catalytic mechanism (31).....	8
Figure 1.6: Structure of diazaborines and 2-(toluene-4-sulfonyl)-benzodiazaborine. ....	10
Figure 1.7: Structure of the 2-(toluene-4-sulfonyl)-benzodiazaborine-NAD adduct bound to ecFabI (pdb code: 1dfg). ....	10
Figure 1.8: Structure of the INH-NAD adduct bound to InhA (pdb code: 1zid) (23).....	11
Figure 1.9: Structure of (A) triclosan bound to ecFabI (pdb code: 1qsg) (22) and (B) PT70 bound to InhA (pdb code: 2x23) (49). ....	13
Figure 1.10: Representative structure of FabI inhibitors.....	16
Figure 1.11: Structures of the phyloquinone (vitamin K <sub>1</sub> ), menaquinone (vitamin K <sub>2</sub> ) and ubiquinone (Q). ....	18
Figure 1.12: Menaquinone biosynthetic pathway in <i>E. coli</i> .....	20
Figure 1.13: Menaquinone biosynthetic pathway in <i>S. coelicolor</i> A3(2). ....	21
Figure 1.14: Representative structures of menaquinone biosynthesis inhibitors.....	23
Figure 2.1: Activation of prodrug isoniazid. Isoniazid and cofactor NAD <sup>+</sup> form INH-NAD adduct. ....	29
Figure 2.2: Structure of the slow onset inhibitor 2-( <i>o</i> -Tolyloxy)-5-hexylphenol (PT70)..	42

Figure 2.3: Active site region of the InhA-NAD <sup>+</sup> -triclosan crystal structure (pdb code: 2b35).....	44
Figure 2.4: Structure of triclosan and 6PP (5-hexyl-2-phenoxyphenol) (50).....	44
Figure 2.5: Progress curve analysis for the inhibition of InhA by PT70 and effect of NAD <sup>+</sup> on the apparent inhibition constant of PT70. ....	51
Figure 2.6: Kinetic scheme for the slow onset inhibition of InhA by PT70. ....	53
Figure 2.7: Loop ordering upon slow binding inhibition. ....	58
Figure 2.8: Close-up of the binding pocket of InhA with bound NAD <sup>+</sup> and PT70.....	59
Figure 2.9: Substrate binding loop conformation.....	67
Figure 2.10: Steric effect between PT70 and side chains of Val203 and Ile215.....	68
Figure 3.1: Structure of Cro-CoA, Oct-CoA, Dec-CoA and DD-CoA. ....	82
Figure 3.2: Kinetic schemes for the inhibition of bpmFabI-1.....	86
Figure 3.3: Sequence alignment of the FabI enzymes from <i>E. coli</i> , <i>F. tularensis</i> and <i>B. pseudomallei</i> . ....	88
Figure 3.4: 12% SDS-PAGE showing the expression and purification of bpmFabI-1 and bpmFabI-2.....	89
Figure 3.5: CD spectra of bpmFabI-1 and bpmFabI-2.....	90
Figure 3.6: Two-substrate steady-state kinetics. ....	92
Figure 3.7: Product inhibition studies to determine the order of substrate binding. ....	93
Figure 3.8: Fluorescence titration of bpmFabI-1 with NADH. ....	93
Figure 3.9: Real-time PCR analysis of bpmFabI-1 and bpmFabI-2.....	96
Figure 3.10: Progress curve and preincubation analysis for the inhibition of bpmFabI-1 by triclosan and PT01.....	99

Figure 4.1: Sequence alignment of enoyl-ACP reductases FabI from <i>E. coli</i> , and FabV from <i>V. cholerae</i> , <i>B. mallei</i> , <i>Y. pestis</i> .....	112
Figure 4.2: Two-substrate steady-state kinetics. ....	114
Figure 4.3: Product inhibition studies to determine the order of substrate binding. ....	114
Figure 4.4: Structure of DD-CoA and <i>cis</i> -5- <i>trans</i> -2-dienoyl-CoA.....	116
Figure 4.5: ecFabI and apo-ypFabV structures comparison.....	125
Figure 4.6: apo-ypFabV structure.....	127
Figure 5.1: Packing of fatty acid chains in a membrane.....	130
Figure 5.2: A generalized desaturase pathway. ....	130
Figure 5.3: Saturated and unsaturated fatty acid biosynthesis pathways in <i>E. coli</i> and <i>S. pneumoniae</i> . ....	133
Figure 5.4: Reactions catalyzed by members of the crotonase superfamily.....	135
Figure 5.5: Structure of <i>trans</i> -2-decenoyl-CoA and <i>cis</i> -3-decenoyl-CoA.....	138
Figure 5.6: Proposed (A) SFA and (B) UFA biosynthesis pathway in <i>B. mallei</i> .....	146
Figure 5.7: FabM reaction using CoA substrate analogue (186).....	147
Figure 5.8: Part of the cloning/expression region in pBAD <i>Myc/His C</i> vector. ....	148
Figure 5.9: Structure of the bmaa0541.....	151
Figure 5.10: Hydrogen bonding interactions between phosphate groups and adenine moiety of CoA and proteins in crotonase superfamily. ....	153
Figure 5.11: Sequence alignment of characterized crotonase superfamily members. ....	154
Figure 5.12: Proposed reaction mechanism catalyzed by <i>trans</i> -2, <i>cis</i> -3-decenoyl-CoA isomerase.....	156
Figure 5.13: Active site structure of <i>trans</i> -2, <i>cis</i> -3-decenoyl-CoA isomerase. ....	157

Figure 6.1: Sequence alignment of crotonase superfamily members.....	161
Figure 6.2: Reaction catalyzed by MenB.....	162
Figure 6.3: Proposed mechanism of reaction catalyzed by MenB (mtMenB numbering) (65).....	163
Figure 6.4: The degradation of OSB-CoA to spirodilactone. ....	164
Figure 6.5: Alternative mechanism of the mtMenB catalyzed reaction.....	164
Figure 6.6: Reaction catalyzed by MenE and MenB .....	166
Figure 6.7: Structure of 2-amino-4-oxo-phenylbutanoic acids and benzoxazinones ...	167
Figure 6.8: Structure of OCPB-CoA .....	181
Figure 6.9: Analysis of OCPB-CoA product by ion trap mass spectrometry.....	183
Figure 6.10: Proposed reaction of OCPB-CoA.....	184
Figure 6.11: HN-CoA mimics structure of MenB product DHNA-CoA. ....	185
Figure 6.12: X-ray structure of mtMenB•AcAc-CoA and sequence alignment of ecMenB and mtMenB.....	187
Figure 6.13: Structure of OSB-CoA and OSB-NCoA.....	188
Figure 6.14: Overlap of mtMenB bound AcAc-CoA (pdb code: 1q51) with and ecMenB bound with OSB-NCoA.....	189
Figure 6.15: 2-amino-4-oxo-phenylbutanoic acids degradation by retro-Michael addition. ....	190
Figure 6.16: Structure of ( <i>E</i> )-4-(2,4-dichlorophenyl)-4-oxobut-2-enoic acid (compound 22).....	191
Figure 6.17: IC <sub>50</sub> of Compound 22 measured at different CoA andATP concentration. ....	192

Figure 6.18: Proposed mechanism of CoA adduct generation through Michael addition. .....	192
Figure 6.19: Structure of 2-amino-3,3-dimethyl-4-oxo-phenyl-butanoic acids (24) and two 4-oxo-4-phenylbutanoic acids (25 and 26).....	193
Figure 6.20: IC <sub>50</sub> of Compound 23 measured at different CoA concentration. ....	194
Figure 6.21: Effect of OSB on K <sub>i</sub> <sup>app</sup> of 23.....	195
Figure 6.22: Proposed structure of the CoA adduct bound to mtMenB. ....	197
Figure 6.23: Interactions between ecMenB and compound 23. ....	198
Figure 6.24: Crystal structure of ecMenB bound with 23.....	200



## List of Tables

Table 1.1: Comparison of the catalytic signatures of enoyl-ACP reductases. ....	7
Table 1.2: Antimicrobial activity of FabI inhibitors. ....	17
Table 1.3: Inhibitors of menaquinone biosynthesis pathway .....	24
Table 2.1: Nucleotide primers .....	34
Table 2.2: IC <sub>50</sub> of selected B ring diphenyl ethers for wild-type and mutant InhA.....	43
Table 2.3: Inhibition and solubility data for B-ring heterocycles.....	48
Table 2.4: Inhibition and solubility data for nitro, amino, amide and piperazine compounds.....	49
Table 2.5: Inhibition of InhA by PT70 and the INH-NAD Adduct .....	54
Table 2.6: Crystallographic data and refinement statistics .....	57
Table 2.7: Kinetic parameters for wild-type and mutant InhA. ....	63
Table 2.8: Inhibition type and constants for PT70 and 6PP binding to wild-type and mutant InhA enzymes.....	64
Table 2.9: Kinetic parameters for wild-type and mutant InhA. ....	69
Table 2.10: Inhibition type and constants for PT70 and 6PP binding to wild-type and mutant InhA.....	69
Table 3.1: Steady-state kinetic parameters for bpmFabI-1.....	91
Table 3.2: Inhibition of ftuFabI and bpmFabI-1 by triclosan.....	98
Table 3.3: Antibacterial activity and inhibition of bpmFabI-1 by triclosan and the diphenyl ethers .....	100
Table 4.1: Kinetic parameters of enoyl-ACP reductases from different organism and their UFA content in the lipid .....	117

Table 4.2: Inhibition of triclosan and Its Analogues for ypFabV and bmFabV .....	120
Table 5.1: Nucleotide primers .....	138
Table 5.2: UFA synthesis pathway and UFA content in the lipid in different bacteria..	143
Table 5.3: Putative UFA biosynthesis genes in <i>B. mallei</i> genome .....	145
Table 6.1: Inhibition data of selective strong hits at 12 $\mu$ M inhibitor .....	167
Table 6.2: <i>In vitro</i> activity of 2-amino-4-oxo-phenylbutanoic acids. ....	169
Table 6.3: Nucleotide primers .....	172
Table 6.4: Kinetic parameters of mtMenB and ecMenB mutants. ....	179
Table 6.5: Kinetic parameter of MenB reaction with/without preincubation. ....	180
Table 6.6: Kinetic parameter of MenB reaction with OSB-CoA and OCPB-CoA as the substrate. ....	184
Table 6.7: Enzyme inhibition and stability of CoA adducts. ....	196
Table 6.8: Enzyme inhibition of compounds with CoA portion replacement. ....	201
Table 6.9: <i>In vitro</i> activity of 1,4-benzoxazine: (Z)-methyl 2-(2-oxo-2H- benzo[b][1,4]oxazin-3(4H)ylidene)acetates. ....	204
Table 6.10: <i>In vitro</i> activity of 1,4-benzoxazine: (Z)-3-(2-aryl-2-oxoethylidene)-3,4- dihydro-2H-benzo[b][1,4]oxazin-2-ones. ....	207
Table 6.11: Enzyme inhibition of of other inhibitors.....	209

## List of Abbreviations

AcAc-CoA	Acetoacetyl CoA
AccABCD	Acetyl-CoA carboxylase
ACP	Acyl carrier protein
AIDS	Acquired immune deficiency syndrome
AMP	Adenosine monophosphate
ATP	Adenosine triphosphate
Bi Bi	Bi-substrate Bi-product
BLAST	Basic Local Alignment Search Tool
<i>B. mallei</i>	<i>Burkholderia mallei</i>
<i>B. pseudomallei</i>	<i>Burkholderia pseudomallei</i>
BSA	Bovine serum albumin
<i>B. subtilis</i>	<i>Bacillus subtilis</i>
bmaFabV	Enoyl-ACP reductase from <i>Burkholderia mallei</i>
bpmFabI	Enoyl-ACP reductase from <i>Burkholderia pseudomallei</i>
bpmFabV	Enoyl-ACP reductase from <i>Burkholderia pseudomallei</i>
calcd	Calculated
CBD	4-Chlorobenzoyl-CoA dehalogenase
CD	Circular dichroism
ClogP	Calculated logarithm of partition coefficient between n-octanol and water
<i>cis-5-trans-2-dienoyl-CoA</i>	(2E,5Z)-Dodeca-2,5-dienoyl-CoA

CoA	Coenzyme A
Cr-ACP	<i>trans</i> -2-Crotonyl-ACP
Cr-CoA	<i>trans</i> -2-Crotonyl-CoA
crotonase	Enoyl-CoA hydratase
Da	Dalton
DD-CoA	<i>trans</i> -2-Dodecenoyl-CoA
Dec-CoA	<i>trans</i> -2-Decenoyl-CoA
DesA	Desaturase
DesB	Desaturase
DHNA	Dihydroxynaphthoic acid
DMSO	Dimethyl sulfoxide
DNA	Deoxyribonucleic acid
DTNB	5,5'-Dithio-bis(2-nitrobenzoic acid)
DTT	Dithiothreitol
DMPK	Drug metabolism/pharmacokinetics
ECI	$\Delta^{3,2}$ -Enoyl-CoA isomerase
ECH	Enoyl-Coenzyme A hydratase
<i>E. coli</i>	<i>Escherichia coli</i>
ecFabI	Enoyl-ACP reductase from <i>Escherichia coli</i>
ecMenB	MenB from <i>E. coli</i>
ecMenE	MenE from <i>E. coli</i>
EDTA	Ethylenediaminetetraacetic acid
ESI	Electrospray ionization
<i>F. tularensis</i>	<i>Francisella tularensis</i>

FabA	$\beta$ -Hydroxyacyl-ACP dehydratase
FabB	$\beta$ -Ketoacyl synthases I
FabF	$\beta$ -Ketoacyl synthases II
FabG	$\beta$ -Ketoacyl-ACP reductase
FabH	$\beta$ -Ketoacyl synthases III
FabI	Enoyl-ACP reductase
FabK	Enoyl-ACP reductase
FabL	Enoyl-ACP reductase
FabM	<i>trans</i> -2, <i>cis</i> -3-decenoyl-ACP isomerase
FabV	Enoyl-ACP reductase
FabZ	$\beta$ -Hydroxyacyl-ACP dehydratase
FAS-I	Eukaryotic fatty acid biosynthesis
FAS-II	Bacterial fatty acid biosynthesis
ftuACP	ACP from <i>F. tularensis</i>
HNA	1-hydroxy-2-naphthoic acid
HPLC	High-performance liquid chromatography
HTS	High-throughput screening
IC <sub>50</sub>	The half maximal inhibitory concentration
INH	Isoniazid
InhA	Enoyl-ACP reductase from <i>Mycobacterium tuberculosis</i>
IPTG	Isopropyl- $\beta$ -d-thiogalactopyranoside
KatG	Mycobacterial catalase-peroxidase

Lauryl-CoA	Dodecanoyl CoA
LB	Luria Broth
logP	Logarithm of partition coefficient between n-octanol and water
<i>M. tuberculosis</i>	<i>Mycobacterium tuberculosis</i>
MALDI-TOF	Matrix-assisted laser desorption/ionization time-of-flight
MDR-TB	multidrug-resistant TB
MenB	1, 4-Dihydroxy-2-naphthoyl-CoA synthase
MenE	OSB-CoA synthase
MIC	Minimal Inhibitory Concentration
MK	Menaquinone
MMCD	methyalmalonyl-CoA decarboxylase
MS	Mass spectrum
MS/MS	Tandem mass spectrometry
MTB	<i>Mycobacterium tuberculosis</i>
mtMenB	MenB from <i>M. tuberculosis</i>
mtMenE	MenE from <i>M. tuberculosis</i>
NAC	<i>N</i> -Acetylcysteamine
NAD <sup>+</sup>	Nicotinamide adenine dinucleotide (oxidized form)
NADH	Nicotinamide adenine dinucleotide (reduced form)
NADPH	Nicotinamide adenine dinucleotide phosphate
NCBI	National Center for Biotechnology Information

NIAID	National institute of allergy and infectious diseases
NMR	Nuclear magnetic resonance
OCPB-CoA	<i>o</i> -(3-carboxypropyl)-benzoic CoA
Oct-CoA	<i>trans</i> -2-Octenoyl-CoA
O.D. 600	Optical density at 600 nm
ORF	Open reading frame
OSB	<i>o</i> -succinylbenzoic acid
<i>P. aeruginosa</i>	<i>Pseudomonas aeruginosa</i>
PCR	Polymerase chain reaction
pdb	Protein data bank
PIPES	Piperazine-N,N'-bis(2-ethanesulfonic acid)
PPi	Pyrophosphate
Q	Ubiquinone
RMSD	Root-mean-square deviation
RND	Resistance-nodulation-division
RT	Room temperature
<i>S. aureus</i>	<i>Staphylococcus aureus</i>
saMenB	MenB from <i>S. aureus</i>
<i>S. pneumoniae</i>	<i>Streptococcus pneumoniae</i>
saFabI	Enoyl-ACP reductase from <i>S. aureus</i>
SAR	Structure activity relationship
SD	standard deviation
SDR	Short chain dehydrogenase/reductase

SDS-PAGE	Sodium dodecyl sulfate polyacrylamide gel electrophoresis
SFA	Saturated fatty acid
sp.	Specie
spp.	Several species
TB	Tuberculosis
THF	Tetrahydrofuran
UFA	Unsaturated fatty acid
<i>V. cholerae</i>	<i>Vibrio cholerae</i>
vcFabV	Enoyl-ACP reductase from <i>Vibrio cholerae</i>
WHO	World Health Organization
WT	Wild type
<i>Y. pestis</i>	<i>Yersinia pestis</i>
ypFabV	Enoyl-ACP reductase from <i>Y. pestis</i>



## Acknowledgments

I would like to express my gratefully and sincerely gratitude to my advisor Prof. Peter J. Tonge for the continuous support of my Ph.D study and research, for his patience, motivation, enthusiasm, encouragement and immense knowledge. His guidance helped me in all the time of research and writing of this thesis. I could not have imagined having a better advisor and mentor for my Ph.D study. For everything you've done for me, Prof. Tonge, thank you !

I would like to thank Prof. Elizabeth M. Boon, the chairperson of my dissertation committee, for her precious suggestions and insightful comments in guiding my research. I am grateful to Prof. Jin Wang, the third member of my dissertation committee, for all his help and advice. It is a pleasure to thank Prof. Stephen G. Walker, the outside member of my committee, for his intelligent questions and comments.

I would like to thank all the members of Tonge group for your stimulating discussion and kind help. I will cherish the happy time in Tonge group forever.

I owe my deepest gratitude to my parents, for giving birth to me at the first place and supporting me spiritually through my life. I am proud of being your daughter.

Words fail me to express my appreciation to my dear husband Airong Song whose love and persistent confidence encourages me to complete this work. It is pleasure to thank my adorable son Dylan H. Song, for inspiring and amazing me every day.

## List of Publications

- **Liu, N.**, Cummings, J. E., England, K., Slayden, R. A., Tonge, P. J.. Mechanism and Inhibition of the FabI Enoyl-ACP Reductase from *Burkholderia pseudomallei*. *J. Antimicrob. Chemother.*, **2011**, 66, 564-573
- Kinnings, S. L., **Liu, N.**, Tonge, P. J., Jackson, R. M., Xie, L., Bourne, P. E.. A machine learning-based method to improve docking scoring functions and its application to drug repurposing. *J. Chem. Inf. Model.*, **2011**, 51, 408-419
- Luckner, S. R.\*, **Liu, N.\***, am Ende, C. W., Tonge, P. J., Kisker, C.. A slow, tight-binding inhibitor of InhA, the enoyl-ACP reductase from *Mycobacterium tuberculosis*. *J. Biol. Chem.*, **2010**, 285, 14330-14337
- Li, X., **Liu, N.**, Zhang, H., Knudson, S. E., Slayden, R. A., Tonge, P. J.. Synthesis and SAR studies of 1,4-benzoxazine MenB inhibitors: Novel antibacterial agents against *Mycobacterium tuberculosis*. *Bioorg. Med. Chem. Lett.* **2010**, 20(21), 6306-6309
- Kinnings, S. L.\*, **Liu, N.\***, Buchmeier, N.\*, Tonge, P. J., Xie, L., Bourne, P. E.. Drug Discovery Using Chemical Systems Biology: Repositioning the Safe Medicine Comtan to Treat Multi-Drug and Extensively Drug Resistant Tuberculosis. *PLoS Comput. Biol.* **2009**, 5(7): e1000423
- am Ende, C. W., Knudson, S. E., **Liu, N.**, Childs, J., Sullivan, T. J., Boyne, M., Xu, H., Gegina, Y., Knudson, D. L., Johnson, F., Peloquin, C. A., Slayden, R. A., Tonge, P. J.. Synthesis and *in vitro* antimycobacterial activity of B-ring modified diaryl ether InhA inhibitors. *Bioorg. Med. Chem. Lett.* **2008**, 18, 3029–3033

- Bonnac, L., Gao, G., Chen, L., Felczak, K., Bennett, E. M., Xu, H., Kim, T., **Liu, N.**, Oh, H., Tonge, P. J., Pankiewicz, K. W.. Synthesis of 4-phenoxybenzamide adenine dinucleotide as NAD analogue with inhibitory activity against enoyl-ACP reductase (InhA) of *Mycobacterium tuberculosis*. *Bioorg. Med. Chem. Lett.* **2007**, 17(16), 4588-4591

\* These authors contributed equally to this work

## Chapter 1 : Fatty acid and Menaquinone biosynthesis pathway as novel target for drug discovery

### *The History of Antibiotics.*

An antibiotic is a substance or compound that can either kills bacteria or inhibits their growth. The term antibiotic was first described by Louis Pasteur and Robert Koch in 1877; they observed that an airborne bacillus could inhibit the growth of *Bacillus anthracis* (1). In the late 1880s, after screening hundreds of dyes against various organisms, Paul Ehrlich discovered a medically useful drug, synthetic antibacterial Salvarsan, to treat syphilis (2). It ushered in both the birth of the antibiotic revolution and the significance of antibiotic discovery. In 1928, Fleming made an important observation concerning the antibiosis by penicillin (3). In the meantime, another synthetic antibiotic Prontosil was developed and manufactured for commercial use by Domagk in 1932 (2). The discovery and development of this first sulfonamide drug opened the era of antibiotics. In 1941, Florey and Chain succeeded in purifying penicillin for clinical use. The purified antibiotic displayed antibacterial activity against a wide range of bacteria. It also had low toxicity and could be taken without causing adverse effects. The development of penicillin led to the 'golden era' of antibiotic discovery (1945-1960) during which most of the current clinically used antibiotics were discovered and characterized (**Figure 1.1**) (4).

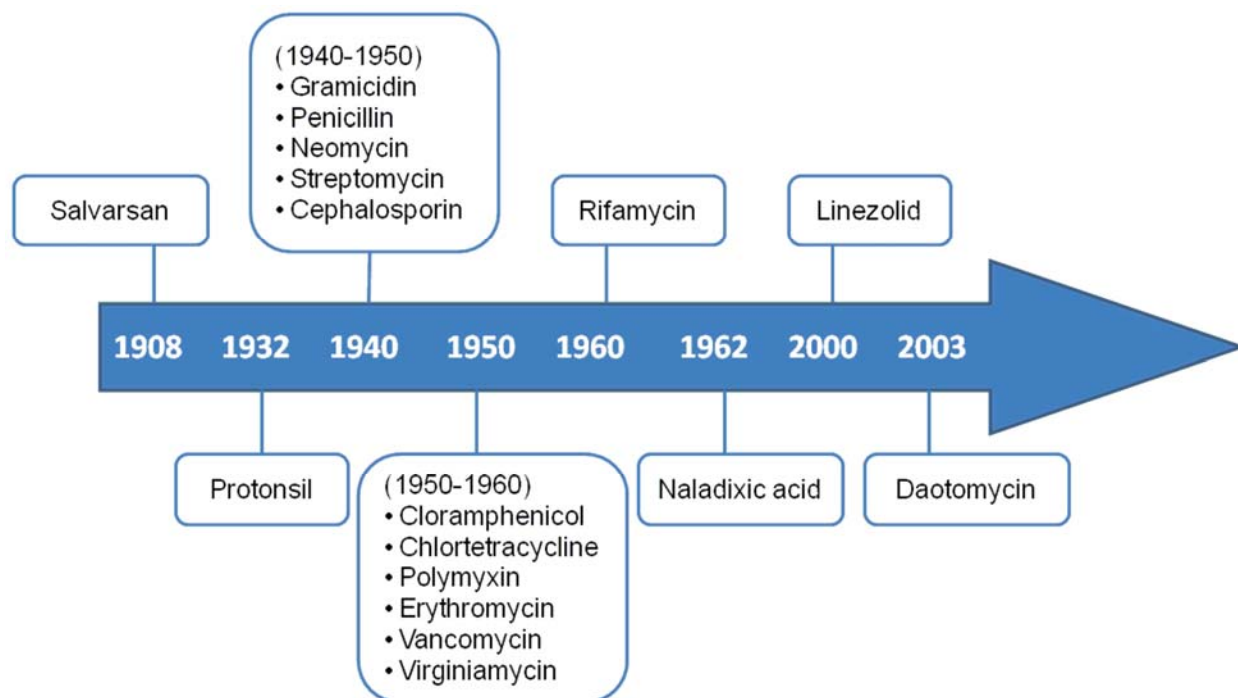


**Figure 1.1: The history of antibiotics development (4).**

However, since the early 1960s, the progress of the new antibiotic discovery significantly slowed down because of complex research and economic reasons (4). Moreover, natural selection led to the emergence of drug-resistance within a few years of antibiotics introduction into the market place (5-7). Consequently, there was an urgent need to launch novel antibacterial agents that can evade current resistance mechanisms.

One strategy to develop new antibiotics is to identify and exploit new molecular targets. This strategy is being favored by the wealth of new genome sequence information (**Figure 1.2**) (8). Once novel validated targets are discovered, appropriate high-throughput screen against diverse compound libraries is carried out. The next

challenge is to optimize and develop these leads toward antibiotics in a medicinal chemistry structure–activity relationship (SAR) study followed by testing lead antimicrobial candidates for safety and efficacy in animal infection models and then in humans.

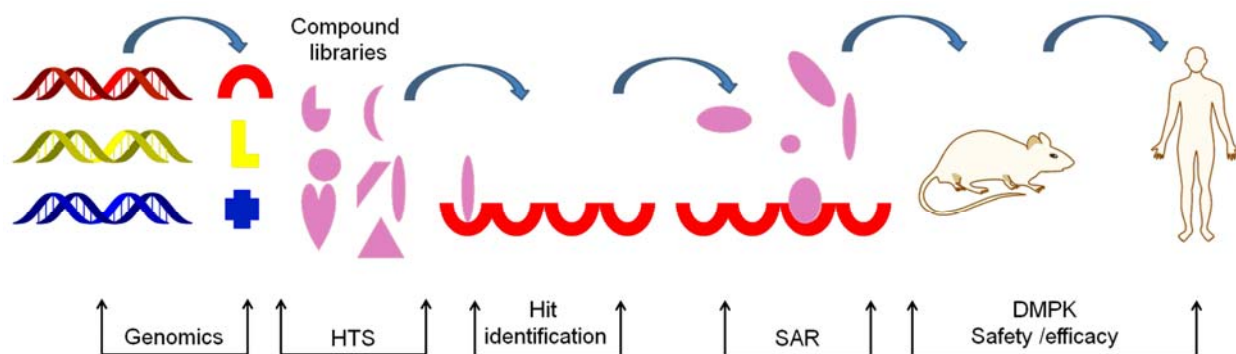


**Figure 1.2: Key steps in the genomics-driven antibiotic drug discovery process (8).**

Abbreviation: HTS, high-throughput screen; SAR, structure–activity relationship; DMPK, drug metabolism and pharmacokinetics.

Our goal is to understand the mechanism of enoyl-ACP reductases from the fatty acid biosynthesis pathway and dihydroxynaphthoyl-CoA synthase from menaquinone biosynthesis pathway in pathogenic bacteria. In addition, we attempt to design and develop potent inhibitors targeting these enzymes.

### *Fatty Acid Biosynthesis (FAS-II) Pathway*

The cell plasma membrane consists of phospholipid bilayers with embedded proteins. It separates the interior of cells from the outside environment. It acts as a permeability barrier for most molecules, and is also involved in a variety of cellular

processes such as cell signaling. Therefore, the cell membrane is essential for cell physiology.

The fatty acid biosynthesis pathway is the principal route for the production of the metabolic precursor for membrane phospholipid acyl chains. In eukaryotes, fatty acid synthesis is catalyzed by individual domains of a single protein including acyl carrier protein domain, the type I fatty acid synthesis (FAS-I). In prokaryotes, fatty acid synthesis is catalyzed by a series of discrete proteins and a separate acyl carrier protein, the type II fatty acid synthesis pathway (FAS-II) (**Figure 1.3**) (9). FAS-I and FAS-II have different active site organization, so enzymes involved in FAS-II pathway are attractive targets for antibiotics. In addition, genetic knockout and knockdown experiments proved that FAS-II pathway is essential for the viability of bacteria, and that fatty acid cannot be scavenged from the host by bacteria (8-10).

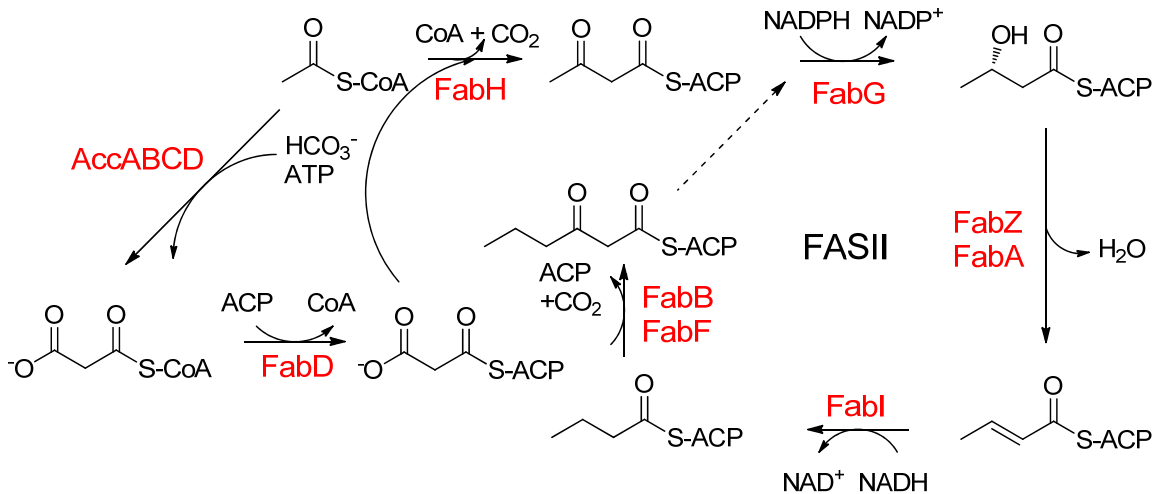


**Figure 1.3: Fatty acid synthesis pathway in *E. coli*.**

AccABCD is the acetyl-CoA carboxylase; FabH is the malonyl-CoA:ACP transacylase; FabG is the  $\beta$ -ketoacyl-ACP reductase; FabA and FabZ are the  $\beta$ -hydroxyacyl-ACP dehydrases; FabI is the enoyl-ACP reductase; FabH, FabB and FabF are the  $\beta$ -ketoacyl-ACP synthases. The initial condensation reaction is catalyzed by FabH, while further rounds of elongation are initiated by FabB or FabF.

FAS-II is composed of two modules: initiation and elongation. The initiation module is catalyzed by acetyl-CoA carboxylase (AccABCD), a multi-subunit protein catalyzing the biotin-dependent carboxylation of acetyl-CoA to malonyl-CoA (11). Then, the malonyl moiety from malonyl-CoA is transferred to the terminal sulfhydryl of acyl carrier protein (ACP) through a transthioesterification reaction catalyzed by malonyl-CoA:ACP transacylase (FabD). ACP acts as the transportation machinery to shuttle substrates among all the enzymes in the subsequent elongation steps (12).

The elongation module is initiated by a condensation reaction between acetyl-CoA and malonyl-ACP, which is catalyzed by the condensing enzyme  $\beta$ -ketoacyl-ACP synthase III (FabH) (13). The  $\beta$ -ketoacyl-ACP is then reduced at the C3 position to produce  $\beta$ -hydroxyacyl-ACP by  $\beta$ -ketoacyl-ACP reductase (FabG) with NADPH as a



cofactor (14, 15). The third step in the elongation cycle is the dehydration of  $\beta$ -hydroxyacyl-ACP to form *trans*-2-enoyl-ACP by  $\beta$ -hydroxyacyl-ACP dehydratase FabZ or FabA (16, 17). Finally, enoyl-ACP is reduced to acyl-ACP by NADH-dependent enoyl-ACP reductase (FabI) to finish the elongation cycle. FabI catalyzes the reaction by reducing the C2 and C3 carbon-carbon double bond of the enoyl-ACP substrate to a single bond using NADH as cofactor and Tyr-Tyr-Lys triad. This elongation cycle repeats until the specific chain length is reached and then a thioesterase cleaves the fatty acids for further cell wall synthesis. In the elongation cycles,  $\beta$ -ketoacyl-ACP synthase I and II (FabB and FabF) are used to condense malonyl-ACP and acyl-ACP substrates generated from the previous cycle.

### *Enoyl-ACP Reductase*

The structure and mechanism of enoyl-ACP reductase FabI in several organisms has been thoroughly studied, such as in *Escherichia coli* (18-22), *Mycobacterium tuberculosis* (23, 24), *Staphylococcus aureus* (25) and *Francisella tularensis* (26). They belong to short-chain alcohol dehydrogenase/reductase superfamily (SDR) and have a highly conserved motif: tyrosine and lysine (Tyr-X<sub>6</sub>-Lys) (**Table 1.1**) (27). The normal enzyme mechanism involves Tyr donating a proton to C2, and NADH donating a hydride to C3 of the enoyl substrate. The Tyr proton is replenished by a proton relay system through Lys, the ribose hydroxyls and a chain of four water molecules that communicate with solvent. The resulting enol then undergoes tautomerization to yield the final product (**Figure 1.4**) (28, 29).

**Table 1.1: Comparison of the catalytic signatures of enoyl-ACP reductases.**

Name	Catalytic signature
<i>M. tuberculosis</i> InhA	Phe-X <sub>8</sub> -Tyr-X <sub>6</sub> -Lys
<i>E. coli</i> FabI	Ser-X <sub>10</sub> -Tyr-X <sub>6</sub> -Lys
<i>B. subtilis</i> FabL	Ser-X <sub>10</sub> -Tyr-X <sub>6</sub> -Lys
<i>V. cholera</i> FabV	Ser-X <sub>10</sub> -Tyr-X <sub>8</sub> -Lys

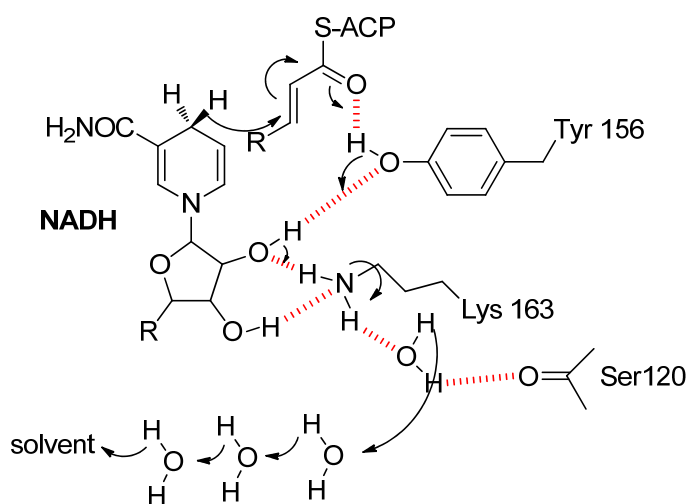


**Figure 1.4: The *E. coli* enoyl-ACP reductase (FabI) catalytic mechanism (29).**

Two other members of the SDR class of enoyl-ACP reductases, FabL (30) and FabV (31-33) make this enzyme family more diverse. *Bacillus subtilis* FabL is only 25 % identical with *E. coli* FabI and uses NADPH as cofactor. *Vibrio cholerae* FabV is 60 % larger than the typical SDR family member and the active site motif is Tyr-X<sub>8</sub>-Lys (32), which is two more residues than FabI and FabL (**Table 1.1**). The mechanism study of

FabV in *Burkholderia mallei* suggests that Y235 has hydrogen bond with K244 and/or K245. This interaction would lower the pK<sub>a</sub> of Y235 and facilitate the ability of this residue to stabilize and protonate the enolate intermediate formed during substrate reduction (**Figure 1.5**) (31).

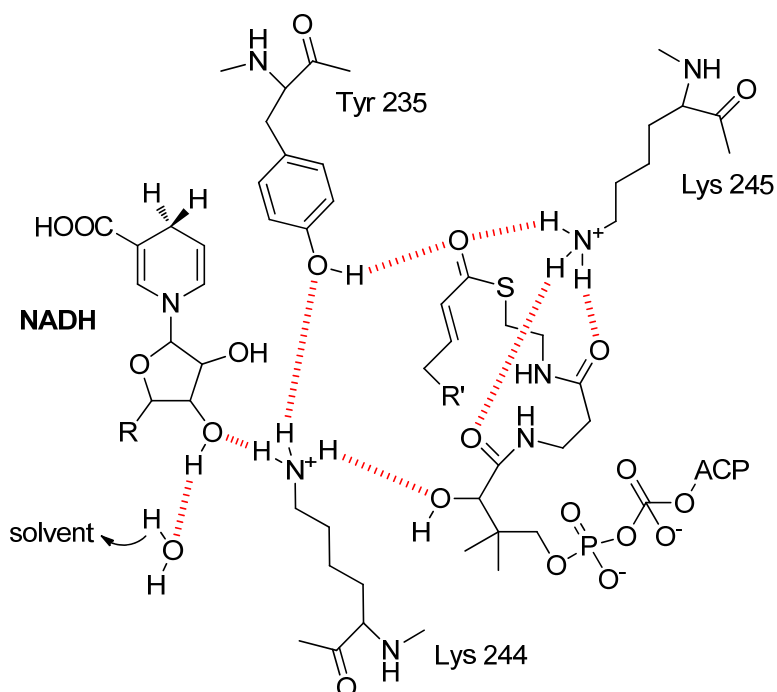


**Figure 1.5: The *Burkholderia mallei* enoyl-ACP reductase (FabV) catalytic mechanism (31).**

Proposed hydrogen bonding network among the three active site residues (Y235, K244, and K245), the cofactor, and the enoyl-ACP substrate.

*Streptococcus pneumoniae* FabK, a flavin-containing protein, is the only enoyl ACP reductase that does not belong to SDR superfamily (34). In this enzyme catalyzed reaction, NADH is the reductant, however it acts indirectly by reducing the tightly bound flavin cofactor. Then the reduced flavin catalyzes the double bond reduction.

#### *Inhibitor of FabI.*

FAS-II pathway offers us several unique binding sites by chemotherapeutic agents. The FabI enzymes have been shown to be essential for bacterial growth (35, 36). Below, we will summarize the current status of efforts to inhibit this enzyme.

The diazaborines are a class of heterocyclic boron-containing compounds that inhibit FabI via the formation of a covalent bond between the boron atom and the 2'-hydroxyl of the NAD<sup>+</sup> ribose (**Figure 1.6 and 1.7**) (18). The drug  $\pi$ -stacks with the nicotinamide ring of NAD<sup>+</sup> and also has van der Waals interactions with the hydrophobic substrate-binding pocket. The boron atom and its associated hydroxyl group occupy the space of the enolate in the putative substrate complex, thus the diazaborine-NAD adduct is a bisubstrate FabI inhibitor (18, 21). SAR studies have shown that the diazamoiety and the boron atom are essential for activity, and the best derivative benzodiazaborine has MIC value as low as 1.25  $\mu\text{g}/\text{mL}$  against *E. coli* and 8  $\mu\text{g}/\text{mL}$  against *M. tuberculosis* H37RV (37-39). However, diazaborines have been abandoned as a medically useful set of compounds, because of their undesirable inhibition of RNA processing in eukaryotic cells (40).

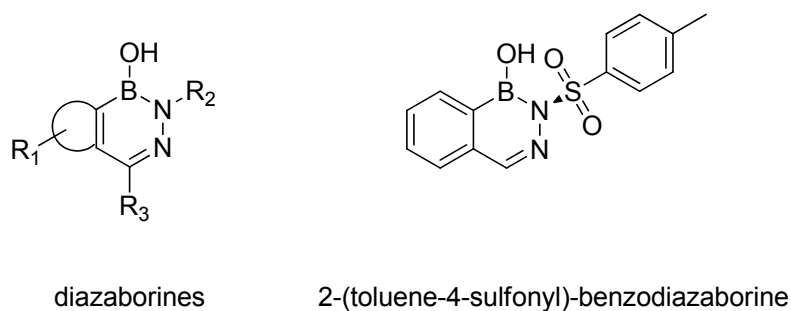


**Figure 1.6: Structure of diazaborines and 2-(toluene-4-sulfonyl)-benzodiazaborine.** R<sub>1</sub> in diazaborines can be benzene, naphthalene, thiophene, furan or pyrrole.

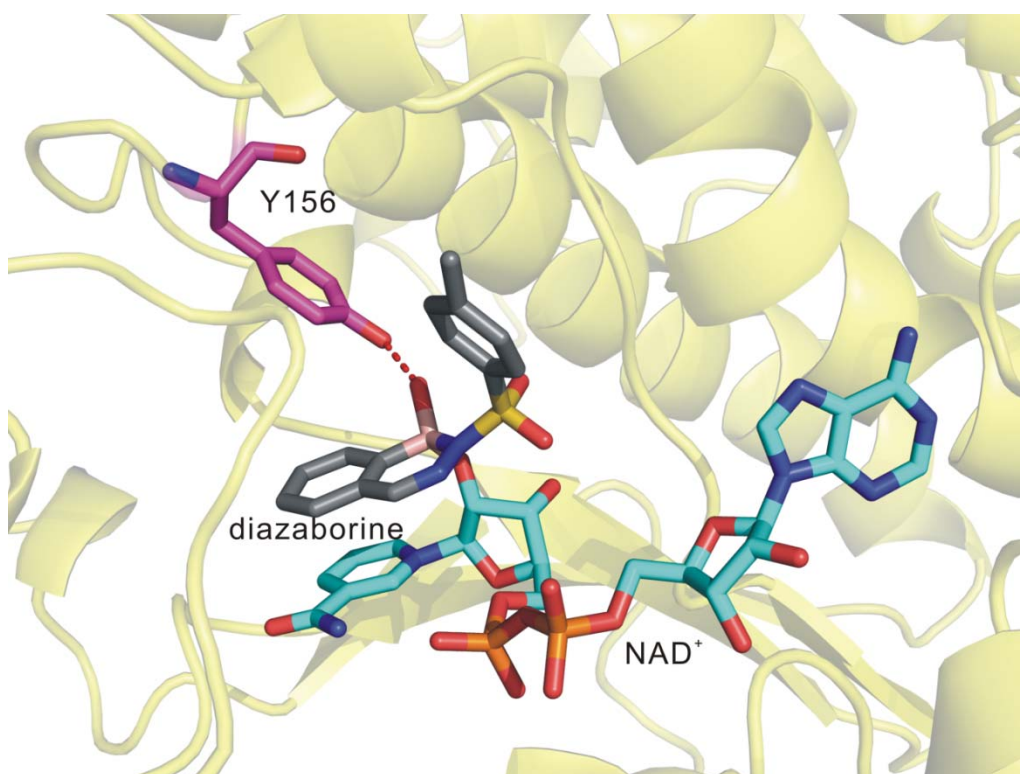


**Figure 1.7: Structure of the 2-(toluene-4-sulfonyl)-benzodiazaborine-NAD adduct bound to ecFabi (pdb code: 1dfg).** The diazaborine is in grey, the NAD<sup>+</sup> is in cyan, Y156 is in magenta.

The anti-mycobacterial properties of isoniazid (INH) have been known for almost 60 years, however the cellular target for this drug remained obscure until 1994 when a missense mutation within the mycobacterial *inhA* gene was shown to confer resistance

to INH (41). The inhibition of INH is dependent on the activation of the mycobacterial catalase-peroxidase enzyme KatG to form an adduct with  $\text{NAD}^+$  (INH-NAD adduct) (42). The INH-NAD adduct is a slow onset inhibitor of InhA with an overall  $K_i$  value of 0.75 nM (43). Structural studies have revealed that the INH-NAD adduct is a bisubstrate inhibitor, and slow onset inhibition is coupled to ordering of the substrate binding loop (Figure 1.8). However, isoniazid resistant strains were isolated almost immediately after its clinical use. The rapid development of isoniazid resistance is due to mutations on KatG (44).

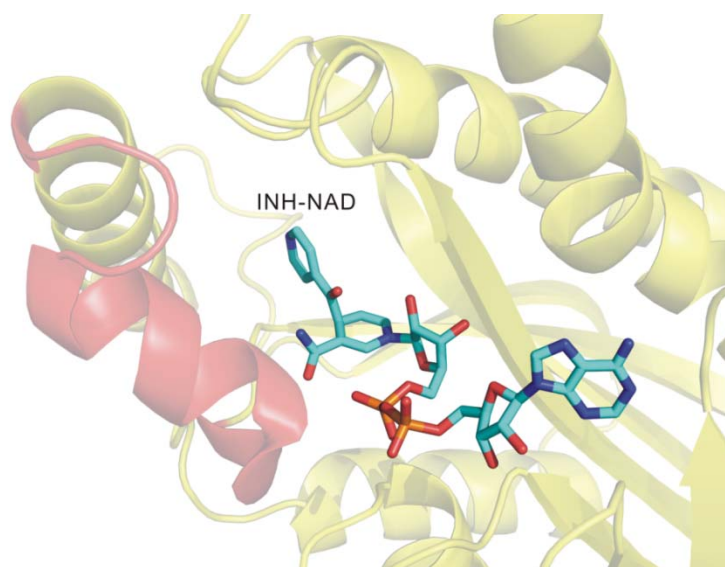


**Figure 1.8: Structure of the INH-NAD adduct bound to InhA (pdb code: 1zid) (23).** The INH-NAD adduct is in cyan, while the substrate binding loop is colored in red.

Triclosan is a slow onset, tight binding inhibitor of FabI from *E. coli*, binding with  $\text{E-NAD}^+$  complex with  $K_i$  value of 7 pM (Figure 1.9A) (45-47). Triclosan's phenol ring makes  $\pi$ -stacking interaction with the nicotinamide ring of  $\text{NAD}^+$ , and the hydroxyl group and ether oxygen of triclosan form hydrogen bonds with both the phenolic oxygen of Try156 and the 2'-hydroxyl of the nicotinamide ribose. Also there are extensive van der

Waals interactions with the protein. Finally, binding of triclosan to ecFabI leads to the ordering of the substrate binding loop, that has been proposed to account for the slow onset step in the formation of enzyme-inhibitor complex (22).

Extensive SAR studies of diphenyl ether scaffold are explored in our group. Diphenyl ether analogues have subnanomolar affinity for FabIs from *S. aureus* (saFabI) (25), *F. tularensis* (ftuFabI) (26) and *M. tuberculosis* (InhA) (48-50) (**Figure 1.9B**), where the lowest MIC values for these compounds against the respective organisms are less than 0.1-1 µg/mL (25, 26, 48-50).

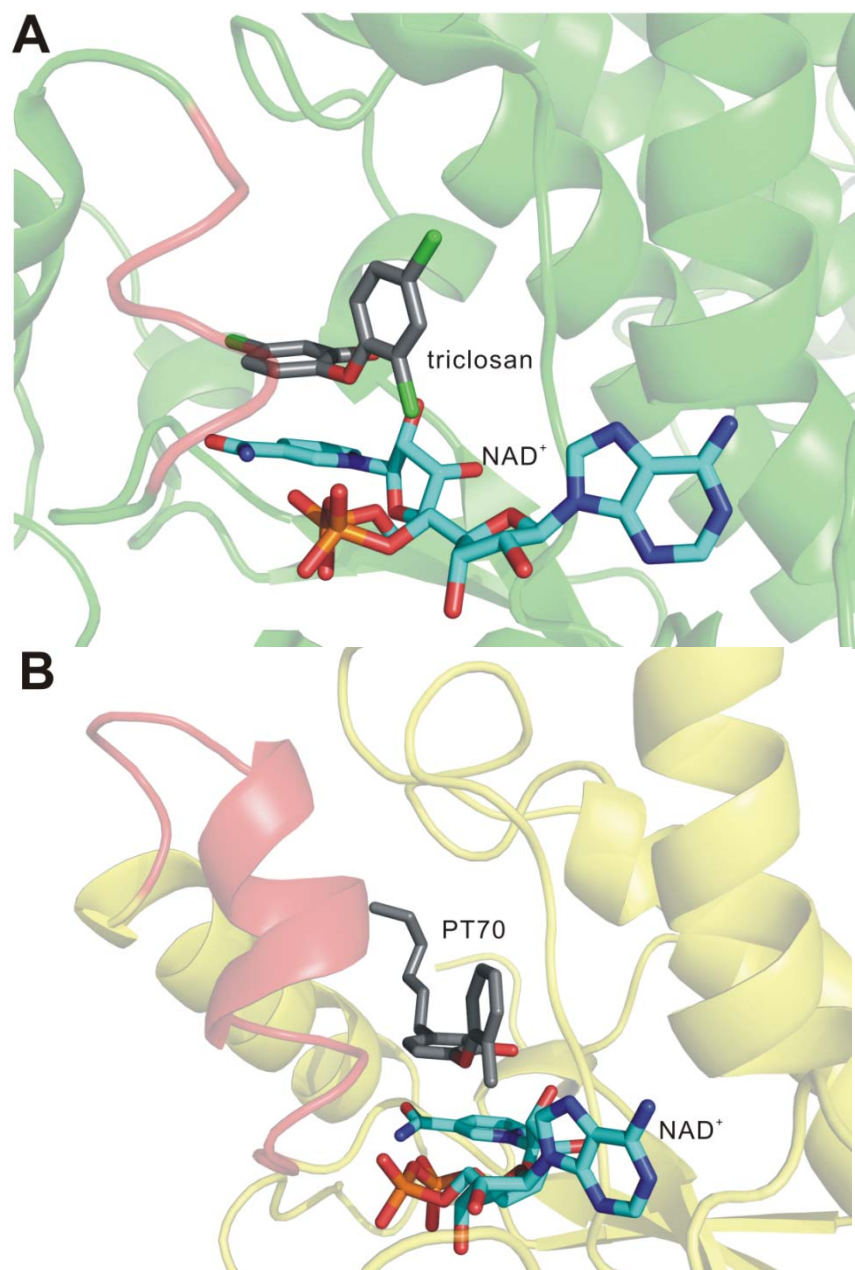
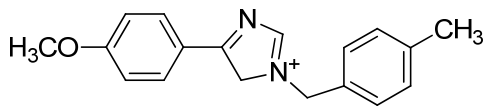


**Figure 1.9: Structure of (A) triclosan bound to ecFabi (pdb code: 1qsg) (22) and (B) PT70 bound to InhA (pdb code: 2x23) (49).**  
The triclosan and PT70 are in grey, NAD<sup>+</sup> is in cyan, the substrate binding loop is colored red.

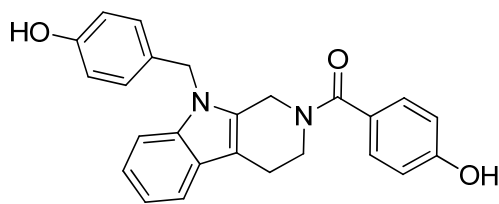


Several new chemical classes of FabI inhibitors have been discovered recently from high throughput screens (**Figure 1.10, Table 1.2**). GlaxoSmithKline screened over 300,000 compounds and identified a benzodiazepine derivative (51). Four related series of inhibitors, imidazoles (52), indoles (53), naphthyridines (51, 54) and aminopyridines (55) were identified after chemical optimization. Screening also identified indole-piperazines (56), pyrazole-based compounds (56) and pyrrolidine carboxamide (57). Structure-based chemical optimization produced compounds with sub-micromolar IC<sub>50</sub> value. Other FabI inhibitors incorporate pyridine and pyridone, such as thiopyridines (58) and 4-pyridone (59). CrystalGenomics Inc. discovered 2-pyridone that has potent antibacterial activity against several drug-resistant strains of *S. aureus* (60).

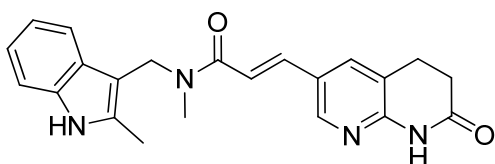
Another chemical class of FabI inhibitors was discovered during exploiting the antibacterial effects of various natural products (**Figure 1.10, Table 1.2**). These studies demonstrated that (-)-gallocatechin gallate (GCG) inhibits both FabI and FabG (61). Linoleic acid (62), iridoid-related aglycone (63), luteolin and curcumin (64) have antimicrobial activity against *S. aureus* and *E. coli*, respectively. Natural compounds are potentially good leads for the development of novel FabI inhibitors due to low toxicity.



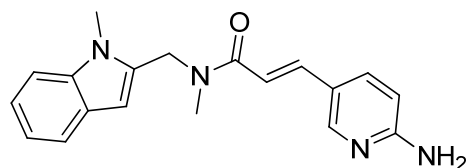
imidazoles



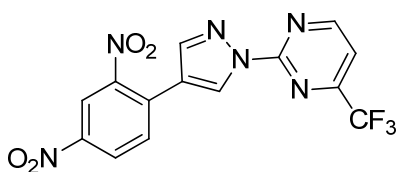
indoles



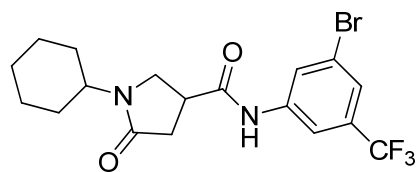
naphthyridines



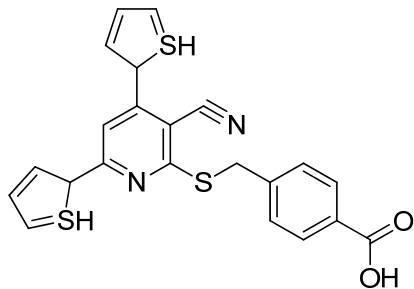
aminopyridines



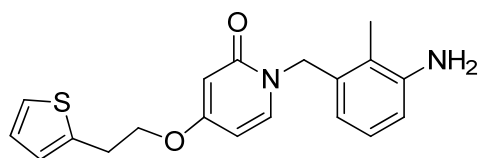
pyrazole



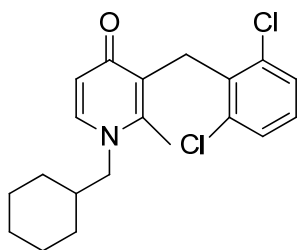
pyrrolidine carboxamide



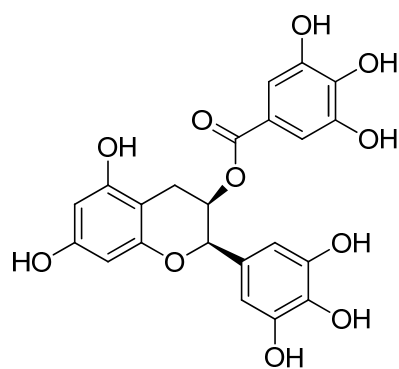
thiopyridine



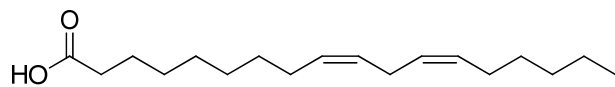
2-pyridone



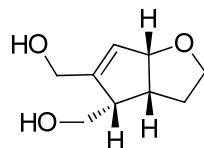
4-pyridone



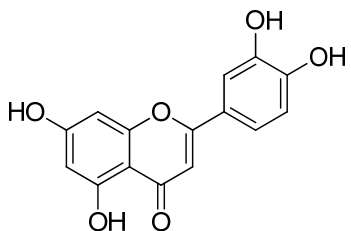
GCG



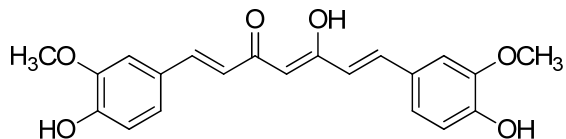
linoleic acid



iridoid-related aglycone



luteolin



curcumin

**Figure 1.10: Representative structure of FabI inhibitors.**

**Table 1.2: Antimicrobial activity of FabI inhibitors.**

Inhibitor	Support for Target	Bacterium	IC <sub>50</sub> ( $\mu$ M)	MIC ( $\mu$ g/mL)
imidazoles	X-ray <sup>a</sup> , OER <sup>b</sup>	<i>S. aureus</i>	0.36	8
indoles	X-ray, OER	<i>S. aureus</i>	0.11	0.5
naphthyridines	X-ray, OER, C14 <sup>c</sup>	<i>S. aureus</i>	0.05	0.016
aminopyridines	X-ray, OER, C14	<i>S. aureus</i>	2.4	0.5
pyrazole	X-ray	<i>M. tuberculosis</i>	N/A	2.5
pyrrolidine carboxamide	X-ray	<i>M. tuberculosis</i>	0.85	62.5
thiopyridines	UEH <sup>d</sup> , C14	<i>S. aureus</i>	4	2
2-pyridone	N/A <sup>e</sup>	<i>S. aureus</i>	N/A	0.5
4-pyridone	N/A	<i>S. aureus</i>	0.22 (ecFabI)	0.25
GCG	C14	<i>S. aureus</i>	5	200
linoleic acid	C14	<i>S. aureus</i>	35	56
iridoid-related aglycone	N/A		100	N/A
luteolin	OER, Kinetics <sup>f</sup>	<i>E. coli</i>	K <sub>i</sub> =7.1	74
curcumin	OER, Kinetics	<i>E. coli</i>	K <sub>i</sub> =15	74

<sup>a</sup> X-ray: structure of co-crystal of inhibitor

<sup>b</sup> OER: over-expression resistance

<sup>c</sup> C14: inhibition of C12-acetate incorporation into fatty acids

<sup>d</sup> UEH: underexpression hypersensitivity assay

<sup>e</sup> N/A: not available

<sup>f</sup> Kinetics: determination of inhibition mode and constants

### Menaquinone Biosynthesis Pathway.

Quinones shuttle electrons between membrane-bound protein complexes in the electron transport chain (65). They include phyloquinone (vitamin K<sub>1</sub>), menaquinone (MK, vitamin K<sub>2</sub>) and ubiquinone (Q). The specific quinones also differ in the number of repeating isoprene units in the side chain of the molecule (**Figure 1.11**).

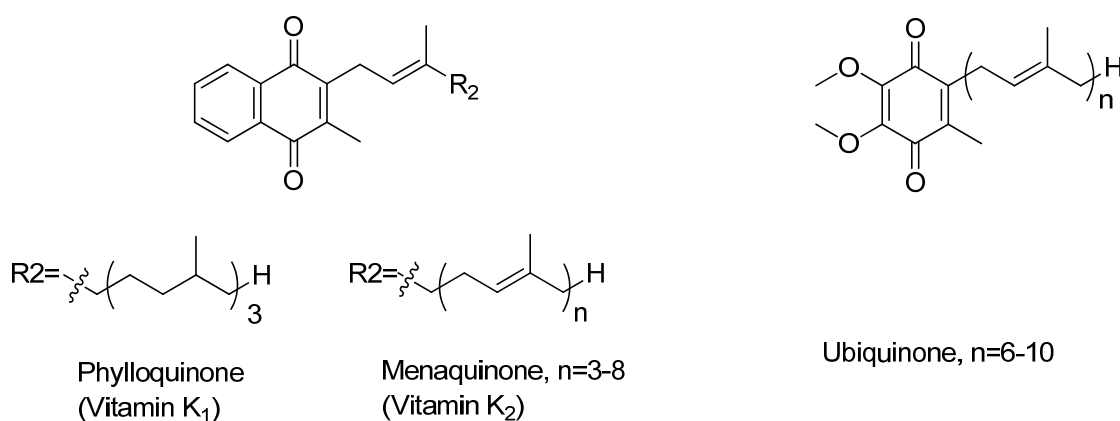


**Figure 1.11: Structures of the phyloquinone (vitamin K<sub>1</sub>), menaquinone (vitamin K<sub>2</sub>) and ubiquinone (Q).**

Acid fast bacteria *M. tuberculosis* utilizes menaquinone as a lipid-soluble electron carrier in their electron transport system (66), while Gram-negative bacteria, such as *E. coli*, utilize ubiquinone under aerobic conditions and menaquinone under anaerobic conditions (67). In humans, ubiquinone (Q<sub>10</sub>) functions as the electron carrier in the respiratory chain (67). There is no direct evidence for the menaquinone utilization in electron transportation by humans. However, menaquinone plays an important role in blood clotting (68). Humans lack the biosynthetic pathway for menaquinone, which must

obtain from intestinal bacteria, therefore the menaquinone biosynthetic pathway is proposed to be a potential drug target.

The menaquinone biosynthesis pathway has been studied extensively in *E. coli* (69-72) (**Figure 1.12**). The biosynthesis of menaquinone is initiated from chorismate and proceeds through a series of menaquinone-specific reactions. Chorismate is initially converted into isochorismate by MenF, isochorismate synthase, and then into 2-succinyl-6-hydroxy-2,4-cyclohexadiene-1-carboxylate (SEPHCHC) by MenD, a thiamin-dependent enzyme. Then the transformation of SEPHCHC to 2-succinyl-6-hydroxy-2, 4-cyclohexadiene-1-carboxylate (SHCHC) requires an additional enzyme, YfbB. The SHCHC is then dehydrated by MenC to yield an aromatic compound, *o*-succinylbenzoate (OSB), followed by the attachment of coenzyme A by MenE to yield *o*-succinylbenzoyl-CoA (OSB-CoA). The sixth step is the conversion of OSB-CoA to 1,4-dihydroxy-2-naphthoyl-CoA (DHNA-CoA) by MenB. After the DHNA-CoA is hydrolyzed to dihydroxynaphthoic acid (DHNA), MenA catalyzes the attachment of the prenyl side chain with the loss of a carboxyl group. The last step of the pathway is the methylation, catalyzed by UbiE, an *S*-adenosylmethionine (SAM)-dependent methyl transferase. The menaquinone pathway in *Bacillus subtilis*, *Mycobacterium phlei* and *M. tuberculosis* is thought to mirror the pathway found in *E. coli* (65, 73, 74).

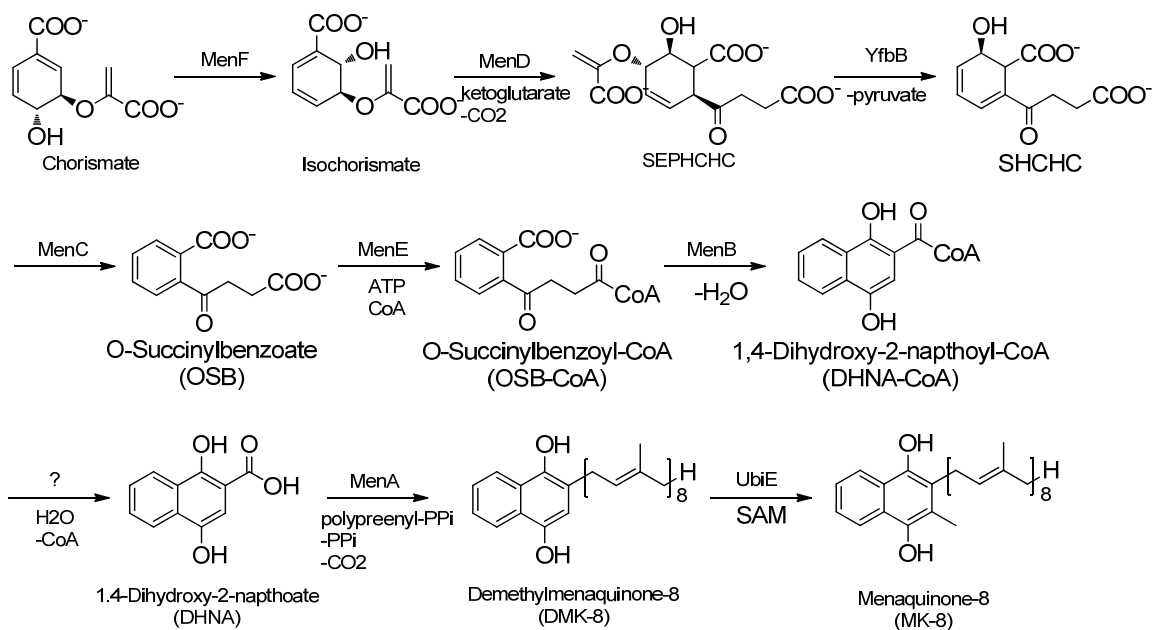


**Figure 1.12: Menaquinone biosynthetic pathway in *E. coli***

Menaquinone is an obligatory component of the electron-transfer pathway in some bacteria. However, a bioinformatics analysis of whole genome sequences has shown that some bacteria do not have homologues of the *men* genes, even though they produce menaquinone, for example *Streptomyces coelicolor* A3(2) (75-77), *Helicobacter pylori*, *Campylobacter jejuni* and lactobacilli (78-81). Recent studies support the existence of an alternative biosynthetic pathway in *S. coelicolor* A3(2), the futasine pathway as illustrated in **Figure 1.13** (82, 83).

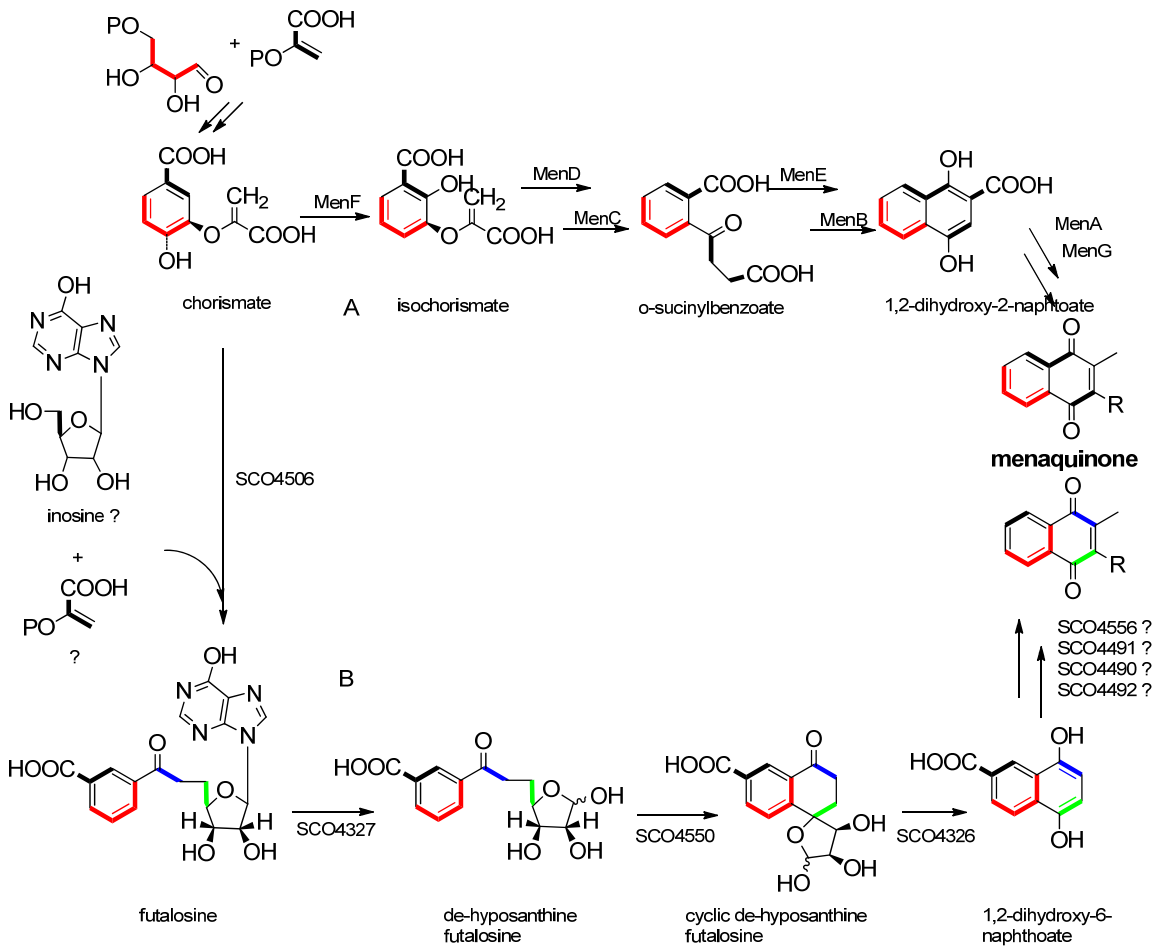
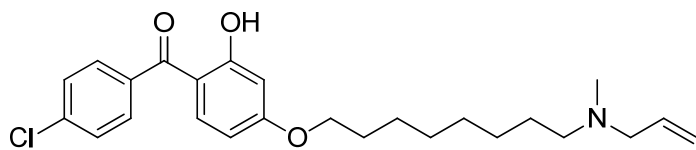


**Figure 1.13: Menaquinone biosynthetic pathway in *S. coelicolor* A3(2).**

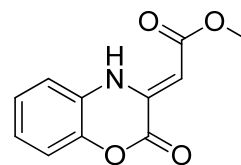


### *Inhibitors of Menaquinone Biosynthesis Pathway*

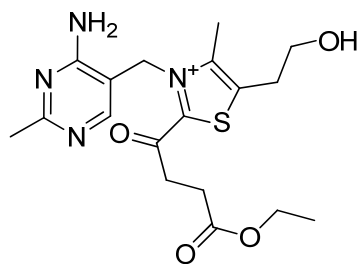
Genetic experiments demonstrated that menaquinone plays an essential role for survival of Gram-positive bacteria (65, 66, 84-87). Consequently, it is speculated that inhibitors of enzymes in menaquinone biosynthesis have the potential to be developed as novel drugs. This speculation is supported by several reports. Inhibition of MenA showed significant growth inhibition for drug-resistant *Mycobacterium* spp. (88). In addition, several 1,4-benzoxazines were identified *via* a high-throughput screen against MenB. Subsequent SAR studies were performed and resulted in the discovery of compounds with excellent antibacterial activity against *M. tuberculosis* H37Rv with MIC value as low as 0.6 µg/mL (89-91). Additionally, oxythiamine derivatives and succinylphosphonate esters were found to be MenD inhibitors (92, 93). Furthermore, a series of vinyl sulfonamides were designed based on MenE enzymatic substrate and an adenylated molecule showed an excellent MenE enzymatic inhibitory activity in both *E. coli* and *Bacillus anthracis* (94, 95) (**Figure 1.14, Table 1.3**).



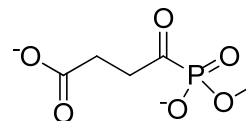
allylaminomethanone-A



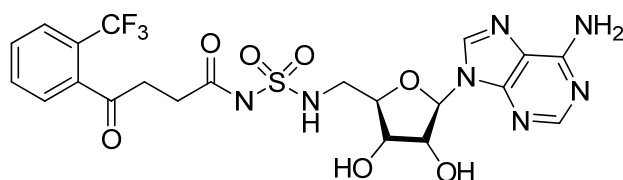
1,4-benzoxazine



oxythiamine



succinylphosphonate ester



vinyl sulfonamide

**Figure 1.14: Representative structures of menaquinone biosynthesis inhibitors.**

**Table 1.3: Inhibitors of menaquinone biosynthesis pathway**

Target	Inhibitor	Support for Target	Bacterium	inhibition ( $\mu\text{M}$ )	MIC ( $\mu\text{g/mL}$ )
<b>MenA</b>	aminomethanone	H3 <sup>a</sup>	<i>M. tuberculosis</i>	N/A	1.5
<b>MenB</b>	1,4-benzoxazines	N/A <sup>b</sup>	<i>M. tuberculosis</i>	10	0.6
<b>MenD</b>	oxythiamine	N/A	<i>S. aureus</i>	25	240
	succinylphosphonate esters	Kinetics <sup>c</sup>	<i>M. tuberculosis</i>	$K_i=0.7$	>128
<b>MenE</b>	vinyl sulfonamides	Kinetics		5	N/A

<sup>a</sup> H3: inhibition of H3 farnesyl-prenyl pyrophosphate incorporation,

<sup>b</sup> N/A; not available,

<sup>c</sup> Kinetics: determination of inhibition mode and constants

However, a recent study by Nakagawa and coworkers found that ubiA prenyltransferase containing 1 (UBIAD1) encoded a human homologue of *E. coli* prenyltransferase menA, and it can cleave the side chain of phylloquinone to release menadione and then prenylate with geranylgeranyl pyrophosphate (GGPP) to form MK-4 (96, 97). Thus, it could argue that UBIADI may convert phylloquinone in humans to MK-4, which can be utilized by Gram-positive pathogens.

In addition, although ubiquinone, phylloquinone and menaquinone in humans and menaquinone in bacteria have completely different functions, all of them have similar structures (**Figure 1.11**). Therefore, drug discovery targeting menaquinone

biosynthesis requires careful consideration of quinone distribution and selectivity against the target protein over other essential quinone-dependent proteins in humans (67).

## *Research Project Overview*

This project focuses on mechanism of enzymes in fatty acid biosynthesis and menaquinone pathways, and structure activity relationship studies on FabI (InhA) and MenB inhibitors.

The enoyl-ACP reductase catalyzes the reduction of the carbon-carbon double bond of the enoyl-ACP substrate. In Chapter 2, 3 and 4, mechanistic characterization and inhibition studies on InhA from *M. tuberculosis*, Fabs from *Burkholderia pseudomallei* and FabV from *Yersinia pestis* are performed.

Interestingly, during the study of FabI in *B. pseudomallei*, we found this organism has high amount of unsaturated fatty acids (UFAs), but lacks *fabA* and *fabB* homologues in common UFA biosynthesis pathway. In Chapter 5, we will identify and study the catalytic mechanism of potential *trans*-2, *cis*-3 enoyl-ACP isomerase (FabM), which is a key enzyme in alternative UFA biosynthesis pathway.

Dihydroxynaphthoyl-CoA synthase (MenB) catalyzes the formation of a carbon-carbon bond through a Dieckmann condensation. In Chapter 6, the study of MenB focuses on the mechanistic comparison of MenB from *M. tuberculosis* and MenB from *E. coli*. In addition, we will perform the SAR studies of MenB inhibitors, that are based on the two types of leads (2-amino-4-oxo-phenylbutanoic acids and benzoxazinones) identified from high throughput screen.

## Chapter 2 : Slow Onset Inhibition of Enoyl-ACP Reductase (InhA) from *Mycobacterium tuberculosis*

This chapter is based on part of work that has been published in:

Synthesis and *in vitro* antimycobacterial activity of B-ring modified diaryl ether InhA inhibitors. am Ende, C. W., Knudson, S. E., **Liu, N.**, Childs, J., Sullivan, T. J., Boyne, M., Xu, H., Gegina, Y., Knudson, D. L., Johnson, F., Peloquin, C. A., Slayden, R. A., Tonge, P. J.. *Bioorg. Med. Chem. Lett.*, **2008**, 18, 3029–3033

A slow, tight-binding inhibitor of InhA, the enoyl-ACP reductase from *Mycobacterium tuberculosis*. Luckner, S. R.\* , **Liu, N.\***, am Ende, C. W., Tonge, P. J., Kisker, C.. *J. Biol. Chem.*, **2010**, 285, 14330-14337

### Background

*Tuberculosis and Mycobacterium tuberculosis.*

*Mycobacterium tuberculosis* is the causative agent of tuberculosis (TB), an infectious disease that is spread all over the world. Two billion people, one-third of the world population, are infected with tuberculosis, and *M. tuberculosis* is responsible for 8.8 million new infections and 1.6 million deaths each year (98). These numbers make

TB as one of the leading infectious causes of death, eclipsed only by AIDS. The emergence of multidrug resistant *M. tuberculosis* strains, that are resistant against the current frontline drugs isoniazid and rifampicin, contribute to the spread and worsen the situation by lengthening the treatment considerably from 6 months to nearly two years and thereby increasing the cost for therapy by 20-fold. Extensively drug resistant strains, that are almost untreatable with current chemotherapeutics, threaten both developing and industrialized countries (99). Novel drugs with activity against drug resistant strains are therefore urgently needed to restrain the disease that was once thought to be under control.

#### *Isoniazid Resistance.*

One of the most effective and widely used drugs for the treatment of tuberculosis is isoniazid (INH). INH is a prodrug that has to be activated by KatG, the mycobacterial catalase-peroxidase, to form together with NAD(H) the INH-NAD adduct (**Figure 2.1**) (42). This adduct is a slow onset inhibitor of InhA, the enoyl-ACP reductase of the mycobacterial FAS-II pathway (41, 43). In this pathway, very long chain fatty acids are generated that act as precursors for mycolic acids, which in turn are essential building blocks of the unusual waxy cell wall of mycobacteria (100). Inhibition of InhA blocks mycolic acid biosynthesis, thereby impairing the integrity of the cell wall, and eventually leading to cell death (101). Since the predominant mechanism of resistance against isoniazid arises from mutations in KatG (42), new compounds that directly target InhA

and circumvent the activation step, are promising candidates for combating multidrug resistant strains of *M. tuberculosis*.

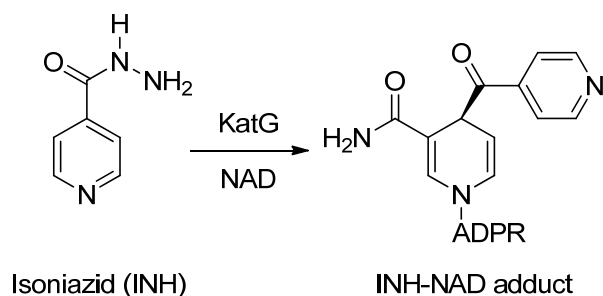


**Figure 2.1: Activation of prodrug isoniazid. Isoniazid and cofactor NAD<sup>+</sup> form INH-NAD adduct.**

#### *Diphenyl Ether Inhibition Activity against InhA Mutant from Isoniazid and Triclosan Resistant Strains.*

To look for new scaffold of good inhibitors of InhA, we get the idea from triclosan. Triclosan is a slow onset inhibitor of FabI, the enoyl-ACP reductase of FAS-II pathway from many organisms including *Escherichia coli* and *Plasmodium falciparum* (18, 22, 45, 56, 102-106). Since InhA and FabI have 46% sequence identity and share a high degree of 3D structural homology, it is thought that triclosan can interact with both enzymes in a similar fashion. It has been shown that triclosan inhibits InhA directly (107). Although it is a relatively weak inhibitor of mycobacterial InhA with  $K_i$  value of 0.2  $\mu\text{M}$  (108), it would be a good starting point to use diphenyl ethers as a scaffold to develop potent InhA inhibitors.

While developing higher binding affinity inhibitors, it is necessary to characterize diphenyl ethers activity against InhA mutants from triclosan resistant strains. In



*Mycobacterium smegmatis*, three mutants selected for resistance to triclosan have been reported (109). They have unique mutations M103T, A124V, and M161V, which are also conserved in *M. tuberculosis*. Therefore, it is necessary to test whether diphenyl ethers are active against these mutant InhAs.

#### *Diphenyl Ether Scaffold Optimization.*

Significant progress has been made to improve its affinity towards InhA: Freundlich and coworkers recently reported the development of potent triclosan derivatives that demonstrated inhibition of InhA in the nanomolar range with MIC values of 5-10 µg/mL (110). In our lab, a series of alkyl diphenyl ethers have been developed using structure based drug design that are nanomolar inhibitors of InhA with MIC values of 1-2 µg/mL against both drug sensitive and drug resistant strains of *M. tuberculosis* (50). However, despite their promising *in vitro* activity, these compounds have limited *in vivo* efficacy (111). This is probably due to these compounds' low solubility. Based on the observed relationship between lipophilicity and *in vivo* efficacy (112, 113), especially as it pertains to antibacterial compounds, it is needed to design diphenyl ether analogues that have increased polarity.

#### *Slow Onset Inhibition.*

Lots of reported compounds have nanomolar binding affinity with InhA (50, 110); however all of them are rapid reversible inhibitors. This is significant given the increasing importance attached to compounds that have long residence times on their targets (see (114) and references therein), as recently demonstrated by the correlation

between residence time and *in vivo* activity for a series of *Francisella tularensis* FabI inhibitors (26). In addition, the highly successful INH-NAD adduct was shown to be a slow onset inhibitor of InhA (43). The crystal structures of InhA (pdb code 2nv6 (115)) and the *Escherichia coli* enoyl reductase (ecFabI), (pdb code 1qg6 (47)) support the hypothesis that slow onset inhibition is coupled to ordering of an active site loop (residues 195-210 in InhA), which leads to a closure of the substrate binding pocket.

Towards the design of slow onset diphenyl ether, we speculated that there must be an entropic penalty for loop ordering. Thus, reducing the conformational flexibility of the lead diphenyl ether might enable ordering of the active site loop thus in turn resulting in slow onset enzyme inhibition.

#### *Project Goal.*

Previous structure-based design studies resulted in the discovery of nanomolar alkyl substituted diphenyl ether inhibitors of InhA. We will test whether these potent inhibitors have activity against InhA mutants found in triclosan strains. Then we will design diphenyl ether analogues which have reduced lipophilicity, increased solubility and *in vivo* efficacy. Based on the knowledge that long drug target residence times is an important factor for *in vivo* drug activity, we set out to generate a slow onset inhibitor of InhA using structure-based drug design, to understand the binding of slow onset inhibitor to InhA and the process of the slow binding inhibition.

## Materials and Methods

### *Expression and Purification of InhA.*

The plasmid of InhA, the *M. tuberculosis* enoyl-ACP reductase, was from previous lab member Dr. Xujie Zhang. InhA was expressed in *E. coli* strain BL21 (DE3) pLysS cell. After transformation, a single colony was used to inoculate 10 mL of Luria Broth (LB) media containing 0.2 mg/mL ampicillin in a 50 mL falcon tube, which was then incubated overnight at 37 °C. The overnight culture was then used to inoculate 1 L of LB media containing 0.2 mg/mL ampicillin, which was incubated at 37 °C until the optical density at 600 nm (O.D. 600) increased to around 0.8. Protein expression was induced by adding 1 mM isopropyl-1-thio- $\beta$ -D-galactopyranoside (IPTG) and the culture was then shaken at 25 °C for 16h. Cells were harvested by centrifugation at 5,000 rpm for 20 min at 4 °C. The cell paste was then resuspended in 30 mL of His binding buffer (5 mM imidazole, 0.5 M NaCl, 20 mM Tris HCl, pH 7.9) and lysed by sonication. Cell debris was removed by centrifugation at 33,000 rpm for 60 min at 4 °C. InhA was purified using His affinity chromatography: the supernatant was loaded onto a His-bind column (1.5 cm x 15 cm) containing 4 mL of His-bind resins (Novagen) that had been charged with 9 mL of charging buffer (50 mM Ni<sub>2</sub>SO<sub>4</sub>). The column was washed with 60 mL of His-binding buffer and 30 mL of wash buffer (60 mM imidazole, 0.5 M NaCl, 20 mM Tris HCl, pH 7.9). Subsequently, the protein was eluted using a gradient of 20 mL elute buffer (60 – 500 mM imidazole, 0.5 M NaCl, 20 mM Tris HCl, pH 7.9). Fractions containing InhA were collected and the imidazole removed using a Sephadex G-25 chromatography (1.5 cm x 55 cm) using Piperazine-1,4-bis(2-ethanesulfonic acid) (PIPES) buffer (30 mM PIPES, 150 mM NaCl, 1.0 mM EDTA, pH 8.0) as storing buffer.

The purity of the protein was shown to be > 95% by 12% SDS-PAGE, which gave an apparent molecular mass of ~28 kDa. The concentration of InhA was determined by measuring the absorption at 280 nm using an extinction coefficient of 30,440 M<sup>-1</sup>cm<sup>-1</sup> calculated from the primary sequence. The enzyme was concentrated by using Centricon-30 (Centricon) and stored at -80 °C after flash freezing with liquid N<sub>2</sub>.

*Site-Directed Mutagenesis, Expression and Purification of InhA Mutants.*

InhA mutant M161V plasmid was from previous lab member from Dr. Xujie Zhang. For other InhA mutants, site-directed mutagenesis was performed using the QuikChange site-directed mutagenesis method with the primers listed in **Table 2.1**. The sequence of each mutant plasmid was confirmed by DNA sequencing. The expression and purification of each InhA mutant followed the same protocol that is described above for the wild-type InhA protein.

**Table 2.1: Nucleotide primers**

<b>Name</b>	<b>Sequence</b>
InhA A124V forward	5' CTTGGCCATCGAAGCATACGAATACACCGAGATGTG 3'
InhA A124V reversed	5' GTCCAAGGGCATCCACATCTCGGTGTATTCGTATG 3'
InhA M103T forward	5' GTCGAAGAACGGGTTGATGCCCGTCCCGGTCTG 3'
InhA M103T reversed	5' GGGTTCATGCCGCAGACCGGGACGGGCATCAAC 3'
InhA A198S forward	5' CTATCCGGACGCTGTTCGATGAGTGCGATC 3'
InhA A198S reversed	5' GATCGCACTCATCGACAGCGTCCGGATAG 3'
InhA A198K forward	G592A 5' CTATCCGGACGCTGAAGATGAGTGCGATC 3' C593A 5' CTATCCGGACGCTGGAGATGAGTGCGATCG 3' G594A 5' CTATCCGGACGCTGAAAATGAGTGCGATCGTC 3'
InhA A198K reversed	G592A 5' GATCGCACTCATCTTCAGCGTCCGGATAG 3' C593A 5' CGATCGCACTCATCTCCAGCGTCCGGATAG 3' G594A 5' GACGATCGCACTCATTTTCAGCGTCCGGATAG 3'
InhA A198D forward	C593A 5' CTATCCGGACGCTGGAGATGAGTGCGATCG 3' G594T 5' CTATCCGGACGCTGGATATGAGTGCGATCGTC 3'
InhA A198D reversed	C593A 5' CGATCGCACTCATCTCCAGCGTCCGGATAG 3'

	G594T
	5' GACGATCGCACTCATATCCAGCGTCCGGATAG 3'
InhA A198V forward	5' CTATCCGGACGCTGGTGATGAGTGCGATCG 3'
InhA A198V reversed	5' CGATCGCACTCATCACCAGCGTCCGGATAG 3'
InhA M199S forward	T596G
	5' GGACGCTGGCGAGGAGTGCGATCGTC 3'
	G597T
	5' GACGATCGCACTCCTCGCCAGCGTCC 3'
InhA M199S reversed	T596G
	5' GACGCTGGCGAGTAGTGCGATCGTC 3'
	G597T
	5' GACGATCGCACTACTCGCCAGCGTC 3'
InhA V203A forward	5' GAGTGCGATCGCGGGCGGTGCGCTC 3'
InhA V203A reversed	5' GAGCGCACCGCCCGCGATCGCACTC 3'
InhA I215A forward	5' CCGGCGCCCAGGCGCAGCTGCTCGAG 3'
InhA I215A reversed	5' CTCGAGCAGCTGCGCCTGGGCGCCGG 3'

---

### *Synthesis of Trans-2-Dodecenoyl-CoA.*

*Trans*-2-dodecenoyl-CoA (DD-CoA) was synthesized from *trans*-2-dodecenoic acid by using the mixed anhydride method as described previously (27). A 25 mL of three-neck round bottom flask was vacuumed and charged with N<sub>2</sub> three times to make sure the reaction is N<sub>2</sub> environment. 8-10 mL of anhydrous THF, followed by 0.882 mL (4.08 mmol) *trans*-2-dodecenoic acid, 0.568 mL (4.08 mmol) triethylamine were added into flask with syringe, and then 0.39 mL (4.08 mmol) ethyl chloroformate was added dropwise. The solution was stirred at room temperature overnight. Next day, the mix

anhydride was separated from salt by filtration and then added dropwise to a CoA solution in 50mM Na<sub>2</sub>CO<sub>3</sub> (pH 8.0), ethanol and ethyl acetate (1:1:1) mixture while being stirred at room temperature. The reaction was monitored by detecting the free thiol concentration in solution with 5,5'-dithio-bis-(2-nitrobenzoic acid) (DTNB). When no free thiol was detected, organic solvents were removed by rotary evaporation. And DD-CoA was purified by HPLC (Shimadzu) using a C-18 semipreparative column. Chromatography was performed with 20 mM ammonium acetate/1.75% acetonitrile as buffer A and 95% acetonitrile as buffer B over 60 min at a flow rate of 4 mL/min. Elution was monitored at 260 nm and 280 nm using a SPD-10A UV-vis detector. Fractions containing DD-CoA were pooled at retention time of 14 min and lyophilized. To remove all ammonium acetate, the product was dissolved in ddH<sub>2</sub>O and lyophilized two more times. ESI-MS ([M - H]<sup>-</sup>) calcd for [C<sub>33</sub>H<sub>53</sub>N<sub>7</sub>O<sub>17</sub> P<sub>3</sub>S]<sup>-</sup>: 946.2, found: 946.2.

#### *Synthesis of Diphenyl Ethers.*

B-ring modified diphenyl ether InhA inhibitors were synthesized by Christopher W. am Ende using the procedure described previously for the synthesis of alkyl-substituted diphenyl ethers (48, 49).

#### *Steady-state Kinetic Assay.*

Kinetic assays using DD-CoA and wild-type InhA were performed as described previously (108). Reactions were initiated by addition of InhA to solutions containing substrate, inhibitor, and NADH in 30 mM PIPES and 150 mM NaCl, pH 6.8. Initial

velocities were measured by monitoring the oxidation of NADH to NAD<sup>+</sup> at 340 nm ( $\epsilon=6300 \text{ M}^{-1}\text{cm}^{-1}$ ) and kinetic parameters ( $k_{\text{cat}}$  and  $k_{\text{cat}}/K_m$ ) were determined as previously described (31).  $IC_{50}$  values were determined by varying the concentration of inhibitor in reactions containing 250  $\mu\text{M}$  NADH, 25  $\mu\text{M}$  DD-CoA and 100 nM InhA. When the assays were performed at 10 nM InhA, the enzyme was stabilized by the addition of glycerol (8%, v/v) and BSA (0.1 mg/mL). The experimental data were analyzed using **equation 2.1**, where I is the inhibitor concentration and y is percent activity.

$$y = 100\%/[1 + (I/IC_{50})] \quad \text{(Equation 2.1)}$$

Inhibition constants ( $K_i$ ) were calculated by determining the  $k_{\text{cat}}$  and  $K_m$  (DDCoA) values at several fixed inhibitor concentrations using the same assay conditions as described above. The inhibition data were analyzed using the standard equation for uncompetitive inhibition. For compounds with  $K_i$  values in the low nanomolar range, initial velocities were determined at a fixed substrate concentration and the data were fit to **equation 2.2**

$$v_i/v_0 = (K_m + S)/(K_m + S[1 + I/K_i]) \quad \text{(Equation 2.2)}$$

where  $v_i$  and  $v_0$  are the initial velocities in the presence and absence of inhibitor. The substrate concentration was fixed at 25  $\mu\text{M}$ , and the inhibitor concentration was varied. Data fitting was performed using Grafit 4.0 (Erithacus Software Ltd.).



### Progress Curve Analysis.

The slow-onset inhibition of InhA by PT70 was monitored by adding the enzyme (5 nM) to assay mixtures containing glycerol (8%), BSA (0.1 mg/mL), DMSO (2% v/v), DD-CoA (300  $\mu$ M), NADH (250  $\mu$ M), NAD<sup>+</sup> (200  $\mu$ M) and inhibitor (0-480 nM). Reactions were monitored until the progress curve became linear, indicating that the steady-state had been reached. To ensure that substrate depletion would not significantly affect the reaction rate, low enzyme concentrations and high substrate concentrations were used. Progress curves were analyzed as described previously (26, 116). This involved fitting the data to **equation 2.3**,

$$A_t = A_0 - v_s t - (v_i - v_s)(1-\gamma) \ln\left\{\frac{[1-\gamma \exp(-k_{obs} t)]}{(1-\gamma)}\right\} (k_{obs} \gamma) \quad \text{(Equation 2.3)}$$

where  $\gamma = [E](1 - v_s / v_i)^2 / [I]$ ,  $v_i$  and  $v_s$  are the initial velocity and steady-state velocity, and  $k_{obs}$  is the observed rate constant for each progress curve. Values of  $k_{obs}$ ,  $v_i$  and  $v_s$  obtained from **equation 2.3** were then fitted to **equation 2.4** and **equation 2.5**, that describe a two-step inhibition mechanism in which rapid binding of the inhibitor to the enzyme is followed by a second slow step that results in the final complex.

$$k_{obs} = k_{-2} + k_2 [I] / (K_{-1}^{app} + [I]) \quad \text{(Equation 2.4)}$$

$$v_s / v_0 = 1 / (1 + [I] / K_i^{app}) \quad \text{(Equation 2.5)}$$

In these equations,  $v_0$  is the initial velocity in the absence of inhibitor.  $K_{-1}^{app}$  and  $K_i^{app}$  are the apparent dissociation constants for the initial enzyme-inhibitor complex (E-I) and the final enzyme-inhibitor complex (E-I\*), respectively.

In addition to monitoring the onset of enzyme inhibition, progress curves were also used to analyze the recovery of enzyme activity resulting from the slow dissociation of inhibitor from EI\*. InhA (0.5  $\mu\text{M}$ ) was preincubated with PT70 (0.3-0.9  $\mu\text{M}$ ) and  $\text{NAD}^+$  (200  $\mu\text{M}$ ) at room temperature. After 5 h, 5  $\mu\text{L}$  of incubation mixture was diluted 100-fold into an assay mixture containing glycerol (8%), BSA (0.1 mg/mL), DMSO (2% v/v), DD-CoA (300  $\mu\text{M}$ ), NADH (250  $\mu\text{M}$ ) and  $\text{NAD}^+$  (200  $\mu\text{M}$ ). Substrate consumption was monitored at 340 nm, and the resulting recovery progress curves were analyzed in a similar fashion as described above (116, 117).

#### *Preincubation Inhibition Assay for Slow Binding Inhibitors.*

Preincubation inhibition assays were performed to determine the preference of PT70 for the different cofactor-bound forms of InhA. These experiments were conducted as described previously (116). InhA (10 nM) was preincubated in the presence of a fixed concentration of DMSO (2%),  $\text{NAD}^+$  (10-200  $\mu\text{M}$ ), NADH (250  $\mu\text{M}$ ) and PT70 (0-1000 nM) for 5 h at 4° C. The mixture was then warmed to room temperature, and the reaction initiated by the addition of DD-CoA (30  $\mu\text{M}$ ). **Equation 2.6** was used to estimate the apparent inhibition constant  $K_i'$ ,

$$v = v_0 / (1 + [I] / K_i') \quad \text{(Equation 2.6)}$$

where  $v$  and  $v_0$  are the initial velocity in the presence and absence of inhibitor, respectively, and  $[I]$  is the inhibitor concentration. The  $K_i'$  values obtained at different  $\text{NAD}^+$  concentrations were then fit to **equations 2.7-2.9**, which describe the binding of

the inhibitor to either E-NAD<sup>+</sup> (**equation 2.7**), E-NADH (**equation 2.8**) or both E-NAD<sup>+</sup> and E-NADH (**equation 2.9**).

$$K_i' = K_1(1 + K_{m'}\text{NAD}/[\text{NAD}^+]) \quad (\text{Equation 2.7})$$

$$K_i' = K_2(1 + [\text{NAD}^+]/K_{m'}\text{NAD}) \quad (\text{Equation 2.8})$$

$$K_i' = K_2(1 + [\text{NAD}^+]/K_{m'}\text{NAD})/[1 + [\text{NAD}^+]/(K_{m'}\text{NAD}K_1/K_2)] \quad (\text{Equation 2.9})$$

$K_1$  and  $K_2$  are inhibition constants for inhibitor binding to E-NAD<sup>+</sup> and E-NADH forms.

#### *Direct Determination of $k_{off}$ .*

Having shown that PT70 bound preferentially to the E-NAD<sup>+</sup> product complex, the rate of dissociation of PT70 from InhA was monitored using <sup>32</sup>P-NAD<sup>+</sup> in order to provide a direct estimate for  $k_{off}$ . These experiments followed a similar protocol to that described previously (43). InhA was incubated with PT70, NAD<sup>+</sup> and <sup>32</sup>P-NAD<sup>+</sup> (800 Ci/mmol) for 5 hours at room temperature to generate the ternary complex formed by InhA, NAD<sup>+</sup> and PT70. After purification using a Sephadex G-75 spin column, 500  $\mu$ L of the complex was diluted into 70 mL of buffer to initiate dissociation of the inhibitor from the enzyme. Since NAD<sup>+</sup> only has a weak affinity for the free enzyme ( $K_d > 2$  mM), dissociation of PT70 from the ternary complex also leads to the release of NAD<sup>+</sup> and <sup>32</sup>P-NAD<sup>+</sup> from the enzyme. Subsequently, 700  $\mu$ L of the diluted complex solution was withdrawn at various time intervals, loaded into a microcon (Satorious 500, 10 kDa), and centrifuged in a microcentrifuge for 1 min at 13,400 rpm. 450  $\mu$ L of the filtrate was collected and the amount of <sup>32</sup>P-NAD<sup>+</sup> quantitated using a scintillation counter. A value

for  $k_{\text{off}}$  was obtained by fitting the data to **equation 2.10**, where  $N_t$  is the radioactive counts (cpm) at time  $t$ , and  $N_0$  is radioactive counts (cpm) following complete dissociation of the complex.

$$N_t = N_0 (1 - \exp(-k_{\text{off}} t)) \quad \text{(Equation 2.10)}$$

#### *Whole Cell Antibacterial Assay.*

Compounds were submitted to Prof. Richard A. Slayden in Department of Microbiology, Immunology and Pathology, Colorado State University, Fort Collins, CO. MIC<sub>90</sub> data were acquired essentially as described previously using the microplate dilution assay (118, 119). Briefly, bacterial cells were grown to early-mid log phase in Middlebrook 7H9 liquid medium containing 10% OADC enrichment and 0.05% Tween-80. 50  $\mu\text{L}$  of bacteria were added to the test wells and compounds were added individually to a final volume of 100  $\mu\text{L}$  per well in 2 fold serial dilutions. Each drug dilution series was performed in triplicate. Plates were incubated at 37 °C for 5-7 days and each well was evaluated for growth or no growth. The MIC was the lowest drug concentration that inhibited visible bacterial growth in all replicates. If alamarBlue® was used as a growth indicator, then the MIC was the lowest drug concentration that maintained a blue color in all replicates. A blue color in the alamarBlue® Assay indicates no bacterial growth whereas a red color in the assay was indicative of cell growth (BioSource International, Inc).

*X-Ray Crystallography of InhA with 2-(o-Tolyloxy)-5-hexylphenol.*

InhA along with the slow onset inhibitor 2-(*o*-Tolyloxy)-5-hexylphenol (PT70) (**Figure 2.2**) was submitted to Dr. Sylvia R. Luckner and Prof. Caroline Kisker at the Rudolf Virchow Center for Experimental Biomedicine, Institute for Structural Biology, University of Wurzburg (Germany). The structure was solved with PT70 bound (49).

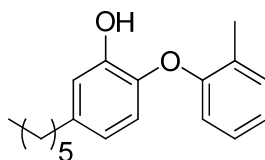


**Figure 2.2: Structure of the slow onset inhibitor 2-(*o*-Tolyloxy)-5-hexylphenol (PT70).**

## Results and Discussion

### *Characterization of the Inhibition of Triclosan-Resistant Mutants by B ring Diphenyl Ethers.*

Three *Mycobacterium smegmatis* mutants selected for resistance to triclosan (109) have different mutations in InhA. Replacement of the mutant chromosomal *inhA* genes with wild-type *inhA* eliminated resistance, suggesting that triclosan resistance is conferred by the point mutations M161V, M103T and A124V. All of these residues are located close to the inhibitor and cofactor (**Figure 2.3**). Our data indicate that these mutations reduce the affinity of the enzyme for triclosan by 5 to 220-fold (**Table 2.2**).

**Table 2.2: IC<sub>50</sub> of selected B ring diphenyl ethers for wild-type and mutant InhA**

InhA	K <sub>i</sub>	
	triclosan	6PP
<b>Wild-type<sup>a</sup></b>	220 ± 20 nM	9.4 ± 0.5 nM
<b>M161V</b>	48 ± 6 μM	1.0 ± 0.1 μM
<b>M103T</b>	3.6 ± 0.3 μM	76 ± 6 nM
<b>A124V</b>	1.2 ± 0.1 μM	29 ± 3 nM

<sup>a</sup> The data were taken from (50).

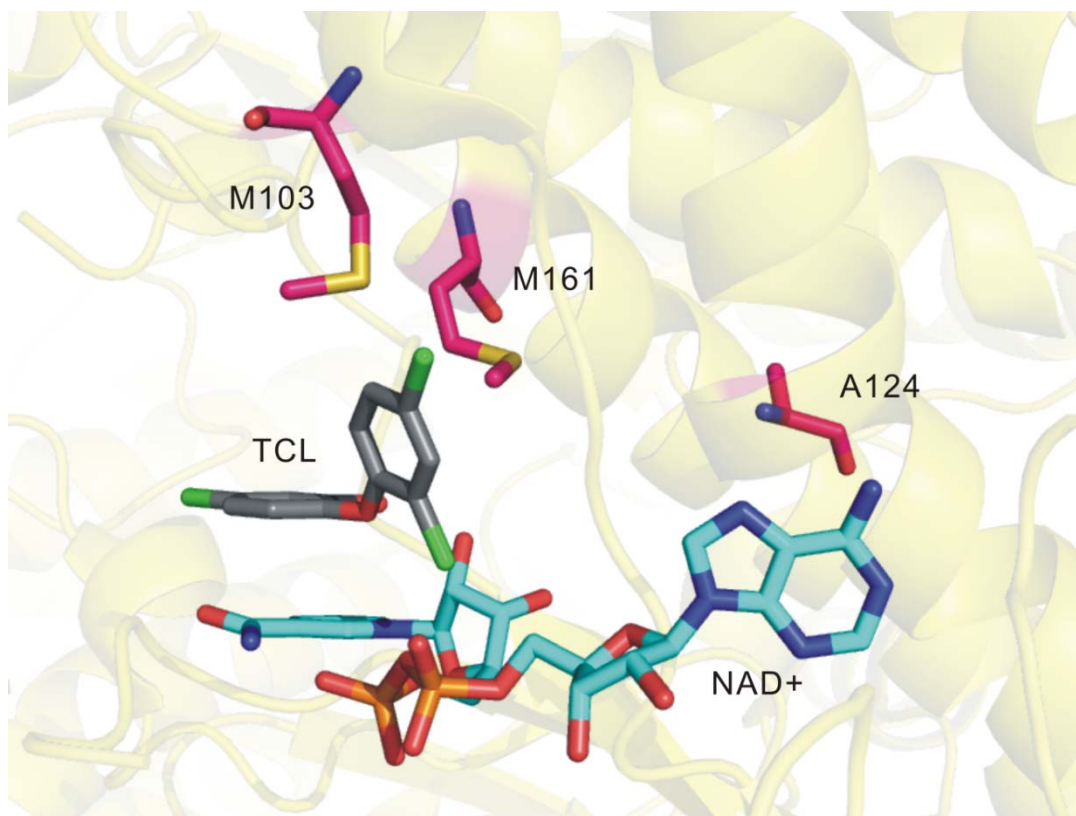


**Figure 2.3: Active site region of the InhA-NAD<sup>+</sup>-triclosan crystal structure (pdb code: 2b35).**

Because diphenyl ether scaffold is designed based on triclosan structure, it is necessary to characterize the inhibition of triclosan-resistant mutants by diphenyl ethers (50). Our data show that, for each mutant, the  $K_i$  difference of 6PP (**Figure 2.4**) between wild-type and mutant is smaller than that of triclosan. Thus, diphenyl ethers are more potent than triclosan for triclosan resistant strain.

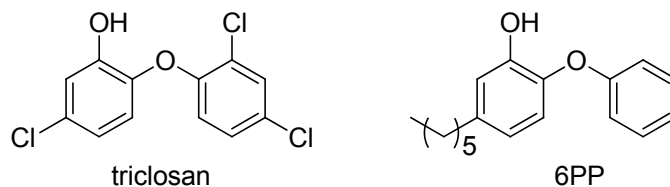


**Figure 2.4: Structure of triclosan and 6PP (5-hexyl-2-phenoxyphenol) (50).**

### *In vitro* Antimycobacterial Activity of B ring Modified Diphenyl Ethers.

Previous structure-based design studies resulted in the discovery of alkyl substituted diphenyl ether inhibitors of InhA, the enoyl reductase from *Mycobacterium tuberculosis*. Compounds such as 5-hexyl-2-phenoxyphenol (6PP) (**Figure 2.4**) are nM inhibitors of InhA and inhibit the growth of both sensitive and isoniazid-resistant strains of *M. tuberculosis* with MIC<sub>90</sub> values of 1–2 µg/mL. However, despite their promising *in vitro* activity, these compounds have ClogP values of over 5 (50).

In efforts to reduce the lipophilicity of the compounds, and potentially enhance compound bioavailability, two classes of molecules in which alternations have been made to the diphenyl ether B ring (48). In one series of compounds we have replaced the B ring with isosteric heterocycles that incorporate nitrogen atoms within the ring, thereby causing little steric perturbation to the overall structure of the molecule. The second series of compounds have nitro, amino, amide, and piperazino functionalities incorporated at the *ortho*, *meta*, or *para* positions of the B ring. This second series of compounds was designed not only to improve solubility but also to systematically identify positions on the B ring which could be substituted without diminishing biological activity.

The *in vitro* activities of the potential inhibitors were evaluated using enzyme inhibition and whole cell antibacterial assays as described previously (**Table 2.3-2.4**).

Incorporation of aromatic nitrogen heterocycles resulted in a significant reduction in both enzyme inhibition and antibacterial activity (**Table 2.3**). The most active compounds, **3**, has MIC<sub>90</sub> values of 3.13 µg/mL, similar to that of 6PP, and has ClogP value of 4.97, compared to 6.47 for the parent compound. In addition it is also worth

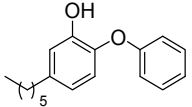
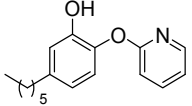
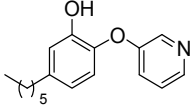
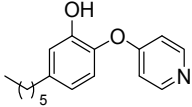
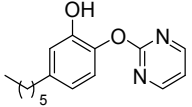
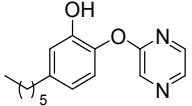
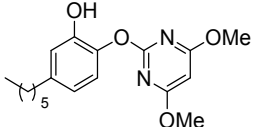
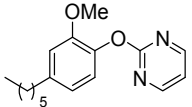


noting that the pyrazine derivative **5** has a ClogP value that is more than one log lower than 6PP, but still only shows a 3-fold increase in MIC<sub>90</sub> compared to the parent compound 6PP (**Table 2.3**).

Introduction of either amino or nitro substituents at the *ortho* and *para* positions had only a minimal effect on activity (**Table 2.4**). In contrast, addition of a bulky substituent at either the *ortho*, *meta*, or *para* position of the B ring of 6PP also resulted in a significant reduction in both enzyme inhibition and antibacterial activity (**Tables 2.4**). The most active compound, **9a**, have MIC<sub>90</sub> values of 3.13 µg/mL, similar to that of 6PP, and have ClogP values of 5.24, compared to 6.47 for the parent compound (**Table 2.4**). In general the MIC values correlated with the IC<sub>50</sub> values for enzyme inhibition. Thus *ortho* and *para* amino substituents (**9a,c**) were well tolerated in addition to the *meta* nitro substituent (**8b**). In these three cases the IC<sub>50</sub> values obtained using 100 nM InhA approached 50% of the enzyme concentration, indicating that these compounds are tight-binding enzyme inhibitors. Additional IC<sub>50</sub> values were determined using 10 and 50 nM InhA in the enzyme assays. Subsequent linear regression analyses of the IC<sub>50</sub> values as a function of enzyme concentration yielded estimates for K<sub>i</sub><sup>app</sup> of 21 ± 3 nM (**8b**), 16 ± 12 nM (**9a**), and 40 ± 3 nM (**9c**). Thus, introduction of a *meta* nitro (**8b**) or an *ortho* amino (**9a**) group into the B ring of the parent compound 6PP has only a minor effect on the affinity of the inhibitor for the enzyme. Compound **9a** is of particular interest because this derivative has an MIC<sub>90</sub> value that is close to the value determined for 6PP. These data provide important information on the structural flexibility of the inhibitor binding-site that will be useful in directing the design of additional compounds.

In conclusion, a series of hexyl diphenyl ethers were synthesized in which the B ring of compound 6PP has been substituted with a variety of groups, or replaced with nitrogen-containing aromatic heterocycles. Several of these new compounds possess  $MIC_{90}$  and  $K_i^{app}$  values similar to that of 6PP while having significantly improved ClogP values. Studies are underway to determine whether the modifications that we have introduced have resulted in an increase in compound bioavailability and an improvement in their *in vivo* antibacterial activity.

**Table 2.3: Inhibition and solubility data for B-ring heterocycles.**

	Structure	IC <sub>50</sub> <sup>a</sup> (nM)	MIC <sub>90</sub> (µg·mL <sup>-1</sup> )	ClogP <sup>b</sup>	logP
<b>6PP</b>		11 ± 1 <sup>c</sup>	2.1 ± 0.9	6.47	5.76
<b>1</b>		11,500 ± 1160	50	4.97	5.06
<b>2</b>		236 ± 31		4.97	
<b>3</b>		160 ± 16	3.13	4.97	4.93
<b>4</b>		8200 ± 980	100.0 ± 0	4.01	4.46
<b>5</b>		650 ± 60	6.25 ± 0	4.01	4.76
<b>6</b>		NI <sup>d</sup>	100	5.50	
<b>7</b>		> 100,000	75 ± 0	4.50	

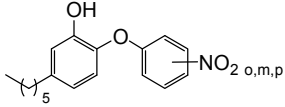
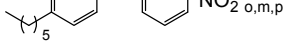
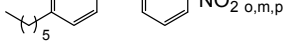
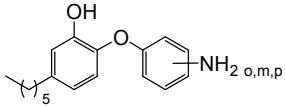
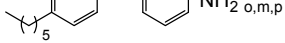
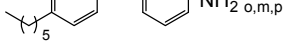
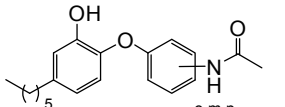
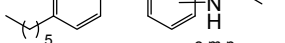
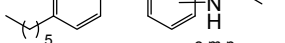
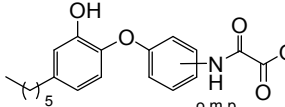
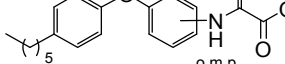
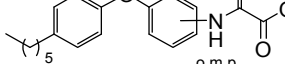
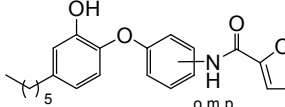
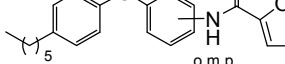
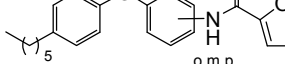
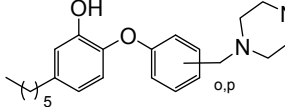
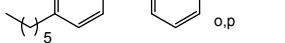
<sup>a</sup>Enzyme concentration is 100 nM.

<sup>b</sup>ClogP values determined using ChemDraw 8.0.

<sup>c</sup>Enzyme concentration is 1 nM.

<sup>d</sup>No inhibition.

**Table 2.4: Inhibition and solubility data for nitro, amino, amide and piperazine compounds.**

Structure	IC <sub>50</sub> <sup>a</sup> (nM)	MIC <sub>90</sub> (µg·mL <sup>-1</sup> )	ClogP <sup>b</sup>	logP
<b>8a</b> 	182 ± 20	12.50	6.21	5.50
<b>8b</b> 	48 ± 6 <sup>c</sup>	12.50	6.21	
<b>8c</b> 	90 ± 10	25.0 ± 0	6.21	5.64
<b>9a</b> 	62 ± 5 <sup>c</sup>	3.13	5.24	5.27
<b>9b</b> 	1090 ± 90	100 ± 0	5.24	
<b>9c</b> 	55 ± 6 <sup>c</sup>	12.50	5.24	4.93
<b>10a</b> 	1550 ± 460	>200 ± 0	4.90	5.28
<b>10b</b> 	5600 ± 770	100	4.90	
<b>10c</b> 	1300 ± 200	50.0 ± 0	4.90	
<b>11a</b> 	2360 ± 200	100.00	4.24	
<b>11b</b> 	580 ± 40	133 ± 58	4.24	
<b>11c</b> 	1930 ± 90	>200 ± 0	4.24	
<b>12a</b> 	3220 ± 550	>200 ± 0	5.76	5.60
<b>12b</b> 	1220 ± 60	>200 ± 0	5.76	5.22
<b>12c</b> 	130 ± 34	>200 ± 0	5.76	5.15
<b>13a</b> 	1315 ± 256		6.66	
<b>13b</b> 	306 ± 46	>100	6.66	

<sup>a</sup>Enzyme concentration is 100 nM.

<sup>b</sup>ClogP values determined using ChemDraw 8.0.

<sup>c</sup>Actual IC<sub>50</sub> may be lower than this value.

### *Kinetic Characterization of PT70.*

Previous work resulted in the development of a series of alkyl-diphenyl ethers that are nanomolar inhibitors of InhA, the enoyl-ACP reductase of *M. tuberculosis* (50). The best inhibitor of this series, 8PP, is active against drug sensitive and drug resistant strains of MTB. Although these inhibitors have high affinity for InhA, they are still rapid reversible inhibitors. Based on previous encouraging results, we rationally designed the slow onset alkyl-diphenyl ethers that directly targets InhA. We speculated that reducing the conformational flexibility of the lead diphenyl ether might enable to promote interactions between the inhibitor and the loop that becomes ordered during slow-onset inhibition, and ordering of the active site loop would in turn result in slow onset enzyme inhibition.

Introduction of a methyl group *ortho* to the diphenyl ether linkage resulted in a compound, PT70 (**Figure 2.2**). The inhibition of InhA by PT70 was characterized by determining the IC<sub>50</sub> values using steady state kinetic methods. The IC<sub>50</sub> values obtained using 100 nM and 10 nM InhA were  $50.3 \pm 7.0$  nM and  $5.3 \pm 0.4$  nM, respectively, indicating that PT70 is a tight binding inhibitor. Progress curve analysis was used to determine if PT70 is also a slow-onset inhibitor of InhA. Reaction conditions were adjusted so that consumption of DD-CoA occurred at a linear rate for up to 30 min. Upon addition of the inhibitor, the turnover velocity decreased exponentially with time, from an initial velocity  $v_i$  to a steady state velocity  $v_s$ . Additionally, with increasing concentrations of PT70, both  $v_i$  and  $v_s$  decreased, while  $k_{obs}$  increased and the time required to reach  $v_s$  decreased (**Figure 2.5 A**). This behaviour is a classic example of slow-onset

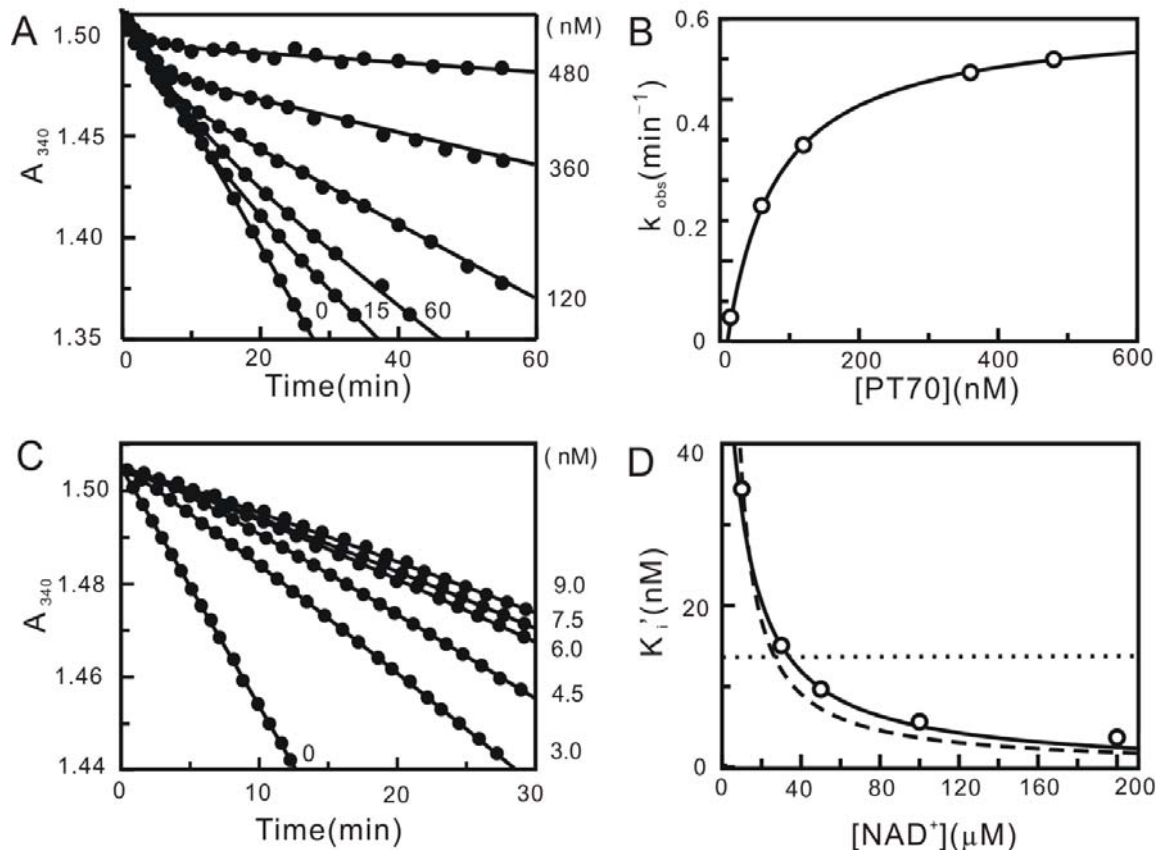


**Figure 2.5: Progress curve analysis for the inhibition of InhA by PT70 and effect of  $\text{NAD}^+$  on the apparent inhibition constant of PT70.**

(A) Progress curves were obtained for inhibitor concentrations ranging from 0 to 480 nM. The solid curves are the best fits of the data to equation 2.3. (B)  $k_{\text{obs}}$  plotted as a hyperbolic function of [PT70] using equation 2.4. (C) Progress curves of InhA activity recovery were obtained for inhibitor concentrations ranging from 0 to 9 nM. The solid curves are the best fits of the data to equation 2.3 to obtain  $k_{\text{obs}}$  which was then plotted against [PT70] using equation 2.4 to obtain  $k_2$ . (D) Effect of  $\text{NAD}^+$  on the apparent inhibition constant of PT70. Fitted curves are shown for equation 2.7 (dashed line;  $K_1 = 0.0146 \pm 0.0009$  nM), equation 2.8 (dotted line;  $K_2 = 13.6 \pm 5.5$  nM), and equation 2.9 (solid line;  $K_1 = 0.022 \pm 0.001$  nM,  $K_2 = 90.6 \pm 9.7$  nM).

inhibition in which the rapid formation of the initial E-I complex is followed by a second slow step leading to the formation of the final E-I\* complex (Figure 2.6). Fitting the data to equation 2.3 provided values for  $v_i$ ,  $v_s$  and  $k_{\text{obs}}$ . The hyperbolic dependence of  $k_{\text{obs}}$  on the concentration of PT70 was fitted to equation 2.4 allowing the calculation of the

constants for the conversion of E-I to E-I\* ( $k_2$  and  $k_{-2}$  in **Figure 2.6**) and also providing a value for  $K_{-1}^{app}$ , the dissociation constant of E-I (**Figure 2.5 B**). The dependence of  $v_s/v_0$  on the concentration of PT70 was analyzed using **equation 2.5** to give  $K_i^{app}$ , the dissociation constant of the final E-I\* complex. The thermodynamic and kinetic constants describing the inhibition of InhA by PT70 are summarized in **Table 2.5**. PT70 initially binds to InhA with a  $K_{-1}^{app}$  value of 62 nM, while the dissociation constant of the final E-I\* complex  $K_i^{app}$  is about 10 times smaller than  $K_{-1}^{app}$  (7.8 nM). Data analysis using **equations 2.3** and **2.4** also provided a value for  $k_{-2}$ , the rate constant for conversion of E-I\* to E-I. Assuming that  $k_{-1} \gg k_2$  and  $k_{-2}$ , then  $k_{-2}$  will be equal to  $k_{off}$ , the dissociation rate constant for the formation of active enzyme from E-I\*. The value of  $k_{-2}$  obtained from progress curve analysis of  $0.041 \text{ min}^{-1}$  is the same within experimental error to the values obtained when the recovery of enzyme activity was monitored (**Figure 2.5 C**,  $0.044 \text{ min}^{-1}$ ), and when  $k_{off}$  was determined directly by following the dissociation of  $^{32}\text{P-NAD}^+$  from the enzyme-inhibitor ternary complex ( $0.043 \text{ min}^{-1}$ ). Thus, the residence time of PT70 on the enzyme ( $1/k_{off}$ ) is 24 min, which is about 3-fold smaller than that of the INH-NAD adduct (**Table 2.5**). Most diphenyl ethers, preferentially bind to the E-NAD<sup>+</sup> product complex of InhA and other FabI enzymes and only occasionally prefer the E-NADH form of the enzyme (26, 45, 50, 108, 120, 121). Preincubation studies were used to examine which form of the enzyme PT70 prefers. InhA and PT70 were preincubated in the presence of saturating NADH (250  $\mu\text{M}$ ) and at different fixed concentrations of NAD<sup>+</sup> (10, 30, 50, 100, 200  $\mu\text{M}$ ). Assays were initiated by adding the substrate DD-CoA to obtain the apparent inhibition constant  $K_i'$  at each concentration of NAD<sup>+</sup>. The dependence of  $K_i'$  on the concentration of NAD<sup>+</sup> was fit to

**equations 2.7-2.9** using a  $K_{mNAD}$  value of 4 mM and a  $K_{mNADH}$  value of 48  $\mu$ M. The dependence of  $K_i'$  on the concentration of  $NAD^+$  was best described by **equation 2.9** (**Figure 2.5 D**), indicating that PT70 binds to both the E- $NAD^+$  and E- $NADH$  forms of the enzyme albeit with a strong (4000-fold) preference for the enzyme-oxidized cofactor product complex ( $K_1 = 0.022$  nM,  $K_2 = 90.6$  nM, **Table 2.5**). The value of  $K_1$  is significantly smaller than that obtained for  $K_i^{app}$  (7.8 nM), however, the latter was determined at a fixed concentration of  $NAD^+$ .

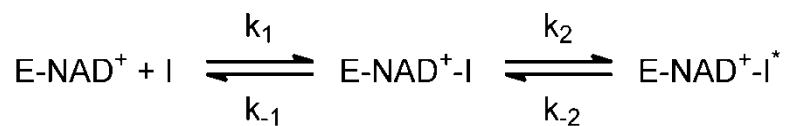


**Figure 2.6: Kinetic scheme for the slow onset inhibition of InhA by PT70.**



**Table 2.5: Inhibition of InhA by PT70 and the INH-NAD Adduct**

Inhibitor	$k_2$ ( $\text{min}^{-1}$ )	$k_{-2}$ ( $\text{min}^{-1}$ )	$t_{1/2}$ <sup>a</sup> (min)	Res time <sup>a</sup> (min)	$K_{-1}^{\text{app}}$ (nM)	$K_i^{\text{app}}$ (nM)	$k_{\text{off}}$ <sup>b</sup> ( $\text{min}^{-1}$ )	$K_1$ <sup>c</sup> (pM)
PT70	$0.46 \pm 0.003$	$0.041 \pm 0.003^e$ $0.044 \pm 0.008^f$	$17 \pm 1$	$24 \pm 2$	$62 \pm 2$	$7.8 \pm 0.4$	$0.043 \pm 0.006$	$22 \pm 1$
INH-NAD <sup>d</sup>	$0.13 \pm 0.01$	$0.016 \pm 0.007$	$43 \pm 12$	$63 \pm 27$	$100 \pm 75$	$5.0 \pm 0.5$	$0.017 \pm 0.001$	

<sup>a</sup> data taken from (43).

<sup>b</sup>  $t_{1/2} = 0.693/k_{\text{off}}$  and residence time =  $1/k_{\text{off}}$  where  $k_{\text{off}} = k_{-1}k_{-2}/(k_{-1}+k_2+k_{-2})$ . Assuming that  $k_{-1} \gg k_2$  and  $k_{-2}$ , then  $k_{\text{off}} \approx k_{-2}$ .

<sup>c</sup>  $k_{\text{off}}$  determined by monitoring the rate of release of  $^{32}\text{P-NAD}^+$  from the ternary enzyme-inhibitor complex.

<sup>d</sup>  $K_1$  determined from preincubation experiments.

<sup>e</sup>  $k_{-2}$  determined by progress curve of enzyme-inhibitor complex formation

<sup>f</sup>  $k_{-2}$  determined by progress curve of enzyme activity recovery

The inhibitor, PT70, shows improved affinity for InhA compared to the first generation compounds reported previously (50, 110). Like the parent compound 5-hexyl-2-phenoxyphenol that lacks the methyl group (6PP, **Figure 2.4**), PT70 binds preferentially to the E-NAD<sup>+</sup> product. However, the  $K_1$  value of 22 pM for PT70 is ~430-fold smaller than the  $K_i'$  value of 9.4 nM for 6PP (50), and thus introduction of the methyl group has dramatically increased the affinity of the inhibitor for the enzyme complex. More importantly, this inhibitor now also displays slow onset inhibition, which is expected to be crucial for its *in vivo* antibacterial activity. Assuming that  $k_{\text{on}}$  for 6PP is limited by the rate of encounter of enzyme and inhibitor ( $10^9 \text{ M}^{-1} \text{ s}^{-1}$ ), then the  $K_i'$  value of 9.4 nM allows  $k_{\text{off}}$  for 6PP to be estimated at  $9.4 \text{ s}^{-1}$ , giving a residence time of 0.1 s for 6PP on the enzyme. This value is in stark contrast to the residence time of 24 min for PT70, a 14,000-fold increase compared to 6PP.

Although measurements of inhibitor residence time are not normally incorporated into drug discovery programs, there is growing evidence that residence time is a critical factor for *in vivo* drug activity (26, 114, 122, 123). In particular, slow onset inhibitors will spend longer times bound to their targets compared to rapid reversible inhibitors, and will remain bound even when free drug concentrations are low. Recent studies with the FabI enzyme from *F. tularensis* highlight the importance of this concept, where it was seen that residence time was a better predictor of *in vivo* activity than the thermodynamic affinity of the inhibitor for the enzyme (26).

#### *Structure of the Ternary InhA•PT70•NAD<sup>+</sup> Complex.*

The binding of PT70 to InhA and the basis for the slow binding step was further characterized by structural studies. Two structures of the ternary InhA•NAD<sup>+</sup>•PT70 complex were solved by Dr. Sylvia R. Luckner. The first structure was solved at a resolution of 2.1 Å resolution, and belongs to space group C222<sub>1</sub> the same space group as in the ternary InhA complex with 5-octyl-2-phenoxyphenol and NAD<sup>+</sup> (8PP, PDB code 2b37(50)). The second structure was obtained at 1.8 Å resolution and belongs to space group P2<sub>1</sub>, which has not been reported for InhA so far (structural data are summarized in **Table 2.6 (Figure 2.7B)**). The slow onset inhibitor PT70 binds to the substrate binding site with the two rings of the inhibitor oriented almost 90° to each other comparable to the rings of the diphenyl ethers 5PP and 8PP described previously (50). Hydrogen bonds are formed between the inhibitor hydroxyl group and Tyr158 and a hydrogen bonding network is formed between the 2'-hydroxyl group of NAD<sup>+</sup> and

Lys165 (**Figure 2.8**, red dotted lines). A  $\pi$ - $\pi$  stacking interaction between the B-ring of PT70 and the nicotinamide ring of  $\text{NAD}^+$  further stabilizes the conformation of the inhibitor. The alkyl chain of PT70 extends into the hydrophobic environment of the substrate binding cavity and forms hydrophobic interactions with residues Phe149 and Tyr158. Most importantly, however, is the substrate binding loop (residues 195-210, helix  $\alpha 6$ ) of the structures reported here, which is ordered and forms a helix that covers the entrance to the active site (**Figure 2.7B**). Hydrophobic interactions are formed between the phenyl rings of the inhibitor and amino acids Ala198, Ile202, Met199 and Val203 of the substrate binding loop (**Figure 2.8**). Ala198 forms hydrophobic interactions with the B-ring methyl group at a distance of 3.4 Å, Ile202 with the B-ring at a distance of 3.7 Å and Met199 interacts with the A-ring at a distance of 3.8 Å. Val203 forms hydrophobic interactions with both phenyl rings at a distance of 4 Å and with the acyl chain of PT70 at 3.7 Å.

Additionally, the PT70 methyl group forms van der Waals contacts to the phosphate groups of the  $\text{NAD}^+$  cofactor, resulting in a 1 Å shift of the B-ring upward relative to its position in 8PP. In contrast, when triclosan is bound to InhA the B-ring is tilted by  $\sim 25^\circ$  towards Ile202 of the substrate binding loop and thereby interferes sterically with the loop residues, pushing the loop away from the substrate cavity instead of keeping it in place (**Figure 2.8**).

**Table 2.6: Crystallographic data and refinement statistics**

	InhA•NAD <sup>+</sup> •PT70 Crystal 1	InhA•NAD <sup>+</sup> •PT70 Crystal 2
<b>Data collection</b>		
Space group	C222 <sub>1</sub>	P2 <sub>1</sub>
Cell dimensions		
<i>a</i> , <i>b</i> , <i>c</i> (Å)	89.80, 157.51, 91.23	88.48, 90.27, 89.56
$\alpha$ , $\beta$ , $\gamma$ (°)	90.00, 90.00, 90.00	90.00, 118.76, 90.00
Resolution (Å)	36.16 - 2.10 (2.21-2.10)	78.57 - 1.81 (1.9-1.81)
<i>R</i> <sub>merge</sub>	0.080 (0.300)	0.101 (0.438)
<i>I</i> / $\sigma$ <i>I</i>	16.0 (2.5)	6.1 (1.7)
Completeness (%)	98.1 (89.7)	92.5 (77.8)
Redundancy	4.4 (2.9)	1.6 (1.4)
<b>Refinement</b>		
Resolution (Å)	2.10	1.81
No. reflections	38141	112861
<i>R</i> <sub>work</sub> / <i>R</i> <sub>free</sub> (%)	17.2 / 21.6	16.8 / 20.3
No. atoms		
Protein	4063	8033
PT70	42	84
NAD <sup>+</sup>	88	176
Water	143	682
<i>B</i> -factors		
Protein	26.2	10.4
PT70	26.9	7.3
NAD <sup>+</sup>	19.7	3.9
Water	29.9	16.0

Root mean square deviations

Bond lengths (Å)	0.013	0.015
Bond angles (°)	1.465	1.534

---

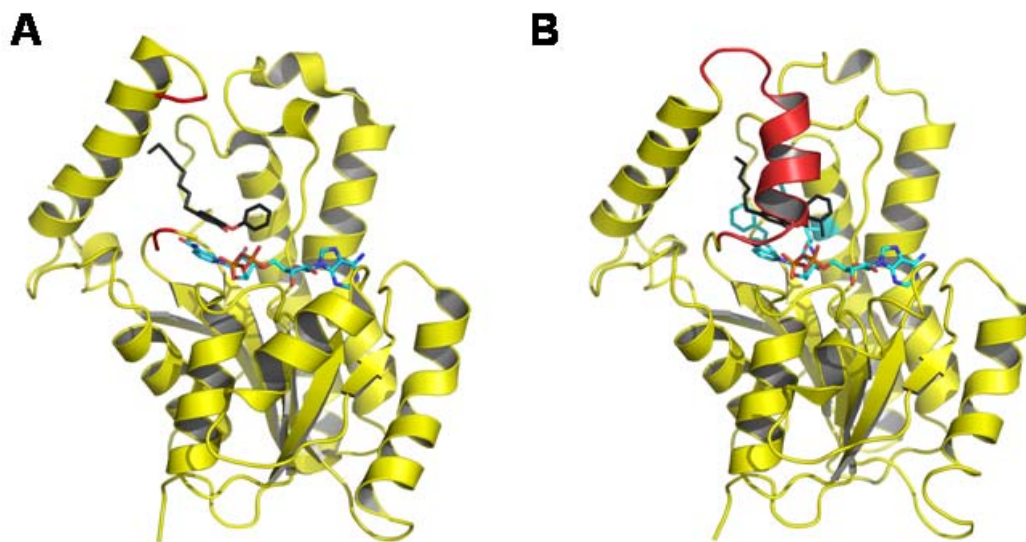


**Figure 2.7: Loop ordering upon slow binding inhibition.**

(A) One monomer of the ternary InhA•NAD<sup>+</sup>•8PP complex (pdb code 2b37) is shown in cartoon representation with the NAD<sup>+</sup> molecule in cyan and the 8PP molecule in black and all-bonds representation. The substrate-binding loop is disordered in the 8PP structure, the loop ends are depicted in red. (B) Monomer of the ternary InhA•NAD<sup>+</sup>•PT70 complex using the same colours and orientation as in A. The substrate binding loop is ordered in this structure and covers the binding pocket (red cartoon). Secondary structure elements for both molecules were assigned with STRIDE (124).

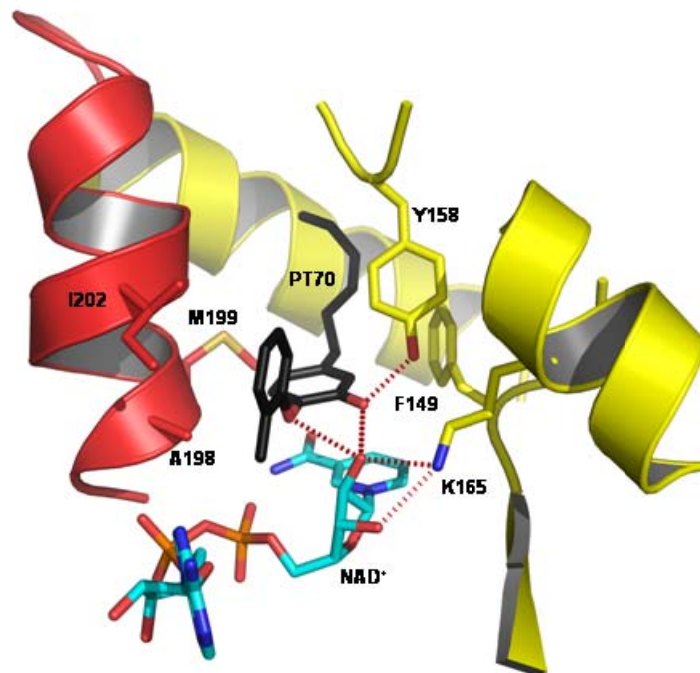


**Figure 2.8: Close-up of the binding pocket of InhA with bound NAD<sup>+</sup> and PT70.** Hydrogen bonds between PT70 (black) and Tyr158 (yellow) as well as the NAD<sup>+</sup> molecule (cyan) are indicated as red dotted lines. The important hydrophobic residues Ala198, Met199 and Ile202 of the substrate binding loop are shown in all bonds representation (red).

It is important to note that Freundlich and coworkers recently reported InhA structures inhibited by triclosan derivatives (110) that have an ordered substrate binding loop in two of the four structures (pdb codes 3fng and 3fnh). However, it was not reported, if the compounds are slow binding inhibitors. The possibility that loop ordering is due to intermolecular contacts in space group  $I4_122$ , which has not been reported so far for InhA structures, cannot be excluded. In this space group residues 197-205 of the substrate binding loop are closely packed with atoms of symmetry related molecules so that interactions due to crystallographic packing could be the reason for the ordered substrate binding loop. This contention is also supported by the fact that the co-crystal structures of InhA with the other inhibitors from this series which crystallized in space group C2 (pdb codes 3fne and 3fnf) remain disordered in the loop segment. In the case of our PT70 structures, that crystallized in space groups  $C222_1$  and  $P2_1$ , crystal contacts can be ruled out to be responsible for loop ordering, and instead the hydrophobic interactions of the residues with the inhibitor itself lead to the formation of the stable helix of the substrate binding loop. Close inspection of the solvent areas between the molecules in the crystal packing demonstrate that the closest contact between two of the loops within the tetramer and the symmetry related molecule is at least  $\sim 5$  Å and no salt bridges or hydrogen bonds exist between the molecules that directly stabilize the loop.

The substrate binding loop of the PT70 bound structure adopts a different conformation compared to other complex structures of InhA with an ordered substrate binding loop like the substrate bound form (pdb code 1bvr (24)), the triclosan derivative JPL inhibited form (pdb code 3fng (110)) and the pyrrolidine carboxamide inhibited form

(pdb code 2h7m (57)). While the loop of the PT70 bound structures is oriented closely to the substrate binding pocket due by hydrophobic interactions to the inhibitor PT70, the loops of the other structures are shifted further out of the pocket. In the fatty acid bound structure, the shift of the substrate binding loop is necessary to widen the binding pocket and accommodate substrates of different lengths. Nevertheless, the fatty acid interacts with residues Ala198, Ile202 and Met199 of the substrate binding loop and thereby the substrate is enclosed inside the pocket. However, due to missing or few interactions with the ligand or even due to steric interference, the substrate binding loops of the JPL and the pyrrolidine carboxamide inhibited structures are shifted further outside relative to the PT70 inhibited structure suggesting that the inhibitor does not get locked inside the pocket. Significantly, in the structures presented here, the side chain of Ile202 is turned towards the B-ring of PT70 and thereby facilitates the hydrophobic interactions and the shift of the substrate binding helix towards closing the active site.

#### *Basis of the PT70 Slow-onset Inhibition*

The crystal structures of the ternary InhA•NAD<sup>+</sup>•PT70 complex reveal how the inhibitor is bound to the active site. The observed hydrophobic interactions and the hydrogen bonding network of PT70 are similar to the observed interactions of previously described triclosan derivatives (50). In addition, however, PT70 generates hydrophobic interactions to amino acids Ala198, Met199 and Ile202 which are part of the substrate binding loop (residues 195-210 in InhA). This substrate binding loop is disordered in InhA structures in the presence of triclosan as well as in the structures with the



improved 5PP and 8PP triclosan derivatives which, despite their improved IC<sub>50</sub> values, remain rapid reversible inhibitors (50). In contrast, triclosan is a slow onset inhibitor of *E. coli* FabI and the corresponding crystal structure shows that the substrate binding loop is ordered (47). The substrate binding loop is also ordered in the crystal structure of InhA inhibited by the slow onset INH-NAD adduct (115). These observations prompted us to speculate that compounds with the ability to cause loop ordering will be slow, tight binding inhibitors of InhA (50). The triclosan bound *E. coli* FabI structure clearly reveals that the inhibitor forms hydrophobic interactions with the loop-amino acids Ala196 and Ala197, which correspond to Ala198 and Met199 in InhA. Additionally, Rozwarski and coworkers (24) identified in the crystal structure of InhA with a C<sub>16</sub> fatty acyl substrate that hydrophobic amino acids of the loop are important for proper substrate binding into the cavity. Interestingly, the last few carbon atoms of the fatty acid interact with the hydrophobic amino acids Ala198, Met199 and Ile202. A fatty acid shorter than 16 carbons might not be accommodated correctly by the enzyme due to missing interactions with Ala198, Met199 and Ile202.

Site-directed mutagenesis was used to replace the hydrophobic amino acids on the substrate binding loop, Ala198 and Met199, and to examine the hypothesized hydrophobic interaction with the PT70 and 6PP inhibitors. Kinetic parameters for wild-type and mutant enzymes are given in **Table 2.7**. The A198S and M199S mutations have relatively little effect on the catalytic parameter (less than 4-fold), with the exception of  $k_{\text{cat}}$  for A198S which is decreased by 17-fold. In contrast, A198K, A198D and A198V showed no activity at 3  $\mu\text{M}$  enzyme.

**Table 2.7: Kinetic parameters for wild-type and mutant InhA.**

<b>InhA</b>	<b><math>k_{\text{cat}}</math></b> ( $\text{min}^{-1}$ )	<b><math>K_{\text{m}}</math></b> ( $\mu\text{M}$ )	<b><math>k_{\text{cat}}/K_{\text{m}}</math></b> ( $\mu\text{M}^{-1}\text{min}^{-1}$ )
<b>wt</b>	$278 \pm 26$	$27 \pm 7$	$10 \pm 3$
<b>A198S</b>	$16 \pm 2$	$7.0 \pm 1.0$	$2.4 \pm 0.3$
<b>A198K</b>	No activity at 3 $\mu\text{M}$ enzyme		
<b>A198D</b>	No activity at 3 $\mu\text{M}$ enzyme		
<b>A198V</b>	No activity at 3 $\mu\text{M}$ enzyme		
<b>M199S</b>	$84 \pm 8$	$22 \pm 2$	$3.9 \pm 0.4$

**Table 2.8** lists the inhibition constants obtained for PT70 and 6PP binding to the wild-type and mutant enzymes. Normal rapid reversible inhibition by PT70 is observed for A198S and M199S. The  $K_i$  value of PT70 against A198S is 2860-fold larger than  $K_i^*$  value of PT70 against wild-type InhA. The  $K_i$  value of PT70 against M199S is 2227-fold larger than  $K_i^*$  value of PT70 against wild-type InhA. Meanwhile,  $K_i$  value for 6PP against A198S is only 18-fold larger than  $K_i$  value of 6PP against wild-type InhA.  $K_i$  value for 6PP against M199S is only 35-fold larger than  $K_i$  value of 6PP against wild-type InhA. These data indicate that that Ala198 and M199 have important hydrophobic interaction with PT70 to have slow onset and tight binding inhibition. These two mutants restrict the conversion from E-I to E-I\* form.

**Table 2.8: Inhibition type and constants for PT70 and 6PP binding to wild-type and mutant InhA enzymes**

InhA	PT70			6PP	
	Slow	$K_i$ (nM)	$K_i^*$ (nM)	Slow	$K_i$ (nM)
<b>wt</b>	Yes	$7.8 \pm 0.4$	$0.022 \pm 0.001$	No	$5.4 \pm 0.5$
<b>A198S</b>	No	$63 \pm 7$	N/A <sup>a</sup>	No	$96 \pm 8$
<b>M199S</b>	No	$49 \pm 5$	N/A	No	$190 \pm 13$

<sup>a</sup>N/A: not available

For M199S,  $K_i$  values of PT70 is 2230-fold larger than for wild-type InhA, while  $K_i$  of 6PP is only 35-fold larger than for wild-type InhA. So the hydrophobic interaction between Met199 and inhibitor is more important for PT70 than 6PP. Although Met199

does not interact directly with that methyl group, but the mutation Met199S still destroy the interaction between Met199 and A ring, so both PT70 and 6PP binding affinity decreases. And lack of this interaction made PT70 lost its slow onset binding inhibition, further reduced affinity for M199S.

These observations strongly support that the interactions with the three amino acids (Ala198, Met199, Ile202) are important determinants for loop ordering. An inhibitor, like PT70, that is able to directly interact with these residues would lead to a defined loop structure. The ordered substrate binding loop covers the entrance to the binding pocket and thereby locks the inhibitor into the cavity and increases its residence time. It is conceivable that the conformational change of the loop poses the slow step observed in the binding studies.

#### *Mechanism of InhA Slow-onset Inhibition.*

All of above study supports the hypothesis that slow onset inhibition is coupled to ordering of the substrate binding loop, however, the slow-onset mechanism of InhA is still not clarified. Based on the observation of the X-ray crystal structures, the substrate binding loop can be defined into three types: closed, open and semi-open conformation. The open conformations are InhA bound with substrate analogues C16-NAC (pdb code: 1bvr) and only with cofactor NAD<sup>+</sup> (pdb code: 2aq8) (**Figure 2.9 A**). The closed conformation is InhA bound with slow-onset inhibitor PT70 (pdb code: 2x23) (**Figure 2.9 B**). Our group member Cheng-Tsung Lai proposed that the conformational transition from open to closed might relate with the experimental

observation of slow onset process. During the conformational transition from open to closed, helix  $\alpha_6$  (residue 197 to 210, in green) moves up, whereas helix  $\alpha_7$  (residue 211 to 226, in hot pink) moves down.

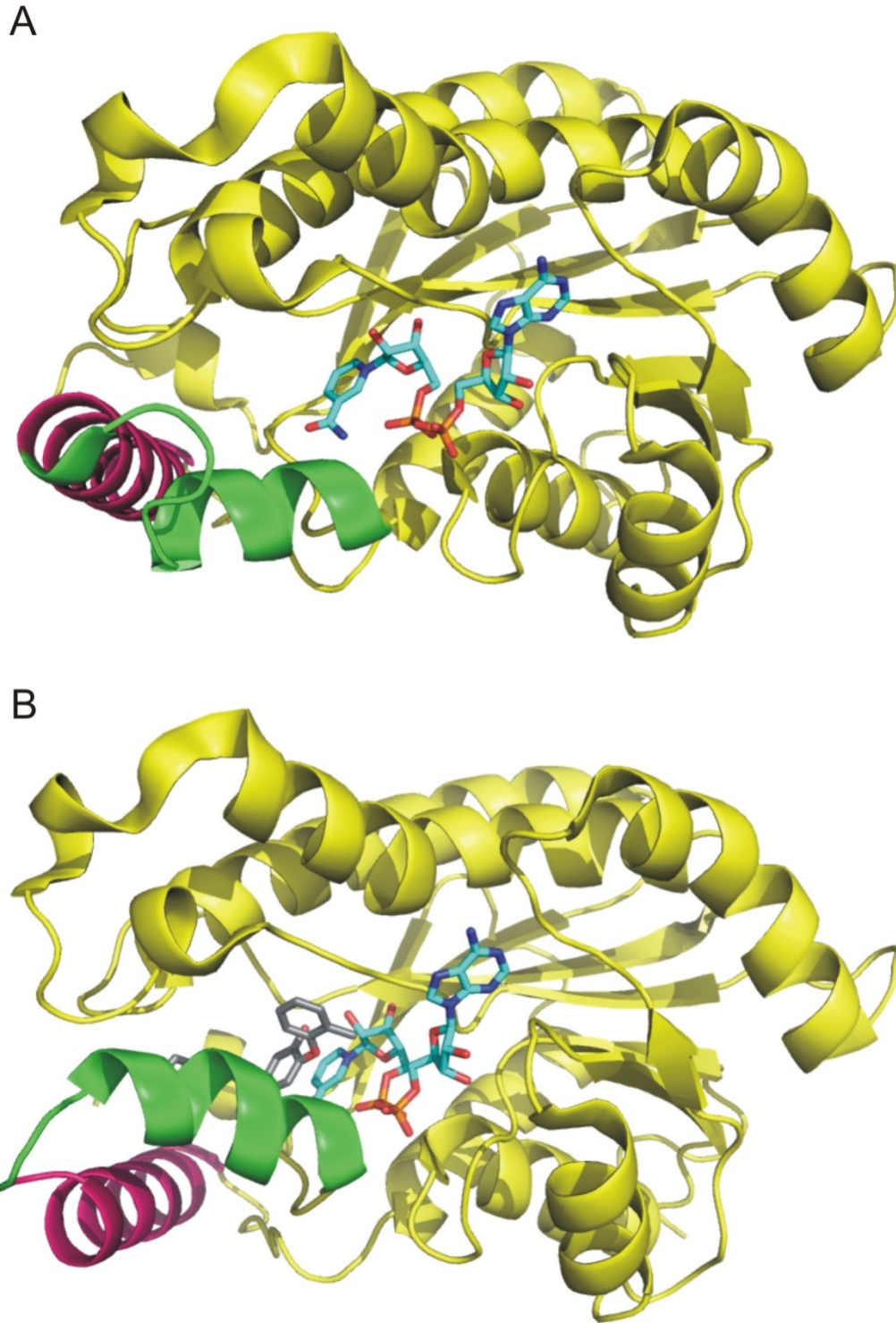


**Figure 2.9: Substrate binding loop conformation.**  
(A) open and (B) closed conformation.

Val203 and Ile215 side chains are on the interface of these two  $\alpha$ -helices, so the steric effect caused by Val203, Ile215 side chains and PT70 alky chain may result the slow conformational transition (**Figure 2.10**).

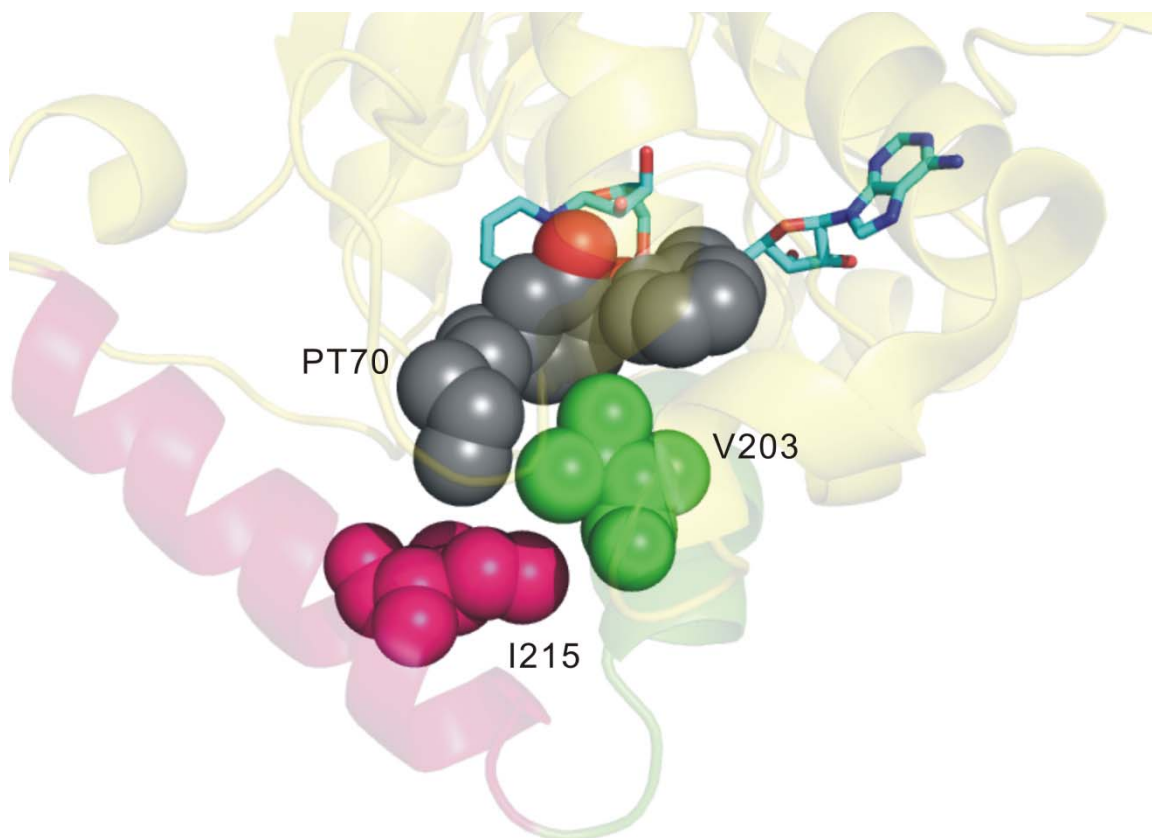


**Figure 2.10: Steric effect between PT70 and side chains of Val203 and Ile215.**

Two mutant InhA V203A and I215A were prepared. Kinetic and Inhibition parameters are given in **Table 2.9-2.10**. The V203A and I215A mutations have little effect on the catalytic parameters (less than 4-fold). In agreement with Cheng-Tsung Lai's hypothesis, because the mutations remove the steric effect during the conformational transition, the PT70 inhibition of V203A and I215A does not exhibit slow

onset inhibition. In addition, lots of important hydrophobic interactions between the inhibitor and Val203 and Ile215 lead to a reduction in the binding affinity.

**Table 2.9: Kinetic parameters for wild-type and mutant InhA.**

<b>InhA</b>	<b>k<sub>cat</sub></b> (min <sup>-1</sup> )	<b>K<sub>m</sub></b> (μM)	<b>k<sub>cat</sub>/K<sub>m</sub></b> (μM <sup>-1</sup> min <sup>-1</sup> )
<b>wt</b>	278 ± 26	27 ± 7	10 ± 3
<b>V203A</b>	78 ± 7	13 ± 3	6 ± 1
<b>I215A</b>	109 ± 5	13 ± 2	8.4 ± 1

**Table 2.10: Inhibition type and constants for PT70 and 6PP binding to wild-type and mutant InhA.**

<b>InhA</b>	<b>PT70</b>			<b>6PP</b>	
	<b>Slow</b>	<b>K<sub>i</sub></b> (nM)	<b>K<sub>i</sub><sup>*</sup></b> (nM)	<b>Slow</b>	<b>K<sub>i</sub></b> (nM)
<b>wt</b>	Yes	7.8 ± 0.4	0.022 ± 0.001	No	5.4 ± 0.5
<b>V203A</b>	No	67 ± 7	N/A <sup>a</sup>	No	160 ± 8
<b>I215A</b>	No	102 ± 12	N/A <sup>a</sup>	No	177 ± 22

<sup>a</sup>N/A: not available



## Conclusions

In conclusion, a series of hexyl diphenyl ethers were designed in which the B ring of compound 6PP has been substituted with a variety of groups, or replaced with nitrogen-containing aromatic heterocycles. Several of these new compounds possess  $MIC_{90}$  and  $K_i^{app}$  values similar to that of 6PP while having significantly improved ClogP values. These modifications may result in an increase in compound bioavailability and an improvement in compound *in vivo* antibacterial activity.

The new characteristics of PT70 facilitate the hydrophobic interactions to the important loop residues of InhA, resulting in slow tight binding inhibition. Our work supports the prediction that slow onset inhibition of enoyl-ACP reductase is indeed coupled to loop ordering. Slow binding and improved residence time are expected to result in significant improvements in *in vivo* antibacterial activity.

### **Chapter 3 : Mechanism and Inhibition of FabI Enoyl-ACP Reductases from *Burkholderia pseudomallei* (bpmFabI-1 and bpmFabI-2)**

This chapter is based on part of work that has been published in:

Mechanism and Inhibition of the FabI Enoyl-ACP Reductase from *Burkholderia pseudomallei*. Liu, N., Cummings, J. E., England, K., Slayden, R. A., Tonge, P. J.. *J. Antimicrob. Chemother.*, 2011, 66, 564-573

#### **Background**

*Melioidosis and Burkholderia pseudomallei.*

*Burkholderia pseudomallei* is classified as a category B bioterrorism pathogen by the US National Institute of Allergy and Infectious Diseases (125, 126). This organism causes the disease melioidosis, which is primarily found in South-East Asia and Northern Australia. Although only a few cases of the disease are reported each year, it is thought that the lack of research and medical facilities in the areas of incidence may have resulted in an underestimate of the numbers of individuals that are affected (127).

Unfortunately, there is no vaccine to prevent melioidosis. Affected patients need two treatment phases: For the first phase, intravenous therapy is carried with ceftazidime or imipenem (or meropenem) as first-line agents, or a beta-lactam/beta-lactamase inhibitor combination as second-line (amoxicillin-clavulanate) agent for six

weeks, or at least fourteen days. For the second eradication phase, patients should take a combination of trimethoprim-sulfamethoxazole and doxycycline with or without chloramphenicol as oral drug for three to six months. Mortality is still very high, even with treatment using the first-line agents, while relapse is often observed (128). So the therapy result is unsatisfactory.

The main reason for inefficient treatment is *B. pseudomallei* is natural resistance to a wide range of classical antimicrobial agents, including third-generation cephalsporins, penicillins, rifamycins, and aminoglycosides. There are several possible resistance mechanisms. First, *B. pseudomallei* contains up to six types of independent secretion systems, such as multidrug resistant efflux pump of the resistance-nodulation-division (RND) family, which is very widespread among *Burkholderia* species. Second, its cell wall lipopolysaccharide (LPS) acts as immunodominant antigen. Third, it can produce hydrated glyocalyx polysaccharide capsule, which will help form slime. This capsule plays an important role in forming microcolonies, so can help resist antibiotic penetration. Of course, these three mechanisms are only parts of the possible resistance mechanism (129-131).

### *Multidrug Resistant Efflux Pump*

Efflux pumps are transport proteins involved in the transportation of toxic substrates (including virtually all classes of clinically relevant antibiotics) from within cells into the external environment (132). These proteins are found in both Gram-positive and Gram-negative bacteria as well as in eukaryotic organisms (133). Efflux pumps have been discovered in nearly all clinically relevant Gram-negative bacteria, and found to be responsible for much of the intrinsic multidrug resistance in Gram-negative bacteria. Broadly specific efflux systems can accommodate a variety of unrelated antimicrobial agents, including antibiotics, biocides, dyes, detergents, and organic solvents (134). In *B. pseudomallei*, AmrAB-OprA and BpeAB-OprB, efflux systems of the resistance-nodulationdivision (RND) family, have been reported to be responsible for the efflux of aminoglycosides and macrolides (135, 136). Other members of the RND family which are responsible for the efflux of antimicrobials in Gram-negative bacteria include AcrAB-TolC of *Escherichia coli* (137); AcrAB homologue of *Salmonella enteric* serovar Typhimurium; MexAB-OprM, MexCD-OprJ, MexEF-OprN, and MexXY-OprM of *Pseudomonas aeruginosa* (138); and CeoAB-OpcM of *Burkholderia cepacia* (134).

### *Targeting on Enoyl ACP Reductase*

Fatty acid biosynthesis (FAS) is used to synthesize the metabolic precursors for membrane phospholipids in the cell wall. In eukaryotes, fatty acid biosynthesis is catalysed by a type I fatty acid synthase (FAS-I), in which the different enzyme activities

are encoded by domains of a large polypeptide. In contrast, fatty acids are synthesized in prokaryotes by a type II pathway (FAS-II) in which each reaction is catalysed by individually encoded enzymes (29). Due to the essential role that fatty acids play in bacterial cell survival and the low degree of sequence homology with the mammalian FAS-I synthase, the FAS-II pathway is thought to be an attractive antibacterial drug target (18, 120). In particular, the FAS-II enoyl-acyl carrier protein (ACP) reductase, which catalyses the final step in the elongation cycle, is thought to be a key regulator of fatty acid biosynthesis and to be essential for the viability of bacteria (36). Although a recent report concluded that the FAS-II pathway in *Streptococcus agalactiae* and, by extension, other Gram-positive bacteria is not essential for growth in the presence of fatty acids (139), the generality of this conclusion, at least with regard to the important nosocomial pathogen *Staphylococcus aureus*, has since been questioned (140). Importantly, there is no evidence that Gram-negative bacteria, such as *B. pseudomallei*, can sequester fatty acids from their environment to counter the impact of FAS-II inhibition, and an overall goal of our program is to validate the FAS-II pathway in *B. pseudomallei* and other pathogenic bacteria as a novel target for drug discovery.

The majority of the FAS-II enzymes are essential for bacterial viability (141). Among the enzyme in FAS-II pathway, the enoyl-ACP reductase, which catalyzes the last reaction in each elongation cycle, has been mostly studied based on the discovery that antibacterial compounds such as triclosan and isoniazid target this enzyme (102, 107, 142). The FabI enoyl-ACP reductase from *E. coli* was first identified (143), and it was initially considered to be the only reductase in bacteria. Subsequently, drug resistance in other pathogens led to the discovery of FabI isoforms: FabK in

*Streptococcus pneumoniae*, a flavin-dependent enoyl-ACP reductase which is insensitive to lead FabI inhibitor triclosan (34); FabL found in *Bacillus subtilis* (30); and FabV recently found in *Vibrio cholera* (32), *Pseudomonas aeruginosa* (33) and *Burkholderia mallei* (31).

It is important to note that more than one enoyl-ACP reductase can be found in certain bacteria. For example, in *Bacillus subtilis*, FabL coexists with FabI (30); in *P. aeruginosa* FabV coexists with FabI (33); in *B. pseudomallei* FabV coexists with FabI (31). However the biological *in vivo* function for each of the different enoyl-ACP reductase, and why some bacteria need more than one enoyl-ACP reductase is still unknown. However, it is possible that all of the present enoyl-ACP reductases have to be inhibited in order to fully compromise fatty acid biosynthesis.

### *Project Goals*

As an initial step in developing novel antibacterials against *B. pseudomallei*, we will study the mechanism of two FabI enoyl-ACP reductase homologues in the type II fatty acid biosynthesis pathway from this organism. Due to the interest in developing chemotherapeutics against *B. pseudomallei*, we will study the inhibition of bpmFabI-1 by triclosan and three other lead diphenyl ethers, and also evaluate the antibacterial activity of these compounds against *B. pseudomallei* and *B. thailandensis*.

## Materials and Methods

### *Cloning, Expression and Purification of bmaFabI-1 and bmaFabI-2.*

Since bpmFabI-1 (BURPS1710b\_2636, chromosome 1: 2917100..2917891) and bpmFabI-2 (BURPS1710b\_A2297, chromosome 2: 2788921..2789682) from *B. pseudomallei* are 100% identical to *bmfabI-1* (BMA1608, chromosome 1: 1671734..1672525) and *bmfabI-2* (BMAA1403, chromosome 2: 1510367..1511128) from *Burkholderia mallei*, genomic DNA from *B. mallei* ATCC 23344 (NCBI Reference Sequence: YP\_102617.1) was used for cloning. Amplification was performed using puReTaq Ready-To-Go PCR Beads (Amersham Biosciences) and following primers (Integrated DNA Technologies):

bmFabI-1 5'-GGAATTCCATATGGGCTTTCTCGACGGTAAAC-3' (forward) and 5'-CCCAAGCTTTTCCTCGAGGCCGGCCATC-3' (reverse),

bmFabI-2 5'-GGAATTCCATATGCGACTTCAGCACAAGC-3' (forward) and 5'-CCCAAGCTTGCCGACGACGTGATAG-3' (reverse). Both PCR products were digested with NdeI and HindIII, and then inserted into the pET23b plasmid (Novagen) so that a His-tag was encoded at the C-terminus of the coding sequence for each protein. In addition, in order to provide a bpmFabI-2 construct with a cleavable N-terminal His-tag, *bmfabI-2* was amplified using the primers 5'-GGAATTCCATATGCGACTTCAGCACAAGC-3' (forward) and 5'-CGCGGATCCTCAGCCGACGACGTGATAG-3' (reverse), digested with NdeI and BamHI, and then inserted into the pET15b plasmid. The correct sequences of the constructed plasmids were confirmed by DNA sequencing (DNA Sequencing Facility, Health Science Center, Stony Brook University).

Protein expression was performed using the *E. coli* strain BL21 (DE3) pLysS cells. After transformation, a single colony was used to inoculate 10 mL of Luria Broth (LB) media containing 0.2 mg/mL ampicillin in a 50 mL falcon tube, which was then incubated overnight at 37 °C. The overnight culture was then used to inoculate 1 L of LB media containing 0.2 mg/mL ampicillin, which was incubated at 37 °C until the optical density at 600 nm (O.D. 600) increased to around 1.0. Protein expression was induced by adding 1 mM isopropyl-1-thio- $\beta$ -D-galactopyranoside (IPTG) and the culture was then shaken at 25 °C for 16h. Cells were harvested by centrifugation at 5,000 rpm for 20 min at 4 °C. The cell paste was then resuspended in 30 mL of His binding buffer (5 mM imidazole, 0.5 M NaCl, 20 mM Tris HCl, pH 7.9) and lysed by sonication. Cell debris was removed by centrifugation at 33,000 rpm for 60 min at 4 °C. FabI was purified using His affinity chromatography. The supernatant was loaded onto a His-bind column (1.5 cm x 15 cm) containing 4 mL of His-bind resins (Novagen) that had been charged with 9 ml of charge buffer (Ni<sup>2+</sup>). The column was washed with 60 mL of His-binding buffer and 30 mL of wash buffer (60 mM imidazole, 0.5 M NaCl, 20 mM Tris HCl, pH 7.9). Subsequently, the protein was eluted using a gradient of 20 mL elute buffer (500 mM imidazole, 0.5 M NaCl, 20 mM Tris HCl, pH 7.9). Fractions containing bpmFabI-1 or bpmFabI-2 were collected and the imidazole removed using a Sephadex G-25 chromatography (1.5 cm x 55 cm) using PIPES buffer (30 mM PIPES, 150 mM NaCl, 1.0 mM EDTA, pH 8.0) as eluent. The purity of the protein was shown to be > 95% by 12% SDS-PAGE, which both gave an apparent molecular mass of ~28 kDa. The concentration of bpmFabI-1 and bpmFabI-2 was determined by measuring the absorption at 280 nm using an extinction coefficient of 13,490 and 16,170 M<sup>-1</sup>cm<sup>-1</sup>.



calculated from the primary sequence. The enzyme was concentrated by using Centricon-10 (Centricon) and stored at -80 °C after flash freezing with liquid N<sub>2</sub>.

#### *Circular Dichroism (CD) Spectroscopy.*

Circular dichroism (CD) spectra of bpmFabI-1 and bpmFabI-2 (15 μM) were recorded at RT on an Aviv model 202SF CD spectrometer (Lakewood, NJ), using a 1-mm path length, 1-nm bandwidth, 1-nm resolution, 0.5-s response time, and a scan speed of 50 nm/min. The secondary structure content of each protein was subsequently estimated using CDNN Deconvolution software (version 2; Bioinformatik.biochemtech.uni-halle.de/cdnn).

#### *Fluorescence Titration Experiments.*

Equilibrium fluorescence titrations were conducted using a Quanta MasterTM-4/2005 spectrometer (Photon Technologies International). Binding experiments were performed at 25 °C using the same buffer as that used for kinetic studies. Microliter aliquots of NADH stock solution (1 mM) were titrated into a 1 mL solution of bpmFabI-1 or bpmFabI-2 (1 μM), and the fluorescence was monitored using 350 nm excitation and 455 nm emission with excitation and emission slit widths of 5.0 and 1.0 nm, respectively. A control experiment was also conducted in which there was no enzyme in the cuvette. The dilution of the protein concentration was kept to a minimum (< 1%). Data were fitted into the following quadratic equation (**equation 3.1**) using Grafit 4.01 (Erithacus Software Ltd.) to get  $K_d$ :

$$\frac{F - F_0}{F(\max) - F_0(\max)} = \frac{(K_d + [E]_0 + [NADH]) - \sqrt{(K_d + [E]_0 + [NADH])^2 - 4K_d[E]_0}}{2[E]_0}$$

**(Equation 3.1)**

Where  $F$  and  $F_0$  are the fluorescence intensity in the presence and absence of bpmFabI,  $F(\max)$  and  $F_0(\max)$  are the maximum fluorescence intensity in the presence and absence of bpmFabI, respectively,  $K_d$  is the dissociation constant,  $[E]_0$  is the enzyme concentration in cuvette,  $[NADH]$  is the concentration of added NADH.

#### *Expression and Purification of ftuACP.*

The open reading frame (NCBI Reference Sequence YP\_170325) which encodes the putative acyl carrier protein (ACP) in *Francisella tularensis* SCHUS4 was amplified by Dr. Hao Lu. The protein product of this ORF is 68% identical and 79% similar to the ACP from *B. mallei* ATCC 23344. Expression and purification of ftuACP followed a similar protocol as for bpmFabI, except the G-25 chromatography buffer is 0.1 M potassium phosphate buffer, pH 8.0. The purified ftuACP was analyzed by 15% SDS-PAGE and MALDI-TOF mass spectrometry. The concentration of the protein was determined by measuring the absorption at 280 nm and by using an extinction coefficient of  $2,560 \text{ M}^{-1}\text{cm}^{-1}$  calculated from the primary sequence. Then protein was stored at 4 °C.

### *Preparation of Crotonyl-ACP (Cro-ACP).*

Purified ftuACP was concentrated to 900  $\mu$ M in 3 mL reaction buffer (0.1 M potassium phosphate buffer, pH 8.0). An equimolar amount of dithiothreitol was added to the above solution. The reaction mixture was then stirred under nitrogen at 0 °C for 2h to ensure complete reduction of the ACP thiol group. Then 1.5-fold molar excess of crotonic anhydride was added to the reaction mixture. After stirring for 15 min at 0 °C, small molecules were removed from the Cro-ACP by chromatography on a Sephadex G-25 column (1.5 cm x 15 cm) using PIPES buffer (30 mM PIPES, 150 mM NaCl and 1 mM EDTA, pH 8.0) as the eluent.

### *Preparation of CoA Substrate Analogues.*

*trans*-2-Dodecenoyl-CoA (DD-CoA) (**Figure 3.1**) was synthesized from *trans*-2-dodecenoic acid using the mixed anhydride method as described previously (27). Briefly, 0.882 mL (4.08 mmol) of acid was dissolved in 10 mL of anhydrous diethyl ether with 0.568 mL (4.08 mmol) of triethylamine. Following the addition of 0.39mL (4.08 mmol) of ethyl chloroformate, salt crystals formed and the solution was stirred at RT overnight. The mixed anhydride was then filtered and added dropwise to a solution of CoA in 50 mM Na<sub>2</sub>CO<sub>3</sub> (pH 8), ethanol, and ethyl acetate (1:1:1) while being stirred at RT. The reaction progress was monitored by following the concentration of free thiol in solution using 5,5'-dithio-bis-(2-nitrobenzoic acid) (DTNB). When no free thiol was detected, organic solvents were removed by rotary evaporation, and DD-CoA was purified by HPLC (Shimadzu) using a C-18 semipreparative column. Chromatography was performed with 20 mM ammonium acetate/1.75% acetonitrile as buffer A and 95%

acetonitrile as buffer B over 60 min at a flow rate of 4 mL/min. Elution was monitored at 260 nm and 280 nm using a SPD-10A UV-vis detector. Fractions containing DD-CoA were pooled at retention time of 14 min and lyophilized. To remove all ammonium acetate, the product was dissolved in ddH<sub>2</sub>O and lyophilized two more times. ESI-MS ([M - H]<sup>-</sup>) calcd for [C<sub>33</sub>H<sub>53</sub>N<sub>7</sub>O<sub>17</sub> P<sub>3</sub>S]<sup>-</sup>: 946.2, found: 946.2.

*trans*-2-Octenoyl-CoA (Oct-CoA) and *trans*-2-decenoyl-CoA (Dec-CoA) (**Figure 3.1**) were synthesized and purified using the same method as described above. The only difference is that they were synthesized from their corresponding acids, *trans*-2-octenoic acid and *trans*-2-decenoic acid, respectively. The retention time for both of them is around 14 min. ESI-MS ([M - H]<sup>-</sup>) calcd for Oct-CoA [C<sub>29</sub>H<sub>48</sub>N<sub>7</sub>O<sub>17</sub>P<sub>3</sub>S]<sup>-</sup>: 891.2, found: 890.2. ESI-MS ([M - H]<sup>-</sup>) calcd for Dec-CoA [C<sub>31</sub>H<sub>52</sub>N<sub>7</sub>O<sub>17</sub> P<sub>3</sub>S]<sup>-</sup>:919.2, found: 918.2.

Crotonyl-CoA (Cro-CoA) (**Figure 3.1**) was prepared by coupling crotonic anhydride with CoA as described previously (144). Crotonic anhydride can be obtained commercially. Crotonic anhydride was added dropwise to a CoA solution in 50 mM Na<sub>2</sub>CO<sub>3</sub> (pH 8.0), ethanol and ethyl acetate (1:1:1). The mixture was stirred at RT. Also the reaction was monitored by detecting free thiol concentration in solution with DTNB. When no free thio was detected, organic solvents were removed by rotary evaporation. As above, crotonoyl-CoA was purified by HPLC (Shimadzu) using a C-18 semipreparative column. Chromatography was performed with 20 mM ammonium acetate/1.75% acetonitrile as buffer A and 95% acetonitrile as buffer B over 60 min at a flow rate of 4 ml/min. Elution was monitored at 260 nm and 280 nm using a SPD-10A

UV-vis detector. Fractions containing Cro-CoA were collected at 14 min. ESI MS calcd for  $[C_{25}H_{40}N_7O_{17}P_3S]^-$  835.1. Found: 834.0

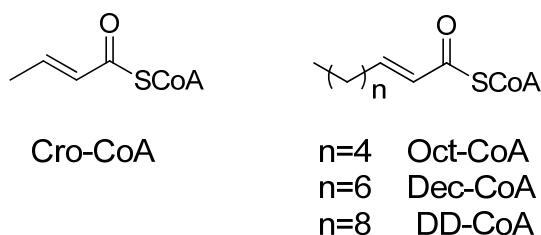


**Figure 3.1: Structure of Cro-CoA, Oct-CoA, Dec-CoA and DD-CoA.**

#### *Steady-state Kinetic Assays.*

All kinetic experiments were performed on a Cary 300 Bio (Varian) spectrometer at 25 °C in 30 mM PIPES buffer pH 6.8 containing 150 mM NaCl and 1.0 mM EDTA. Initial velocities were measured by monitoring the oxidation of NADH to NAD<sup>+</sup> at 340 nm ( $\epsilon = 6,300 \text{ M}^{-1} \text{ cm}^{-1}$ ), and kinetic parameters ( $k_{cat}$  and  $k_{cat}/K_m$ ) were determined as previously described (31).

Initial characterization of the enzyme mechanism was performed in reaction mixtures containing 30 nM bpmFabI-1 and by measuring initial velocities at several fixed concentrations of NADH (50, 120, 190 and 250  $\mu\text{M}$ ) and by varying the concentration of Oct-CoA (16-128  $\mu\text{M}$ ), or at a fixed concentration of Oct-CoA (16, 32, 64 and 128  $\mu\text{M}$ ) and by varying the concentrations of NADH (50-250  $\mu\text{M}$ ). Double reciprocal plots were then used to differentiate between ping-pong or ternary-complex mechanisms. To further investigate the binding order of the two substrates, product inhibition studies

were performed in which the concentration of each substrate (NADH and Oct-CoA) was varied in the presence of the NAD<sup>+</sup> product (0, 200 and 2000 μM). Lineweaver-Burk plots were subsequently used to determine whether enzyme inhibition was competitive, uncompetitive or noncompetitive.

### *Progress Curve Analysis.*

Progress curve analysis was performed to identify slow onset inhibitors of bpmFabI-1. Reactions were performed by adding enzyme (5 nM) to assay mixtures containing glycerol (8%, v/v), BSA (0.1 mg/ml), DMSO (2%, v/v), Oct-CoA (300 μM), NADH (250 μM), NAD<sup>+</sup> (200 μM) and inhibitor (0-1000 nM). Reactions were monitored until the progress curve became linear, indicating that the steady-state had been reached. In this protocol, the low enzyme concentration and high substrate concentration ensure that substrate depletion was minimized so that the progress curves in the absence of inhibitors were approximately linear over a period of 30 min (47, 145). Because triclosan and the diphenyl ether inhibitors bind to other Fabs in presence of NAD<sup>+</sup>, 200 μM NAD<sup>+</sup> was added so that the NAD<sup>+</sup> concentration was constant during progress curve data collection. Subsequently the data were fit to the integrated rate equation (**equation 3.2**):

$$A_t = A_0 - v_s t - (v_i - v_s) * (1 - \gamma) * \ln \left\{ \frac{[1 - \gamma * \exp(-k_{obs} * t)]}{1 - \gamma} \right\} T / (k_{obs} * \gamma)$$

**(Equation 3.2)**

where  $A_t$  and  $A_0$  are the absorbances at time  $t$  and time 0,  $v_i$  and  $v_s$  are the initial velocity and steady-state velocity from the progress curve, respectively,  $t$  is time,  $\gamma = [E]^*(1 - v_s/v_i)^2/[I]$ , and  $k_{obs}$  is the observed rate constant for each curve. The  $k_{obs}$  values were then analyzed using **equation 3.3**, that describes a two-step inhibition mechanism in which the initial rapid binding of inhibitor to enzyme is followed by a second slow step that leads to formation of the final enzyme-inhibitor complex (E-I\*) (**Figure 3.2A**).

$$k_{obs} = k_{-2} + k_2[I]/(K_{-1}^{app} + [I]) \quad \text{(Equation 3.3)}$$

In **equation 3.3**,  $k_2$  and  $k_{-2}$  are the association and dissociation rates for the second step, respectively, and  $K_{-1}^{app}$  is the apparent dissociation constant for the initial enzyme-inhibitor complex (E-I).

#### *Inhibition of bpmFabI-1 by Triclosan and Select Diphenyl Ether Inhibitors.*

Preincubation assays were performed to obtain the true inhibition constants and to determine the preference of slow onset inhibitors for the different cofactor-bound forms of bpmFabI-1. Enzyme (5 nM) was preincubated in the presence of a fixed concentration of DMSO (2% v/v),  $\text{NAD}^+$  (10-200  $\mu\text{M}$ ), NADH (250  $\mu\text{M}$ ) and inhibitors (0-1000 nM) for 5h at 4 °C. After warming to RT, assays were initiated by the addition of Oct-CoA (30  $\mu\text{M}$ ). **Equation 3.4** was used to estimate the apparent inhibition constant  $K_i'$

$$v = v_0 / (1 + [I] / K_i') \quad \text{(Equation 3.4)}$$

where  $v_0$  is the rate in the absence of inhibitor and  $[I]$  is the inhibitor concentration.

The experiment was repeated at varying concentrations of  $\text{NAD}^+$  (10-200  $\mu\text{M}$ ) and the mechanism of inhibition with respect to  $\text{NAD}^+$  was determined by fitting the data to following **equation 3.5-3.7**.  $K_1$  and  $K_2$  are defined in **Figure 3.2** and represent the equilibrium constants for inhibitor binding to E- $\text{NAD}^+$  and E-NADH, respectively.

Inhibitor binds exclusively to the E- $\text{NAD}^+$  form

$$K_i' = K_1([NAD^+] + K_{m,NAD})/[NAD^+] \quad \text{(Equation 3.5)}$$

Inhibitor binds exclusively to the E-NADH form

$$K_i' = K_2([NAD^+] + K_{m,NAD})/K_{m,NAD} \quad \text{(Equation 3.6)}$$

Inhibitor binds to both the E- $\text{NAD}^+$  form and E-NADH forms

$$K_i' = K_2 \left\{ \frac{(1 + \frac{[NAD^+]}{K_{m,NAD}})}{1 + \frac{[NAD^+]}{(K_{m,NAD}K_1/K_2)}} \right\} \quad \text{(Equation 3.7)}$$

Where the  $K_{m,NAD}$  value for  $\text{NAD}^+$  was calculated from **equation 3.8**:

$$K_{m,NAD} = K_{i,NAD}(1 + [NADH]/K_{m,NADH}) \quad \text{(Equation 3.8)}$$

and  $K_{i,NAD}$  is the dissociation constant of  $\text{NAD}^+$ . Equation X presumes that  $\text{NAD}^+$  is a competitive inhibitor with respect to NADH as was shown by the product inhibition studies.



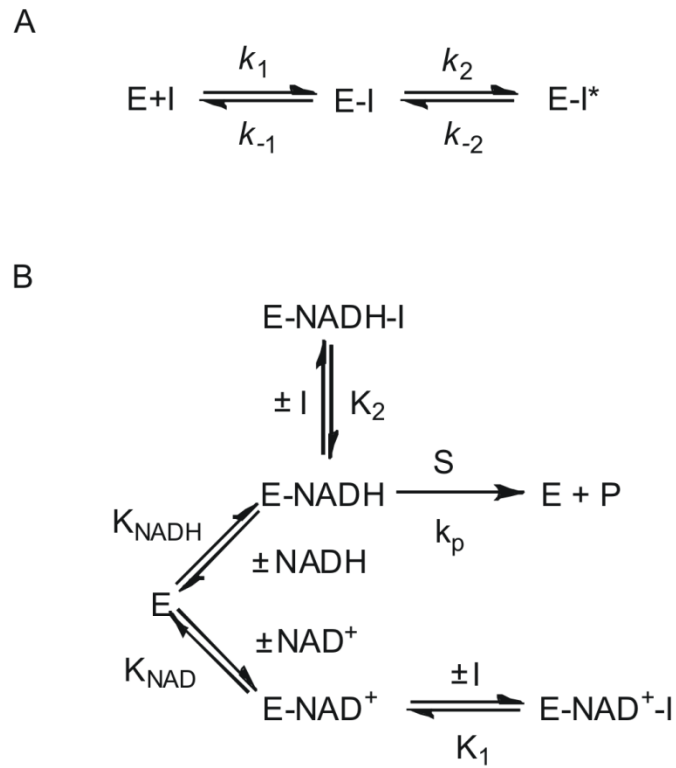


**Figure 3.2: Kinetic schemes for the inhibition of bpmFabI-1.**

(A) Slow-onset inhibition in which formation of the final E-I\* inhibitor complex occurs in two steps. (B) Kinetic scheme for the interaction of inhibitors with E-NAD<sup>+</sup> and E-NADH.

## Results and Discussion

### *Cloning, Overexpression and Purification of bpmFabI-1 and bpmFabI-2.*

In order to identify putative FabI homologues in *B. pseudomallei*, the sequences of the FabI proteins from *E. coli* (ecFabI) and from *F. tularensis* (ftuFabI) were used as the query sequence for a BLAST analysis of proteins encoded in the *B. pseudomallei* genome. This analysis revealed that there are two FabI homologues, one on each of the chromosomes with bpmFabI-1 encoded on chromosome 1 having 63.9% identity over 252 residues to ecFabI and 61.6% identity over 258 residues to ftuFabI, and bpmFabI-2 encoded on chromosome 2 with 42.4% identity over 252 residues to ecFabI and 40.9% identity over 252 residues to ftuFabI. In addition, this analysis also revealed 41.4% identity over 251 residues between bpmFabI-1 and bpmFabI-2 in which active site residues were conserved between both enzymes (22) (**Figure 3.3**).

```

ecFabI      MGFLSGKRILVTGVASKLSIAYGIAQAMHREGAELAFTYQNDKLGKRVVEFAAQLGSDIV 60
ftuFabI     MGFLAGKKILITGLLSNKS IAYGIAKAMHREGAELAFTYVG-QFKDRVEKLCAEFNPAAV 59
bpmFabIa    MGFLDGKRILLTGLLSNRSIAYGIAKACKREGAELAFTYVGDREKDRITEFAAEFGSELV 60
bpmFabIb    MR-LQHKRGLIIGIANENSIAFGCARVMREQGAELALTYLNEKAEPYVRPLAQRLD SRLV 59
* * * * * : : * * * * * : : * * * * * : : * * * * * : : * * * * * : : * * * * *

ecFabI      LQCDVAEDASIDTMFAELGKVPKFDGFGVHSIGFAPGDQLDGDYVNAVVTREGFKIAHDIS 120
ftuFabI     LPCDVISDQEIKDLFVELGKVVWDGLDAIVHSIAFAPRDQLEGNFIDCVTREGFSIAHDIS 119
bpmFabIa    FPDVDADDAQIDALFASLKTHWDSLDGLVHSIGFAPREAIAGDFLDGLTRENFRIAHDIS 120
bpmFabIb    VPCDVREPGRLEDV FARIAQEWGQLDFVLHSIAYAPKEDLHRRVTDCS-QAGFAMAMDVS 118
. * * * . . : : * . : * : * * * : * * : : : : : * * * * *

ecFabI      SYSFVAMAKACRSM LNP-GSALLTLSYLGAERAI PNYNVMGLAKASLEANVRYMANAMGP 179
ftuFabI     AYSFAALAKEGRSMMKNRNASMVALTYIGA EKAMPSYNTMGVAKASLEATVRYTALALGE 179
bpmFabIa    AYSFPALAKAALPMLSD-DASLLTLSYLGAERAI PNYNTMGLAKAALEASVRYLAVSLGA 179
bpmFabIb    CHSFIRVARLAEPLMTN-GGCLLTVTFYGAERAVEDYNLMGPVKAALLEGSVRYLAEELGP 177
. : * * * : * : . : : . : : : : : * * * * * : * * * * * . * * * * * * * * *

EcFabI      EGVRVNAISAGPIRTLAASGIKDFRKMLAHCEAVTPIRRTVTI EDVGNSAAFLCSDLSAG 239
ftuFabI     DGIKVNAVSA GPIKTLAASGISNFKKMLDYNAMVSP LKKNVDIMEVGNTVAFLCSDMATG 239
bpmFabIa    KGV RVNAISAGPIKTLAASGIKSFGKILDFVESNSPLKRNVTIEQVGNAGAFLLS DLSAG 239
bpmFabIb    RRIRVHALSPG PLKTRAASGIDRFDALLERVRERTPGHRLVDIDDVGHVAAFLASDDAAA 237
. : * : * * * * * : * * * * * . * * * * * : * * * * * : * * * * * : : .

ecFabI      ISGEVVHV DGGFSIAA--MNELELK 262
ftuFabI     ITGEVVHV DAGYHCVS--MGNVL-- 260
bpmFabIa    VTAEVMHV DSGFN AVVGGMAGLEE- 263
bpmFabIb    LTGNVEYIDGGYHVVG----- 253
. : : . * : : * * * : .

```

**Figure 3.3: Sequence alignment of the FabI enzymes from *E. coli*, *F. tularensis* and *B. pseudomallei*.**

Residues in rectangle contribute to the substrate binding loop. The three active site residues are highlighted by star. The sequence alignment was performed using Clustal W (146), and the figure was made using Jalview (147).

Following overexpression in *E. coli*, the two FabI homologues were purified to homogeneity using His-tag affinity chromatography, following which the N-terminal His-tag was removed from bpmFabI-2 using biotinylated thrombin. SDS-PAGE demonstrated that each protein was > 95% pure and provided apparent molecular mass of 28 kDa in each case, consistent with the predicted molecular mass of 27,770 Da and 27,823Da for bpmFabI-1 and bpmFabI-2, respectively (**Figure 3.4**).

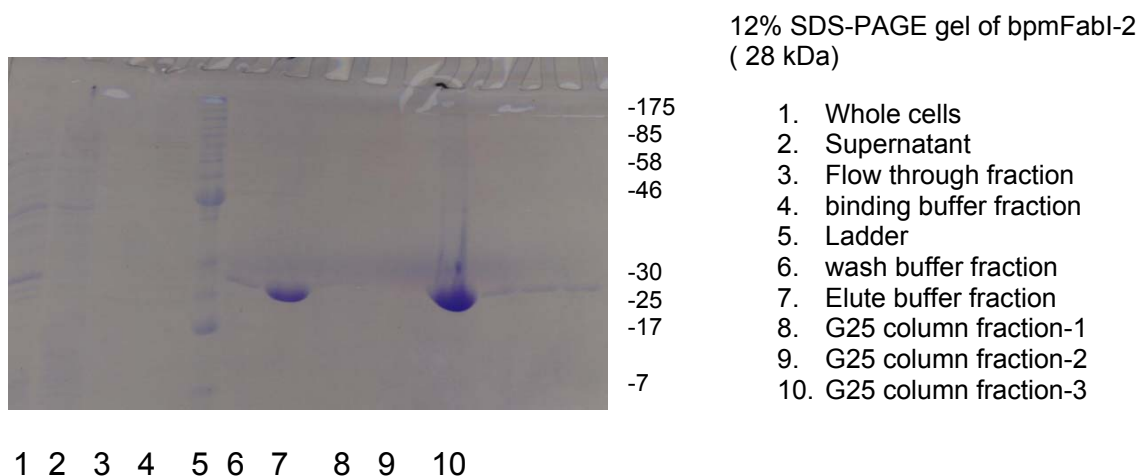
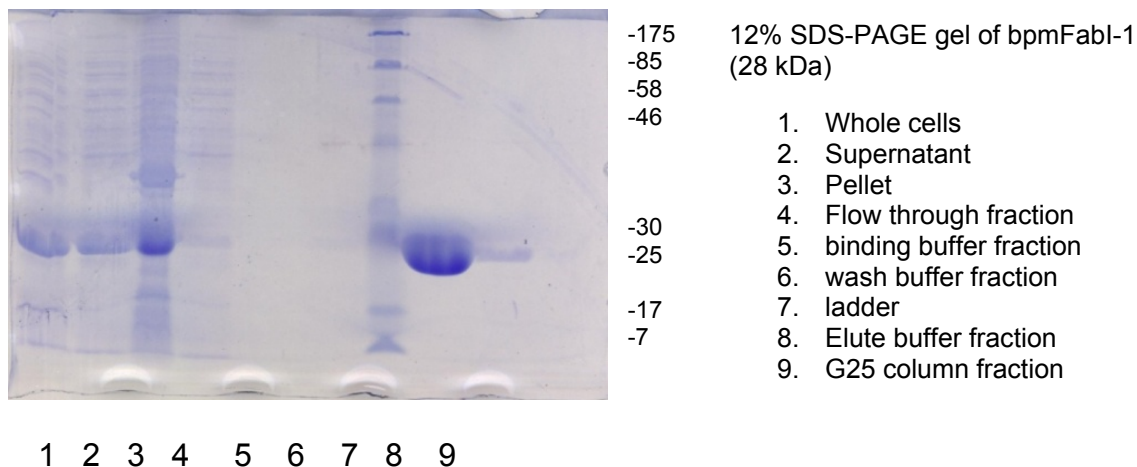


**Figure 3.4: 12% SDS-PAGE showing the expression and purification of bpmFabI-1 and bpmFabI-2.**

The secondary structure of bpmFabI-1 and bpmFabI-2 were estimated by CD spectroscopy (**Figure 3.5**). Data analysis indicated that the  $\alpha$ -helical content of bpmFabI-1 and bpmFabI-2 were 39.2% and 45.0%, respectively, while the  $\beta$ -sheet contents were 15.8% and 14.9%, respectively.

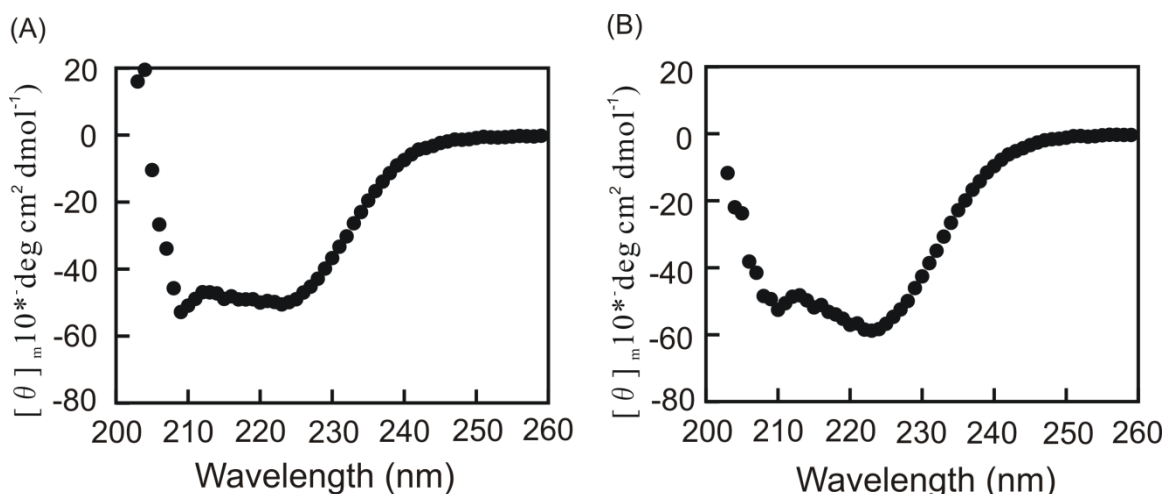


**Figure 3.5: CD spectra of bpmFabI-1 and bpmFabI-2.**

(A) bpmFabI-1, (B) bpmFabI-2. Spectra were recorded at 25 °C in 30 mM PIPES buffer pH 8.0 containing, 150 mM NaCl and 1.0 mM EDTA.

#### *Catalytic Activity of bpmFabI-1 and bpmFabI-2.*

While the natural substrates for the FabI enzymes are fatty acid thioesters of acyl carrier protein (ACP), all FabIs evaluated to date are able to accept enoyl substrates based on CoA or other artificial carrier molecules (26, 46, 47, 120, 148). Consequently, enoyl-CoA substrates are normally used to assay these enzymes since acyl-CoAs are significantly easier to synthesize and purify compared to the corresponding enoyl-ACPs. To demonstrate that the recombinant enzyme is also capable of catalyzing the reduction of ACP substrates, the ACP from *F. tularensis* SCHU S4 (ftuACP), which is 68% identical to the putative ACP from *B. mallei*, was expressed and purified. A chemical coupling reaction with crotonic anhydride was subsequently used to synthesize Cro-ACP. The steady-state kinetic parameters for bpmFabI-1 are summarized in **Table 3.1**, where it can be seen that bpmFabI-1 is able to catalyze the reduction of Cro-ftuACP and a variety of the CoA substrates, confirming that gene product of

BURPS1710b\_2636 is an enoyl-ACP reductase. The  $k_{\text{cat}}/K_m$  values vary by a factor of 300, from Cro-CoA to DD-CoA, indicating that the enzyme catalyzes the reduction of long chain fatty acids most efficiently. High concentrations of Dec-CoA and DD-CoA resulted in substrate inhibition, possibly as a result of binding to the NADH binding site. Consequently, the observed variation in  $k_{\text{cat}}/K_m$  through the enoyl-CoA substrate series may actually be an underestimate. Due to substrate inhibition observed with the longer acyl chain substrate, Oct-CoA was used for the progress curve analysis where high substrate concentrations are required. The increase in  $k_{\text{cat}}/K_m$  from Cro-CoA to Cro-ACP is due primarily to a reduction in  $K_m$  for the ACP substrate, consistent with the expectation that ACP is the preferred substrate carrier for this class of enzyme (149).

**Table 3.1: Steady-state kinetic parameters for bpmFabI-1**

Substrate	$k_{\text{cat}}$ ( $\text{min}^{-1}$ )	$K_m$ ( $\mu\text{M}$ )	$k_{\text{cat}}/K_m$ ( $\mu\text{M}^{-1} \text{min}^{-1}$ )
Cro-CoA	$215 \pm 8$	$188 \pm 15$	$1.2 \pm 0.1$
Cro-ACP	$242 \pm 22$	$27 \pm 6$	$9 \pm 2$
Oct-CoA	$1700 \pm 132$	$160 \pm 22$	$11 \pm 1$
Dec-CoA	$335 \pm 10$	$5.6 \pm 0.7$	$60 \pm 8$
DD-CoA	$504 \pm 6$	$1.7 \pm 0.1$	$300 \pm 17$

As expected for an enoyl-ACP reductase, double-reciprocal plots of the kinetic data displayed intersecting lines to the left of the Y-axis, consistent with a ternary-complex mechanism (**Figure 3.6**) (150, 151) To further determine whether the reaction proceeded via an ordered Bi Bi mechanism or a random Bi Bi mechanism, product

inhibition studies were conducted (**Figure 3.7**) which showed that  $\text{NAD}^+$  is a competitive inhibitor with respect to NADH, and a mixed-type competitive inhibitor with respect to Oct-CoA. This inhibition pattern is consistent with an ordered Bi Bi mechanism in which NADH binds first to the enzyme (150, 151). Consistent with this result, fluorescence titration experiments demonstrated that NADH was able to bind to the free enzyme with a  $K_d$  value of  $1.02 \pm 0.02 \mu\text{M}$  (**Figure 3.8**).

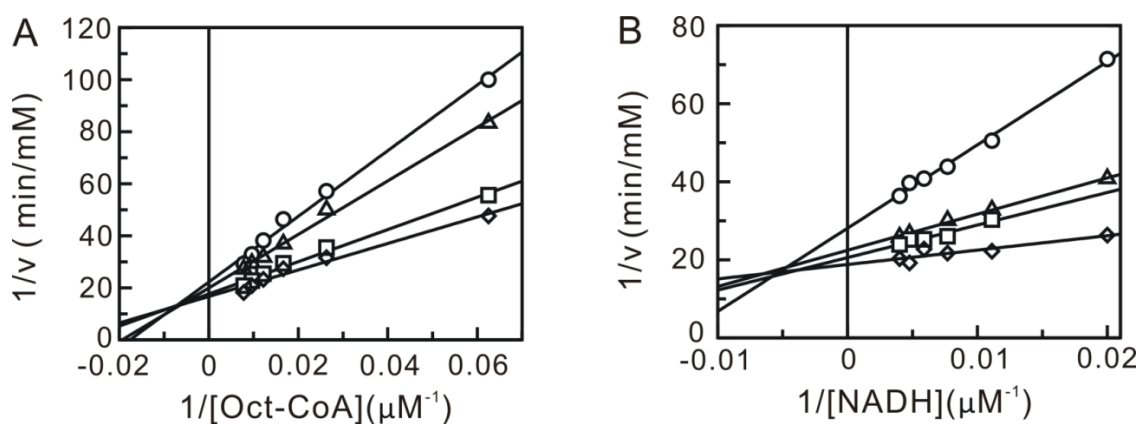


**Figure 3.6: Two-substrate steady-state kinetics.**

Initial velocity patterns: **(A)**  $1/v$  versus  $1/[\text{Oct-CoA}]$  double-reciprocal plot in which  $[\text{NADH}]$  was fixed at 50 ( $\circ$ ), 120 ( $\Delta$ ), 190 ( $\square$ ) and 250  $\mu\text{M}$  ( $\diamond$ ). **(B)**  $1/v$  versus  $1/[\text{NADH}]$  double-reciprocal plot in which  $[\text{Oct-CoA}]$  was fixed at 16 ( $\circ$ ), 32 ( $\Delta$ ), 64 ( $\square$ ) and 128  $\mu\text{M}$  ( $\diamond$ ).

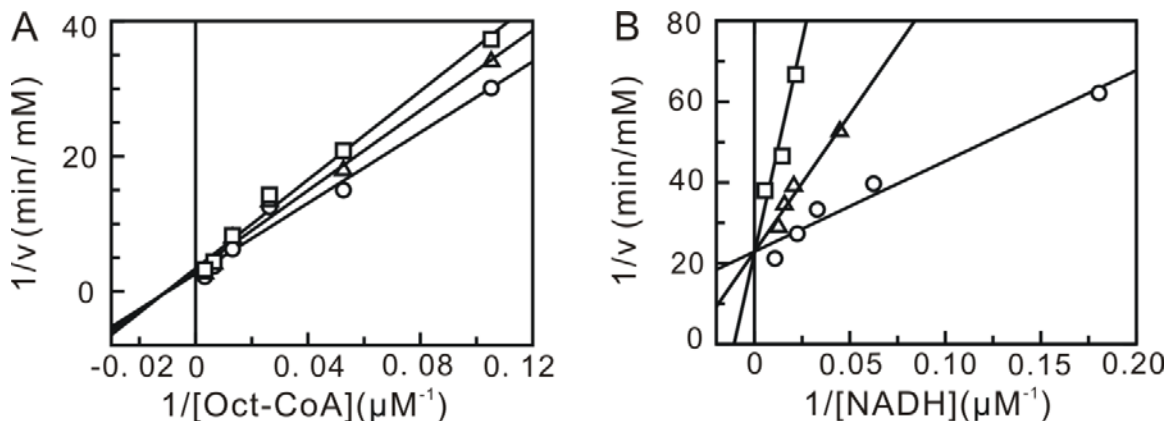


**Figure 3.7: Product inhibition studies to determine the order of substrate binding.** Assays were performed by varying the concentration of one substrate at a fixed concentration of the second substrate and in the presence of  $\text{NAD}^+$ . Initial velocity patterns: **(A)**  $1/v$  versus  $1/[\text{Oct-CoA}]$  double-reciprocal plot in which  $[\text{NAD}^+]$  was fixed at 0 ( $\circ$ ), 200 ( $\Delta$ ) and 2000  $\mu\text{M}$  ( $\square$ ). **(B)**  $1/v$  versus  $1/[\text{NADH}]$  double-reciprocal plot in which  $[\text{NAD}^+]$  was fixed at 0 ( $\circ$ ), 200 ( $\Delta$ ) and 2000  $\mu\text{M}$  ( $\square$ ).

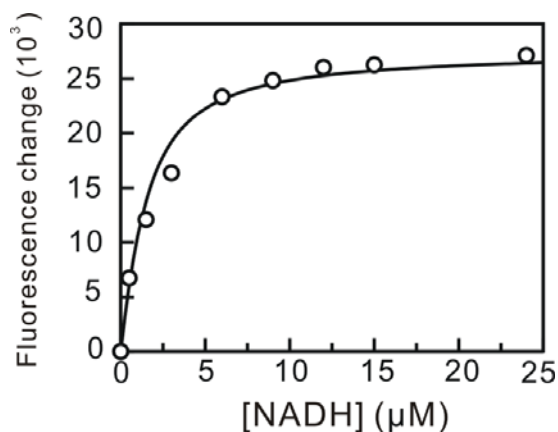


**Figure 3.8: Fluorescence titration of bpmFabI-1 with NADH.**

The plot shows the change in fluorescence when 1  $\mu\text{M}$  bpmFabI-1 is titrated with NADH. The solid line is the best fit of the data to the Scatchard equation with  $K_d = 1.02 \pm 0.02 \mu\text{M}$ .

In contrast bpmFabI-2 was not active with any substrate tested, a result that was unaffected by removal of the His-tag purification sequence from this protein. Crotonyl-ACP was also used to evaluate whether the lack of activity detected with bpmFabI-2



was simply the result of a complete inability to accept CoA-base substrates. However, bpmFabI-2 was also inactive with crotonyl-ACP.

Currently it is not known why bpmFabI-2 is inactive. However, either the enzyme is not folded correctly or we have so far not presented the enzyme with the correct substrate. In order to ascertain whether activity was lost during purification we evaluated the enoyl-ACP reductase activity of the *E. coli* cell lysate following overexpression of bpmFabI-2. However no activity, above that assigned to the endogenous *E. coli* enzymes, could be detected. In addition, bpmFabI-2 is soluble suggesting that if the protein is incorrectly folded it is not grossly so, while CD spectroscopy revealed that bpmFabI-2 has similar secondary structure content to bpmfFabI-1. Further perusal of the sequence data reveals a minor change in the alignment of the catalytic residues between bpmFabI-2 and the other FabI enzymes. Similar to other FabI short chain dehydrogenase reductases (SDRs), bpmFabI-1 has the typical Y-Y-K catalytic triad, specifically Y146-Y156-K163 (152). However in bpmFabI-2, the residue equivalent to Y146 is displaced by one residue to position 147 so that a phenylalanine occupies position 146. In ecFabI, ftuFabI and bpmFabI-1 the sequence around Y146 is L-S/T-**Y-L-G-A-E-R/K**, whereas in bpmFabI-2 it is L-T-**F-Y-G-A-E-R**. Experiments with ecFabI have shown that Y146 plays a key role in catalysis (149), and it is plausible that the position of Y146 in bpmFabI-2 has been altered to accommodate an alternative substrate. Interestingly, fluorescence titration reveals that bpmFabI-2 binds NADH with a  $K_d$  value of  $1.07 \pm 0.02 \mu\text{M}$ . Thus we currently hypothesize that while bpmFabI-2 is a NAD-dependent enzyme, it does not catalyze the reduction of fatty acid substrates. In

this regard, we note that the SDR family proteins catalyze the oxidation/reduction of a wide range of substrates (152).

To provide additional information on the role of bpmFabI-2, the transcriptional activity of both FabI homologues was evaluated using RT-PCR. This analysis demonstrates that *bpmFabI-1* is strongly transcribed while the transcriptional level of *bpmFabI-2* is at least 1000-fold less than that for *bpmFabI-1* (**Figure 3.9**). These data support the importance of bpmFabI-1 in the fatty acid biosynthesis pathway and indicate that bpmFabI-2, if indeed it is an enoyl-ACP reductase, is not required for fatty acid biosynthesis under the growth conditions employed. In this regard, it has previously been observed that chromosome 1 encodes many of the core functions associated with central metabolism and cell growth of *B. pseudomallei*, whereas chromosome 2 encodes accessory functions associated with adaptation and survival in atypical conditions, possibly accounting for the lack of bpmFabI-2 expression observed here (153). Thus, we cannot rule out the possibility that bpmFabI-2 assumes one or more important functions under alternative growth conditions, e.g. when the organism replicates *in vivo*.

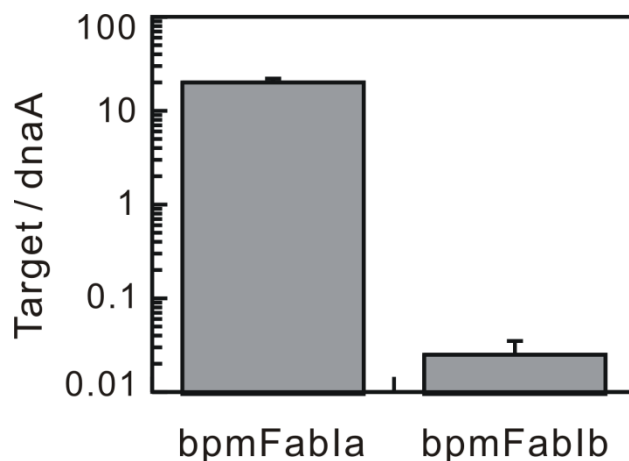


**Figure 3.9: Real-time PCR analysis of bpmFabl-1 and bpmFabl-2.**

Data are mean values  $\pm$  SD from independent biological samples. Values were calculated using total number of targets of bpmFabl-1 or bpmFabl-2 compared to dnaA.

#### *Antimicrobial Activity of the Diphenyl Ether bpmFabl-1 Inhibitors*

Triclosan is a potent inhibitor of the FabI enzymes from organisms such as *E. coli* (46, 47), *F. tularensis* (26) and *S. aureus* (25). This molecule has been used as a starting point for developing long residence time diphenyl ether inhibitors of ftuFabI in addition to the FabI from *M. tuberculosis* (mtFabI, InhA) (49, 50) which is relatively insensitive to triclosan (108). Slow onset inhibition of the FabI enzymes is coupled to ordering of a loop of amino acids close to the active site (22, 26, 49, 120), and the long residence time of the slow onset inhibitors is thought to be critical for *in vivo* drug activity (114, 120, 122, 154-156) as demonstrated directly by us for a series of inhibitors of ftuFabI (26). Consequently, as a prelude to rational inhibitor discovery, we were interested in assessing the ability of the diphenyl ether class of compounds to inhibit this

enzyme and to determine the ability of these compounds to inhibit growth of *B. pseudomallei*.

Progress curve analysis was used to demonstrate that all four diphenyl ethers tested were slow onset inhibitors of bpmFabI-1 (26, 157). Representative data are shown in **Figure 3.10** for the inhibition of bpmFabI-1 by triclosan. In these experiments sufficient substrate is used so that the reaction rate is linear for a significant period of time (30 min) in the absence of inhibitor, and so that the observation of curvature in the presence of inhibitor can be used as a diagnostic for slow onset inhibition. In **Figure 3.10 A** it can be seen that in the presence of triclosan the rate decreased exponentially with time, from an initial velocity ( $v_i$ ) to a steady-state velocity ( $v_s$ ). In addition, both  $v_i$  and  $v_s$  decreased with increasing inhibitor concentration, while  $k_{obs}$  increased and the time required to reach  $v_s$  decreased (**Figure 3.10 A**). This behavior is a classic example of slow-onset inhibition in which the rapid formation of the initial E-I complex is followed by a second slow step leading to the formation of the final E-I\* complex (**Figure 3.2 A**). Fitting the data to **equation 3.1**, provided values for  $v_i$ ,  $v_s$  and  $k_{obs}$ . The hyperbolic dependence of  $k_{obs}$  on the concentration of inhibitor was then fit to **equation 3.2** (**Figure 3.10 B**), allowing the calculation of the kinetic constants for the interconversion of E-I and E-I\*, and also providing a value for  $K_{-1}^{app}$ , the dissociation constant of E-I (**Table 3.2**). Assuming that the rate of dissociation of the inhibitor from the enzyme ( $k_{off}$ ) can be approximated by  $k_{-2}$ , the residence time of triclosan on bpmFabI-1 ( $1/k_{-2}$ ) is 35 min, which is similar to that determined previously for the inhibition of ftuFabI by triclosan (26) (**Table 3.2**).

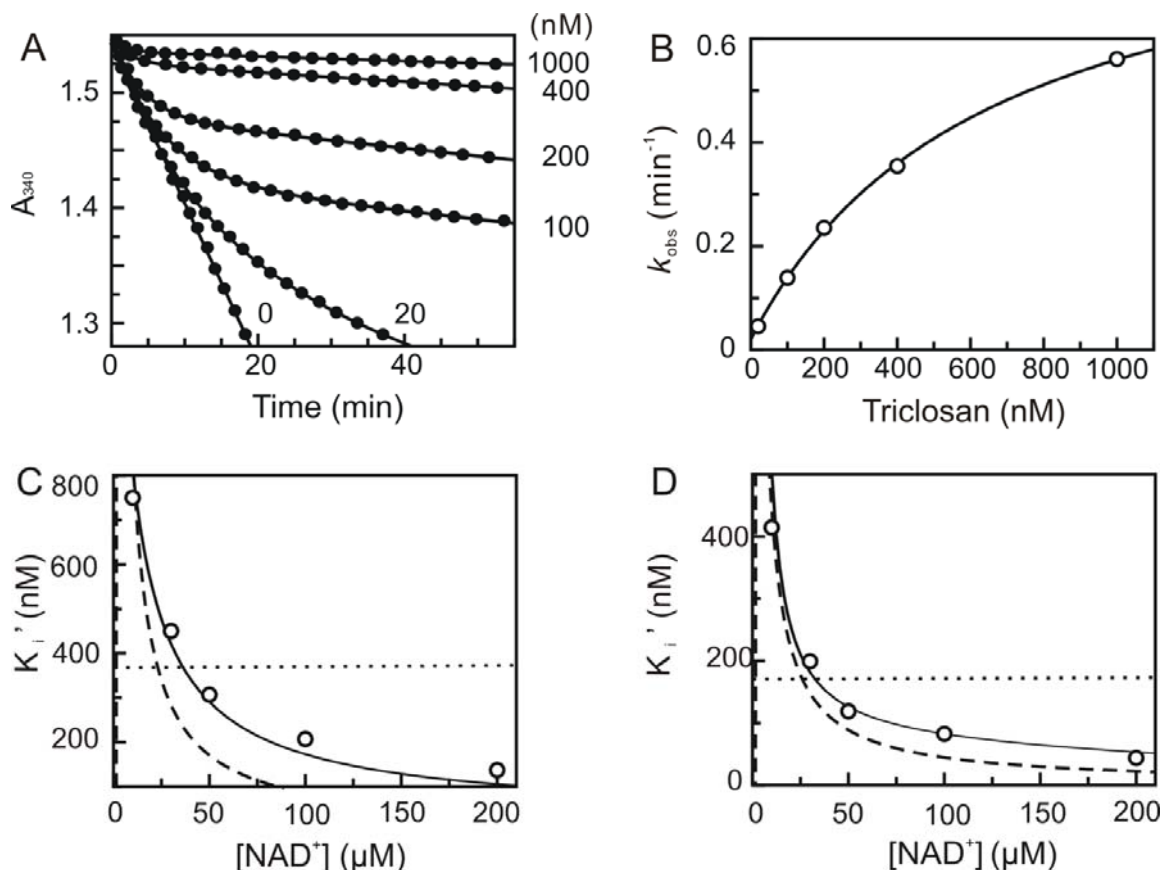
**Table 3.2: Inhibition of ftuFabI and bpmFabI-1 by triclosan**

Enzyme inhibitor pair	$k_2$ ( $\text{min}^{-1}$ )	$k_{-2}$ ( $\text{min}^{-1}$ )	$t_{1/2}$ (min)	$K_{-1}^{\text{app}}$ (nM)	$K_1$ (nM)
ftuFabI-triclosan <sup>a</sup>	0.56±0.04	0.025±0.003	28±2	407±48	0.051± 0.003
bpmFabI-1-triclosan	0.87±0.03	0.020±0.006	35±8	647±50	1.57±0.13

<sup>a</sup> data taken from (26).

Since most diphenyl ethers preferentially bind to the FabI-NAD<sup>+</sup> product complex and only occasionally prefer the FabI-NADH form of the enzyme (22, 45, 108, 120), we performed preincubation experiments with the diphenyl ether inhibitors and bpmFabI-1(26). This enables the dependence of enzyme inhibition on NADH or NAD<sup>+</sup> to be evaluated and also provides the true thermodynamic affinity of the inhibitor for E-NAD<sup>+</sup> ( $K_1$ ) and E-NADH ( $K_2$ ) (**Figure 3.2 B**). Following preincubation of bpmFabI-1 with inhibitor in the presence of saturating NADH and various concentrations of NAD<sup>+</sup> for 5 h, the reaction was initiated by adding Oct-CoA to obtain the apparent inhibition constant  $K_i'$  at each  $[\text{NAD}^+]$ . Subsequently, the dependence of  $K_i'$  on  $[\text{NAD}^+]$  was examined. For triclosan, the dependence of  $K_i'$  on  $[\text{NAD}^+]$  was best described by the equation in which the inhibitor binds to both E-NAD<sup>+</sup> and E-NADH forms of bpmFabI-1 (**Figure 3.10 C**), albeit with a ~1,000-fold preference for E-NAD<sup>+</sup>. The  $K_1$  and  $K_2$  values determined using this method were 1.57 nM and 1.10  $\mu\text{M}$ , respectively (**Table 3.3**). The three other diphenyl ethers behaved similarly to triclosan (**Table 3.3**) with representative

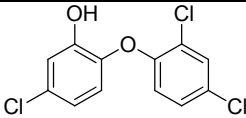
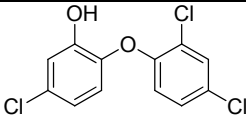
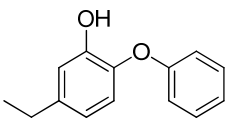
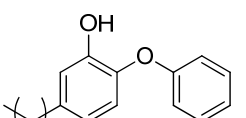
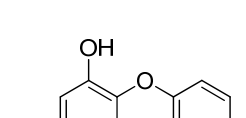
data shown in **Figure 3.10 D** for PT01. Thus, all four compounds tested are slow onset inhibitors of bpmFabI-1 with nanomolar affinity for the E-NAD<sup>+</sup> form of this enzyme.



**Figure 3.10: Progress curve and preincubation analysis for the inhibition of bpmFabI-1 by triclosan and PT01.**

(A) Progress curves were obtained for triclosan concentrations ranging from 0 - 1000 nM. The solid lines are the best fits of the data to equation 1. (B)  $k_{obs}$  from Figure 2.9 A plotted as a hyperbolic function of [triclosan] using equation 2. (C) The effect of NAD<sup>+</sup> on the apparent inhibition constant of triclosan. The solid, dashed and dotted lines are the fits of the data to equations in which the inhibitor binds to both E-NADH and E-NAD<sup>+</sup> (solid line), only E-NAD<sup>+</sup> (dashed line) or only E-NADH (dotted line) (26). The best fit (solid line) is obtained using  $K_i' = K_2(1 + [\text{NAD}^+]/K_{m'}^{\text{NAD}})/[1 + [\text{NAD}^+]/(K_{m'}^{\text{NAD}} K_1/K_2)]$ , with  $K_1 = 1.57 \pm 0.13$  nM and  $K_2 = 1096 \pm 74$  nM. (D) The effect of NAD<sup>+</sup> on the apparent inhibition constant of PT01. The solid, dashed and dotted lines are as described in 6C, and the best fit (solid line) is again obtained with the equation in which PT01 binds to both E-NAD<sup>+</sup> and E-NADH with  $K_1 = 0.51 \pm 0.04$  nM and  $K_2 = 910 \pm 101$  nM.

**Table 3.3: Antibacterial activity and inhibition of bpmFabI-1 by triclosan and the diphenyl ethers**

Inhibitor		$K_1$ (nM)	$K_2$ (nM)	<i>B. pseudomallei</i> MIC ( $\mu\text{g/mL}$ )	<i>B. thailandensis</i>	
					E264 MIC ( $\mu\text{g/mL}$ )	Bt38 MIC ( $\mu\text{g/mL}$ )
<b>Triclosan</b>		1.57 $\pm 0.13$	1096 $\pm 74$	30	30	0.2-0.5
<b>PT01</b>		0.51 $\pm 0.04$	910 $\pm 101$	72	72	0.2-0.5
<b>PT02</b>		1.30 $\pm 0.10$	361 $\pm 14$	>250	>250	1.2
<b>PT03</b>		1.80 $\pm 0.20$	428 $\pm 20$	>250	>250	33

The ability of the diphenyl ethers to inhibit bacterial growth was also evaluated. MIC values against *B. pseudomallei* varied from 30 and 70 µg/mL for triclosan and PT01, respectively, to >250 µg/mL for PT02 and PT03 (**Table 3.3**). Since efflux is a major mechanism of drug resistance in *Burkholderia spp.* (135), we also evaluated antibacterial activity using a *B. thailandensis* strain (Bt38) in which the bpeAB-oprB and amrAB efflux pumps have been disabled (136). FabI-1 and FabI-2 in *B. pseudomallei* and *B. thailandensis* are very similar with 98% and 97% identity, respectively, so it is likely that the FabI-1 enzyme in *B. thailandensis* is also very sensitive to the compounds used in this study. As a control we first determined MIC values for the diphenyl ethers against a wild-type strain of *B. thailandensis* (E264), and observed the same values as those determined for *B. pseudomallei*, ranged from 30 µg/mL for triclosan and 70 µg/mL for PT01, to 250 µg/mL for PT02 and PT03 (**Table 3.3**). However, MICs for pump mutant strain Bt38 were dramatically reduced, with values of 0.2-0.5 µg/mL for triclosan and PT01, 1.2 µg/mL for PT02 and 33 µg/mL for PT03 (**Table 3.3**), in the range observed for this class of compounds with other sensitive organisms (25, 26, 50), suggesting that their antibacterial activity is due to FabI-1 inhibition in Bt38. Since all four compounds have similar affinities for bpmFabI-1, it is presently unclear why the MIC values of PT02 and PT03 differ from those of triclosan and PT01 for the three strains tested. Clearly, all are substrates for the efflux pumps that have been inactivated in Bt38, since the MIC values are lower for this strain; however, it is plausible that PT02 and, especially, PT03 are substrates for additional efflux system(s) or detoxification pathways that are still present in Bt38, or that these compounds have more difficulty in crossing the cell wall.



Finally, it is important to comment on the presence of the FabV enoyl-ACP reductase homologue in *B. pseudomallei*. In addition to the two FabI homologues, *B. pseudomallei* also contains a homologue of the recently discovered FabV enoyl-ACP reductase (31, 33). It is currently not clear what role FabI and FabV play in *Burkholderia spp.* However it is possible that both have to be inhibited in order to fully compromise fatty acid biosynthesis, a view that is supported by recent work on *Pseudomonas aeruginosa* PAO1 (33). Like *B. pseudomallei*, *P. aeruginosa* also contains both FabI (paFabI) and FabV (paFabV) homologues, which are 65% and 74% identical, respectively, to the corresponding enzymes in *B. pseudomallei*. Interestingly, Wang, Cronan and co-workers have demonstrated that deletion of the gene for paFabV leads to a >2,000-fold increase in sensitivity of *P. aeruginosa* to triclosan (MIC >2,000 to 1 µg/mL), supporting their conclusion that triclosan resistance in this organism is due to the presence of the 'triclosan-resistant' FabV enzyme rather than to efflux (33). However, in the case of *Burkholderia spp.*, experiments with strain Bt38 indicate that efflux plays an important role in modulating the sensitivity of this organism to triclosan and the other diphenyl ethers. Additionally, the triclosan MIC value for Bt38 of 0.2-0.5 µg/mL is similar to that of the *P. aeruginosa* FabV knockout strain, indicating that in *Burkholderia* either both enzymes are essential or that this concentration is sufficient to inhibit both bpmFabI-1 and bpmFabV. In this regard we know that the  $K_i$  value of triclosan for bpmFabV is 0.4 µM (0.12 µg/mL) (31), which is similar to the MIC value for the efflux pump mutant strain. Thus, even though bpmFabV is ~250-fold less sensitive to triclosan than bpmFabI-1, the concentration of inhibitor required to prevent bacterial growth is indeed sufficient to inhibit both enoyl-ACP reductases. Currently we are

constructing genetic knockouts of the respective genes in *B. thailandensis* and *B. pseudomallei* to provide additional insight into the function of FabI and FabV in *Burkholderia spp.* and to evaluate the mechanism of action of the enoyl-ACP reductase inhibitors.

## Conclusions

As an initial step in developing novel antibacterials against *Burkholderia pseudomallei*, we have characterized the FabI enoyl-ACP reductase homologues in FAS-II pathway from this organism and performed an initial enzyme inhibition study. A BLAST analysis identified two FabI enoyl-ACP reductase homologues, bpmFabI-1 and bpmFabI-2, in the *B. pseudomallei* genome, which were cloned, overexpressed in *E. coli* and purified. Steady-state kinetics was used to determine the reaction mechanism and the sensitivity of bpmFabI-1 to four diphenyl ethers. The antibacterial activity of the inhibitors was assessed using a wild-type strain of *Burkholderia thailandensis* (E264) and an efflux pump mutant (Bt38). Consistent with its annotation as an enoyl-ACP reductase, bpmFabI-1 catalysed the NADH-dependent reduction of DD-CoA via a sequential Bi Bi mechanism. In contrast, bpmFabI-2 was inactive with all substrates tested and only *bpmfabI-1* was transcriptionally active under the growth conditions employed. The sensitivity of bpmFabI-1 to four diphenyl ethers was evaluated and in each case the compounds were slow-onset inhibitors with  $K_i$  values of 0.5–2 nM. In addition, triclosan and PT01 had MIC values of 30 and 70  $\mu\text{g}/\text{mL}$  for *B. pseudomallei* as well as a wild-type strain of *B. thailandensis* (E264), but MIC values of < 1  $\mu\text{g}/\text{mL}$  for the efflux pump mutant Bt38. A reduction in MIC values was also observed for the pump mutant strain with the other diphenyl ethers. We conclude provided that efflux can be circumvented, bpmFabI-1 is a suitable target for drug discovery.

## **Chapter 4 : Mechanism and Inhibition of the FabV enoyl-ACP Reductase from *Yersinia pestis***

### **Background**

#### *Plague*

Plague, a widespread zoonotic disease, has had devastating effects on the human population throughout history. The three major historical plague epidemics—plague of Justinian, Black Death, and Third Pandemic—have caused millions of death in the European continent, as well as worldwide after the spread of the disease (158). It has lodged itself permanently in the world's list of highly infectious diseases.

The main carrier of this zoonotic disease has been identified to be infected rodents and the vector of transmission to humans has long been established to be fleas, ticks and body lice (158, 159). The transmission route through the flea has been established: after an infected blood meal, an antibacterial mechanism of the flea causes the containment of the bacteria within its stomach which are eventually regurgitated into the mammalian blood during the feeding process (160).

There are three main forms of manifestation of the plague: bubonic, septicemic, and pneumonic plague. In the most common form, bubonic plague, pathogenic bacteria spreads through the lymphatics until it reaches a lymph node, and stimulates severe haemorrhagic inflammation that causes the lymph nodes to expand. The expansion of lymph nodes is the cause of the characteristic "bubo" associated with the disease (158). Lymphatics ultimately drain into the bloodstream, so the plague

pathogenic bacteria may enter the blood and travel to almost any part of the body, and result in septicemic plague. The pneumonic plague, the extremely deadly form, is normally spread by aerosolic propagation when airborne droplets were produced by acts of coughing and sneezing by infected humans (158). Secondary pneumonic plague can develop after the initial bubonic manifestation, when the bacteria spread to the lungs in the human host.

### *Yersinia pestis*

*Yersinia pestis* is a Gram-negative bacterium which has been identified as the plague-causing pathogen by both Alexandre Yersin and Shibasaburo Kitasato independently in 1894 (158). *Y. pestis* has gained attention as a possible biological warfare agent (161) and the Centers for Disease Control and Prevention (CDC) has classified it as a category A bioterrorism pathogen.

Streptomycin has been used to treat plague for about 60 years (162) and still remains the drug of choice. However, because streptomycin is bacteriolytic, it should be administered with care to prevent the development of endotoxic shock. Due to its toxicity, patients are gradually switched to another antibiotics, usually tetracycline (158). Because antibiotics may provide little immediate relief to patients who are infected with antibiotic resistant strain, some antibacterial investigations have been carried on the anti-plague antibody as therapeutics (163).

### *FabV, the fourth Enoyl-ACP Reductase*

The majority of the FAS-II enzymes are essential for bacterial viability (141). Among the enzymes found in the FAS-II pathway, the enoyl-ACP reductase, which catalyzes the last reaction in each elongation cycle, has been mostly studied based on the discovery of antibacterial compounds that target this enzyme (102, 107, 142). The FabI enoyl-ACP reductase from *E. coli* was first identified (143), and it was initially considered to be the only reductase in bacteria. Subsequently, drug resistance in other pathogens led to the discovery of FabI isoforms: FabK in *Streptococcus pneumonia* (34), FabL in *Bacillus subtilis* (30), and FabV, the most recently discovered class of the enoyl-ACP reductase, originally identified in *Vibrio cholera* by Cronan and co-workers (32). Recently, FabV was identified in *B. mallei*, and there was a detailed kinetic analysis of the enzyme mechanism and inhibition by triclosan (31).

### *Project Goal*

Enoyl-ACP reductase in *Y. pestis* has not been characterized and remains relatively unexplored. Based on the protein sequence similarity, we predict that there is only one enoyl-ACP reductase, and that this enoyl-ACP reductase belongs to the class of FabV. This project is focused on characterizing the mechanism of FabV in *Y. pestis* and identifying potential inhibitors for *Y. pestis* as well as all other infectious pathogens containing FabV. The outcome of this project will further enhance our knowledge of the FAS-II pathway in *Y. pestis* and lead to the development of antibiotics.

## Materials and Methods

### *Cloning, Expression, and Purification of ypFabV*

A putative *fabV* gene from *Y. pestis* CO92 genome was identified using BLAST sequence alignment with FabV found in *Vibrio cholera*, and amplified using the following primers (Integrated DNA Technologies): 5'-CCGCTCGAGATGATTATAAAACCACGTGTA-3' (forward) and 5'-CCGGAATTCTTAACCCTGAATCAAGTTAGG-3' (reverse). PCR product was digested with XhoI and EcoRI, and then inserted into the pET15b plasmid (Novagen) so that a His-tag was encoded at the N-terminus of the coding sequence. The constructed plasmids were confirmed by the DNA sequencing (DNA Sequencing Facility, Health Science Center, Stony Brook University).

Protein expression was performed using the *E. coli* strain BL21 (DE3) pLysS cells. After transformation, a single colony was used to inoculate 10 mL of Luria Broth (LB) media containing 0.2 mg/mL ampicillin in a 50 mL falcon tube, which was then incubated overnight at 37 °C. The overnight culture was used to inoculate 1 L of LB media containing 0.2 mg/mL ampicillin, which was incubated at 37 °C until the optical density at 600 nm (O.D. 600) increased to around 1.0. Protein expression was induced by adding 1 mM isopropyl-1-thio- $\beta$ -D-galactopyranoside (IPTG) and the culture was then shaken at 25 °C for 16h. Cells were harvested by centrifugation at 5,000 rpm for 20 min at 4 °C. The cell pellet was resuspended in 30 mL of binding buffer (5 mM imidazole, 0.5 M NaCl, 20 mM Tris-HCl, pH 7.9) and was lysed by sonication. The cell lysate was ultracentrifuged at 33,000 rpm for 1 hour at 4 °C to pellet the cell debris and the supernatant was then loaded onto a His-bind column (1.5 cm  $\times$  15 cm) which

contained around 4 mL of His-bind resin (Novagen) charged with charge buffer ( $\text{Ni}^{2+}$ ). The column was equilibrated with binding buffer before loading. The flow-through from the supernatant was collected and 60 mL of binding buffer was used to wash the column. After that, 60 mL of wash buffer (60 mM imidazole, 0.5 M NaCl, 20 mM Tris-HCl, pH 7.9) was used to wash the column. Finally, the ypFabV was eluted by 30 mL of eluent buffer (1M imidazole, 0.5 M NaCl, 30 mM Tris-HCl, pH 7.9) and collected in fractions. The presence of ypFabV in the collected fractions was tested with a spectrophotometer at 280 nm. The fractions with protein were combined and loaded onto a Sephadex G-25 chromatography (1.5 cm  $\times$  55 cm) to remove imidazole using PIPES buffer (30 mM PIPES, 150 mM NaCl and 1 mM EDTA, pH 8.0) as the eluent. The protein was >95% pure shown by 12% SDS-PAGE, which gave an apparent molecular mass of ~43 kDa. The concentration of the protein was measured by obtaining the absorption at 280 nm using the extinction coefficient ( $\epsilon$ ) of  $46,610 \text{ M}^{-1}\text{cm}^{-1}$  calculated from the primary sequence. The final concentrated protein was flash frozen and stored at  $-80 \text{ }^\circ\text{C}$ .

#### *Synthesis of Trans-2-dodecenoyl-CoA, Cis-5-trans-2-dienoyl-CoA and Lauryl-CoA*

*trans*-2-Dodecenoyl-CoA (DD-CoA), *cis*-5-*trans*-2-dienoyl-CoA and lauryl-CoA were synthesized from *trans*-2-decenoic acid, *cis*-5-*trans*-2-dienoic acid and lauric acid, respectively, using the mixed anhydride method (108, 148). ESI-MS ( $[\text{M} - \text{H}]^-$ ) calculated for DD-CoA [ $\text{C}_{33}\text{H}_{53}\text{N}_7\text{O}_{17} \text{P}_3\text{S}$ ] $^-$ : 946.2, found: 946.2. ESI-MS ( $[\text{M} - \text{H}]^-$ ) calculated for *cis*-5-*trans*-2-dienoyl-CoA [ $\text{C}_{33}\text{H}_{51}\text{N}_7\text{O}_{17} \text{P}_3\text{S}$ ] $^-$ : 944.7, found: 944.7. ESI-MS ( $[\text{M} - \text{H}]^-$ ) calculated for lauryl-CoA [ $\text{C}_{33}\text{H}_{55}\text{N}_7\text{O}_{17} \text{P}_3\text{S}$ ] $^-$ : 948.7, found: 948.7.



### *Steady-State Kinetics Analysis*

All kinetic experiments were performed on a Cary 300 Bio (Varian) spectrometer at 25 °C in 30 mM PIPES buffer pH 6.8 containing 150 mM NaCl and 1.0 mM EDTA. Initial velocities were measured by monitoring the oxidation of NADH to NAD<sup>+</sup> at 340 nm ( $\epsilon = 6,300 \text{ M}^{-1} \text{ cm}^{-1}$ ), and kinetic parameters ( $k_{cat}$  and  $k_{cat}/K_m$ ) were determined as previously described (31).

Initial characterization of the enzyme mechanism was performed in reaction mixtures containing 30 nM ypFabV, and measuring initial velocities at several fixed concentrations of NADH (50, 120, 190 and 250  $\mu\text{M}$ ) and by varying the concentration of DD-CoA (16-128  $\mu\text{M}$ ), or at a fixed concentration of DD-CoA (16, 32, 64 and 128  $\mu\text{M}$ ) and by varying the concentration of NADH (50-250  $\mu\text{M}$ ). Double reciprocal plots were then used to differentiate between ping pong or ternary-complex mechanisms. To further investigate the binding order of the two substrates, product inhibition studies were performed in which the concentration of each substrate (NADH and DD-CoA) was varied in the presence of the NAD<sup>+</sup> product (0, 50 and 100  $\mu\text{M}$ ). Lineweaver-Burk plots were subsequently used to determine whether enzyme inhibition was competitive, uncompetitive or noncompetitive.

### *Inhibition by Diphenyl Ether Compounds*

Kinetic assays using DD-CoA and ypFabV were performed as described previously (108). Reactions were initiated by addition of 15 nM ypFabV to solutions containing 250  $\mu\text{M}$  NADH, 30  $\mu\text{M}$  DD-CoA and 100  $\mu\text{M}$  inhibitor.

## Results and Discussion

### *Bioinformatic Analysis.*

Sequence similarity studies revealed that enoyl-ACP reductase, especially FabV, is well conserved among several clinically important pathogens, such as *Vibrio cholera* (32), *Pseudomonas aeruginosa* (33), and *Burkholderia spp.* (31). To identify putative enoyl-ACP reductase homologues in *Y. pestis*, the sequences of FabI from *E. coli* (ecFabI), FabL from *B. subtilis*, FabK from *S. pneumoniae*, and FabV from *V. cholerae* (vcFabV) were used as templates for a BLAST analysis of *Y. pestis* CO92 genome. Open reading frame YPO4104 was identified as vcFabV homologue. The putative ypFabV was found to be 86% homologous to FabV in *Vibrio cholera* (vcFabV), and has conserved active site residues (**Figure 4.1**).

```

ecFabI      -----MGFLSG-----KRILVTGVASKLSIAYGIA 25
vcFabV      MI IKPKIRGFICTTTHPVGCEANVKEQIAYTKAQGPIKNA PKRVLVVGSSSGYGLSSRIA 60
bmFabV      MI IKPRVRGFICVTTHPAGCAASVREQIAYVARRGPIERGPKKVLVI GASTGYGLAARIA 60
ypFabV      MI IKPRVRGFICVTAHPTGCEANVKQIDYVTTTEGPIANGPKRVLVI GASTGYGLAARIT 60
              : : *:* * * : : * :

ecFabI      QAMHREGAELAFYQNDKLGKR-----VEEFAAQLGSDIVLQ-----CDVAEDA 69
vcFabV      AAFGGGAATIGVFFEKPGTDKKPGTAGFYNAAAFDKLAHEAGLYAKSLNGDAF SNEAKQK 120
bmFabV      AAFVGGAATLGVFFERAPADAKPGTAGWYNSAAFHDEAAAARGLQATSVNGDAF SDEIKHK 120
ypFabV      AAFGCGADTLGVFFERPGEEKPGTSGWYNSAAFHKFAAQKGLYAKSLNGDAF SDEIKQL 120
              * : . : . : . : . : . : . : * * : : . :

ecFabI      SIDTMFAELGKVPKFDGFGVHSIGFAPG-----DQLDGDY 104
vcFabV      AIELIKQDLGQIDLVVYSLASPVKMPD TGELVRSALKPIGETYTTSTAVDTNKDVIIEAS 180
bmFabV      TIDAI RRDLGQVDLVVYSVAAPRRTHPKTVGTHQSTLKPIGHAVRLRGIDTNEAIKEITL 180
ypFabV      TIDAIKQDLGQVDQVIYSLASPRRTHPKTGEVFNSALKPIGNVNLRLGLD TDKEVIKESV 180
              :* : : *:* : . . . . * : :

ecFabI      VNAVTRREGFKIAHDIS---SYSFVAMAKACRSMLNPGSALLTLSV LGAERAI PNYN--VM 159
vcFabV      VEPATEQEIADTVTMGGQDWELWIQALEEAGVLAEGCKTVAYSYIGTELTPV IYWDGAL 240
bmFabV      LQPATPDEIADTVAVMGGEDWRMWIDALDAAGVLDGAKT TAFTYLG EQVTHDIYWNGSI 240
ypFabV      LQPATQSEIDSTVAVMGGEDWQMWIDALLDAGVLAEGAQT TAFTYLG EKITHDIYWNGSI 240
              : : * : : : : : * : * : : * : * : : * :

ecFabI      GLAKASLEANVRYMANAMGPEGV-RVNAISAGPIRTLAASC I KDFRKM LAHCEAVTP--- 215
vcFabV      GRAKMDLDRAATAINEKLAAKGG-TANVAVLKSVVTOASSA TPVMPLYIAMVFKMKREQG 299
bmFabV      GEAKKDLDRTVLALRGKLAARGG-DARVSVLKAVVTOASSA TPMMPLYLSLLFKVMKARG 299
ypFabV      GAAKDL DQKVLAIRESLAAHGGGDARVSVLKAVVTOASSA TPMMPLYLSLLFKVMKEKG 300
              * * * . : . : : . . . * . . . : * * : * * : : :

ecFabI      -----IRRTVTIEDVGNSAAFLCSDLSAGISGEVV 245
vcFabV      VHEGCMEQIYRMFSQRLYKEDGSAPEVDDHNRLRLDDWELRDD IQQHCRDLWPQITTENL 359
bmFabV      THEGCI EQVDGLLRDSLY---SAQPHVDAEGR LRADRL ELDPAVQARVLELWDQVTDNDL 356
ypFabV      THEGCI EQVYSLYKDSL C---GDSPHMDQEGRLRADYKELDPEVQNVQQLWDQVTDNDI 357
              * : : : * : : :

ecFabI      HVDGGFSIAAMNELELK----- 262
vcFabV      RELTDYDMYKEEFIKLFGFGIEGIDYDADVNPEVEFDVIDIE 401
bmFabV      YTLLTDFAGYKAEFLRLFGFGIDGVDYDAPVEPNVRIPNLIE- 397
ypFabV      YQLTDFVGYKSEFLNLFGFGIDGVDYDADVNPDVKIPNLIQG 399
              . : : : *

```

**Figure 4.1: Sequence alignment of enoyl-ACP reductases FabI from *E. coli*, and FabV from *V. cholerae*, *B. mallei*, *Y. pestis*.** Active sites are labeled in red, key residues for inhibitor binding are labeled in blue.

Subsequently, the ypFabV was cloned, expressed, and purified, giving a protein with a molecular mass of ~43 kDa on SDS-PAGE, consistent with the expected molecular mass of 43346 Da. The enzyme was shown to catalyze the NADH-dependent reduction of DD-CoA, demonstrating that ypFabV has *in vitro* enzymatic activity characteristic of an enoyl-ACP reductase.

### *Kinetic Mechanism.*

The Michaelis-Menten constants for DD-CoA were then determined by varying the concentration of DD-CoA at a saturating concentration of NADH. The values of  $k_{cat}$ ,  $K_{m,DD-CoA}$  and  $k_{cat}/K_m$  obtained using this method were  $1270 \pm 140 \text{ min}^{-1}$ ,  $17 \pm 2 \text{ }\mu\text{M}$ , and  $34 \pm 4 \text{ }\mu\text{M}^{-1} \text{ min}^{-1}$ , respectively, which is comparable with bmFabV (31).

In order to discriminate between ternary complex mechanism or ping pong mechanism of substrate binding, a matrix of initial velocities was measured at different concentrations of DD-CoA and NADH, and the kinetic data were then analyzed using double-reciprocal plots (**Figure 4.2**). It was shown that all the lines obtained from the bi substrate kinetic data intersected each other at a single point in both double reciprocal plots. This indicated that ypFabV catalyzes substrate reduction through a ternary complex mechanism, which was also the same for bmFabV(31). To further determine whether the reaction proceeded via an ordered Bi Bi mechanism or a random Bi Bi mechanism, product inhibition studies were conducted (**Figure 4.3**) which showed that  $\text{NAD}^+$  is a competitive inhibitor with respect to NADH, and a noncompetitive inhibitor with respect to DD-CoA. This inhibition pattern is consistent with an ordered Bi Bi mechanism in which NADH binds first to the enzyme (25, 151).

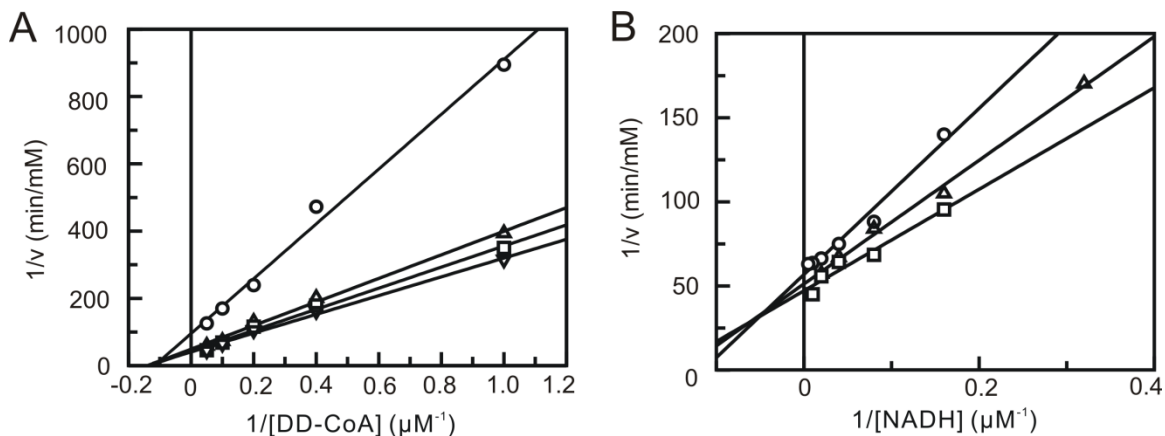


**Figure 4.2: Two-substrate steady-state kinetics.**

Initial velocity patterns: **(A)**  $1/v$  versus  $1/[DD-CoA]$  double-reciprocal plot in which  $[NADH]$  was fixed at 10 ( $\circ$ ), 33 ( $\Delta$ ), 100 ( $\square$ ) and 250  $\mu M$  ( $\nabla$ ). **(B)**  $1/v$  versus  $1/[NADH]$  double-reciprocal plot in which  $[DD-CoA]$  was fixed at 6 ( $\circ$ ), 12 ( $\Delta$ ) and 24  $\mu M$  ( $\square$ ).

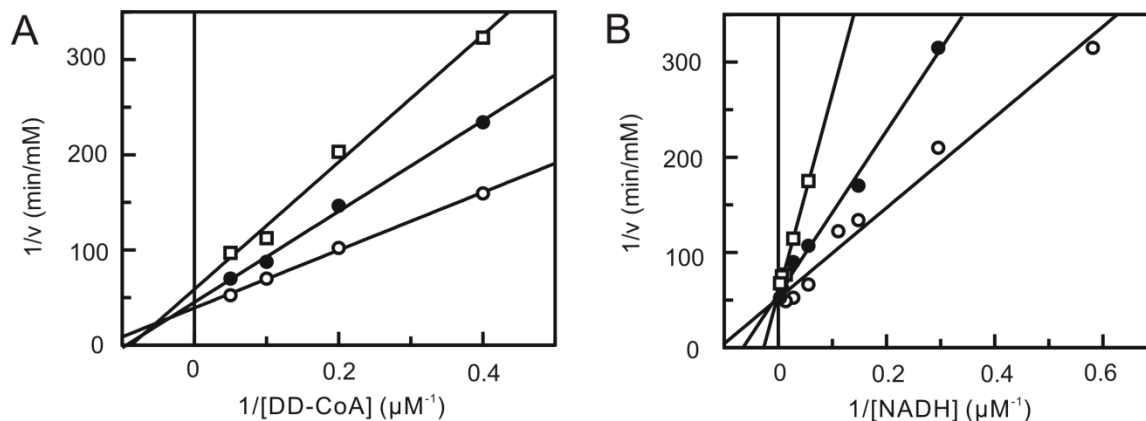


**Figure 4.3: Product inhibition studies to determine the order of substrate binding.**

Assays were performed by varying the concentration of one substrate at a fixed concentration of the second substrate and in the presence of  $NAD^+$ . Initial velocity patterns: **(A)**  $1/v$  versus  $1/[DD-CoA]$  double-reciprocal plot in which  $[NAD^+]$  was fixed at 0 ( $\circ$ ), 50 ( $\bullet$ ) and 100  $\mu M$  ( $\square$ ). **(B)**  $1/v$  versus  $1/[NADH]$  double-reciprocal plot in which  $[NAD^+]$  was fixed at 0 ( $\circ$ ), 50 ( $\bullet$ ) and 100  $\mu M$  ( $\square$ ).

*Preference toward Saturated Acyl Chain Substrate and Unsaturated Acyl Chain Substrate.*

From previous study (**Table 4.1**), the FabI enzymes from *E. coli* and *F. tularensis*, which are the only enoyl-ACP reductase in the corresponding organisms, can efficiently catalyze the reduction of both DD-CoA and *cis-5-trans-2*-dienoyl-CoA. Interestingly, the ratio of  $k_{cat}/K_m$  values toward the unsaturated substrate and saturated substrate correlate with their unsaturated fatty acid (UFA) content in the lipids from the respective organism. In *S. aureus*, saFabI has no activity toward *cis-5-trans-2*-dienoyl-CoA, which is also consistent with the trace amount of UFAs in its lipids. In *B. mallei*, bmaFabI can only poorly catalyze *cis-5-trans-2*-dienoyl-CoA, so the ratio of  $k_{cat}/K_m$  values toward *cis-5-trans-2*-dienoyl-CoA and DD-CoA is only 0.003, which is significantly not consistent with the UFA percentage of *B. mallei*. The inefficiency of the bmaFabI toward unsaturated substrate *cis-5-trans-2*-dienoyl-CoA, may be because of the presence of another enoyl-ACP reductase bmaFabV, which can efficiently catalyze the reduction of unsaturated substrate for UFA biosynthesis with a 90-fold increase in  $k_{cat}/K_m$  ratio compared to bmaFabI. Consequently, we hypothesize that bacteria may control their UFA/SFA ratio by regulating the enoyl-ACP reductase activity toward different intermediates in both SFA and UFA biosynthesis pathway.

*Y. pestis* has large amount of UFA with UFA/SFA ratio of 32%. Interestingly, it only has one enoyl-ACP reductase (FabV). We would like to explore whether we can extend above hypothesis to *Y. pestis*. We synthesized two substrates that mimicked the intermediates from both the SFA and UFA biosynthesis pathways (**Figure 4.4**), and evaluated ypFabV catalysis efficiency for both of the two substrates. Consistent with the

observance in above bacteria, ypFabV can catalyze both unsaturated and saturated substrate with similar  $k_{cat}/K_m$  values (UFA/SFA), correlating with the high UFA percentage in its lipids.

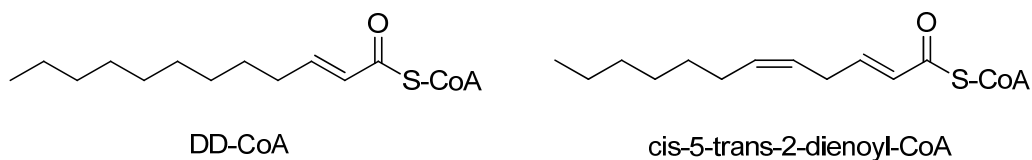


**Figure 4.4: Structure of DD-CoA and *cis-5-trans-2-dienoyl-CoA***

Kinetic parameters of ypFabV were measured and are shown in **Table 4.1**. The parameters of different enoyl-ACP reductases (ecFabI, ftuFabI, saFabI, bmFabI and bmFabV) and the percentage of monounsaturated fatty acids from the lipids of corresponding organism are also listed.

**Table 4.1: Kinetic parameters of enoyl-ACP reductases from different organism and their UFA content in the lipid**

<b>Enzymes</b>	<b>DD-CoA</b> $k_{cat}/K_m$ ( $\mu\text{M}^{-1}\text{s}^{-1}$ )	<b><i>cis-5-trans-2-</i></b> <b>dienoyl-CoA</b> $k_{cat}/K_m$ ( $\mu\text{M}^{-1}\text{s}^{-1}$ )	<b>Ratio<sup>c</sup></b>	<b>UFA% in</b> <b>each</b> <b>organism<sup>d</sup></b>
<b>ecFabI</b>	24 ± 6	8.4 ± 1.3	0.35	33
<b>ftuFabI</b>	570 ± 36	7.6 ± 0.6	0.013	1.2
<b>saFabI</b>	0.8 ± 0.1 <sup>a</sup>	Inactive <sup>a</sup>	0	Trace
<b>bmFabI</b>	300 ± 18	0.92 ± 0.06 <sup>b</sup>	0.003	32
<b>bmFabV</b>	497 ± 19 <sup>b</sup>	85 ± 3 <sup>b</sup>	0.17	
<b>ypFabV</b>	88	88	1	32

<sup>a</sup>Data measured by Dr. Hua Xu

<sup>b</sup>Data measured by Dr. Hao Lu

<sup>c</sup>Ratio= *cis-5-trans-2*-dienoyl-CoA / DD-CoA (  $k_{cat}/K_m$  values)

<sup>d</sup>Percentage of monounsaturated fatty acid obtained from (3, 164-167)

In summary, all of above data demonstrated that to have a high UFA content in cellular lipids, the enoyl-ACP reductase has to be capable of efficiently reducing the unsaturated intermediates in the UFA biosynthesis pathway. If there is only one enoyl-ACP reductase, either FabI or FabV, the only enoyl-ACP reductase will catalyze both unsaturated and saturated substrate efficiently. If there are two enoyl-ACP reductases, both FabI and FabV, FabI will serve as the enoyl-ACP reductase in SFA biosynthesis, while FabV competes with FabI to divert the intermediates to UFA biosynthesis.



### *Inhibition of ypFabV by diphenyl ethers.*

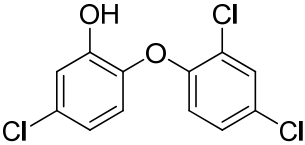
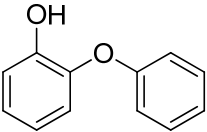
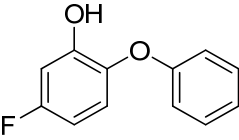
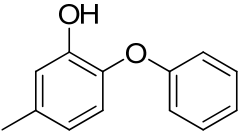
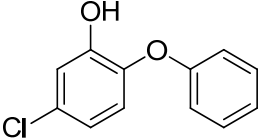
Triclosan is a potent inhibitor of FabI enzyme from a variety of organisms. Studies with the FabI enzymes from *E. coli* (9, 47, 120), *F. tularensis* (26) and *B. pseudomallei* (168) have revealed that triclosan is a slow-onset inhibitor. However, it is a rapid reversible inhibitor of InhA from *M. tuberculosis* with a  $K_i$  value of only 0.2  $\mu\text{M}$  (108) compared to  $K_i$  values of 5 pM, 50 pM and 1.5 nM for ecFabI, ftuFabI and bpmFabI-1, respectively (26, 46, 168). Rational structure-based drug discovery has successfully resulted in diphenyl ether-based inhibitors of InhA with improved affinity (48-50) that are slow-onset inhibitors of the enzyme (49). Because of our success in modifying diphenyl ethers to high-affinity slow-onset inhibitors of InhA, we would like to study the inhibition of ypFabV by diphenyl ethers.

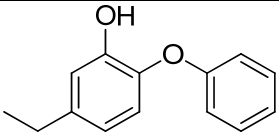
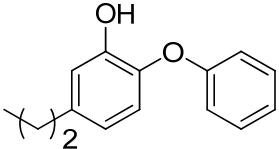
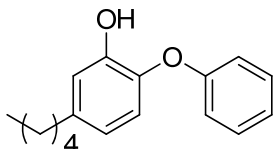
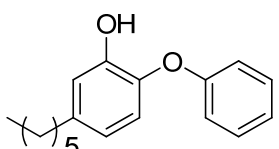
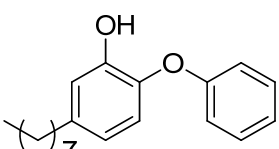
Previously, we reported that the electronic and steric properties of A-ring are essential for the binding affinity of triclosan analogues for InhA (50). To investigate the electronic effect, we replaced the chlorine atom with a stronger electron withdrawing group (fluorine) (**PT55**) and electron donating group (methyl group) (**PT53**). To investigate the steric effect, we replaced the chlorine with different lengths of alkyl groups to generate analogues (**PT01-05**, **PT07**). From previous InhA work, introduction of different function groups on B-ring can affect the binding affinity probably due to hydrophobic interactions or steric interactions between the substituent and enzyme (48-50). Therefore, we evaluated the enzyme inhibition activity of **PT52** with no substituent, **PT16-18** with amide group, **PT70** with methyl group.

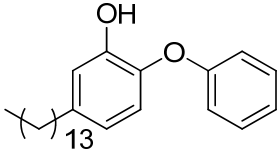
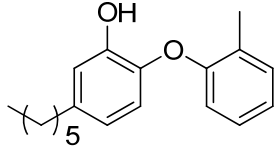
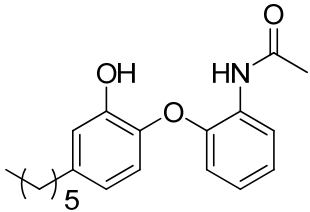
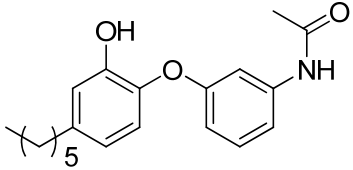
Enzyme inhibition data are summarized in **Table 4.2**. For all the compounds, the binding affinities were very weak, so we didn't measure their accurate  $\text{IC}_{50}$  values, but

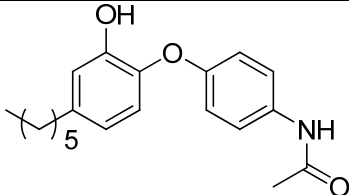
only measured their enzyme activity at 100  $\mu$ M inhibitor. In addition, previous research has shown that triclosan is a slow binding inhibitor of ecFabI with picomolar affinity (47). However, different from FabI, the study of ypFabV, same as bmFabV (31), shows triclosan and diphenyl ethers are rapid reversible inhibitors of FabV. So we conclude that diphenyl ether is not a good scaffold for ypFabV. In addition, this *in vitro* inhibition data is consistent with MIC values of *Y. pestis* (**Table 4.2**).

**Table 4.2: Inhibition of triclosan and Its Analogues for ypFabV and bmFabV**

		ypFabV (15 nM)	bmFabV <sup>a</sup>	<i>Y. pestis</i> ( $\mu\text{g/mL}$ )
#	Inhibitor	activity %  at 100 $\mu\text{M}$	$K_i$ ( $\mu\text{M}$ )	MIC
PT54		54 %	$0.42 \pm 0.02$	
<b>Modification of A-ring at 5-position</b>				
PT51		94%	$12.8 \pm 0.5$	>40
PT55		64 %	$5.3 \pm 0.3$	>40
PT53		62 %	$3.7 \pm 0.1$	
PT52		60%	$1.1 \pm 0.1$	>40

#	Inhibitor	ypFabV (15 nM) activity % at 100 $\mu$ M	bmFabV <sup>a</sup> K <sub>i</sub> ( $\mu$ M)	<i>Y. pestis</i> ( $\mu$ g/mL) MIC
PT01		72 %	0.28 $\pm$ 0.02	>40
PT02		56%	0.19 $\pm$ 0.01	20-40
PT03		61 %	0.11 $\pm$ 0.01	>40
PT04		70 %	1.6 $\pm$ 0.1	>40
PT05		74 %	6.2 $\pm$ 0.2	

#	Inhibitor	ypFabV (15 nM) activity % at 100 $\mu$ M	bmFabV <sup>a</sup> K <sub>i</sub> ( $\mu$ M)	<i>Y. pestis</i> ( $\mu$ g/mL) MIC
PT07		82 %	N/A	
<b>Modification of B-ring at <i>ortho</i>-, <i>meta</i>- or <i>para</i>-position</b>				
PT70		81 %	N/A	>40
PT16		88 %	3.9 $\pm$ 0.5	
PT17		100 %	No inhibition at 30 $\mu$ M	

#	Inhibitor	ypFabV (15 nM)	bmFabV <sup>a</sup>	<i>Y. pestis</i> ( $\mu\text{g/mL}$ )
		activity %  at 100 $\mu\text{M}$	$K_i$ ( $\mu\text{M}$ )	MIC
PT18		89%	3.3 $\pm$ 0.4	

<sup>a</sup> Data is from Dr. Hao Lu

To study the reason for weak binding affinity, apo-ypFabV was crystallized by Maria Hirschbeck in Dr. Caroline Kisker group in Rudolf Virchow Center for Experimental Biomedicine, Institute for Structural Biology University of Wurzburg, then compared with ecFabI-NAD<sup>+</sup>-triclosan structure. In the structure of ternary complex ecFabI-NAD<sup>+</sup>-triclosan, there are several important interactions: hydrogen bonds are formed between the inhibitor A-ring hydroxyl group and Tyr156, and a hydrogen bonding network is formed between the 2'-hydroxyl group of NAD<sup>+</sup> and Lys163. A  $\pi$ - $\pi$  stacking interaction between the A-ring of triclosan and the nicotinamide ring of NAD<sup>+</sup> further stabilizes the conformation of the inhibitor. The A-ring chlorine of triclosan extends into the hydrophobic environment of the substrate binding cavity and forms hydrophobic interactions with residues Tyr146 and Tyr156. A-ring chlorine also forms an

edge-on  $\pi$  interaction with the aromatic ring of Phe203. Additionally, hydrophobic interactions are formed between the two phenyl rings of the inhibitor and amino acids Ala196, Ile200, and Ala197 of the substrate-binding loop. B-ring *ortho*-Cl forms hydrophobic interactions with Ala196 at a distance of 3.5 Å, B-ring interacts with Ile200 at a distance of 4.0 Å. A-ring interacts with Ala197 at a distance of 3.9 Å. A-ring and B-ring forms hydrophobic interactions with Ile200 at a distance of 3.9 Å and 3.5 Å, respectively.

According to the protein sequence alignment, most of the residues which play a key role in inhibitor binding with ecFabI are conserved in FabV; however, Ala197 and Phe203 in ecFabI are replaced by Ser and Met, respectively. These amino acid replacements, from Ala to Ser with polar side chain and from Phe to Met without phenyl ring, may greatly affect the inhibitor binding. In addition, because of the beta hairpin loop (Pro142-Ser155) (**Figure 4.5B**) pointing out of the binding pocket, some of the hydrophobic interaction partners (Ile92-Ala95) (**Figure 4.5A**) of the B-ring of the inhibitors are missing. This might also affect the triclosan binding.

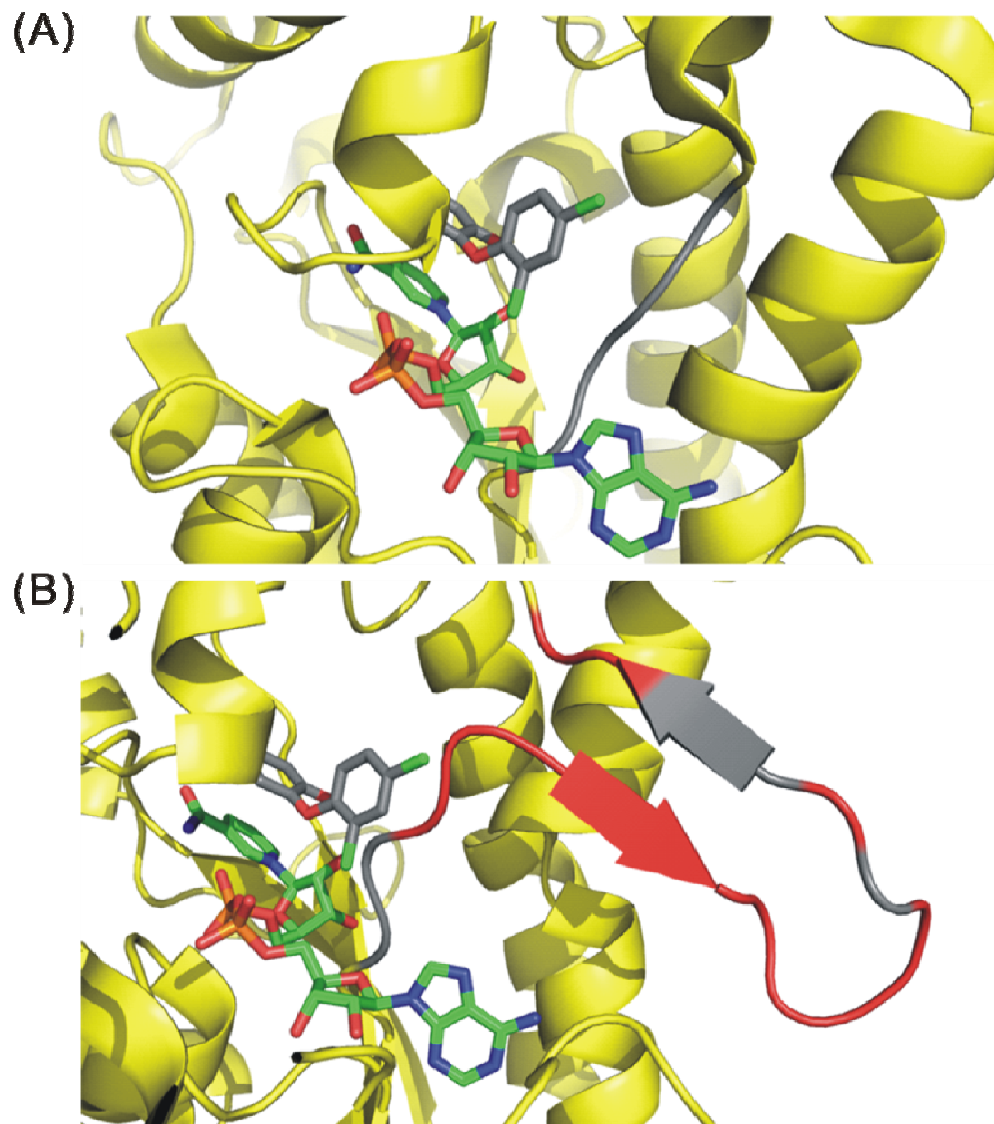


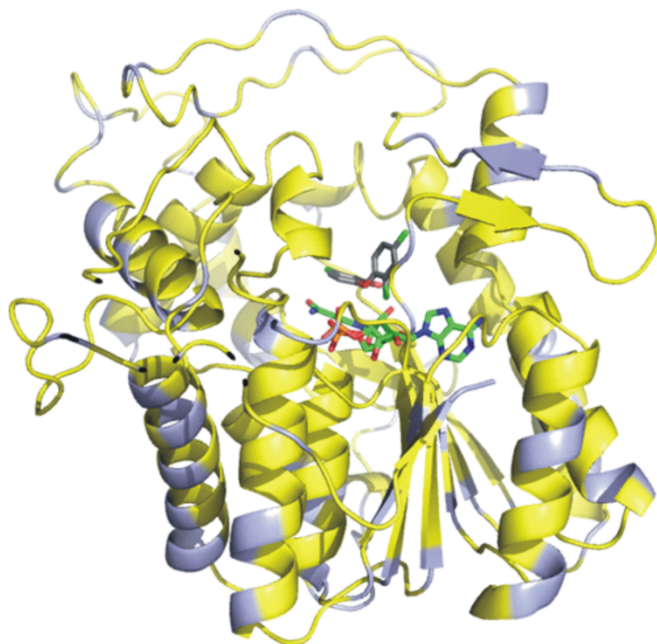
**Figure 4.5: ecFabI and apo-ypFabV structures comparison.**

(A) Structures of triclosan (gray molecule) in complex with NAD<sup>+</sup> (green molecule) and *E. coli* FabI (1QSG.pdb). Ile92-Ala95 are hydrophobic residues, labeled in gray. (B) apo-ypFabV structure was overlapped with structure of triclosan bound to ecFabI (1QSG.pdb). Pro142-Ser155, hydrophobic residues are labeled in gray, hydrophilic residues are labeled in red.



Interestingly, diphenyl ethers have much lower binding affinity with bmFabV (**Table 4.2**), which is 75% identical and 84% similar to ypFabV. To explain ypFabV resistance, we speculate even their protein sequence is very similar; their crystal structure may be different, especially at some important residues for inhibitor binding. In ypFabV, most residues which are not conserved in bmFabV, in light blue (**Figure 4.6A**), are far away from the inhibitor binding site. However, Leu139 and Ser141 in ypFabV (**Figure 4.6B**), which are replaced by Val and Ala in bmFabV, respectively, are closely adjacent to NAD<sup>+</sup> and triclosan binding site. Consequently, we speculate these two residues, especially Ser141, may leads to unfavorable interaction and weak binding between ypFabV and diphenyl ethers. In future, we can compare crystal structure of both ypFabV and bmFabV to further explore it.

(A)



(B)

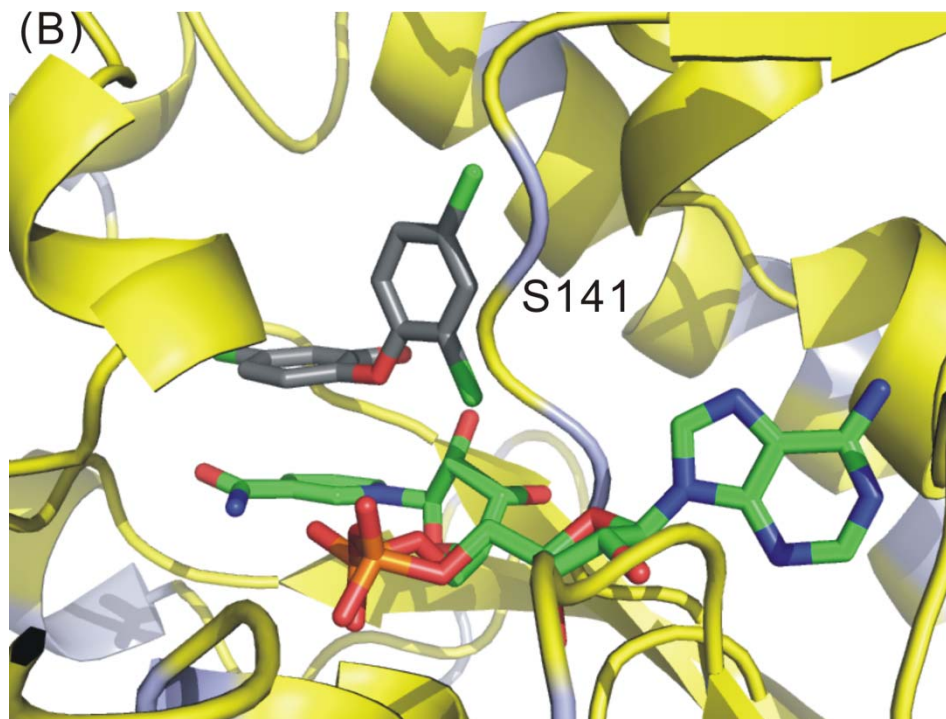


**Figure 4.6: apo-ypFabV structure.**

(A) apo-ypFabV structure was overlapped with structure of triclosan bound to ecFabI (1QSG.pdb). Residues which are not conserved in bmFabV are in light blue. (B) Zoom-in crystal structure of inhibitor binding site.

## Conclusion

In summary, the FabV among various bacteria have shown high conservation of active site residues. Steady-state kinetics analysis has also demonstrated that ypFabV catalyzes the reduction of enoyl-ACP substrates through an ordered Bi Bi mechanism in which NADH binds first to the enzyme.

FabV, as the only enoyl ACP reductase FabV in *Y. pestis*, will be a good drug target. However, diphenyl ethers are not promising leads for developing potent FabV inhibitors. In future, we can identify lead inhibitor from high throughput screening.

Since there is only one enoyl ACP reductase FabV, *Y. pestis* is a good example to study the FabV activity *in vivo*, for example, the possibility of thermal control of lipid fluidity by changing UFA/SFA ratio, which is regulated by the enoyl-ACP reductase activity toward saturated and unsaturated substrates.

## Chapter 5 : Identification of putative *trans*-2, *cis*-3-decenoyl-CoA isomerase in *Burkholderia mallei*

### Introduction

#### *Bacterial Unsaturated Fatty Acid (UFA) Biosynthesis*

The cell membrane physically separates the intracellular components from the extracellular environment. It is semi-permeable and able to regulate what enters and exits the cell, thus facilitating the transport of materials needed for survival. This function is dependent on the physical state of lipid bilayers in the cell membrane (169). At the physiological temperature, the bilayers of most organisms are entirely or mostly fluid. However, at lower temperature, membrane lipid bilayers undergo a reversible change from fluid (disordered) to nonfluid (ordered) array of fatty acid acyl chains (170, 171).

Unsaturated fatty acids (UFAs) exhibit steric hindrance due to the rigid kink of *cis* double bond in the phospholipid acyl chains, thus UFAs cannot pack as tightly as saturated fatty acids (SFAs) (**Figure 5.1**) (172). UFAs' characteristics allow them to have lower transition temperature than SFAs, which is the temperature at the midpoint between the fluid and non-fluid states. The membrane lipid fluidity seems to be controlled by incorporation of more UFAs as the temperature decreases (173). In most bacteria, the dominant forms of UFAs (C16:1 *cis*-9 acid, C18:1 *cis*-9 acid and C18:1 *cis*-11 acid) are the straight-chain monounsaturated fatty acids predominately with 16 and 18 carbon chain lengths.

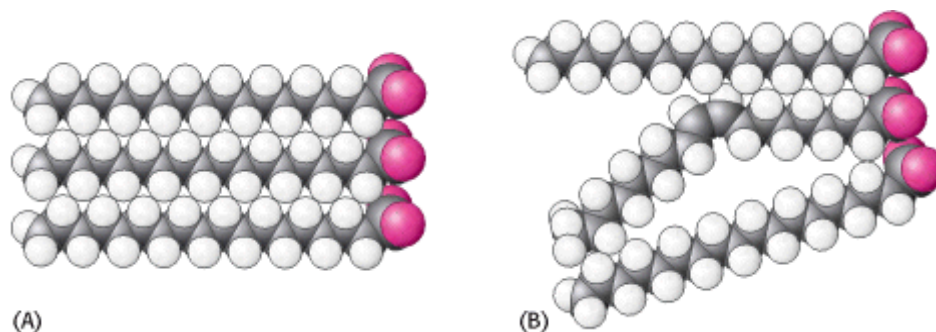


**Figure 5.1: Packing of fatty acid chains in a membrane.**

The space-filling model shows the packing of **(A)** three molecules of stearic acid (C18:0) and **(B)** a molecule of oleic acid (C18:1 cis-9) between two molecules of stearic acid. The highly ordered packing of fatty acid chains is disrupted by the presence of *cis* double bond (173).

Eukaryotes (174) and some bacteria, such as *Pseudomonas aeruginosa* (175) and cyanobacteria (176), have completely separate systems for the synthesis of SFAs and UFAs. UFAs are synthesized from SFAs by fatty acid desaturases (DesA or DesB) that convert single bonds to double bonds through O<sub>2</sub>-dependent desaturation reactions (177). DesA desaturates acyl chains of the membrane bilayer phospholipids, whereas DesB desaturates acyl chains of CoA substrates (**Figure 5.2**) (176, 178-183).

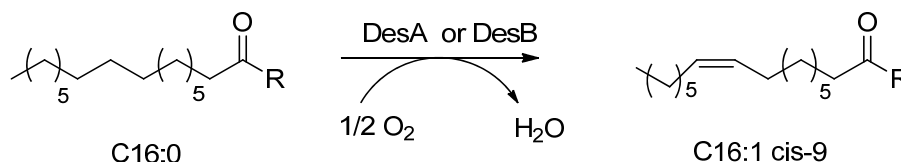


**Figure 5.2: A generalized desaturase pathway.**

For DesA and DesB, the R group would be the 1-acyl-lisophospholipid moiety of a phospholipid molecule and CoA, respectively.

An alternative UFA biosynthesis pathway was identified when Knorad Bloch became interested in how anaerobically growing bacteria synthesize UFAs. Bloch and his coworkers found both obligate (Clostridia) and facultatively anaerobic bacteria (*E. coli*) contain two dominant UFAs: palmitoleic acid (C16:1 *cis*-9 acid) and *cis*-vaccenic acid (C18:1 *cis*-11 acid) (169). They concluded that there must be an O<sub>2</sub>-independent UFA biosynthesis pathway. The mechanism of this O<sub>2</sub>-independent UFA biosynthesis pathway was elucidated with the  $\gamma$ -proteobacterium *E. coli* as the prototype of such pathways (170, 184). In this pathway, synthesis of UFA requires three enzymes, FabA, FabB and FabF (**Figure 5.3 A**).

FabA is a bifunctional key enzyme in both SFA and UFA biosynthesis pathway. It catalyzes dehydration and isomerization of  $\beta$ -hydroxydecanoyl-ACP, and produces *trans*-2-decenoyl-ACP (the starting point of SFA biosynthesis) and *cis*-3-decenoyl-ACP (the starting point of UFA biosynthesis) (9, 185). *Cis*-3-decenoyl-ACP cannot be reduced by the *trans*-2-enoyl-ACP reductase, the subsequent enzyme in SFA biosynthesis (184, 186). Therefore, it directly enters a condensation reaction catalyzed by  $\beta$ -ketoacyl synthase in UFA biosynthesis.

$\beta$ -ketoacyl transferases, FabB and FabF, catalyze the condensation of a wide range of long-chain acyl-ACPs (187). FabB is responsible for a condensation reaction that cannot be catalyzed by FabF, namely, elongation of *cis*-3-decenoyl-ACP, a rate-limiting step in UFAs synthesis (188). FabF is required to convert the C16 to C18 unsaturated species (189), and plays an essential role in the thermal regulation of fatty acid composition (190, 191).

Recently, the flood of sequenced bacterial genomes shows that only  $\alpha$ - and  $\gamma$ -proteobacteria have *fabA* and *fabB* homologues (9). A bioinformatics analysis of the genome sequence of *Streptococcus pneumonia*, a Bacillus shaped bacterium, shows it does not have homologues of either *fabA* or *fabB*, even though it produces significant amount (35%) of monounsaturated fatty acids. Rock and his coworkers supported the existence of an alternative O<sub>2</sub>-independent UFA biosynthesis pathway (186). In this new pathway, *fabM* in the FAS-II pathway gene cluster encodes a *trans*-2, *cis*-3-decenoyl-ACP isomerase (FabM) (**Figure 5.3B**). It carries out the isomerization of *trans*-2-decenoyl-ACP to *cis*-3-decenoyl-ACP, but it is not capable of catalyzing the dehydration of  $\beta$ -hydroxydecanoyl-ACP.

Interestingly, Zhang and coworkers found that *Pseudomonas aeruginosa*, a  $\gamma$ -proteobacterium, had one O<sub>2</sub>-independent (FabA/ FabB) (192) and two O<sub>2</sub>-dependent (DesA and DesB) UFA pathways (175). Therefore, to synthesize the major UFAs (C16:1 *cis*-9 acid, C18:1 *cis*-9 acid and C18:1 *cis*-11 acid), bacteria may utilize more than one UFA biosynthesis pathway.

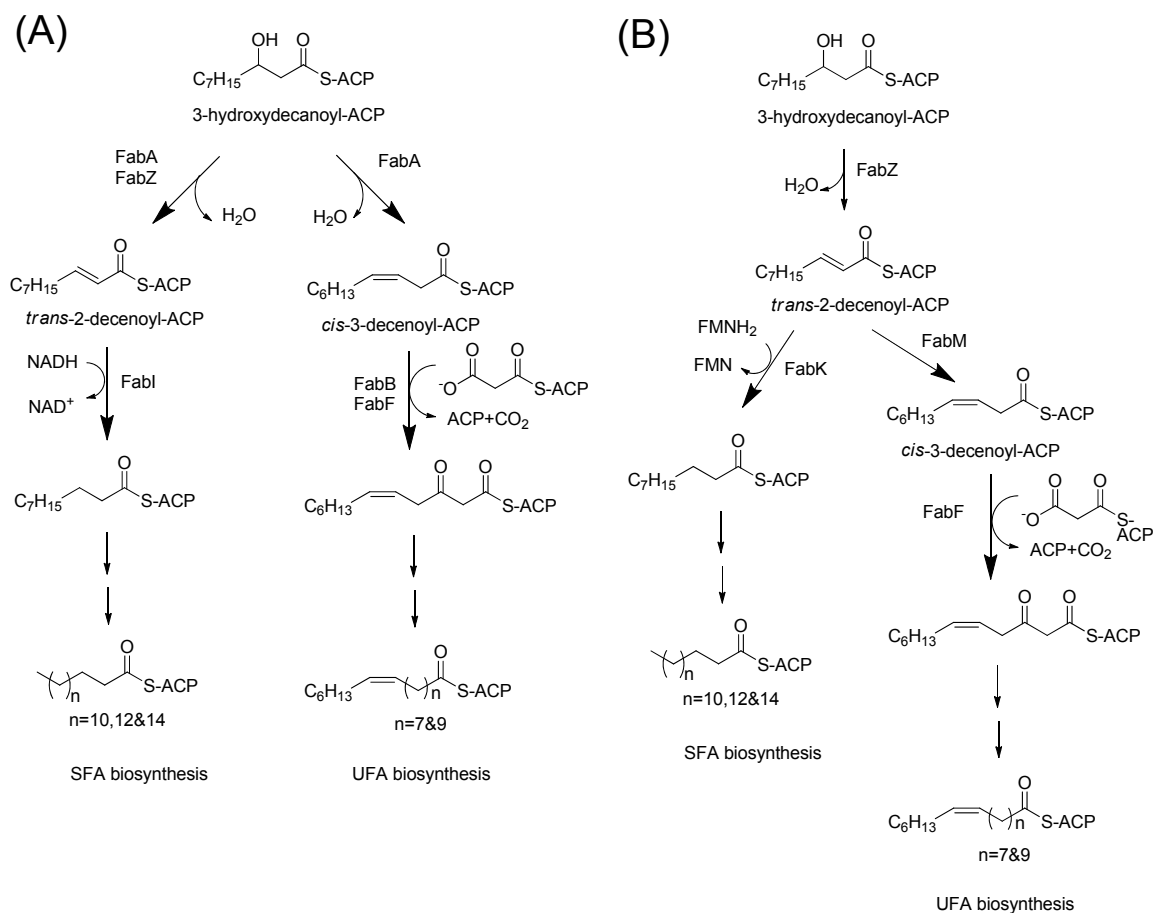


**Figure 5.3: Saturated and unsaturated fatty acid biosynthesis pathways in *E. coli* and *S. pneumoniae*.**

(A) SFA and UFA biosynthesis pathways in *E. coli* (29); (B) SFA and UFA biosynthesis pathways in *S. pneumoniae* (34, 186).



### *Putative trans-2, cis-3-Decenoyl-CoA Isomerase (FabM) in B. mallei*

Like other  $\beta$ -proteobacteria, *B. mallei* does not have *fabA* and *fabB* homologue in its genome (186). Yet this organism produces a high amount (32%) of unsaturated fatty acids. It is interesting to identify the enzyme(s) responsible for UFAs biosynthesis pathways in *B. mallei*. By BLAST analysis, Dr. Hao Lu speculated that *bmaa0541* might encode the *trans-2, cis-3-decenoyl-CoA* isomerase (FabM), which may be in UFA biosynthesis pathway in *B. mallei*.

FabM was first identified to be involved in UFA biosynthesis pathway in *S. pneumonia* by Rock and his coworkers (186). It is biochemically characterized as *trans-2, cis-3-decenoyl-ACP* isomerase (**Figure 5.3B**). The *in vitro* reconstituted fatty acid synthase assay and mass spectrometry analysis indicated that FabM was capable of isomerizing *trans-2-decenoyl-ACP*. And a direct assay with substrate analogue, *N*-acetylcysteamine thioesters (NAC thioesters), showed that FabM alone is capable of catalyzing the isomerization of enoyl-thioesters.

### *Crotonase Superfamily*

The *bmaa0541* is a member of the crotonase superfamily. This superfamily is known to catalyze a wide range of reactions (193). Several enzymes in this family are well studied, such as enoyl-CoA hydratase (crotonase) (194), methylmalonyl-CoA decarboxylation (195), 1,4-dihydroxy-2-naphthoyl-CoA synthase (65), 4-chlorobenzoyl-CoA dehalogenase (196, 197) and  $\Delta^{3,2}$ -enoyl-CoA isomerase (198, 199) (**Figure 5.4**). The wide varieties of chemistry represented by this family are catalyzed by enzymes

divergent in amino acid sequence but closely related overall structure. In all known structure of this family crystallized with substrate analogues, the carbonyl oxygen atom of the thioester on the substrate is bound in an oxyanion hole, which activates the substrate for the conversion catalyzed by the active-site residues of the respective enzymes.

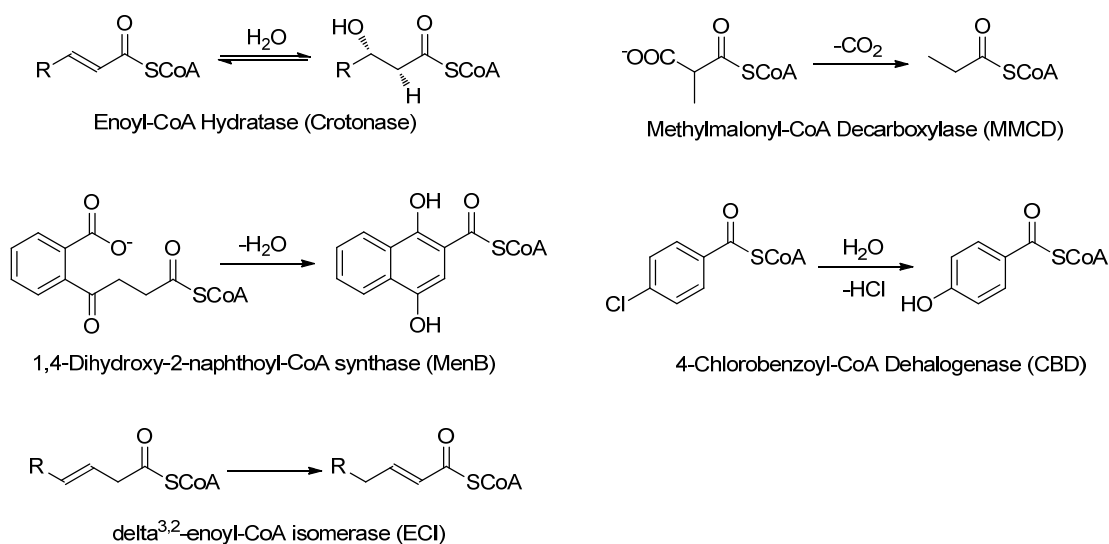


**Figure 5.4: Reactions catalyzed by members of the crotonase superfamily.**

Crotonase superfamily can catalyze various reactions, for example, hydration, decarboxylation, Dieckmann condensation, dehalogenation and isomerization.

*Project Goals*

We hypothesized that the *bmaa0541* gene encoded the FabM in *B. mallei*. Its function and catalytic mechanism will be explored based on previous study on the crotonase superfamily.

## Materials and Methods

### *Cloning, Expression, and Purification of the bmaa0541*

The *bmaa0541* gene was identified from *B. mallei* genome through BLAST sequence alignment using the *S. pneumoniae* FabM as bait. It was amplified from *bmaa0541*-pBAD *Myc/His C* plasmid (made by Dr. Hao Lu) with the following primers (Integrated DNA Technologies) 5'-GGAATTCCATATGTCCTACCAGACGATTCGCATC-3' (forward) and 5'-CGCGGATCCTCAGCGTCCTTCGAAGCGAGG-3' (reverse). The PCR product was digested with NdeI and BamHI-HF, and then inserted into the pET15b plasmid (Novagen) so that a His-tag was encoded at the N-terminus of the coding sequence for the protein. The correct sequence of the constructed plasmid was confirmed by the DNA sequencing (DNA Sequencing Facility, Health Science Center, Stony Brook University).

Protein expression was performed using the *E. coli* strain BL21 (DE3) cell. After transformation, a single colony was used to inoculate 10 mL of LB media containing 0.2 mg/mL of ampicillin, which was then incubated overnight at 37 °C. The overnight culture was used to inoculate 1 L of LB media containing 0.2 mg/ml of ampicillin, and incubated at 37 °C until the optical density at 600 nm (O.D. 600) increased to around 1.0. Protein expression was induced by the addition of 1.0 mM IPTG and the culture was then shaken at 25 °C for 16h. Cells were harvested by centrifugation at 5,000 rpm for 20 min at 4 °C. The cell pellet was resuspended in 30 mL of binding buffer (5 mM imidazole, 0.5 M NaCl, 20 mM Tris-HCl, pH 7.9) and was lysed by 3 passages through a French Press cell (1,000 psi). The cell lysate was ultracentrifuged at 33,000 rpm for 1 hour at 4

°C to pellet the cell debris and the supernatant was then loaded onto a His-bind column (1.5 cm × 15 cm) which contained 4 mL of His-bind resin (Novagen) charged with charging buffer (50 mM Ni<sub>2</sub>SO<sub>4</sub>). The column was equilibrated with binding buffer. Then 60 mL of binding buffer (5 mM imidazole, 0.5 M NaCl, 20 mM Tris-HCl, pH 7.9) was used to wash the column. After that, 60 mL of wash buffer (60 mM imidazole, 0.5 M NaCl, 20 mM Tris-HCl, pH 7.9) was used to wash the column. Finally, the protein was eluted with 30 mL of eluent buffer (1M imidazole, 0.5 M NaCl, 30 mM Tris-HCl, pH 7.9). The fractions containing protein were collected and loaded onto a Sephadex G-25 chromatography (1.5 cm × 55 cm) to remove imidazole using PIPES buffer (30 mM PIPES, 150 mM NaCl and 1 mM EDTA, pH 8.0) as the eluent. The purity of the protein was shown to be >95% by 12% SDS-PAGE, which gave an apparent molecular mass of ~28 kDa. The concentration of the protein was measured by obtaining the A<sub>280</sub> using an extinction coefficient (ε) of 21,030 M<sup>-1</sup>cm<sup>-1</sup> calculated from the primary sequence. The final concentrated protein was flash frozen and stored at -80 °C.

#### *Cloning, Expression and Purification of the bmaa0541 Mutants*

The bmaa0541 mutants D145E and D145N were prepared using Quikchange site-directed mutagenesis with the following primers (**Table 5.1**). The procedure for the expression and purification of mutants was used as described for wild-type bmaa0541.

**Table 5.1: Nucleotide primers**

Name	Sequence
D145E forward	5' CCTCGTTCCGGAATCCGGCGGCACG 3'
D145E reversed	5' CGTGCCGCCGGATTCCGGAACGAGG 3'
D145N forward	5' GGCCTCGTTCCGAATCCGGCGGCAC3'
D145N reversed	5' GTGCCGCCGGAATTCGGAACGAGGCC 3'

*Synthesis of trans-2-Decenoyl-CoA and cis-3-Decenoyl-CoA.*

*Cis-3-decenoic acid* was synthesized by Dr. Gopal Reddy in our lab. According to the modified anhydride method, *trans-2-decenoyl-CoA* and *cis-3-decenoyl-CoA* was synthesized with *trans-2-dodecenoic acid* and *cis-3-decenoic acid*, respectively (**Figure 5.5**) (27). Both ESI-MS ( $[M - H]^-$ ) calcd for  $[C_{31}H_{53}N_7O_{17}P_3S]^-$ : 918.7, found: 918.7.

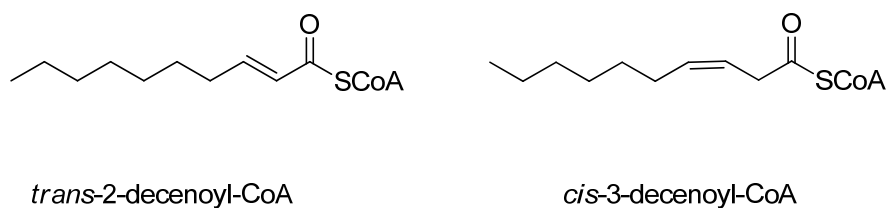


**Figure 5.5: Structure of *trans-2-decenoyl-CoA* and *cis-3-decenoyl-CoA*.**

### *Preparation of trans-2-Decenoyl-ecACP and cis-3-Decenoyl-ecACP*

The protein product of the ORF b1094, which encodes the putative acyl carrier protein (ACP) in *E. coli*, is 74% identical to the ACP from *B. mallei* ATCC 23344. *ecACP* was cloned into the pET-23b plasmid (Novagen) and placed in frame with a C-terminal His-tag sequence by Carla Neckles.

*ecACP* was expressed in BL21(DE3)*plysS* cells. Transformed cells were induced with 0.5 mM isopropyl- $\beta$ -D-thiogalactopyranoside (IPTG) at an OD<sub>600</sub> of 0.8 and harvested by centrifugation after shaking for 10 h at 18 °C. The cell pellet was resuspended in 30 mL of His-binding buffer (5 mM imidazole, 0.5 M NaCl, 20 mM Tris HCl, pH 7.9) and lysed by sonication. Cell debris was removed by centrifugation at 33,000 rpm for 60 min at 4 °C. *ecACP* was purified using His affinity chromatography: the supernatant was loaded onto a His-bind column (1.5 cm x 15 cm) containing 4 mL of His-bind resin (Novagen) that had been charged with 9 mL of charge buffer (50 mM Ni<sub>2</sub>SO<sub>4</sub>). The column was washed with 60 mL of His-binding buffer and 30 mL of wash buffer (60 mM imidazole, 0.5 M NaCl, 20 mM Tris HCl, pH 7.9). Subsequently, the protein was eluted using 20 mL elute buffer (500 mM imidazole, 0.5 M NaCl, 20 mM Tris HCl, pH 7.9). Fractions containing *ecACP* were collected and the imidazole removed by dialysis in storage buffer (20 mM Tris HCl, pH 7.0). The concentration of *ecACP* was determined by measuring the absorption at 280 nm using an extinction coefficient of 1,280 M<sup>-1</sup>cm<sup>-1</sup> calculated from the primary sequence. The protein was analyzed by SDS-PAGE which showed a dominant band of 8.6 kDa. The enzyme was concentrated by using Centricon-3 (Amicon) and stored at -80 °C.

Subsequently, 25  $\mu\text{M}$  of ecACP was incubated with 75  $\mu\text{M}$  *cis*-3-decenoyl-CoA or *trans*-2-decenoyl-CoA, 1 mM dithiothreitol (DTT) and 1  $\mu\text{M}$  Sfp in 75 mM Tris HCl, 10 mM  $\text{MgCl}_2$ , pH 7.5 buffer for 2h at 37°C. *cis*-3-decenoyl-ecACP and *trans*-2-decenoyl-ecACP were purified by MonoQ 5/50 strong anion exchange column on the ÄKTA Purifier. Chromatography was performed with 20 mM Tris HCl, pH 7.0 as buffer A and 20 mM Tris HCl, 800 mM NaCl, pH 7.0 as buffer B over 25 min at a flow rate of 1 mL/min. Fractions containing *cis*-3-decenoyl-ecACP and *trans*-2-decenoyl-ecACP were pooled, concentrated, and loaded onto Sephadex G-75 size exclusion chromatography to separate isoforms and byproducts from the desired product and exchange product to buffer A.

#### *Enzymatic Activity of the bmaa0541*

A solution containing 100  $\mu\text{M}$  of *trans*-2-decenoyl-CoA or *cis*-3-decenoyl-CoA or 30  $\mu\text{M}$  of *trans*-2-decenoyl-ACP or *cis*-3-decenoyl-ACP in 10 mM potassium phosphate buffer (pH 7.0) was placed in a cuvette. 600 nM bmaa0541 was added to initiate the reaction. The isomerase activity was measured using a Cary 300 Bio (Varian) spectrophotometer to monitor the absorbance changing at 263 nm ( $\epsilon = 6,700 \text{ M}^{-1}\text{cm}^{-1}$ ) (186).

## Results and Discussion

### *Putative UFAs Biosynthesis Pathways in B. mallei*

Since there are four UFA biosynthesis pathways, which are two desaturases dependent on molecular O<sub>2</sub> and the two UFA biosynthesis pathways independent of molecular O<sub>2</sub>, and they can potentially coexist as combinations, it is difficult to predict how many and which UFA biosynthesis pathways *B. mallei* may utilize. We speculate that the type of UFA biosynthesis pathway that is present may be related to the growth condition (with or without O<sub>2</sub>), and the percentage of UFA that is present.

The availability of bacterial genome sequence allowed us to find the enzyme(s) homologues responsible for different UFA biosynthesis pathways. Here we used the sequences of FabA from *E. coli*, FabM from *S. pneumonia* and DesA and DesB from *P. aeruginosa* as the query sequence for a BLAST analysis of proteins encoded in different bacterial genomes. In addition, the growth condition and the percentage of UFA were also summarized in **Table 5.2** and **Table 5.3**.

Unfortunately, we can only conclude that anaerobic bacteria do not have the O<sub>2</sub>-dependent UFA biosynthesis pathway. Interestingly, aerobic bacteria, such as *P. aeruginosa* and *E. coli*, can have O<sub>2</sub>-independent UFA biosynthesis pathway. Beside these, we cannot observe any correlation between growth conditions and the UFA biosynthesis method or correlation between the amount of UFA and the number of UFA synthesis pathways. Therefore, based on the UFA utilization pattern in other bacteria, it is hard to predict the pattern in *B. mallei*.

However, BLAST analysis showed that in *B. mallei* an ORF (*bmaa0541*) encodes an enzyme that is 31% identical and 50% similar to FabM from *S. pneumoniae*, and an



ORF (*bma2237*) encodes an enzyme that is 54% identical and 71% similar to DesA from *P. aeruginosa*, suggesting the existence of putative FabM and DesA homologues in *B. mallei* (**Table 5.3 and Figure 5.6**). Therefore, we speculate that *B. mallei* may utilize the FabM/FabF O<sub>2</sub>-independent pathway as in *S. pneumonia*, and the DesA O<sub>2</sub>-dependent pathway as in *P. aeruginosa*.

**Table 5.2: UFA synthesis pathway and UFA content in the lipid in different bacteria**

Bacteria <sup>a</sup>	Class <sup>d</sup>	UFA synthesis pathway				UFA% <sup>i</sup>	Ref
		With O <sub>2</sub>		Without O <sub>2</sub>			
		DesA	DesB	FabA/B	FabM/F		
<b>Aerobic<sup>b</sup></b>							
<i>P. aeruginosa</i>	γ <sup>e</sup>	●	●	●	○	45%	(200)
<i>C. hominis</i>	γ	-	-	○	-	44%	(201)
<i>B. mallei</i>	B <sup>f</sup>	○	-	-	○	32%	(202)
<i>B. cereus</i>	B <sup>g</sup>	-	○	○	○	17%	(203)
<i>F. tularensis</i>	γ	-	-	○	-	1.2%	(204)
<i>B. sphaericus</i>	B	-	-	○	-	trace	(205)
<i>E. corrodens</i>	β	-	-	○	-	50%	(201)
<i>E. coli</i>	γ	-	○	●	-	33%	(165)
<i>E. faecalis</i>	B	-	-	●	-	28%	(203)
<i>S. enteritidis</i>	γ	-	-	○	-	21%	(165)
<i>L. monocytogenes</i>	B	-	-	○	-	2.1%	(165)

<i>S. aureus</i>	B	-	-	○	-	trace	(165)
<b>Anaerobic<sup>c</sup></b>							
<i>S. pneumoniae</i>	B	-	-	-	●	35%	(206)
<i>C. thermocellum</i>	C <sup>h</sup>	-	-	○	-	trace	(207)
<i>Y. pestis</i>	γ	-	-	○	-	32%	(167)

<sup>a</sup> Bacteria's full name: *P. aeruginosa*: *Pseudomonas aeruginosa*, *C. hominis*: *Cardiobacterium hominis*, *B. mallei*: *Burkholderia mallei*, *B. cereus*: *Bacillus cereus*, *F. tularensis*: *Francisella tularensis*, *B. sphaericus*: *Bacillus sphaericus*, *S. pneumonia*: *Streptococcus pneumonia*, *C. thermocellum*: *Clostridium thermocellum*, *E. corrodens*: *Eikenella corrodens*, *E. coli*: *Escherichia coli*, *Y. pestis*: *Yersinia pestis*, *E. faecalis*: *Enterococcus faecalis*, *S. enteritidis*: *Salmonella enterica enterica*, *L. monocytogenes*: *Listeria monocytogenes*, *S. aureus*: *Staphylococcus aureus*

<sup>b,c</sup> Bacteria growth condition for UFA% measurement

<sup>d</sup> Scientific classification

<sup>e</sup> Kingdom: Bacteria, Phylum: Proteobacteria, Class: γ Proteobacteria

<sup>f</sup> Kingdom: Bacteria, Phylum: Proteobacteria, Class: β Proteobacteria

<sup>g</sup> Kingdom: Bacteria, Phylum: Firmicutes, Class: Bacilli

<sup>h</sup> Kingdom: Bacteria, Division: Firmicutes, Class: Clostridia

● Existence of this pathway is published

- No homologue is found through BLAST

○ Putative homologue is found through BLAST

<sup>i</sup> Percentage of major straight-chain monounsaturated fatty acids: C16:1 cis-9 acid, C18:1 cis-9 acid and C18:1 cis-11 acid.

**Table 5.3: Putative UFA biosynthesis genes in *B. mallei* genome**

	<b>Bait</b>	<b>Putative gene in <i>B. mallei</i></b>	<b>Identity</b>	<b>Similarity</b>
<b>O<sub>2</sub>-dependent pathway</b>				
<i>P. aeruginosa</i>	DesA (PA0286)	<i>bma2237</i>	211/389 (54%)	277/389 (71%)
	DesB (PA4888)	--- <sup>a</sup>	--- <sup>a</sup>	--- <sup>a</sup>
<b>O<sub>2</sub>-independent pathway</b>				
<i>E. coli</i>	FabA (b0954)	--- <sup>a</sup>	--- <sup>a</sup>	--- <sup>a</sup>
	FabB (b2323)	<i>bma0534</i>	158/412 (38%)	227/412 (55%)
<i>S. pneumoniae</i>	FabM (SPG_0381)	<i>bmaa0541</i>	91/252 (36%)	141/252 (55%)
	FabF (SPG_0388)	<i>bma0534</i>	177/411 (43%)	250/411 (60%)

<sup>a</sup> no homologue is found through BLAST.

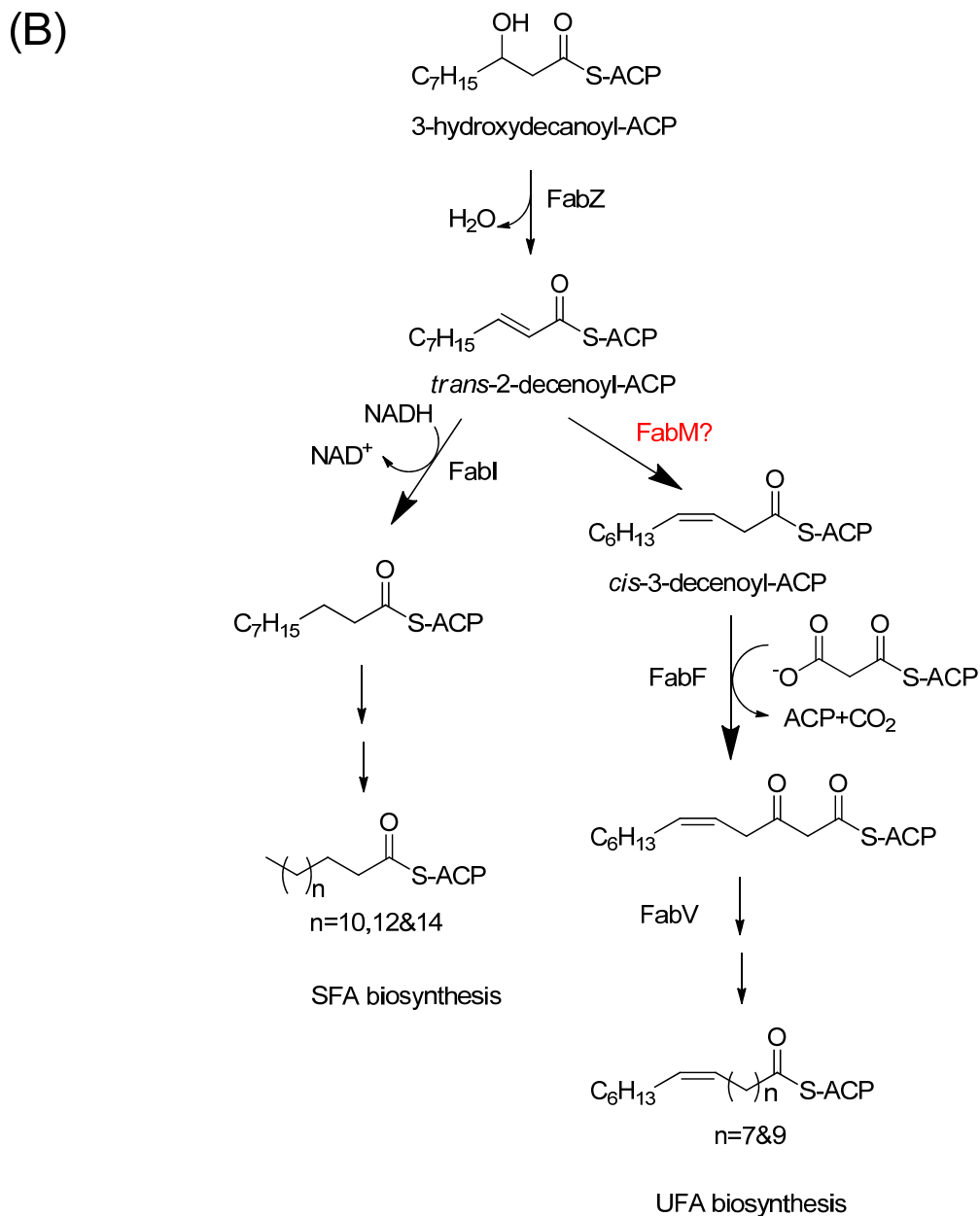
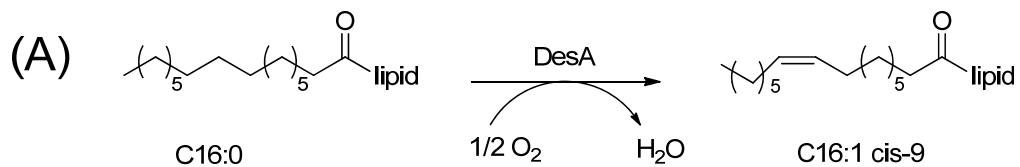
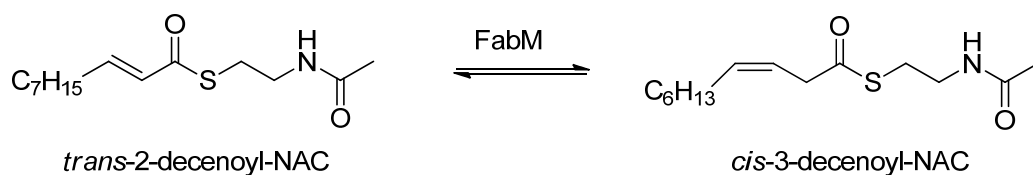


Figure 5.6: Proposed (A) SFA and (B) UFA biosynthesis pathway in *B. mallei*.

### *In vitro* Activity of the Putative *trans*-2, *cis*-3-enoyl-ACP Isomerase (FabM)

In several bacteria, including *B. mallei*, the enzymes involved in fatty acid biosynthesis are highly specific for ACP substrates, but in many cases these enzymes can utilize substrate analogues in biochemical assays, such as acyl-CoA and acyl-NAC, which have similar  $k_{\text{cat}}/K_m$  values (25), (14, 25, 26, 168, 208). These substrate analogues are significantly easier to synthesize and purify compared to the corresponding acyl-ACPs. In addition, it was previously shown that FabM from *S. pneumoniae* can catalyze the isomerization of the substrate analogue *trans*-2-decenoyl-NAC. The conversion of *trans*-2-decenoyl-NAC to *cis*-3-decenoyl-NAC can be monitored by a decrease in absorbance at 263 nm due to the loss of conjugation in the product (Figure 5.7) (186). Therefore, the activity of the putative FabM in *B. mallei* was first evaluated with *trans*-2-decenoyl-NAC and *trans*-2-decenoyl-CoA.



**Figure 5.7: FabM reaction using CoA substrate analogue (186)**

The *bmaa0541* gene was amplified and inserted into pBAD Myc/His C plasmid using the 5' NcoI and 3' HindIII restriction sites with a His-tag at the C-terminus by Dr. Hao Lu. However, purified protein has no activity with either *trans*-2-decenoyl-NAC or *cis*-3-decenoyl-NAC. It was speculated that the native structure of this protein had been

disturbed by a large segment attached at the C-terminus from the encoding sequencing of the pBAD *Myc/His C* vector (**Figure 5.8**).

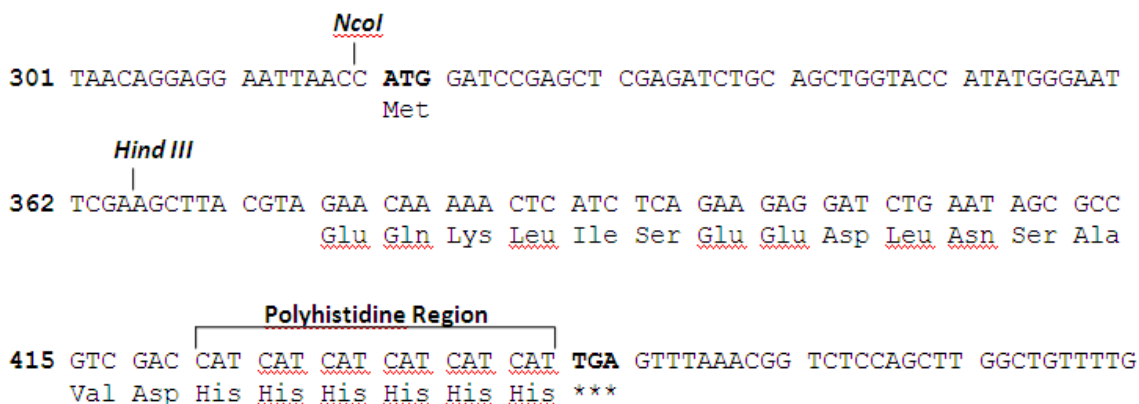


**Figure 5.8: Part of the cloning/expression region in pBAD *Myc/His C* vector.**

Therefore, to remove the large amino acids segment, the *bmaa0541* gene was amplified and inserted into pET15b vector so that a His-tag was encoded at the N-terminus. Following overexpression in *E. coli*, the *bmaa0541* was purified to homogeneity using His-tag affinity chromatography and size exclusion chromatography. SDS-PAGE demonstrated that the protein was > 95% pure and provided apparent molecular mass of 28 kDa, consistent with the predicted molecular mass of 28,400 Da.

Using 100  $\mu$ M *trans*-2-decenoyl-CoA and 8  $\mu$ g protein in the biochemical assay, we found that the *bmaa0541* is able to catalyze *trans*-2-decenoyl-CoA to *cis*-3-decenoyl-CoA with initial velocity of 70 pmol/min. The initial velocity of the reaction is comparable with that of FabM from *S. pneumonia* (200 pmol/min) (186). However, the yield of product is only 1%, since the equilibrium favors the substrate (**Figure 5.7**). So

we speculate the low yield is because the formation of expected product *cis*-3-decenoyl-CoA is thermodynamically unfavorable. Because the enzymatic reaction is reversible, we synthesized *cis*-3-decenoyl-CoA and tested the enzyme activity, in which an increase of absorbance at 263 nm should be observed during the enzyme reaction. In agreement with our prediction, the yield is 15%, higher than that of using *trans*-2-decenoyl-CoA as substrate analogue. However, the reaction is still not complete. We speculate it could be caused by substrate inhibition.

To prove that the bmaa0541 is a *trans*-2, *cis*-3-decenoyl-ACP isomerase, we need to test the enzyme activity with ACP substrate. The ACP from *E. coli* (ecACP), which is 74% identical to the putative ACP from *B. mallei* (bmACP), was expressed and purified. An enzymatic coupling reaction with *trans*-2-decenoyl-CoA or *cis*-3-decenoyl-CoA was subsequently used to synthesize *trans*-2-decenoyl-ecACP and *cis*-3-decenoyl-ecACP. Unfortunately, the enzyme was inactive toward both substrates.

One explanation of the above data is that the bmaa0541 ACP binding pocket cannot tolerate the difference between ecACP and bmACP. However, ACP is a highly structurally conserved protein, that consists of a 3- or 4-helix bundle (209). bmACP has 78 residues and ecACP has 79 residues, and have 74% sequence identity. Due to the conserved structure, similar size and amino acid sequence between ecACP and bmACP, we could negate the possibility that the bmACP binding pocket cannot uptake ecACP.

An analysis of the putative FAS-II genes in *B. mallei* genome shows that only the *bmaa0541* gene locates in chromosome 2 and other genes locate in chromosome 1. However, in the case of *S. pneumoniae*, all of the genes required for FAS-II are located



in a single cluster (186). It suggests that the transcription of the *bmaa0541* gene and other FAS-II genes may be separately regulated. And the *bmaa0541* gene may be not related to FAS-II pathway. Therefore, based on the enzyme activity, we speculate the *bmaa054* is not an ACP-dependent enzyme, but a CoA-dependent enzyme.

The real FabM in *B. mallei* has not been identified. There are four possibilities. The first possibility is that the *bma1803* or *bma1438* located on chromosome 1, which has 29% and 28% identity with the *fabM* from *S. pneumonia*, respectively, are the *fabM* in *B. mallei*. The second possibility is that FabZ from *B. mallei* can function like the *E. coli* FabA enzyme which can catalyze both dehydration and isomerization. The third possibility is that *B. mallei* utilizes another mechanism to introduce a double bond into the growing acyl chain of fatty acids. The fourth one is that *B. mallei* only utilizes O<sub>2</sub>-dependent DesA to introduce double bond in UFA.

#### *Crystal Structure of the bmaa0541.*

Recently, X-ray structure of the *bmaa0541* was solved by Huei Jiun Li. The overall fold displays a right hand spiral with a core composed of  $\beta$ -sheets surrounded by  $\alpha$ -helices (**Figure 5.9**). Based on the sequence and structure similarity, the *bmaa0541* is a member of crotonase superfamily.



**Figure 5.9: Structure of the bmaa0541.**  
X-ray structure is solved by Huei Jiun Li in our lab.

Most members in the crotonase superfamily are CoA-dependent enzymes. Structure and sequence alignment with the crotonase superfamily enzymes revealed that there are always one or more Arg or Lys residue adjacent to the 4-phosphate of pantothenic acid and the phosphate of the CoA nucleotide (**Figure 5.10 and 5.11**). The hydrogen bond between Arg or Lys and CoA is highly conserved. In addition, in most of the enzymes, there is a Phe that forms a hydrophobic interaction with the adenine moiety on CoA.

CurF ECH2 domain from *L. majuscula* and FabM from *S. pneumoniae* are the two crotonase superfamily members shown to accept ACP-linked substrates. The CurF

ECH2 domain is shown to have higher specificity for ACP-linked substrate. It appears that the side chain of Y73 blocks the hydrogen bond between R38 in CurF ECH2 and CoA, so CoA is a poorer substrate of CurF ECH2 (**Figure 5.10**).

spFabM is another crotonase superfamily member shown to have ACP-linked substrate as the natural substrate. However, based on the sequence alignment, it appears that it has very similar substrate binding residues as other CoA-dependent enzymes, and has no bulky group, such as Phe or Tyr, in the position of Y73 in CurF ECH2 (**Figure 5.11**). The X-ray structure of spFabM is not available; therefore we don't know what strategy spFabM uses to discriminate CoA-linked substrates.

Structural and sequence alignment of the bmaa0541 with crotonase superfamily enzymes showed that in the bmaa0541, K26, R60 and F252 are in similar position as other CoA-binding residues in CoA-dependent enzymes (**Figure 5.10 and 5.11**). In addition, there is no bulky group, such as Phe or Tyr, blocking the interaction between Arg and CoA. Therefore, based on the structural alignment, we speculate that the bmaa0541 could be a CoA-dependent enzyme, which is consistent with our current data that it selects CoA-linked substrates in the activity assay.

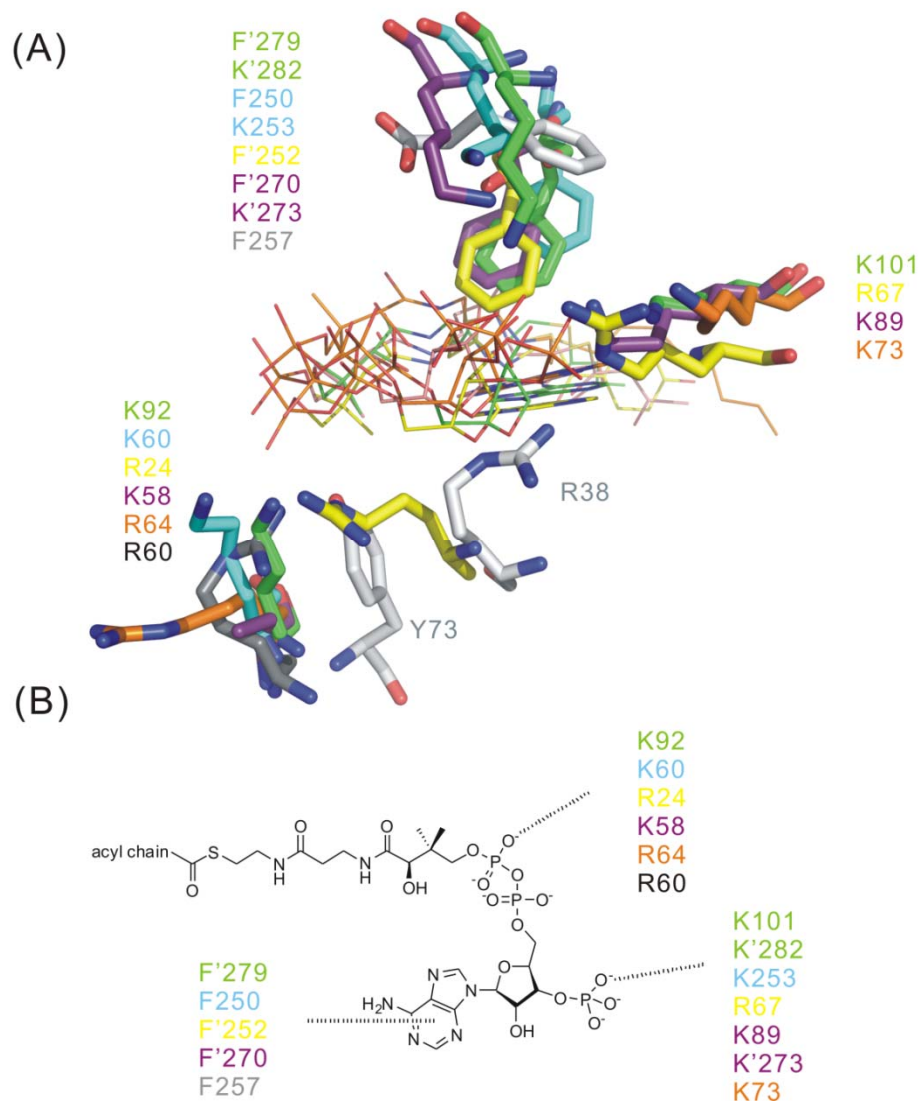


**Figure 5.10: Hydrogen bonding interactions between phosphate groups and adenine moiety of CoA and proteins in crotonase superfamily.**

(A) Crystal structure, (B) Schematic drawing. CoA ligands are in lines, and CoA binding residues are in stick. Enoyl-CoA hydratase (ECH) (pdb code: 1DUB) is in green, Methylmalonyl-CoA decarboxylase (MMCD) (pdb code: 1EF8) is in cyan, 4-Chlorobenzoyl-CoA dehalogenase (CBD) (pdb code: 1JXZ) is in yellow, 1,4-Dihydroxy-2-naphthoyl-CoA synthase (MenB) from *E. coli* is in purple,  $\Delta^{3,2}$ -enoyl-CoA isomerase (ECI) (pdb code: 1K39) is in orange, the bmaa0541 is in black and CurF ECH2 (pdb code: 2Q34) is in light grey. Residue followed by a prime indicates that the residue is from the neighboring subunit.

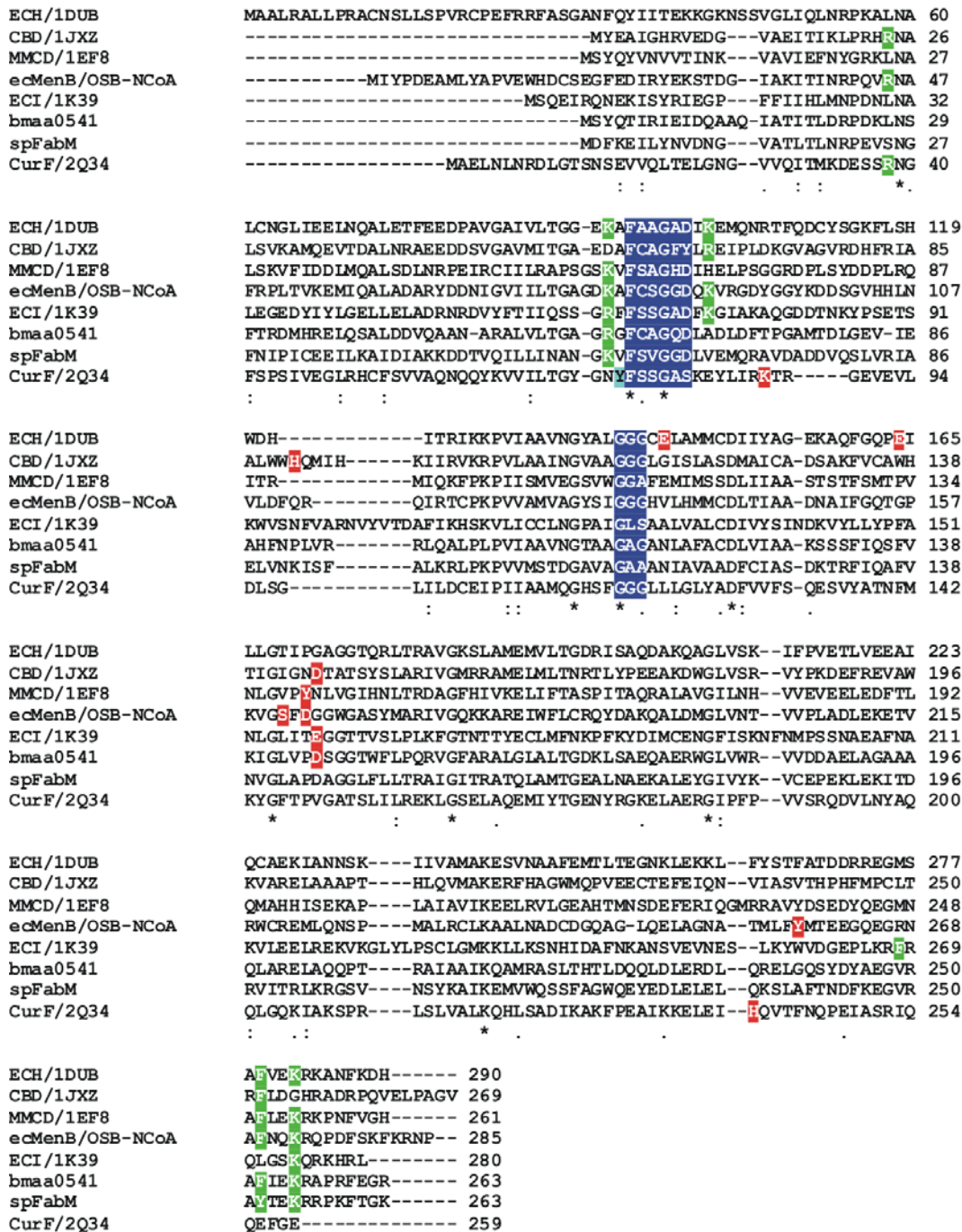


**Figure 5.11: Sequence alignment of characterized crotonase superfamily members.**

Residues of the oxanyon hole are in blue. Characterized catalytic residues are in red. CoA binding residues are in green. The Y73 in CurF is in light blue. The sequence alignment was performed using Clustal W (146), and the figure was made using Jalview (147).

## Catalytic Mechanism

In the crotonase superfamily the oxyanion hole residues have been retained for the stabilization of enolate anion intermediates, while new residues have been selected to alter the substrate specificity and the catalyzed chemistry (193, 210-212). The oxyanion hole is composed of two parts in which two amide protons form hydrogen bonds with oxyanion intermediate. The first part is formed by sequence motif FXXGXD, with the second-to-last residue in the sequence contributing its amide proton. The second part is formed by the sequence motif GXG, with the second residue contributing its amide (Figure 5.11).

Based on our current data, we propose that the bmaa0541 is a *trans*-2, *cis*-3-enoyl-CoA isomerase. Analysis of its sequence suggests one possible active site residue D145 and two possible oxyanion hole residues, Q66 and A113. To verify the importance of this proposed catalytic residue, site-directed mutagenesis was performed to replace D145 in wild type *trans*-2, *cis*-3-enoyl-CoA isomerase. D145E and D145N were prepared. The D145E mutant at 3  $\mu$ M showed 10-fold smaller initial velocity than wild type, while D145N mutant at 3  $\mu$ M showed no activity. These data indicate that D145 in *trans*-2, *cis*-3-enoyl-CoA isomerase is essential for catalysis.

$\Delta^{3,2}$ -enoyl-CoA isomerase, a member of crotonase superfamily, catalyzes similar reaction, converting *cis*-3-enoyl-CoA or *trans*-3-enoyl-CoA into *trans*-2-enoyl-CoA. Its reaction is the reverse of the *trans*-2, *cis*-3-enoyl-CoA isomerase-catalyzed reaction. Therefore, these two enzymes are likely to share similar active site configurations, and their active-site residues might serve similar catalytic functions. Based on the mechanism of  $\Delta^{3,2}$ -enoyl-CoA isomerase (199), the mechanism of *trans*-2, *cis*-3-enoyl-

CoA isomerase is proposed (**Figure 5.12**). D145 acts as a base to shift the double bond by proton abstraction from C4 and subsequent proton donation to C2, while Q66 and A113 stabilize the enolate intermediate. In X-ray structure, essential residues Q66, A113 stabilize the enolate intermediate. In X-ray structure, essential residues Q66, A113 and D145 are positioned consistent with the proposed mechanism (**Figure 5.13**).

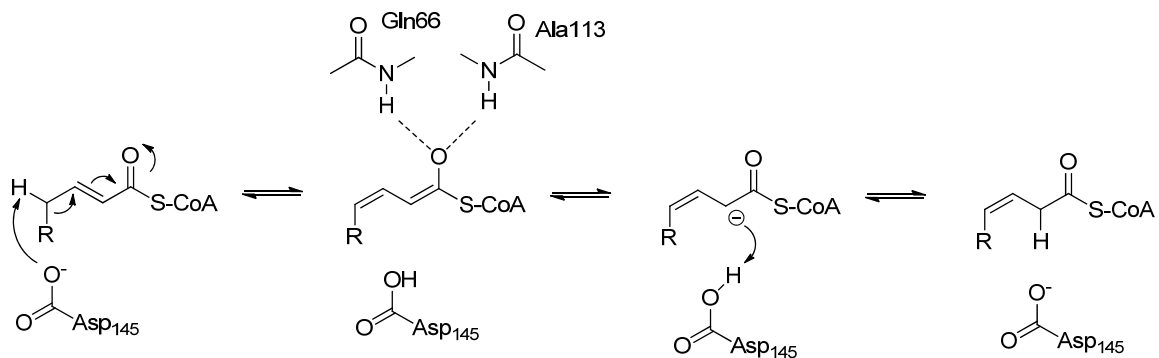


**Figure 5.12: Proposed reaction mechanism catalyzed by *trans*-2, *cis*-3-decenoyl-CoA isomerase.**

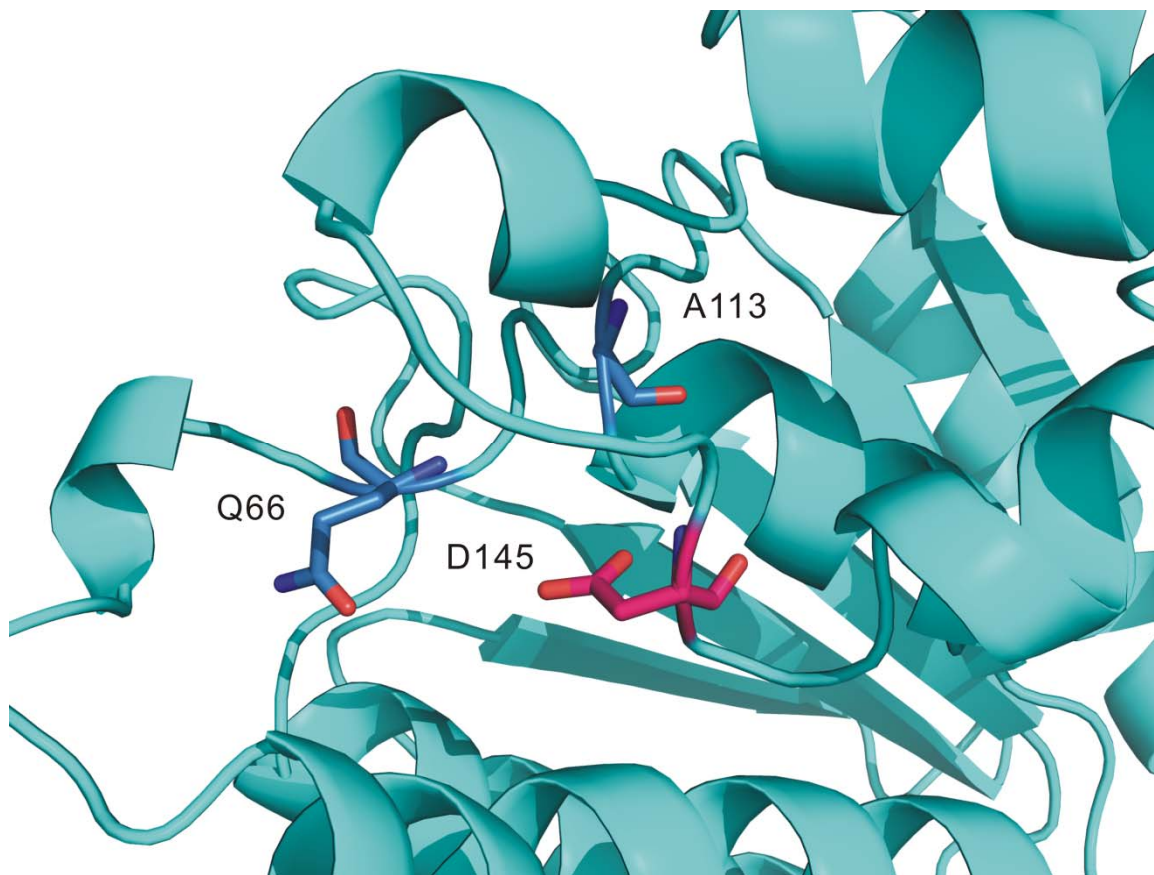


**Figure 5.13: Active site structure of *trans*-2, *cis*-3-decenoyl-CoA isomerase.** Active-site residue D145 is labeled in magenta and oxyanion hole residues Q66 and A113 are labeled in blue. X-ray structure is solved by Hwei Jiun Li in our lab.



## Conclusions

Here we report the cloning, expression and purification of the bmaa0541. We propose the bmaa0541 is a *trans*-2, *cis*-3-enoyl-ACP isomerase. However, kinetic data show that it specifically uptake CoA-linked substrate only, and it does not uptake ACP-linked substrate. Therefore, we speculate that it is a *trans*-2, *cis*-3-enoyl-CoA isomerase. Crystal structure also showed that it has a similar substrate binding pocket as CoA-dependent enzymes. Through sequence alignment with other members in crotonase superfamily, conserved residues of Q66 (oxyanion hole), A113 (oxyanion hole) and D145 (active site) are predicted to be essential for enzyme catalysis.

## Chapter 6 : Mechanism and Inhibition of the Dihydroxynaphthoyl-CoA Synthase (MenB) from *Mycobacterium tuberculosis*

This chapter is based on part of work that has been published in:

Li, X., Liu, N., Zhang, H., Knudson, S. E., Slayden, R. A., Tonge, P. J.. Synthesis and SAR studies of 1,4-benzoxazine MenB inhibitors: Novel antibacterial agents against *Mycobacterium tuberculosis*. *Bioorg. Med. Chem. Lett.* **2010**, 20(21), 6306-6309

### Background

*Crotonase Superfamily.*

MenB catalyzes the ring-closing dehydration of *o*-succinylbenzoyl-CoA (OSB-CoA) to form 1,4-dihydroxy-2-naphthoyl-CoA (DHNA-CoA), an intermediate in the menaquinone biosynthetic pathway. According to its structural scaffold of a right-handed spiral composed of a core of  $\beta$ -sheets surrounded by  $\alpha$ -helices, MenB belongs to the crotonase superfamily.

In the crotonase superfamily, the oxyanion hole is conserved to stabilize a common enolate anion intermediate (210-213). It is composed of two hydrogen bond donor. One donor is provided by the sequence motif FXXGXD, with the second-to-last residue in the sequence contributing its amide proton. The second donor is provided by the sequence motif GXG (normally GGG), with the second residue contributing its

amide (**Figure 6.1**). In contrast, the catalytic residues of crotonase superfamily are diverse to catalyze the various reactions, including hydration (214-216), double bond isomerization (217), Dieckmann condensation (65), reverse Dieckmann condensation (218), decarboxylation (195) and dehalogenation (196).



### *Mechanism of MenB Catalyzed Reaction.*

MenB catalyzes the formation of a carbon-carbon bond through a Dieckmann condensation (220, 221) (**Figure 6.2**). Previous X-ray structure and kinetics study led to the proposed reaction mechanism (65) shown in **Figure 6.3**. In the reaction, the aliphatic OSB carboxylate is activated by the formation of a CoA thioester that results in an acidification of the  $\alpha$ -protons. Subsequently, the thioester is deprotonated to form an enolate intermediate and a  $\beta$ -keto ester is generated through the nucleophilic attack of the enolate anion on the phenyl carboxylate. The enzyme catalyzes the reaction by stabilizing the enolate anion (65). The driving force of this ring closure reaction may be supplied by the aromatization process.

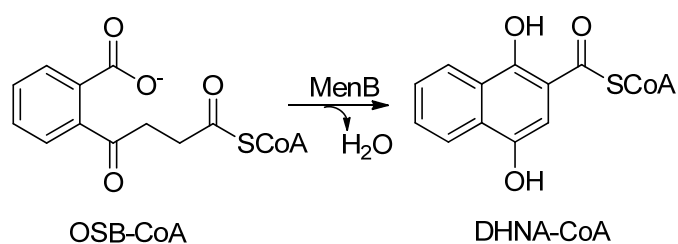


**Figure 6.2: Reaction catalyzed by MenB.**

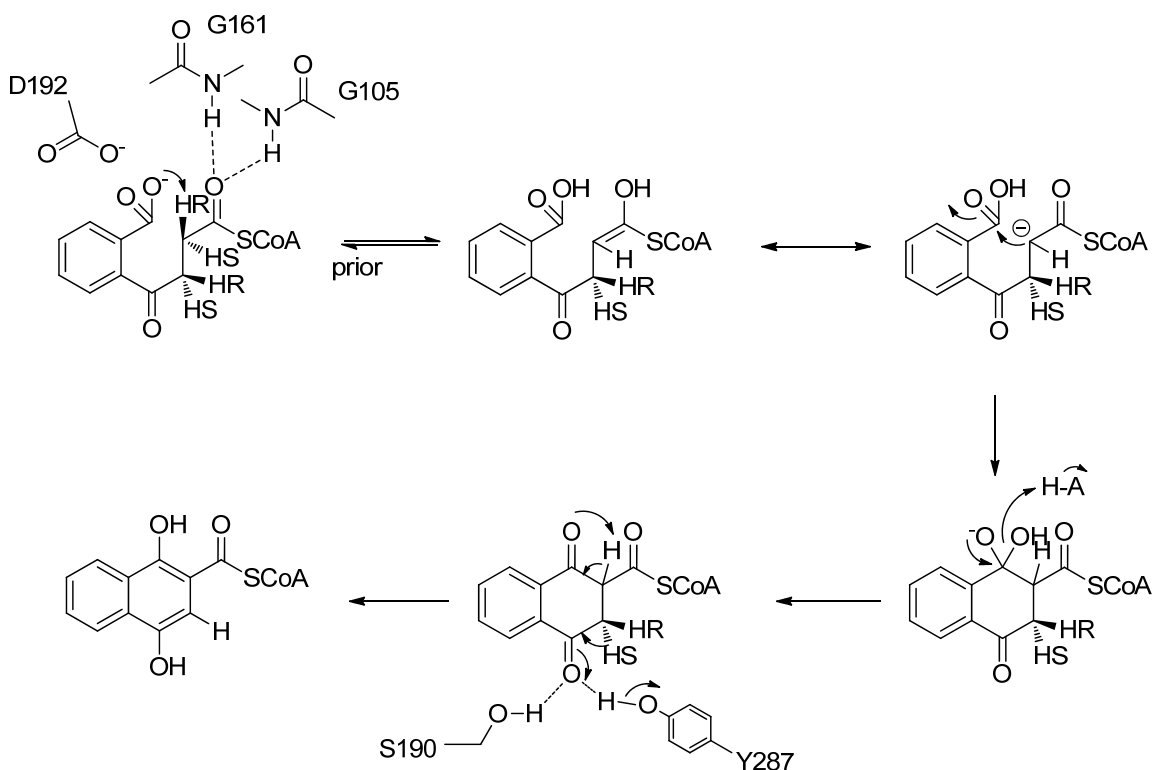


**Figure 6.3: Proposed mechanism of reaction catalyzed by MenB (mtMenB numbering) (65).**

Sequence alignment (**Figure 6.1**) of MenB analogues for several bacterial species shows that all of them have conserved active site residues S190, D192 and Y287 (mtMenB numbering). However, in *M. tuberculosis* there is one more interesting residue D185 close to active site. In addition, OSB-CoA is unstable, and easily decomposes to spirodilactone with lactone as intermediate (**Figure 6.4**). Therefore, Dr. Huaning Zhang proposed an alternative mechanism for mtMenB, with D185 and the lactone of OSB-CoA involved (**Figure 6.5**). mtMenB utilizes the lactone OSB-CoA as a substrate in which the phenyl carboxylate is activated. The catalytic residue D185 functions as a base and facilitates the water to abstract the pro-2*R* proton.

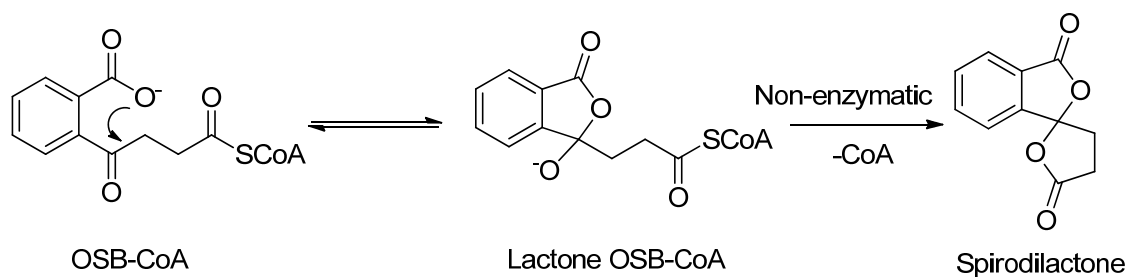


**Figure 6.4: The degradation of OSB-CoA to spirodilactone.**

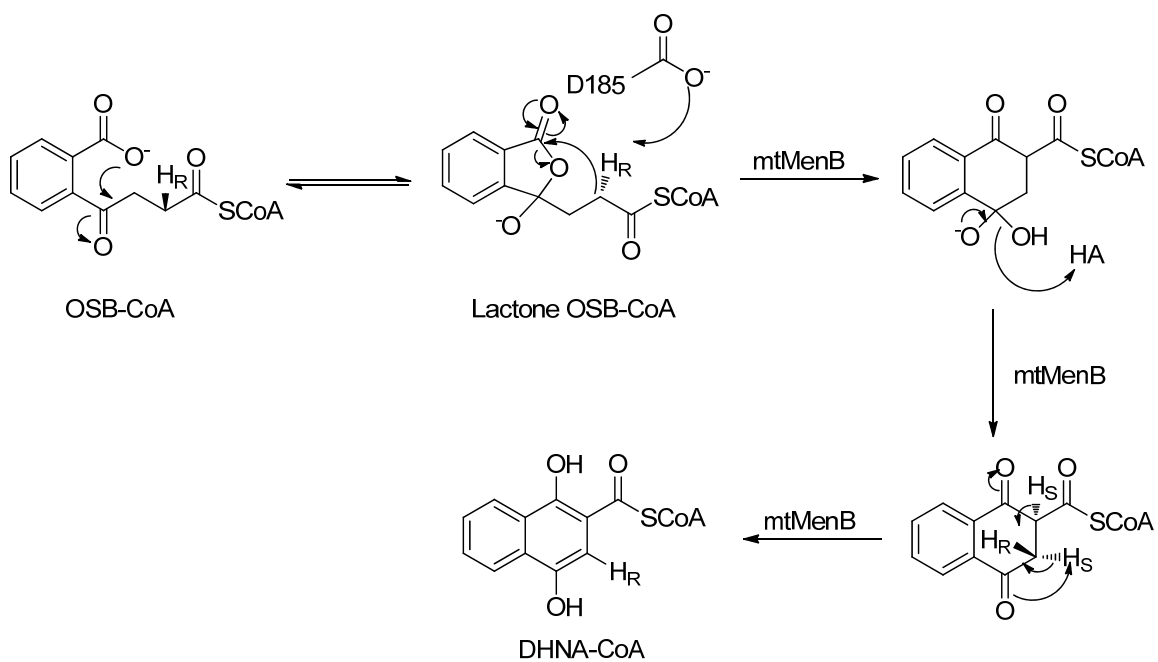


**Figure 6.5: Alternative mechanism of the mtMenB catalyzed reaction.**  
Proposed by Dr. Huaning Zhang.

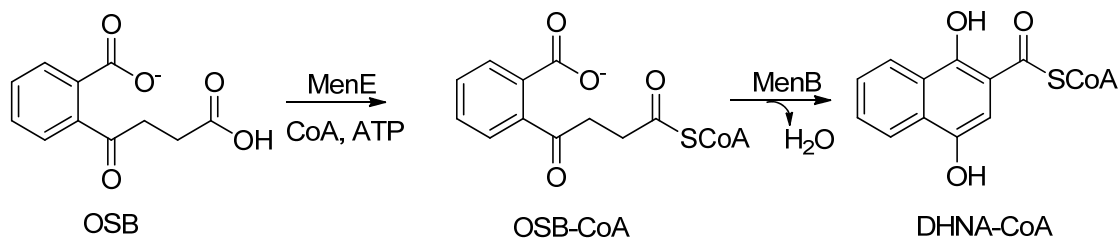
### *High throughput screen of potent inhibitors of mtMenB*

There is debate on whether *menB* is an essential gene. It has been claimed that expression of MenB is closely related to the production of menaquinone, therefore this enzyme is a potential drug target. In addition, a *menB* mutant in *B. subtilis* can only be complemented by DHNA supplementation for normal growth requirement (222, 223). Furthermore, under O<sub>2</sub> limiting condition, *menB* gene is over expressed to produce more menaquinone as a mechanism of survival (224). However, some claimed that by using the transposon site hybridization method *menB* is identified as a non-essential gene for optimal growth of *Mycobacterium leprae*, a close relative of *M. tuberculosis* (87). We support the hypothesis that MenB is a key enzyme required for the menaquinone synthesis, and therefore MenB is a putative drug target.

In order to provide a foundation for discovery of MenB inhibitors, around 105,091 small drug-like molecules from the library of Known Bioactives (Pilot screening) and Commercial Compounds at the ICCB-Longwood Screening Facility at Harvard Medical School were screened by Dr. Huaning Zhang and Xiaokai Li. Following the primary screen, only 455 hits had at least 30% enzyme inhibition. Within the small pool of positive hits, two compounds (1548L21 and 1486C16) were identified as promising scaffolds. 1548L21 (**Table 6.1**) has the backbone of OSB moiety of MenB substrate. In contrast, 1486C16 (**Table 6.1**) is reminiscent of the product DHNA-CoA. Since MenB's substrate OSB-CoA is not stable, the ecMenE/mtMenB coupled assay (**Figure 6.6**) was used for screening. The ability of each compound to inhibit MenE was also evaluated by directly monitoring the formation of pyrophosphate (PPi) by MenE and the ecMenE/mtMenB coupled assay using 50 nM MenE. However, no inhibition against

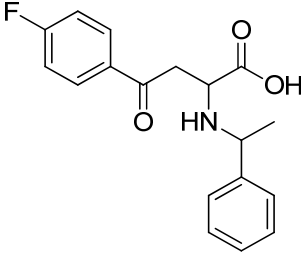
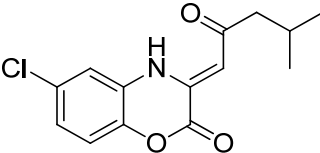


MenE was observed at 50  $\mu\text{M}$  inhibitor, suggesting that this compound class primarily targets MenB in the coupled assay. Subsequent SAR studies have primarily focused on the structure of “substrate-like” 2-amino-4-oxo-phenylbutanoic acids and “product-like” benzoxazinones (**Figure 6.7**).



**Figure 6.6: Reaction catalyzed by MenE and MenB**

**Table 6.1: Inhibition data of selective strong hits at 12  $\mu$ M inhibitor**

ID No.	Structure	Activity (%)
1548L21		64.7
1486C16		79.4

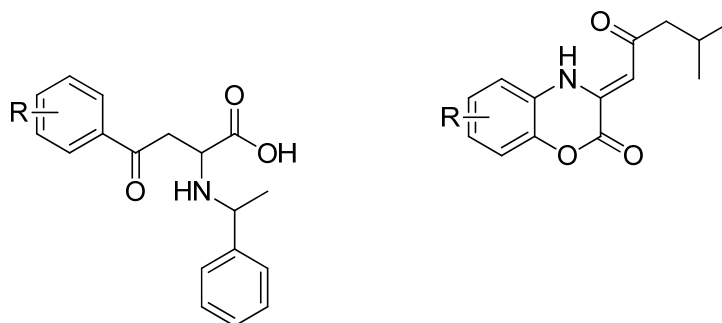


**Figure 6.7: Structure of 2-amino-4-oxo-phenylbutanoic acids and benzoxazinones**

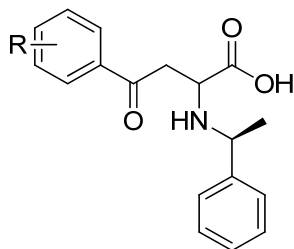
Xiaokai Li designed and synthesized analogues of 1548L21 (**Table 6.2**), which contain the OSB moiety with the different substitutions on the aromatic ring. Their inhibition ability was evaluated by ecMenE/mtMenB coupled assay. However, although several compounds showed promising *in vitro* activity in both enzyme inhibition and antimicrobial activity assays, there was a poor correlation between these assays.

### *Project Goals.*

In this chapter, we will focus on the MenB reaction by comparing the mechanism of the *M. tuberculosis* MenB enzyme with the *E. coli* MenB enzyme. The outcome of this project will further enhance our knowledge on the functional role of D185 for catalysis.

Due to the interest in developing chemotherapeutics against *M. tuberculosis*, we will discuss our efforts to explain the poor SAR of analogues of 1548L21. In addition, we will discuss the activity of a series of inhibitors that mimic the substrate OSB-CoA or product DHNA-CoA.

**Table 6.2: *In vitro* activity of 2-amino-4-oxo-phenylbutanoic acids.**



Compound	R	IC <sub>50</sub> ( $\mu$ M)	MIC ( $\mu$ g/mL)
1	H	112.1 $\pm$ 10.6	6.25
2	4-F	13.2 $\pm$ 0.75	12.5
3	4-Cl	8.54 $\pm$ 0.80	50.0
4	4-Br	105.4 $\pm$ 15.0	12.5
5	4-NO <sub>2</sub>	>150	100
6	4-OMe	>150	12.5
7	2-F	8.70 $\pm$ 0.80	25.0
8	2-Cl	8.50 $\pm$ 0.80	50.0
9	2-Br	0.60 $\pm$ 0.07	12.5
10	2-I	0.63 $\pm$ 0.03	6.25
11	2-NO <sub>2</sub>	2.10 $\pm$ 0.22	12.5
12	2-CF <sub>3</sub>	2.10 $\pm$ 0.19	25.0
13	2-OMe	>150	12.5
14	3-Cl	>150	12.5
15	3-NO <sub>2</sub>	>150	100
16	2,4-diF	1.40 $\pm$ 0.18	6.25
17	2-Cl, 4-F	1.10 $\pm$ 0.08	12.5
18	2-Br, 4-F	0.43 $\pm$ 0.32	12.5
19	2-CF <sub>3</sub> , 4-F	0.82 $\pm$ 0.09	12.5
20	2,4-diCl	0.26 $\pm$ 0.02	25.0
21	2,6-diCl	7.11 $\pm$ 0.11	1.56

## Materials and Methods

### *Expression and purification of mtMenB and ecMenB.*

The *menb* gene *Rv0548c* (945 bp) from *M. tuberculosis* was cloned into the pET-15b plasmid (Novagen) and placed in frame with an N-terminal His-tag sequence by Dr. Yuguo Feng (65). MenB from *M. tuberculosis*, was expressed in *E. coli* CodonPlus cells. Transformed cells were induced with 1 mM IPTG at an OD<sub>600</sub> of 0.8 and harvested by centrifugation after shaking for 12 h at 25 °C. The cell pellet was resuspended in 30 mL of His-binding buffer (5 mM imidazole, 0.5 M NaCl, 20 mM Tris HCl, pH 7.9) and lysed by 3 passages through a French Press cell (1,000 psi). Cell debris was removed by centrifugation at 33,000 rpm for 60 min at 4 °C. The supernatant was applied onto a His-bind column (1.5 cm × 15 cm), which contained 4 mL of His-bind resin (Novagen) charged with charging buffer (50 mM Ni<sub>2</sub>SO<sub>4</sub>). The column was equilibrated with binding buffer. Then 60 mL of binding buffer (5 mM imidazole, 0.5 M NaCl, 20 mM Tris-HCl, pH 7.9) was used to wash the column. After that, 60 mL of wash buffer (60 mM imidazole, 0.5 M NaCl, 20 mM Tris-HCl, pH 7.9) was used to wash the column. Finally, mtMenB was eluted using a gradient of 60-500 mM imidazole in 0.5 M NaCl, 20 mM Tris-HCl, pH 7.9. Fractions containing mtMenB were collected and the imidazole removed by G-25 chromatography (1.5 cm × 55 cm) using 20 mM NaH<sub>2</sub>PO<sub>4</sub>, 0.1 M NaCl at pH 7.0, as the eluent. The concentration of mtMenB was determined by measuring the absorption at 280 nm using an extinction coefficient of 41,370 M<sup>-1</sup>cm<sup>-1</sup> calculated from the primary sequence. The protein was analyzed by SDS-PAGE which showed a dominant band of 37 kDa. The enzyme was concentrated by using Centricon-30 (Amicon) and stored at -80 °C.

The *menb* gene *b2262* (858 bp) from *E. coli* was cloned into the pET-15b plasmid (Novagen) and placed in frame with an N-terminal His-tag sequence by Dr. Yuguo Feng. Protein expression was performed using BL21 (DE3) cells. Expression and purification followed the same protocol as described above for mtMenB. However, ecMenB is not stable with a His-tag sequence; therefore, N-terminal His-tag was cleaved by biotinylated thrombin overnight at RT after purification. The concentration of MenB was determined by measuring the absorption at 280 nm using an extinction coefficient of 36,040 M<sup>-1</sup>cm<sup>-1</sup> calculated from the primary sequence. The protein was analyzed by SDS-PAGE which showed a dominant band of 31 kDa. The enzyme was concentrated by using Centricon-30 (Amicon) and stored at -80 °C.

*Site-Directed Mutagenesis, Expression and Purification of MenB Mutants.*

mtMenB mutants D185N, S190A, D192N and Y287F were from previous work (65). For other mutants, site-directed mutagenesis was performed using the QuikChange mutagenesis kit from Stratagene using the primers listed in **Table 6.3**. The sequence of each mutant plasmid was confirmed by ABI DNA sequencing, and the expression and purification of each MenB mutant followed the same protocol that is described above for the wild-type MenB protein.

**Table 6.3: Nucleotide primers**

<b>Name</b>	<b>Sequence</b>
<b>mtMenB</b>	
D185G forward	5' CGCTTCAAGCAGACCGGGGCCGACGTCGGCAGC 3'
D185G reversed	5' GCTGCCGACGTCGGCCCCGGTCTGCTTGAAGCG 3'
D185E forward	5' CTTCAAGCAGACCGAGGCCGACGTCGGCAG 3'
D185E reversed	5' CTGCCGACGTCGGCCTCGGTCTGCTTGAAG 3'
<b>ecMenB</b>	
G156D forward	5' GCCATCTTCGGTCAGACTGACCCGAAAGTCGGT 3'
G156D reversed	5' GGAGGAACCGACTTTCGGGTCAGTCTGACCGAA 3'
P157A forward	5' GGTCAGACTGACGCGAAAGTCGGTTC 3'
P157A reversed	5' GAACCGACTTTCGCGTCAGTCTGACC 3'
K158D forward	A472G 5' GTCAGACTGACGCGGAAGTCGGTTCCTTC 3' A474T 5' GTCAGACTGACGCGGAAGTCGGTTCCTTC 3'
K158D reversed	A472G 5' GAAGGAACCGACTTCCGCGTCAGTCTGAC 3' A474T 5' GAAGGAACCGACTTCCGCGTCAGTCTGAC 3'

### *Expression and purification of ecMenE*

ecMenE, the *mene* gene *b2260* (1356 bp) from *E. coli*, was previously amplified by PCR from genomic DNA, cloned into the pET-15b plasmid (Novagen) and placed in frame with an N-terminal His-tag sequence by Dr. Yuguo Feng. Protein expression was performed using *E. coli* BL21 (DE3) cells. Transformed cells were grown in 800 mL of LB media containing 0.2 mg/mL ampicillin and induction was achieved using 1 mM IPTG overnight at 25 °C. Cells were harvested by centrifugation at 5,000 rpm for 20 min at 4 °C, resuspended in 30 mL of His-binding buffer (5 mM imidazole, 0.5 M NaCl, 20 mM Tris HCl, pH 7.9) and lysed by 3 passages through a French Press cell (1,000 psi). Cell debris was removed by centrifugation at 33,000 rpm for 60 min at 4 °C. MenB was purified using His affinity chromatography: the supernatant was loaded to a column containing 3 mL of His-bind resin (Novagen), charged with 9 mL of charge buffer (50 mM Ni<sub>2</sub>SO<sub>4</sub>). The column was washed with 20 mL of His-binding buffer and 20 mL of wash buffer (60 mM imidazole, 0.5 M NaCl, 20 mM Tris HCl, pH 7.9). ecMenE was eluted using a gradient of 20 mL elute buffer (0.5 M imidazole, 0.5 M NaCl, 20 mM Tris HCl, pH 7.9). Fractions containing ecMenE were collected and the imidazole removed by chromatography on G-25 resin using 20 mM NaH<sub>2</sub>PO<sub>4</sub>, 0.1 M NaCl at pH 7.0, as storing buffer. The concentration of ecMenE was determined by measuring the absorption at 280 nm using an extinction coefficient of 104,770 M<sup>-1</sup>cm<sup>-1</sup> calculated from the primary sequence. The enzyme was concentrated by using Centricon-30 (Amicon) and stored at -80 °C.



### *Coupled kinetic assay of MenB reaction.*

OSB-CoA, the substrate for MenB, is unstable and rapidly decomposes to spirodilactone. Therefore, we used a coupled assay with ecMenE to assay the MenB reaction. ecMenE is the preceding enzyme in the menaquinone biosynthesis pathway that synthesizes OSB-CoA *in situ* (**Figure 6.6**). Coupled reaction was performed in 20 mM NaH<sub>2</sub>PO<sub>4</sub>, 150 mM NaCl, 1 mM MgCl<sub>2</sub> at pH 7.0, and an excess of ecMenE. Formation of DHNA-CoA was monitored on a CARY-300 spectrophotometer at 25 °C by following the increase in absorption at 392 nm using an extinction coefficient of 4, 000 M<sup>-1</sup>cm<sup>-1</sup>.

IC<sub>50</sub> values were calculated by fitting the initial velocity data (v<sub>i</sub>) obtained at different inhibitor concentrations ([I]) to **equation 6.1** using Grafit 4.0.

$$y = 100\%/[1 + (I/IC_{50})] \quad \text{(Equation 6.1)}$$

### *Inhibition of mtMenB by 27 and 23.*

For **27**, inhibition mechanism was characterized by measuring initial velocities at a fixed concentration of 120 μM ATP, 120 μM CoA, 2 μM ecMenE and 150 nM mtMenB and at various concentrations of OSB (7.5-90 μM) and **7** (0, 380, 570 and 1275 nM). Data was analyzed in Lineweaver Burk plot. The dissociate constant (K<sub>i</sub> and K<sub>i</sub>') was analyzed using **Equation 6.2**, which described noncompetitive inhibition.

$$\frac{1}{v} = \frac{K_m}{v_{max}} \left( \frac{1}{[S]} \right) \left( 1 + \frac{[I]}{K_i} \right) + \frac{1}{v_{max}} \left( 1 + \frac{[I]}{K_i'} \right) \quad \text{(Equation 6.2)}$$

where [S] is the concentration of OSB, [I] is the concentration of inhibitor added,  $K_m$  is the Michaelis-Menten constant for OSB,  $V_{max}$  is the maximum velocity,  $K_i$  and  $K_i'$  are the inhibition constants.

Inhibition mechanism and dissociate constants of **27** were also characterized by measuring initial velocities at various concentrations of **27** (0-4350 nM) and OSB (7.5-90  $\mu$ M) in reaction mixtures containing 120  $\mu$ M ATP, 120  $\mu$ M CoA, 2  $\mu$ M ecMenE and 150 nM mtMenB. Values of  $K_i^{app}$  and [E] obtained from **Equation 6.3** were then fitted to **Equation 6.4-6.6**, which describe noncompetitive, competitive and uncompetitive, respectively.

$$\frac{v_i}{v_0} = 1 - \frac{([E]+[I]+K_i^{app}) - \sqrt{([E]+[I]+K_i^{app})^2 - 4[E][I]}}{2[E]} \quad \text{(Equation 6.3)}$$

where  $v_i$  and  $v_0$  are the initial velocities in the presence and absence of inhibitor,  $K_i^{app}$  is the apparent dissociation constant.

$$K_i^{app} = K_i \left( 1 + \frac{[S]}{K_m} \right) + \frac{1}{2} [E] \quad \text{(Equation 6.4)}$$

$$K_i^{app} = K_i' \left( 1 + \frac{K_m}{[S]} \right) + \frac{1}{2} [E] \quad \text{(Equation 6.5)}$$

$$K_i^{app} = \frac{[S]+K_m}{\left(\frac{K_m}{K_i}\right) + ([S]/K_i')} + \frac{1}{2} [E] \quad \text{(Equation 6.6)}$$

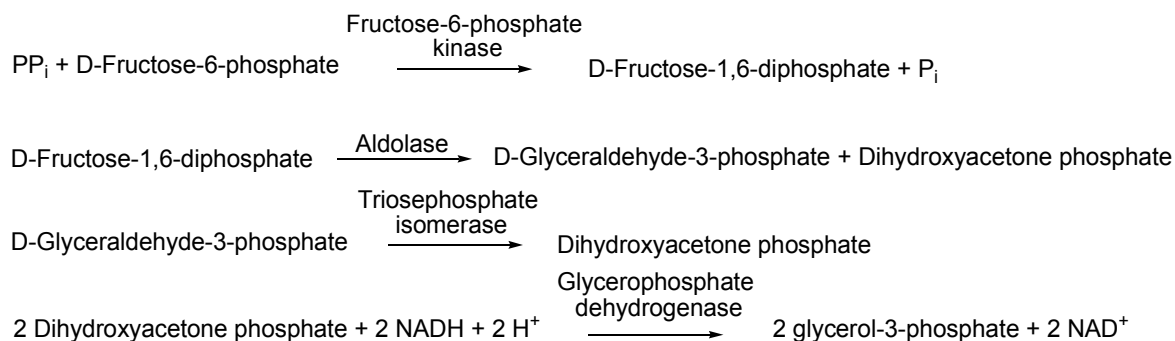
For **23**, inhibition mechanism was characterized by measuring initial velocities at various concentrations of **23** (0-4350 nM) and OSB (7.5-90  $\mu$ M) in reaction mixtures containing 120  $\mu$ M ATP, 120  $\mu$ M CoA, 2  $\mu$ M ecMenE and 150 nM mtMenB. Values of  $K_i^{app}$  and [E] obtained from **Equation 6.3** were then fitted to **Equation 6.4-6.6**.

### *Preincubation assay.*

The preincubation of ecMenE, ATP, CoA and OSB was performed in 20 mM NaH<sub>2</sub>PO<sub>4</sub>, 150 mM NaCl, 1 mM MgCl<sub>2</sub> at pH 7.0 and an excess of ecMenE for 3 min to allow complete conversion of OSB to OSB-CoA. The MenB reaction was initiated by the addition of MenB. Formation of DHNA-CoA was monitored on a CARY-300 spectrophotometer at 25 °C by following the increase in absorption at 392 nm using an extinction coefficient of 4, 000 M<sup>-1</sup>cm<sup>-1</sup>.

### *Pyrophosphate release assay.*

Pyrophosphate (PPi) was produced in the reaction catalyzed by MenE. The concentration of PPi was measured by PPi release assay according to the following coupled reactions. Two moles of NADH were oxidized to NAD<sup>+</sup> per mole of pyrophosphate consumed. The reaction was monitored on a CARY-300 spectrophotometer at 25 °C at 340 nm using an extinction coefficient of 6, 220 M<sup>-1</sup>cm<sup>-1</sup>.



*Synthesis of o-(3-carboxypropyl)-benzoyl CoA (OCPB-CoA).*

OCPB-CoA was synthesized by incubating 13  $\mu$ M ATP, 13  $\mu$ M CoA, 13  $\mu$ M OCPB and 6.5  $\mu$ M ecMenE in 10 mL phosphate buffer (20 mM NaH<sub>2</sub>PO<sub>4</sub>, 0.1 M NaCl, 1 mM MgCl<sub>2</sub> at pH 7.0) for 3 h at RT. The reaction mixture was then purified by semi-preparative HPLC (Vydac C18 column, 10  $\mu$ m particle, 10 mm i.d., 250 mm length) with a linear gradient (0-40% acetonitrile in 20 mM ammonia acetate in 40 min). OCPB-CoA was collected, frozen and lyophilized. ESI-MS [M-H<sup>-</sup>]: calculated 956.18 (C<sub>32</sub>H<sub>45</sub>N<sub>7</sub>O<sub>19</sub>P<sub>3</sub>S<sup>-</sup>); found 956.2.

*Determination of M. tuberculosis antimicrobial activity.*

The MIC is the lowest concentration of compound that inhibit visible growth of *M. tuberculosis* H37Rv. Data were acquired by Susan E. Knudson in the Department of Bioagricultural Sciences and Pest Management at Colorado State University.

## Results and Discussion

### *Role of D185 in mtMenB and G156 in ecMenB*

Based on previous study, Dr. Huaning Zhang proposed a new reaction mechanism for mtMenB, in which D185 functions as a base to abstract the  $\alpha$ -proton on the substrate lactone of OSB-CoA. Then carbon-carbon bond is formed through nucleophilic attack (**Figure 6.5**).

The catalytic residue D185 in mtMenB is replaced by G156 in ecMenB homologue. Site-directed mutagenesis was used to replace D185 and to examine its role in the overall reaction. mtMenB mutants D185G, D185N, and D185E were expressed and purified. The kinetic parameters are given in **Table 6.4**. The D185N and D185G mutants showed no activity, while the D185E mutant has a 60-fold reduced  $k_{\text{cat}}/K_m$  value compared with wild type mtMenB. The replacement of this residue with a glycine or asparagine causes a complete loss of activity, while even subtle change such as the replacement of D185 with a glutamate causes a dramatic decrease in activity. The ecMenB mutant G156D was also prepared, and this mutant also demonstrates no activity. These data clearly indicate that interestingly although D185 and G156 have very different side chain, both of them play a critical role in their reactions, respectively.

There are two possibilities: (1) D185 and G156 may play important catalytic role, so mtMenB and ecMenB utilize different mechanism as Dr. Huaning Zhang proposed, (2) D185 and G156 may play important structural role in guiding the active site residue organization or the substrate OSB-CoA's correct binding pose.

**Table 6.4: Kinetic parameters of mtMenB and ecMenB mutants.**

	$k_{\text{cat}}$ ( $\text{min}^{-1}$ )	$K_{\text{m}}$ ( $\mu\text{M}$ )	$k_{\text{cat}}/K_{\text{m}}$ ( $\text{min}^{-1} \mu\text{M}^{-1}$ )
<b>mtMenB</b>			
wt	$26.2 \pm 0.5$	$15.0 \pm 1.1$	$1.75 \pm 0.03$
D185E	$0.14 \pm 0.01$	$4.8 \pm 0.3$	$0.029 \pm 0.004$
D185N, D185G	No activity at 3 $\mu\text{M}$ enzyme		
<b>ecMenB</b>			
wt	$1.40 \pm 0.06$	$26.6 \pm 4.6$	$0.05 \pm 0.002$
G156D	No activity at 3 $\mu\text{M}$ enzyme		

First, we investigate whether mtMenB and ecMenB utilize different mechanisms as Dr. Huaning Zhang proposed. In order to explore the possibility that the OSB-CoA lactone is the substrate for mtMenB and OSB-CoA is the substrate for ecMenB, preincubation assay was performed with 4  $\mu\text{M}$  ecMenE for 3 min at 25 °C. PPI release assay showed that under this condition all of the OSB was converted to OSB-CoA in 3 min. Since OSB-CoA is not stable and will be converted to spirodilactone with a half-life of 15 min at 30 °C and more than 2 hours at 0 °C (220), we assume that more than 90% of the substrate do not convert to spirodilactone and are in the equilibrium between OSB-CoA and lactone OSB-CoA during the 3 min incubation. The values of  $k_{\text{cat}}/K_{\text{m}}$  values without preincubation, were  $1.75 \text{ min}^{-1} \mu\text{M}^{-1}$  and  $0.05 \text{ min}^{-1} \mu\text{M}^{-1}$ , for mtMenB and ecMenB, respectively. The values of  $k_{\text{cat}}/K_{\text{m}}$  values with preincubation were  $1.77 \text{ min}^{-1} \mu\text{M}^{-1}$  and  $0.05 \text{ min}^{-1} \mu\text{M}^{-1}$  (**Table 6.5**). So for both mtMenB and ecMenB, their  $k_{\text{cat}}/K_{\text{m}}$

values with and without preincubation are almost same within experimental error, indicating that both MenBs catalyze the reaction through same mechanism with preference of OSB-CoA as the substrate. It is worth to pointing out here we assume that after 3 min incubation more than 90% of the substrate are in the equilibrium between OSB-CoA and lactone OSB-CoA. In future we would like to prove lactone of OSB-CoA formation and the equilibrium between OSB-CoA and lactone of OSB-CoA by NMR spectroscopy.

**Table 6.5: Kinetic parameter of MenB reaction with/without preincubation.**

	$k_{cat}$ ( $\text{min}^{-1}$ )	$K_m$ ( $\mu\text{M}$ )	$k_{cat}/K_m$ ( $\text{min}^{-1} \mu\text{M}^{-1}$ )
<b>mtMenB</b>			
No incubation	$26.2 \pm 0.5$	$15.0 \pm 1.1$	$1.75 \pm 0.03$
Pre-incubation	$32.3 \pm 1.3$	$18.2 \pm 2.2$	$1.77 \pm 0.07$
<b>ecMenB</b>			
No incubation	$1.4 \pm 0.06$	$26.6 \pm 4.6$	$0.05 \pm 0.002$
Pre-incubation	$1.4 \pm 0.1$	$31.1 \pm 5.3$	$0.05 \pm 0.002$

The major difference between the two catalytic mechanisms is that the keto carbonyl group of OSB-CoA may or may not be involved in the catalysis (**Figure 6.3 and 6.5**) (65). To investigate the two mechanisms, a substrate analogue OCPB-CoA was synthesized (**Figure 6.8**). OCPB-CoA has similar structures to the OSB-CoA, but lacks the keto carbonyl group. Therefore, if MenB is using the mechanism with keto

carbonyl group involved, a reaction cannot happen with OCPB-CoA as substrate.

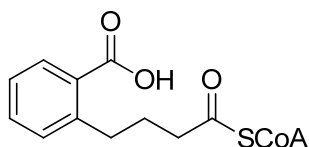
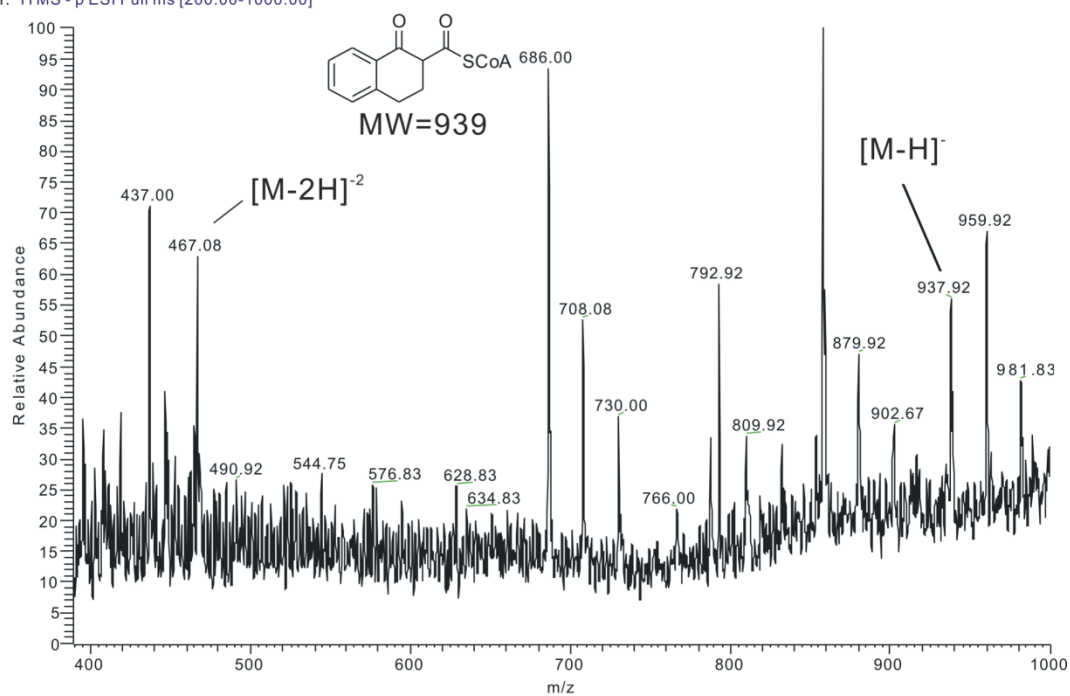


**Figure 6.8: Structure of OCPB-CoA**

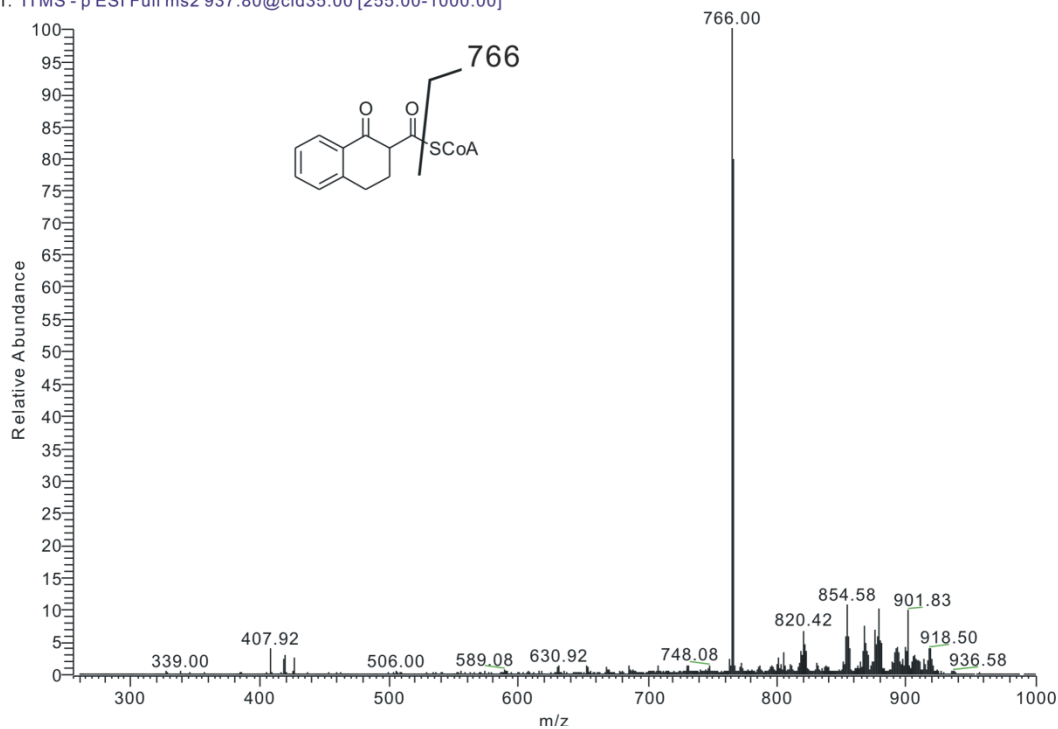
OCPB-CoA (120  $\mu$ M) was incubated with mtMenB or ecMenB. The formation of a new peak at 372 nm was observed for both MenBs. In order to confirm the structure of the product, reaction mixture was purified by HPLC. Product has the molecular mass of 938.92 by MS/MS (**Figure 6.9**) (OCPB-CoA has the molecular mass of 957.21). These molecular masses led to the proposed reaction with 1-hydroxy-2-naphthoyl-CoA (HN-CoA) as the product, shown in **Figure 6.10**. This product formation supports the published MenB mechanism (65).



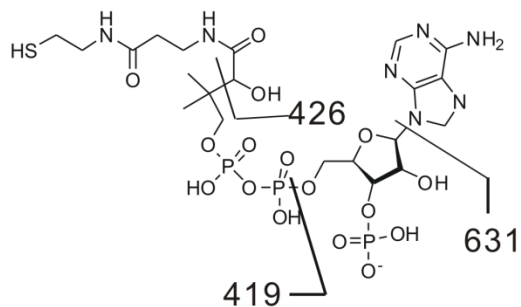
(A) RR090928\_CoA\_1 #774-831 RT: 1.79-1.92 AV: 58 SM: 15G NL: 9.12E2  
T: ITMS - pESI Full ms [200.00-1000.00]



(B) RR090928\_CoA\_2 #298-309 RT: 3.54-3.93 AV: 12 NL: 2.28E2  
T: ITMS - pESI Full ms2 937.80@cid35.00 [255.00-1000.00]



(C)



RR090928\_CoA\_2#176-199 RT: 1.13-1.62 AV: 24 SM: 7G NL: 1.13E1  
T: ITMS - p ESI Full ms3 937.80@cid35.00 766.00@cid0.00 [210.00-1000.00]

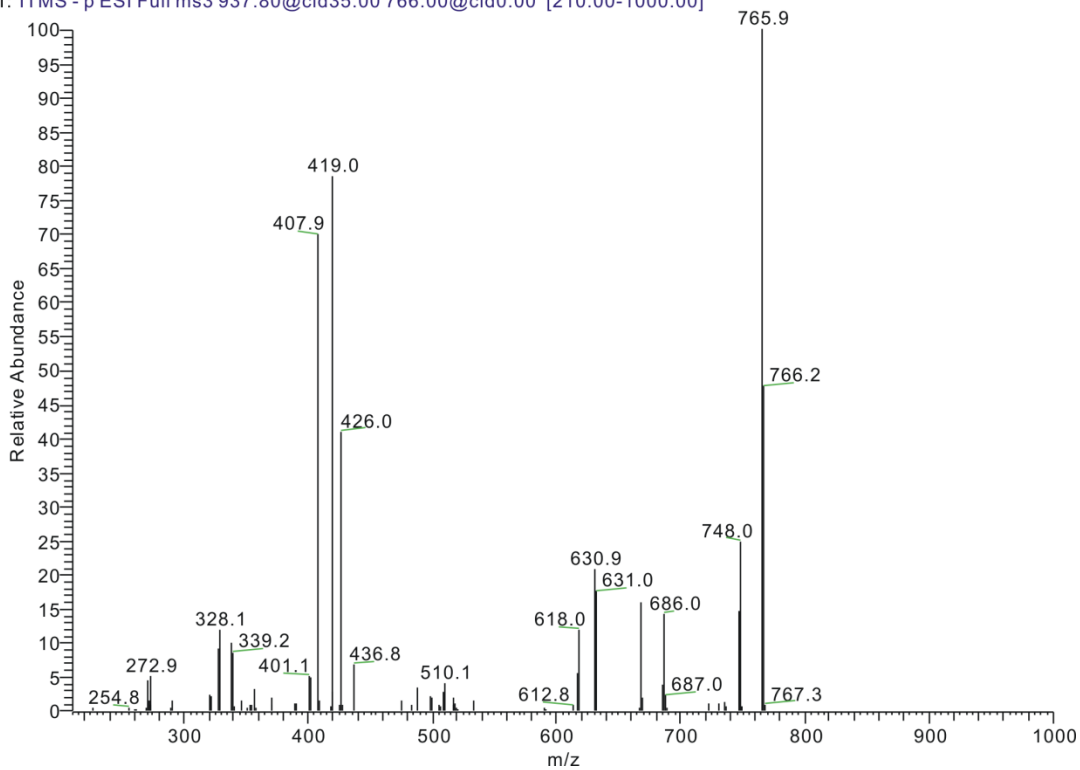


**Figure 6.9: Analysis of OCPB-CoA product by ion trap mass spectrometry.**

(A) Mass Spectrum of sample OCPB-CoA reaction product, (B) MS/MS spectrum of  $m/z$  938, (C) MS<sup>3</sup> of  $m/z$  766.

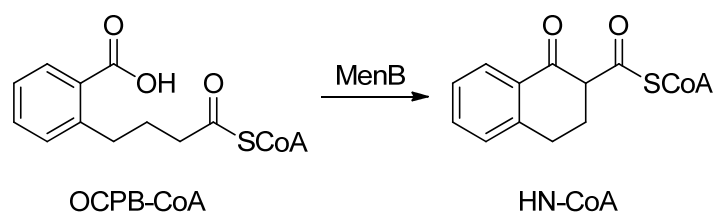


**Figure 6.10: Proposed reaction of OCPB-CoA.**

However, even OCPB-CoA can be catalyzed by both MenBs, the  $k_{cat}/K_m$  values significantly decrease by 12500-fold and 160-fold for mtMenB and ecMenB, respectively (**Table 6.6**). Therefore, we cannot conclude whether OCPB-CoA is the substrate of enzyme reaction, or whether the keto carbonyl group is important for the enzyme catalysis.

**Table 6.6: Kinetic parameter of MenB reaction with OSB-CoA and OCPB-CoA as the substrate.**

	$k_{cat}$ ( $\text{min}^{-1}$ )	$K_m$ ( $\mu\text{M}$ )	$k_{cat}/K_m$ ( $\text{min}^{-1} \mu\text{M}^{-1}$ )
<b>mtMenB (D185)</b>			
OSB-CoA	$26.2 \pm 0.5$	$15.0 \pm 1.1$	$1.75 \pm 0.03$
OCPB-CoA	$0.015 \pm 0.002$	$106 \pm 31$	$0.00014 \pm 0.00004$
<b>ecMenB (G156)</b>			
OSB-CoA	$1.40 \pm 0.06$	$26.6 \pm 4.6$	$0.05 \pm 0.002$
OCPB-CoA	$0.018 \pm 0.003$	$63 \pm 30$	$0.0003 \pm 0.0001$

In order to further characterize the product, higher concentration of OCPB-CoA was incubated with MenBs to obtain more product. Unfortunately, reaction was not complete and stopped with 10% yield. Our speculation is that reaction product (HN-CoA) inhibits the enzyme's activity.

We performed enzyme inhibition assay with the limited amount of purified product. In agreement with above prediction,  $IC_{50}$  value of the product is 200 nM when mtMenB concentration was 150 nM. The OCPB-CoA's resemblance of the product DHNA-CoA may account for the tight binding affinity (**Figure 6.11**). Therefore, this scaffold is a promising foundation for the development of MenB inhibitor.

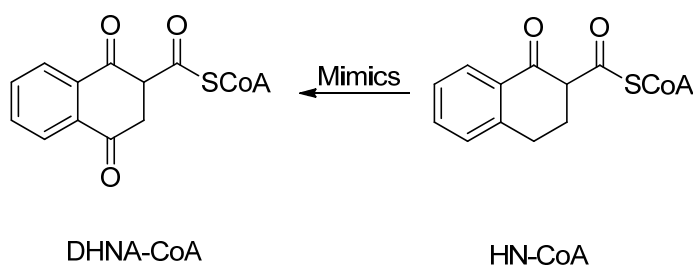


**Figure 6.11: HN-CoA mimics structure of MenB product DHNA-CoA.**

The current experimental data suggest that the catalytic mechanism of mtMenB and ecMenB are the same, and the D185 in mtMenB does not play a catalytic role. Therefore, we are interested in exploring the structural role of D185 in mtMenB, and the reason that mutation D185G in mtMenB and G156D in ecMenB are fatal to MenB activity, respectively.

According to the X-ray structure of mtMenB•AcAc-CoA, D185 is on the  $\alpha$ -helix

adjacent to the catalytic residue D192 (**Figure 6.12A**). It is likely that the mutation of D185G and G156D may affect the  $\alpha$ -helix structure and the correct position of D192. So mutagenesis is performed to replace the intervening 8-residue sequence between catalytic residues D185 and D192 (mtMenB numbering) into ecMenB (**Figure 6.12B**). Site-directed mutagenesis is performed sequentially as described above to produce the triple mutant G156D/P157A/K158D ecMenB. Kinetic assays show that this mutant still demonstrates no activity. The double mutant G156D/P157A also lack activity. While these results confirm the importance of these residues in ecMenB catalysis, experiments and further mutagenesis in the surrounding shell in an attempt to restore activity will give insight into the mechanisms of ecMenB vs. mtMenB.

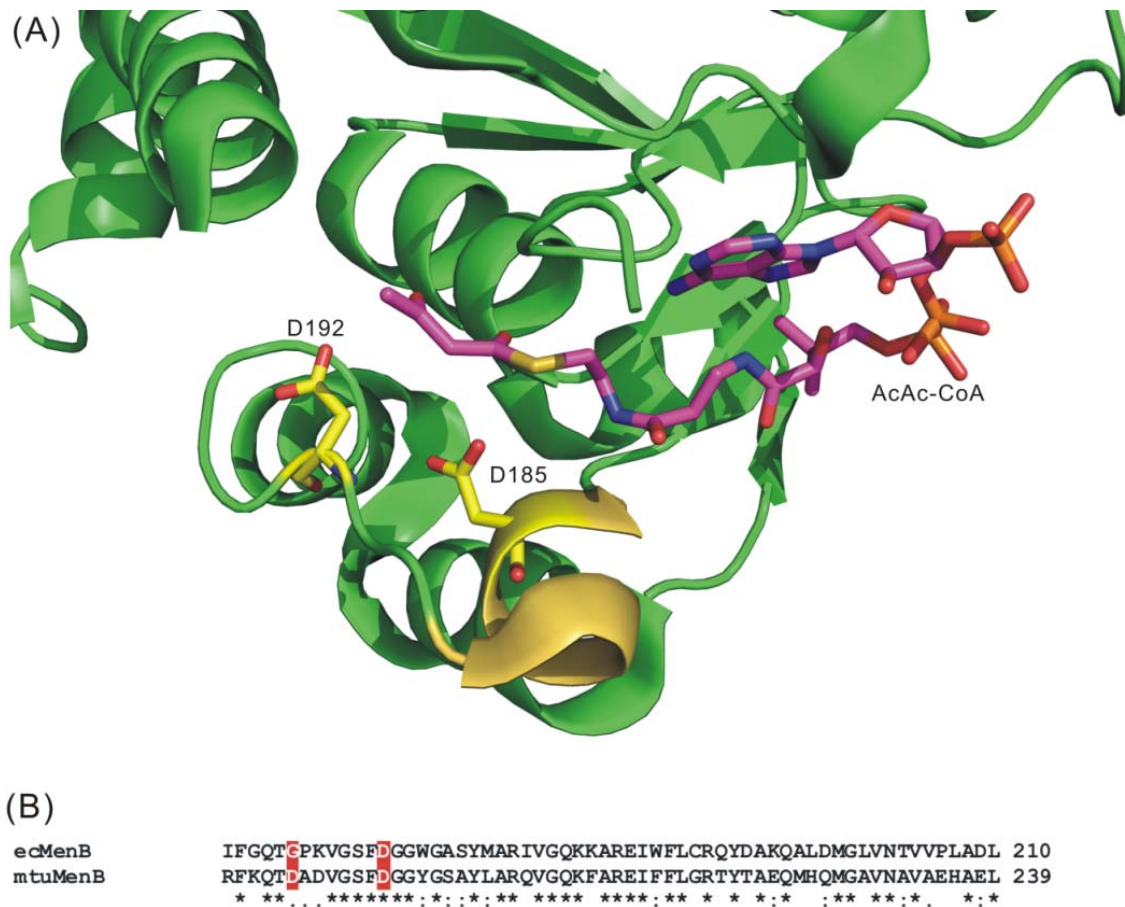


**Figure 6.12: X-ray structure of mtMenB•AcAc-CoA and sequence alignment of ecMenB and mtMenB.**

(A) X-ray structure of mtMenB•AcAc-CoA, D185 and D192 are shown in yellow stick,  $\alpha$ -helix is in yellow, (B) Sequence alignment of ecMenB and mtMenB, G156 and D163 in ecMenB and D185 and D192 in mtMenB are highlighted in red.

To better understand MenB's structure, Huei Jiun Li tried to crystallized mtMenB and ecMenB with the substrate analogue OSB-NCoA (**Figure 6.13**). Unfortunately, the OSB portion of OSB-NCoA is missing in the mtMenB•OSB-NCoA X-ray structure. However, OSB-NCoA was well-defined in the ecMenB•OSB-NCoA X-ray structure. This new structure can be superimposed with the mtMenB bound with acetoacetyl-CoA (AcAc-CoA) very well with RMSD value of 1.20 Å (**Figure 6.14A**). In the superimposed structure, D185 in mtMenB is very close to the carbonyl of OSB-NCoA within hydrogen

bond distance. So we speculate that D185 is important for substrate analogue OSB-NCoA's correct binding. In the case of ecMenB, a water molecule is in the same position as the oxygen atom on the D185's side chain. So D185 in mtMenB is replaced with G156 and water in ecMenB (**Figure 6.14B**). It indicated that mtMenB and ecMenB are using different substrate-binding strategy. Single-residue mutations, neither D185G in mtMenB or G156D in ecMenB, cannot recover the substrate-binding strategy, due to the presence of the water molecule; therefore these two mutants lost activity.

In summary, based on the current data, mtMenB and ecMenB use the same mechanism (65). D185 in mtMenB and G156 in ecMenB play an important structural role in substrate binding. In addition, HN-CoA is discovered as a promising lead inhibitor for mtMenB.

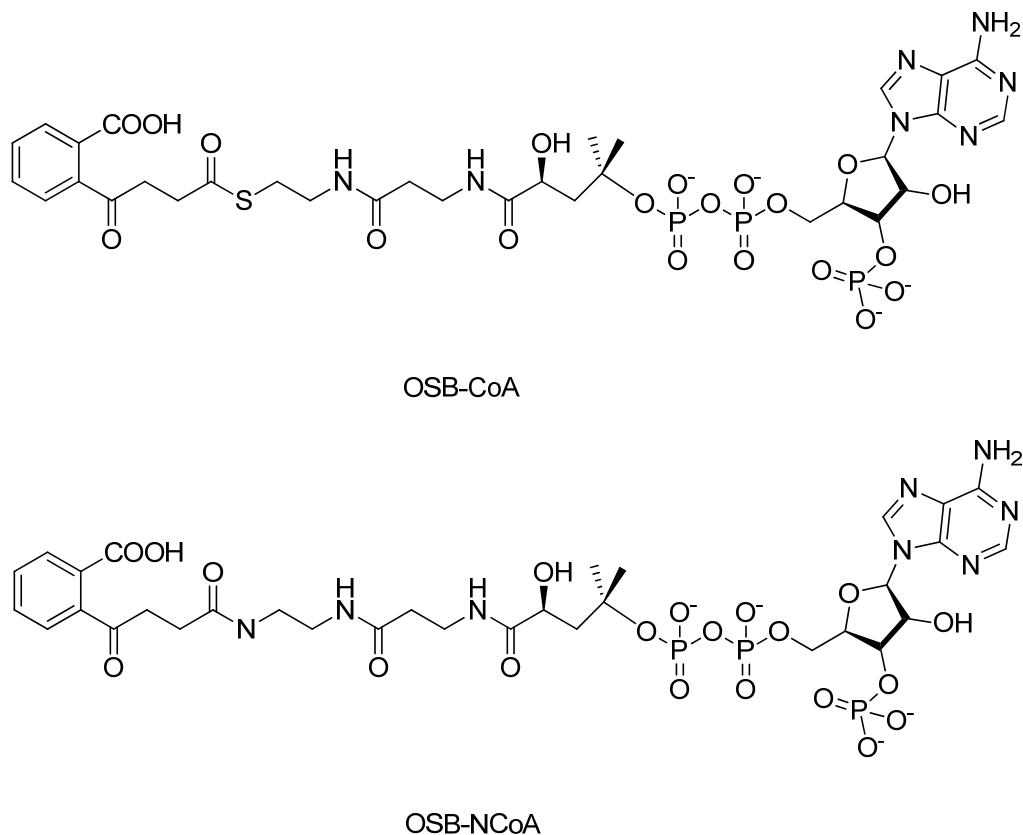
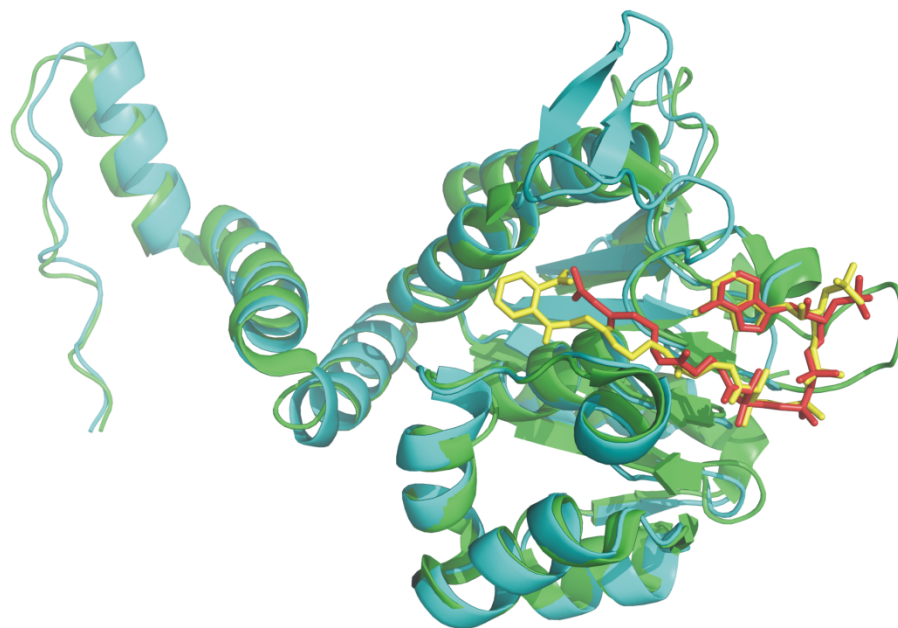


**Figure 6.13: Structure of OSB-CoA and OSB-NCoA.**

(A)



(B)

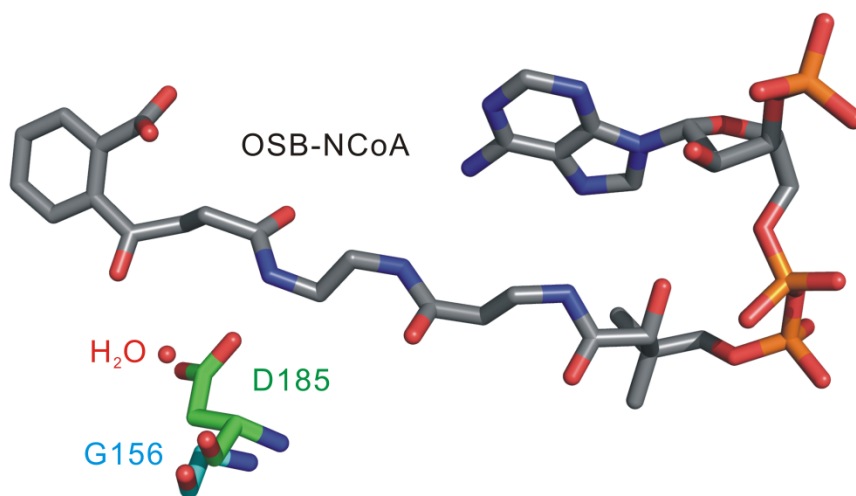


**Figure 6.14: Overlap of mtMenB bound AcAc-CoA (pdb code: 1q51) with and ecMenB bound with OSB-NCoA.**

(A) Superimposition of X-ray structure of mtMenB (in green)•AcAc-CoA (in red) and ecMenB (in cyan)•OSB-NCoA (in yellow) with RMSD of 1.20 Å. (B) D185 in mtMenB is replaced with G156 and water in ecMenB.



### Discovery of “substrate-like” inhibitors.

Based on the structure of “substrate-like” 2-amino-4-oxo-phenylbutanoic acids, Xiaokai Li synthesized analogues of 1548L21, which contain the OSB moiety with different substitutions on the aromatic ring. The synthesized compounds were evaluated for their ability to inhibit the reaction catalyzed by mtMenB as well as the growth of *M. tuberculosis* H37Rv. However, there was a poor correlation between enzyme inhibition and antimicrobial activity (**Table 6.2**).

As a prelude to explain the poor correlation, compound stability was evaluated by Xiaokai Li. Data suggest that this series of compounds are very unstable. For example, half-life ( $t_{1/2}$ ) of compound **8** is only 0.4 hour (**Table 6.2**). Therefore, during the  $IC_{50}$  measurements, these compounds degraded. It was speculated that these inhibitors readily undergo retro-Michael addition (225), which leads to generation of the (*E*)-benzoylacrylic acid and the amine (**Figure 6.15**).

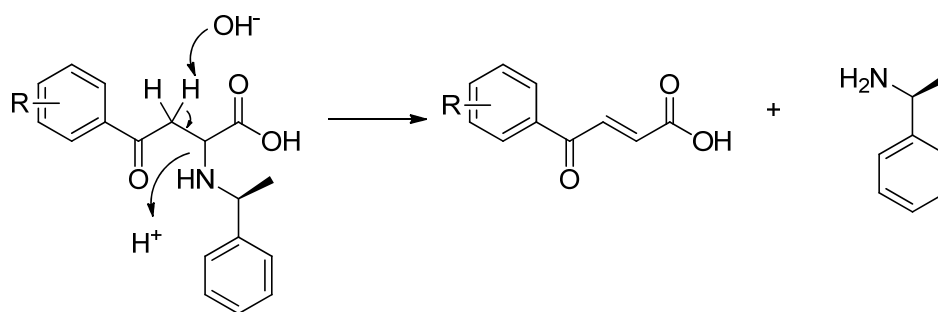


**Figure 6.15: 2-amino-4-oxo-phenylbutanoic acids degradation by retro-Michael addition.**

The (*E*)-benzoylacrylic acid product was then prepared, and their inhibition activity against mtMenB was characterized. Interestingly, the  $IC_{50}$  values for inhibition

were dependent on the CoA concentration and independent of the ATP concentration. For example, for (*E*)-4-(2,4-dichlorophenyl)-4-oxobut-2-enoic acid **22** (**Figure 6.16**), the IC<sub>50</sub> value varied from 0.2 to 1.4 μM when CoA concentration is varied from 30 to 120 μM. In contrast, the IC<sub>50</sub> value was constant at 0.2 μM when the ATP concentration was fixed at 30, 60, 120 μM (**Figure 6.17**). In addition, if **22** was incubated with OSB, CoA, ATP and ecMenE at RT for 45 min, the inhibition activity increase. Since the IC<sub>50</sub> value was dependent on both CoA concentration and incubation time, we speculated that **22**, as the Michael acceptor, might react with the free CoA present in the reaction to generate the final CoA adduct **23**, and that inhibition of mtMenB might result from the CoA adduct **23** (**Figure 6.18**).

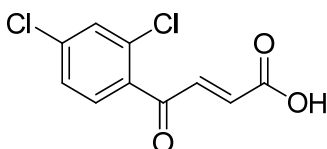


**Figure 6.16:** Structure of (*E*)-4-(2,4-dichlorophenyl)-4-oxobut-2-enoic acid (compound **22**).

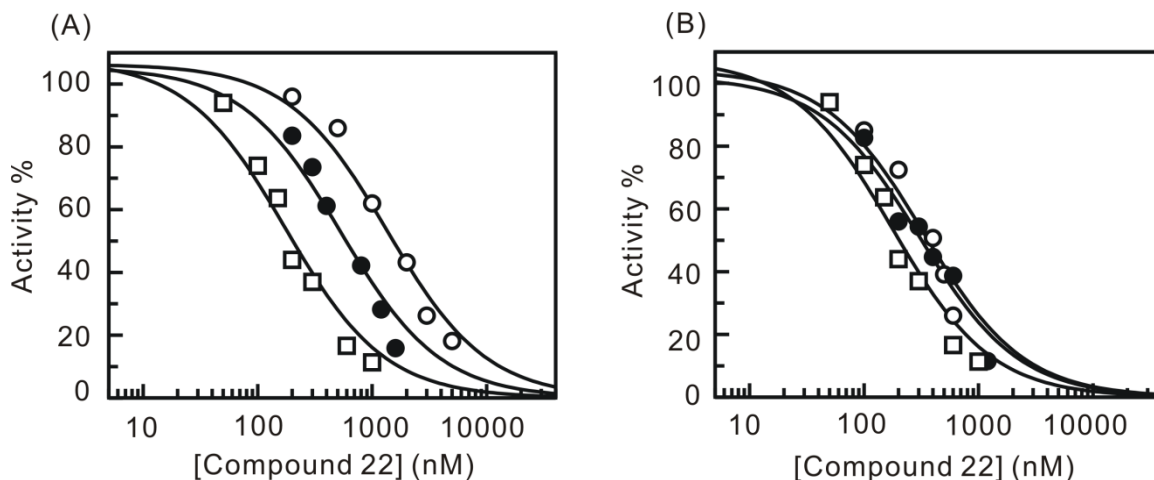


**Figure 6.17: IC<sub>50</sub> of Compound 22 measured at different CoA and ATP concentration.**

(A) CoA concentration was fixed at 30 μM (○), 60 μM (●) and 120 μM (□), (B) ATP concentration was fixed at 30 μM (○), 60 μM (●) and 120 μM (□).

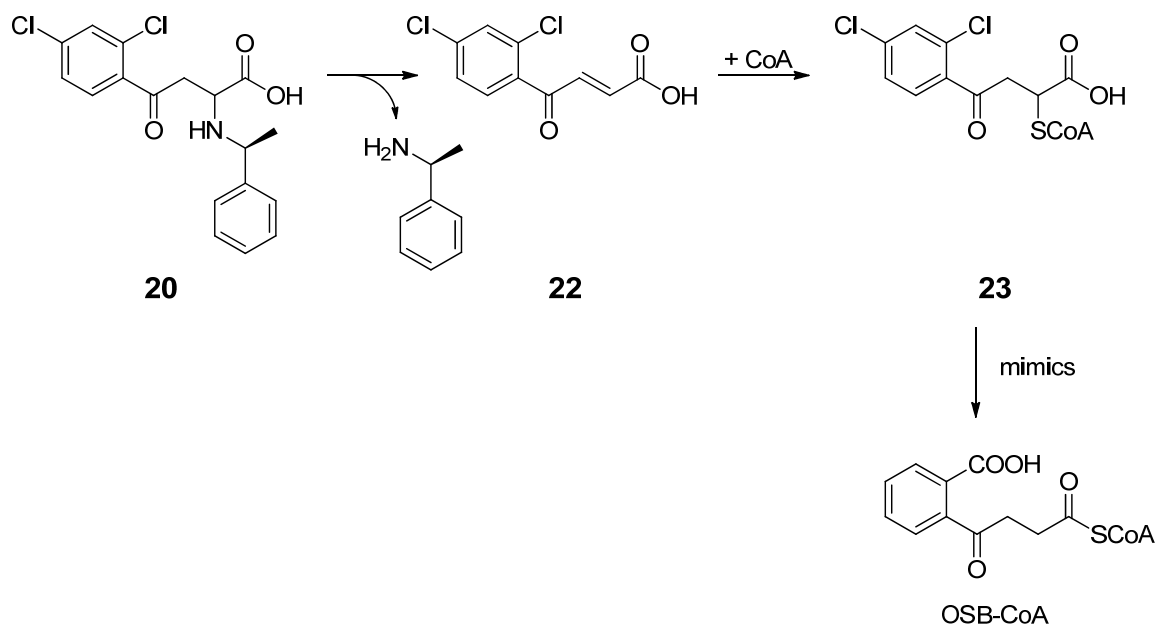


**Figure 6.18: Proposed mechanism of CoA adduct generation through Michael addition.**

To evaluate this prediction, Xiaokai Li synthesized some stable compounds which cannot undergo retro-Michael addition or Michael addition with free CoA, as a control. In 2-amino-4-oxo-phenylbutanoic acids, since the acidity of the proton adjacent to the ketone determine the rate of the retro-Michael addition, 2-amino-3,3-dimethyl-4-oxo-phenyl-butanoic acid (**24**) was synthesized. In this compound, the acidic hydrogen was replaced with a methyl group, so that no hydrogen cannot be abstracted to form the (*E*)-benzoylacrylic acid. In addition, 4-oxo-4-phenylbutanoic acids (**25** and **26**, **Figure 6.19**) were synthesized. These compounds do not have unsaturated carbonyl, so they cannot form CoA adduct. In agreement with our prediction, all of these compounds have no inhibition activity at 200  $\mu$ M. Thus, we believe that CoA adducts are the real inhibitors of MenB.

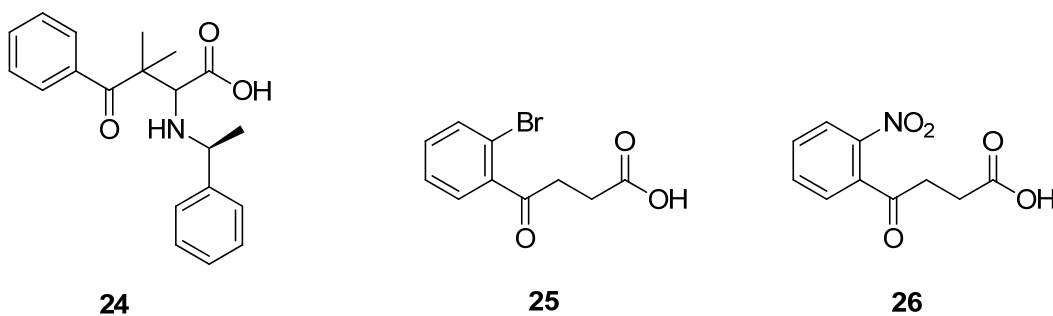


**Figure 6.19: Structure of 2-amino-3,3-dimethyl-4-oxo-phenyl-butanoic acids (**24**) and two 4-oxo-4-phenylbutanoic acids (**25** and **26**).**

To gain direct experimental evidence with this prediction, **22** was incubated with CoA, ATP and ecMenE in MenB reaction buffer (pH=7) at RT for 2h and the major product was purified by HPLC. ESI-MS and NMR data confirmed that the CoA thiol had

added to the C2 carbon of the acid through Michael addition, to generate compound **23** (**Figure 6.18**). Stability assays suggested that **23** is much more stable than **20**, with half life of 11.4 hr. Therefore, we speculate that **23** is the active inhibitor, whose structure is reminiscent of the MenB substrate OSB-CoA (**Figure 6.18**). In agreement with this prediction,  $IC_{50}$  of the CoA adduct **23** was independent on CoA concentration (**Figure 6.20**).

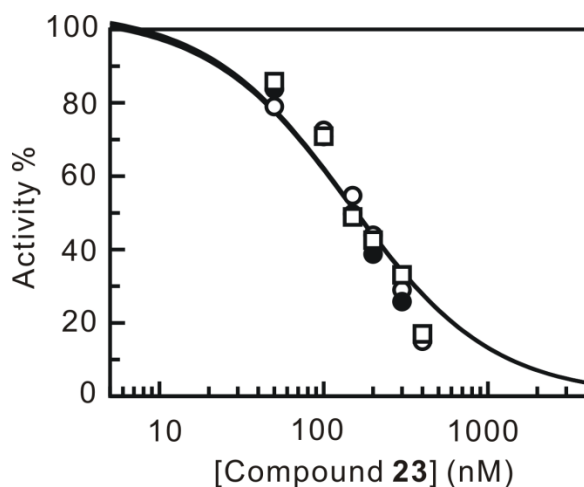


**Figure 6.20:  $IC_{50}$  of Compound 23 measured at different CoA concentration.** CoA concentration was fixed at 30  $\mu$ M (○), 60  $\mu$ M (●) and 120  $\mu$ M (□).

In order to gain further mechanistic insight, we used steady state kinetic methods to study the inhibition of mtMenB by **23**. Inhibition mechanism was characterized by measuring initial velocities at various concentrations of **23** (0-4350 nM) and OSB (7.5-90  $\mu$ M) in reaction mixtures containing 120  $\mu$ M ATP, 120  $\mu$ M CoA, 2  $\mu$ M ecMenE and 150 nM mtMenB. Values of  $K_i^{app}$  and  $[E]$  obtained from **equation 6.3** were then fitted to **equation 6.4-6.6**. The dependence of  $K_i^{app}$  and  $[E]$  was best described by **equation 6.6**, indicating **23** is a noncompetitive inhibitor  $K_i$  value of  $49 \pm 6$  nM and  $K_i'$  value of  $286 \pm 7$  nM (**Figure 6.21**). From the data fitting, enzyme concentration was fitted as 125 nM,

which was less than the concentration calculated from UV absorbance. It is reasonable that some enzyme may not be active. In order to account for noncompetitive inhibition, we speculate that the binding of inhibitor to one subunit in the mtMenB homohexamer can modulate the activity of adjacent subunits.

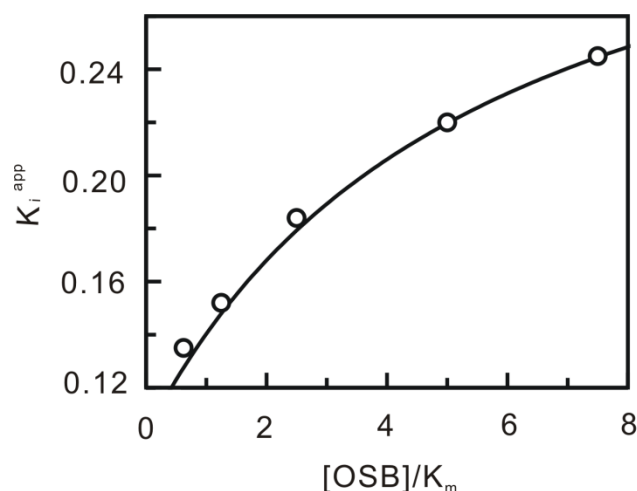
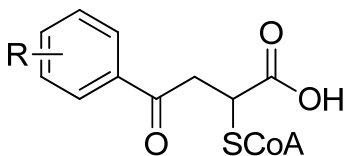


**Figure 6.21: Effect of OSB on  $K_i^{\text{app}}$  of **23**.** Fitted curve is shown for **equation 6.6** (solid line;  $K_i = 49 \pm 6$  nM,  $K_i' = 286 \pm 7$  nM).

Above enzyme inhibition data were very promising, therefore analogues (**27-35**) of CoA adduct **23** were synthesized. SAR for inhibition of mtMenB by the CoA adducts was evaluated using the coupled assay (**Table 6.7**). In general, incorporation of a bulky substituent at either *meta* or *para* position of the phenyl group resulted in significant reduction in enzyme inhibition (**28** and **35**). Incorporation of electron-donating substituents at either *ortho* or *para* positions of the aromatic ring also decreased inhibitor potency (**27**, **28** and **34**). In contrast, introduction of an electron-withdrawing substituent into the aromatic ring resulted in an increase in enzyme inhibition (**29-33**).

**Table 6.7: Enzyme inhibition and stability of CoA adducts.**



Compound	R	IC <sub>50</sub> (nM)	K <sub>i</sub> (nM)	K <sub>i</sub> ' (nM)	h <sub>1/2</sub> <sup>a</sup> (hr)
<b>23</b>	2,4-diCl	106±26	49±6	286±7	11.4
<b>27</b>	4-Cl	468±62	271±71	1830±193	>100
<b>28</b>	4-OMe	33500±2600			36.5
<b>29</b>	2-F	204±37			53.3
<b>30</b>	2-Cl	103±23			>100
<b>31</b>	2-Br	135±22			99.0
<b>32</b>	2-I	421±57			43.3
<b>33</b>	2-NO <sub>2</sub>	154±24			86.6
<b>34</b>	2-OMe	12100±1000			38.5
<b>35</b>	3-Cl	14100±1500			18.7
<b>36</b>	2-NO <sub>2</sub>	32100±3300			
<b>37</b>	2,4-diCl	2200±200			

<sup>a</sup> half life at pH 7.4 and 25°C, measured by Xiaokai Li

Analysis of the mtMenB structure and reaction mechanism suggests an explanation for the high affinity of the CoA adducts. The structural homology of mtMenB with the crotonase family suggests that catalysis by MenB involves formation of a CoA thioester enolate, which is stabilized by the oxyanion hole characteristic of this class of enzymes (65). We speculate that the CoA adducts can adopt a bound structure that resembles the CoA thioester enolate (**Figure 6.22**), which may account for the high affinity of these compounds for mtMenB.

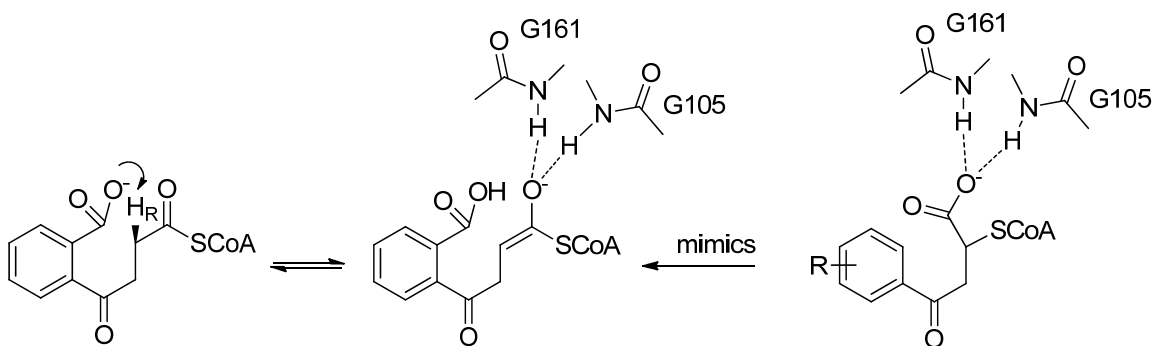


**Figure 6.22: Proposed structure of the CoA adduct bound to mtMenB.**

The binding of CoA adducts to MenB was further characterized by X-ray study. Compound **23** was co-crystallized with mtMenB and ecMenB. Unfortunately, only ecMenB•**23** produced crystals. Crystal structure was then solved by Huei Jiun Li. ecMenB binds to **23** through hydrogen bonds, salt bridges and hydrophobic interaction, resembling the binding between mtMenB and AcAc-CoA (65). ecMenB binds to **23** through hydrogen bond between free carboxylate in **23** and nitrogen atoms of oxyanion hole (G86 and G133, ecMenB numbering) (**Figure 6.23**). mtMenB and ecMenB share 48% identity and 61% similarity. Their oxyanion hole residues together with catalytic



residues (S161, D163 and Y258, ecMenB numbering; S190, D192 and Y287, mtMenB numbering) are conserved. In addition, their crystal structure overlap well (**Figure 6.14A**). Consequently, we predict **23** would adopt a similar bound structure in mtMenB as in ecMenB. Furthermore this structure with extensive hydrogen bonds, salt bridges and hydrophobic interaction accounts for the high affinity of **23** for mtMenB.

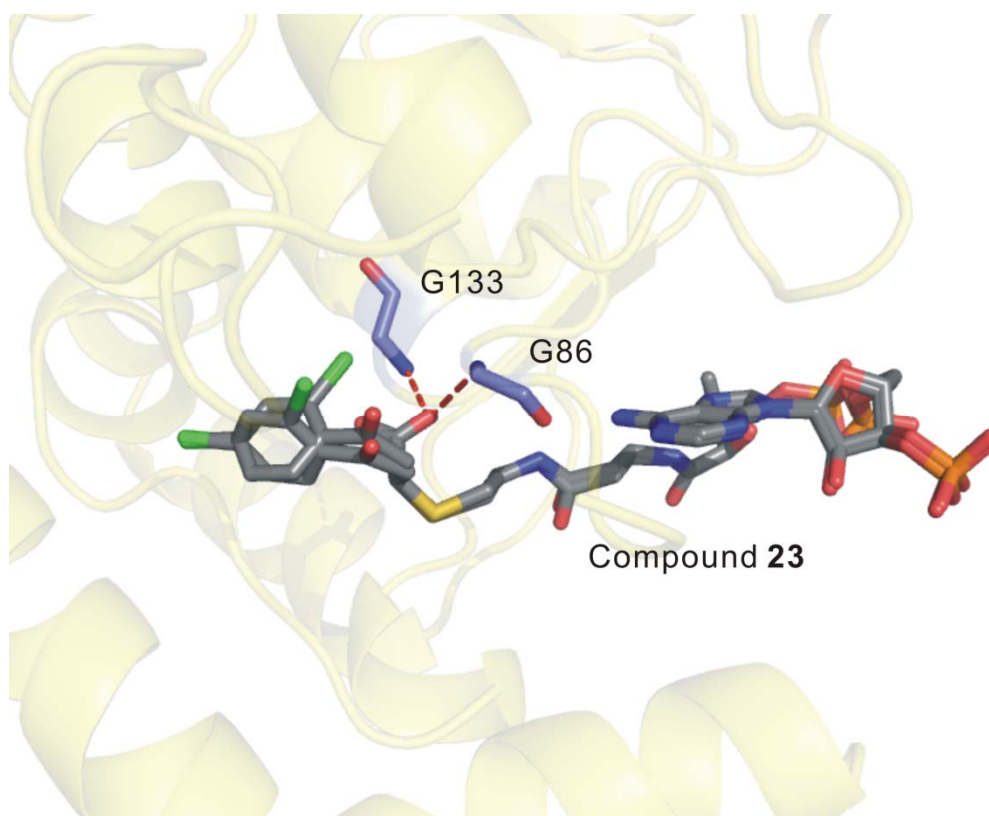


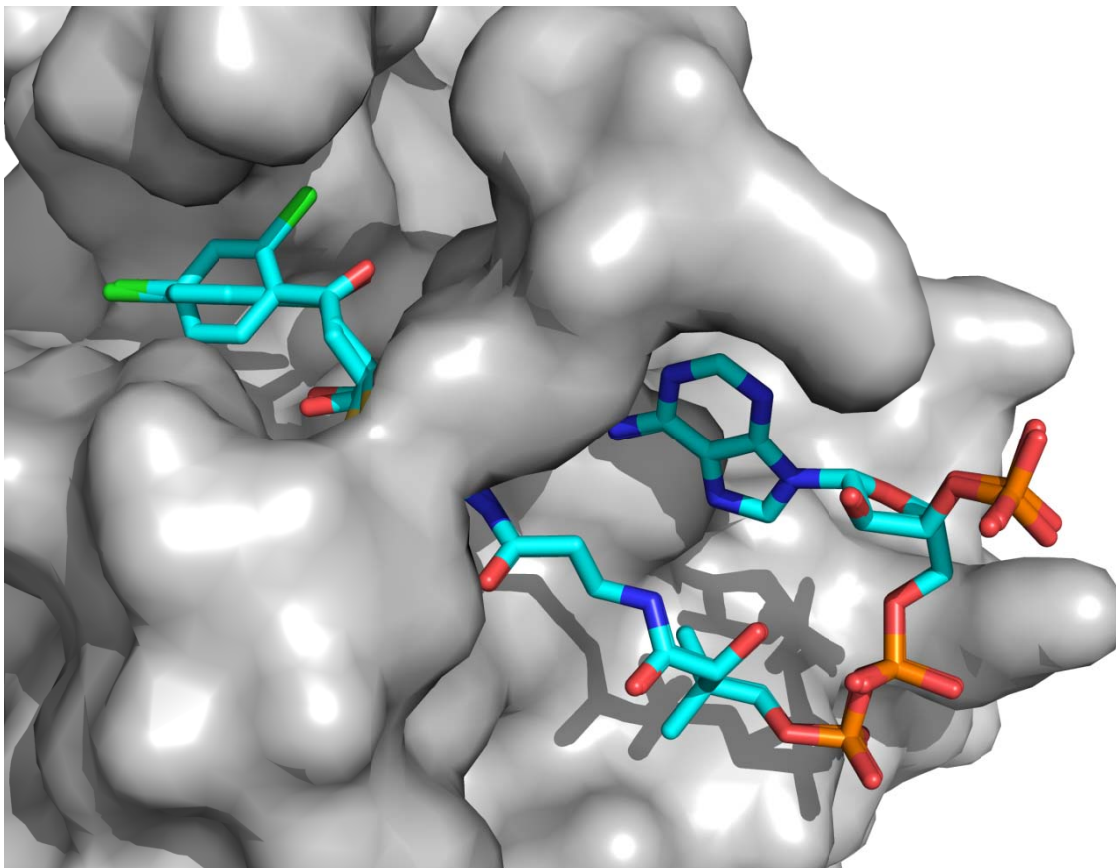
**Figure 6.23: Interactions between ecMenB and compound 23.**  
Two conformations of 23 are superimposed.

An important aspect of the binding mode is the location of the free carboxylate in the CoA adduct. Consequently Xiaokai Li synthesized two OSB-CoA thioester analogues (**36** and **37**), which have similar structures to the CoA adducts but lack the free carboxylate group. Compared with the CoA adducts, the CoA thioesters have much lower affinity for mtMenB (**Table 6.7**) with **36** having an  $IC_{50}$  value of 32  $\mu$ M compared

to 150 nM for the corresponding adduct and **37** having the IC<sub>50</sub> value of 2 μM compared to 100 nM for the corresponding adduct, thus supporting the importance of the free carboxylate for CoA adduct binding.

The only drawback of the CoA adduct is that CoA moiety is too hydrophilic to cross the cell membrane; therefore the CoA based molecule cannot be a good drug-like inhibitor. In agreement, the antimicrobial activity of the CoA adducts is very weak, presumably due to poor uptake by the bacteria. In the crystal structure of ecMenB bound with compound **23**, there are two binding pockets: the active site and CoA binding site (**Figure 6.24**). The portion of the inhibitor in the active site pocket is responsible for the inhibitor binding specificity, while the highly hydrophilic portion of the inhibitor in the CoA binding pocket is responsible for tight binding. To increase the hydrophobicity of CoA adducts, several CoA surrogates were designed and synthesized. In general, CoA surrogates have weaker activity than CoA adducts (**Table 6.8**). If the phosphate group is absent on the ribose (**38**), compound would have lower binding affinity for mtMenB compared to parent compound **23**, with IC<sub>50</sub> value of 506 nM. If adenine is absent, or if both ribose and phosphate group (**39** and **40**) are absent, compounds would have even lower binding affinity, with IC<sub>50</sub> value of 170 μM (**39**) and 29 μM (**40**). In addition, based on the structure of CoA, more compounds were designed to replace adenine, ribose and phosphate group (**41-46**), however, their binding affinity is much lower than parent compound **23** by >150-fold. This result also supports that the disruption of hydrogen bonding with enzyme compromises the inhibition, and that the CoA moiety is essential for the high binding affinity. Further studies are required to fully

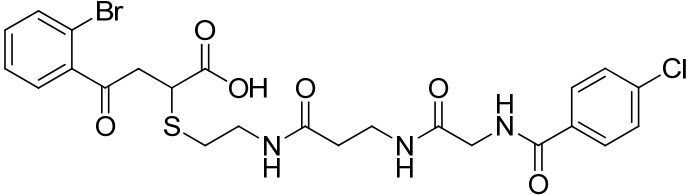
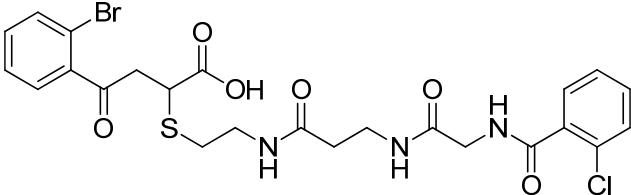
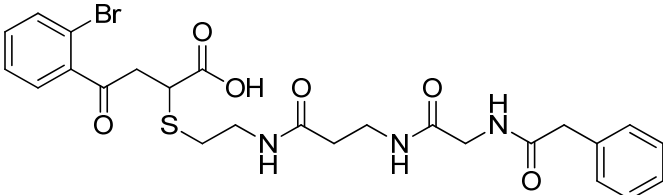
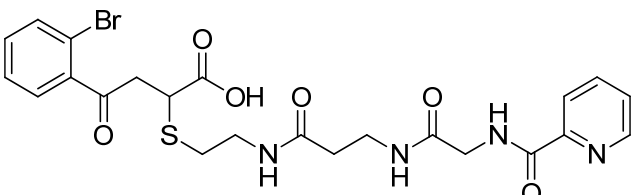
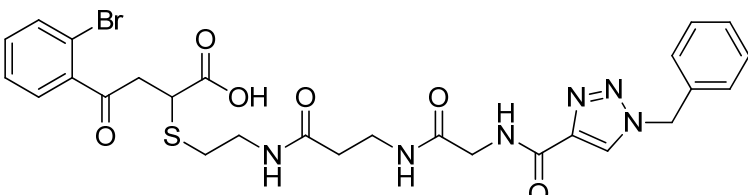
understand the binding of the CoA moiety and to design better CoA moiety replacement.



**Figure 6.24: Crystal structure of ecMenB bound with 23.**

**Table 6.8: Enzyme inhibition of compounds with CoA portion replacement.**

Compound	IC <sub>50</sub>
<b>23</b>	106 ± 26 nM
<b>38</b>	506 ± 60 nM
<b>39</b>	~170.0 μM
<b>40</b>	28.5 ± 6 μM
<b>41</b>	14 ± 1 μM

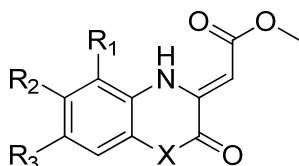
Compound	IC <sub>50</sub>
<b>42</b> 	19 ± 3 μM
<b>43</b> 	18 ± 4 μM
<b>44</b> 	75 ± 4 μM
<b>45</b> 	23 ± 4 μM
<b>46</b> 	77 ± 17 μM

*Discovery of “product-like” inhibitors.*

Based on the structure of “product-like” benzoxazinones, analogues of 1486C16 (**Table 6.1**) were synthesized by Xiaokai Li. The synthesized compounds were evaluated for their ability to inhibit the reaction catalyzed by mtMenB as well as the growth of *M. tuberculosis* H37Rv (**Table 6.9**).

Since a coupled assay was used, the ability of these compounds to inhibit ecMenE was evaluated. Three inhibitors (**47**, **56**, **57**) were randomly selected to test ecMenE inhibition by directly monitoring the formation of PPI (226) and by the ecMenE/mtMenB coupled assay using a limiting concentration of ecMenE. However, none of inhibitors affected ecMenE activity at a concentration of 50  $\mu$ M. Therefore, this series of inhibitors specifically inhibit MenB.

**Table 6.9: *In vitro* activity of 1,4-benzoxazine: (Z)-methyl 2-(2-oxo-2H-benzo[b][1,4]oxazin-3(4H)ylidene)acetates.**



Compound	R <sub>1</sub>	R <sub>2</sub>	R <sub>3</sub>	X	IC <sub>50</sub> ( $\mu$ M)	K <sub>i</sub> ( $\mu$ M)	K <sub>i</sub> ' ( $\mu$ M)	MIC ( $\mu$ g/mL)
47	H	H	H	N	>122			>100
48	H	H	H	S	>140			>100
49	H	H	H	O	10.0 $\pm$ 1.0	9.1	67.0	0.64
50	Me	H	H	O	24.1 $\pm$ 1.8			25
51	H	Me	H	O	23.1 $\pm$ 1.0			>100
52	H	H	Me	O	18.2 $\pm$ 2.8			100
53	H	F	H	O	27.0 $\pm$ 3.0	11.5	10.1	0.63
54	H	H	F	O	30.0 $\pm$ 3.7			0.63
55	H	Cl	H	O	46.3 $\pm$ 3.5	22.5	18.5	5
56	H	H	Cl	O	35.7 $\pm$ 4.8			0.63
57	H	NO <sub>2</sub>	H	O	28.2 $\pm$ 4.4			50
58	H	H	NO <sub>2</sub>	O	20.3 $\pm$ 1.8			>100
59	H	EtSO <sub>2</sub>	H	O	17.9 $\pm$ 3.0			>100

Compounds with quinoxaline (**47**) or benzothiazine (**48**) cores had significantly higher MIC value, indicating that the benzoxazine core is essential for antibacterial activity. Several compounds had low MIC value ( $< 1\mu\text{g/mL}$ ), in which there was either no substituent on the benzoxazine core (**49**), or in which  $R^2 = \text{F}$  (**53**) or  $R^3 = \text{F}$  or  $\text{Cl}$  (**54**, **56**). Introduction of larger electron withdrawing groups ( $R^2 = \text{Cl}$  (**55**),  $R^2 = \text{NO}_2$  (**57**),  $R^3 = \text{NO}_2$  (**58**),  $R^2 = \text{EtSO}_2$  (**59**)) or an electron donating groups such as methyl (**50**, **51**, **52**), resulted in a significant reduction ( $>100$ -fold) in antibacterial activity. This suggested that the effect on antibacterial activity is affected by the size of the substituent, but not from electronic effects.

Although the substitution of benzoxazine core had a dramatic effect on antibacterial activity, the impact of the inhibition of MenB was much less obvious. Although it can be seen from **Table 6.9** that the benzoxazine core is essential for mtMenB inhibition,  $\text{IC}_{50}$  values for benzoxazine analogues only changed by 4-5 fold. These data suggest that there is little correlation between  $\text{IC}_{50}$  and MIC value. Thus these inhibitors may have some other target(s) in the bacteria. In addition, other factors such as altered cell permeability and/or evasion of detoxification strategies may also modulate antibacterial activity.

In order to gain further mechanistic insight, we used steady state kinetic methods to study the inhibition of mtMenB by **49**. These studies revealed that **49**, is a noncompetitive inhibitor with respect to the substrate OSB-CoA, with a  $K_i$  value of  $9.1\mu\text{M}$  and a  $K_i'$  value of  $67\mu\text{M}$ , respectively.

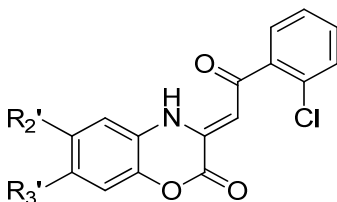
To further study the antimicrobial properties of the 1,4-benzoxazines, Xiaokai Li designed and synthesized a second series of compounds in which the methyl ester was



replaced with a substituted phenyl ring (**Table 6.10**). MIC values of **61** and **64** increased by 5-fold, and MIC values of **66** increased by 2.5-fold compared to analogues in **Table 6.8**, however, none of these compounds (**61-67**) were able to inhibit mtMenB up to 100  $\mu$ M. Thus, introduction of a bulky group into the side chain significantly affects the ability of the 1,4-benzoxazines to inhibit mtMenB. The data suggest that activity might be improved by reducing the size of the side chain (227-229), and that while a portion of their antibacterial activity could stem from an ability to inhibit mtMenB, there must be additional targets for these compounds in the cell.

For both series of benzoxazinones, introduction of a methyl group into the benzoxazine ring (**48-50**, **62**, **63**) abolished antibacterial activity shown by MIC value. Thus, both of them likely have a common target in the cell, and inhibition of which is very sensitive to methylation.

**Table 6.10: *In vitro* activity of 1,4-benzoxazine: (Z)-3-(2-aryl-2-oxoethylidene)-3,4-dihydro-2H-benzo[*b*][1,4]oxazin-2-ones.**

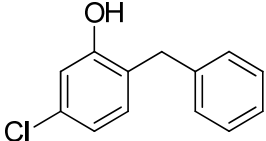
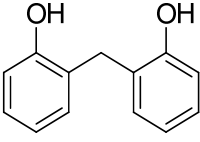
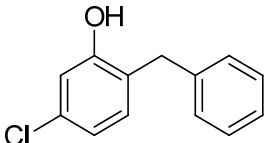
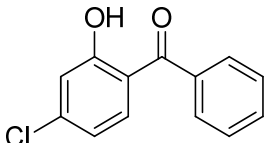
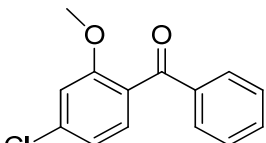
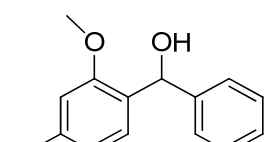


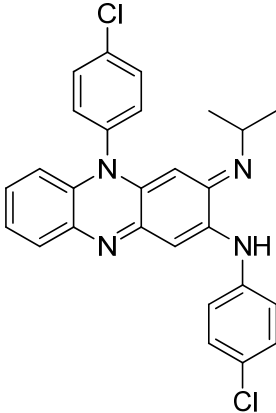
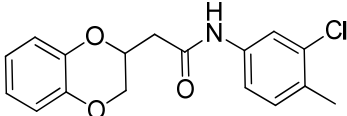
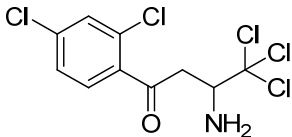
Compound	R <sub>2</sub> '	R <sub>3</sub> '	Enzyme Inhibition	MIC (µg/mL)
61	H	H		3.13
62	Me	H		100
63	H	Me		>100
64	F	H	No inhibition at 100 µM	3.13
65	H	F		1.56
66	Cl	H		12.5
67	H	Cl		3.13

*In vitro enzymatic inhibition assay of other inhibitors.*

To look for novel scaffold of mtMenB inhibitor, we also evaluated enzyme inhibition activity of a few inhibitors from our lab, or that are commercially available. However, none of them were able to inhibit mtMenB up to concentration of 200  $\mu$ M (**Table 6.11**).

**Table 6.11: Enzyme inhibition of of other inhibitors.**

Compound	Enzyme Inhibition
68 	$IC_{50} > 220 \mu M$
69 	No inhibition at 200 $\mu M$
70 	No inhibition at 200 $\mu M$
71 	No inhibition at 200 $\mu M$
72 	No inhibition at 200 $\mu M$
73 	No inhibition at 200 $\mu M$

Compound	Enzyme Inhibition
<b>74</b> 	IC <sub>50</sub> >140 μM
<b>75</b> 	100 μM Not dissolved  10 μM No inhibition
<b>76</b> 	200 μM Not dissolved  100 μM, No inhibition

## Conclusions

MenB, an enzyme in the menaquinone biosynthesis pathway, catalyzes the Dieckmann condensation of OSB-CoA to DHNA-CoA. mtMenB differs from ecMenB by an active site Asp residue in place of Gly. Based on current data, mtMenB and ecMenB utilize same mechanism with OSB-CoA as the substrate. In addition, D185 in mtMenB and G156 in ecMenB play an important structural role in substrate binding. Interestingly, HN-CoA was a MenB inhibitor and will be investigated for future inhibition studies.

Two series of inhibitors of mtMenB including the “substrate-like” 2-amino-4-oxo-phenylbutanoic acids and the “product-like” benzoxazinones were identified from high throughput screen. Our studies explained the reason for poor SAR observed in “substrate-like” 2-amino-4-oxo-phenylbutanoic acids analogues, and then identified a series of 2-CoA-4-oxo-4-(substituted phenyl) butanoic acids as the potent inhibitors of mtMenB with the best  $K_i$  value of 18 nM. In addition, we have identified a group of “product-like” 1,4-benzoxazines with promising *in vitro* antibacterial activity toward *M. tuberculosis* H37Rv with MIC value of 0.63  $\mu\text{g/mL}$ . However, the current SAR data suggest that these compounds act by binding to additional unknown targets within the cell, which need to be further investigated.

## Bibliography

1. Landsberg, H. Prelude to the Discovery of Penicillin. (1949) *Isis* 40, 225-227.
2. Bosch, F., and Rosich, L. The contributions of Paul Ehrlich to pharmacology: A tribute on the occasion of the centenary of his Nobel Prize. (2008) *Pharmacol.* 82, 171-179.
3. Fleming, A. Penicillin. (1941) *Br. Med. J.* 1941, 386-386.
4. Wright, G. D. The antibiotic resistome: the nexus of chemical and genetic diversity. (2007) *Nat. Rev. Microbiol.* 5, 175-186.
5. McGowan, J. E. Resistance in nonfermenting gram-negative bacteria: Multidrug resistance to the maximum. (2006) *Am. J. Infect. Control* 34, S29-S37.
6. Chopra, I., Hodgson, J., Metcalf, B., and Poste, G. New approaches to the control of infections caused by antibiotic-resistant bacteria. An industry perspective. (1996) *JAMA* 275, 401-403.
7. Levy, S. B., and Marshall, B. Antibacterial resistance worldwide: causes, challenges and responses. (2004) *Nat. Med.* 10, S122-S129.
8. McDevitt, D., and Rosenberg, M. Exploiting genomics to discover new antibiotics. (2001) *Trends Microbiol.* 9, 611-617.
9. Campbell, J. W., and Cronan, J. E. Bacterial fatty acid biosynthesis: Targets for antibacterial drug discovery. (2001) *Annu. Rev. Microbiol.* 55, 305-332.
10. Payne, D. J., Warren, P. V., Holmes, D. J., Ji, Y. D., and Lonsdale, J. T. Bacterial fatty-acid biosynthesis: a genomics-driven target for antibacterial drug discovery. (2001) *Drug Discov. Today* 6, 537-544.

11. Cronan, J. E., and Waldrop, G. L. Multi-subunit acetyl-CoA carboxylases. (2002) *Prog. Lipid Res.* 41, 407-435.
12. Ruch, F. E., and Vagelos, P. R. Characterization of a Malonyl-Enzyme Intermediate and Identification of Malonyl Binding-Site in Malonyl Coenzyme-a-Acyl Carrier Protein Transacylase of Escherichia-Coli. (1973) *J. Biol. Chem.* 248, 8095-8106.
13. Jackowski, S., and Rock, C. O. Acetoacetyl-Acyl Carrier Protein Synthase, a Potential Regulator of Fatty-Acid Biosynthesis in Bacteria. (1987) *J. Biol. Chem.* 262, 7927-7931.
14. Price, A. C., Zhang, Y. M., Rock, C. O., and White, S. W. Structure of beta-ketoacyl-[acyl carrier protein] reductase from Escherichia coli: Negative cooperativity and its structural basis. (2001) *Biochemistry* 40, 12772-12781.
15. Price, A. C., Zhang, Y. M., Rock, C. O., and White, S. W. Cofactor-induced conformational rearrangements establish a catalytically competent active site and a proton relay conduit in FabG. (2004) *Structure* 12, 417-428.
16. Kimber, M. S., Martin, F., Lu, Y. J., Houston, S., Vedadi, M., Dharamsi, A., Fiebig, K. M., Schmid, M., and Rock, C. O. The structure of (3R)-hydroxyacyl-acyl carrier protein dehydratase (FabZ) from Pseudomonas aeruginosa. (2004) *J. Biol. Chem.* 279, 52593-52602.
17. Leesong, M., Henderson, B. S., Gillig, J. R., Schwab, J. M., and Smith, J. L. Structure of a dehydratase-isomerase from the bacterial pathway for biosynthesis of unsaturated fatty acids: Two catalytic activities in one active site. (1996) *Structure* 4, 253-264.



18. Baldock, C., Rafferty, J. B., Sedelnikova, S. E., Baker, P. J., Stuitje, A. R., Slabas, A. R., Hawkes, T. R., and Rice, D. W. A mechanism of drug action revealed by structural studies of enoyl reductase. (1996) *Science* 274, 2107-2110.
19. Baldock, C., Rafferty, J. B., Stuitje, A. R., Slabas, A. R., and Rice, D. W. The X-ray structure of *Escherichia coli* enoyl reductase with bound NAD(+) at 2.1 angstrom resolution. (1998) *J. Med. Biol.* 284, 1529-1546.
20. Roujeinikova, A., Levy, C. W., Rowsell, S., Sedelnikova, S., Baker, P. J., Minshull, C. A., Mistry, A., Colls, J. G., Camble, R., Stuitje, A. R., Slabas, A. R., Rafferty, J. B., Pauptit, R. A., Viner, R., and Rice, D. W. Crystallographic analysis of triclosan bound to enoyl reductase. (1999) *J. Med. Biol.* 294, 527-535.
21. Roujeinikova, A., Sedelnikova, S., de Boer, G. J., Stuitje, A. R., Slabas, A. R., Rafferty, J. B., and Rice, D. W. Inhibitor binding studies on enoyl reductase reveal conformational changes related to substrate recognition. (1999) *J. Biol. Chem.* 274, 30811-30817.
22. Stewart, M. J., Parikh, S., Xiao, G. P., Tonge, P. J., and Kisker, C. Structural basis and mechanism of enoyl reductase inhibition by triclosan. (1999) *J. Mol. Biol.* 290, 859-865.
23. Rozwarski, D. A., Grant, G. A., Barton, D. H. R., Jacobs, W. R., and Sacchettini, J. C. Modification of the NADH of the isoniazid target (InhA) from *Mycobacterium tuberculosis*. (1998) *Science* 279, 98-102.
24. Rozwarski, D. A., Vilcheze, C., Sugantino, M., Bittman, R., and Sacchettini, J. C. Crystal structure of the *Mycobacterium tuberculosis* enoyl-ACP reductase, InhA,

- in complex with NAD(+) and a C16 fatty acyl substrate. (1999) *J. Biol. Chem.* 274, 15582-15589.
25. Xu, H., Sullivan, T. J., Sekiguchi, J. I., Kirikae, T., Ojima, I., Stratton, C. F., Mao, W. M., Rock, F. L., Alley, M. R. K., Johnson, F., Walker, S. G., and Tonge, P. J. Mechanism and inhibition of saFabI, the enoyl reductase from *Staphylococcus aureus*. (2008) *Biochemistry* 47, 4228-4236.
  26. Lu, H., England, K., Ende, C. A., Truglio, J. J., Luckner, S., Reddy, B. G., Marlenee, N. L., Knudson, S. E., Knudson, D. L., Bowen, R. A., Kisker, C., Slayden, R. A., and Tonge, P. J. Slow-Onset Inhibition of the FabI Enoyl Reductase from *Francisella tularensis*: Residence Time and in Vivo Activity. (2009) *ACS Chem. Biol.* 4, 221-231.
  27. Parikh, S., Moynihan, D. P., Xiao, G. P., and Tonge, P. J. Roles of tyrosine 158 and lysine 165 in the catalytic mechanism of InhA, the enoyl-ACP reductase from *Mycobacterium tuberculosis*. (1999) *Biochemistry* 38, 13623-13634.
  28. Rafferty, J. B., Simon, J. W., Baldock, C., Artymiuk, P. J., Baker, P. J., Stuitje, A. R., Slabas, A. R., and Rice, D. W. Common Themes in Redox Chemistry Emerge from the X-Ray Structure of Oilseed Rape (*Brassica-Napus*) Enoyl Acyl Carrier Protein Reductase. (1995) *Structure* 3, 927-938.
  29. White, S. W., Zheng, J., Zhang, Y. M., and Rock, C. O. The structural biology of type II fatty acid biosynthesis. (2005) *Annu. Rev. Biochem.* 74, 791-831.
  30. Heath, R. J., Su, N., Murphy, C. K., and Rock, C. O. The enoyl-[acyl-carrier-protein] reductases FabI and FabL from *Bacillus subtilis*. (2000) *J. Biol. Chem.* 275, 40128-40133.

31. Lu, H., and Tonge, P. J. Mechanism and Inhibition of the FabV Enoyl-ACP Reductase from *Burkholderia mallei*. (2010) *Biochemistry* 49, 1281-1289.
32. Massengo-Tiasse, R. P., and Cronan, J. E. *Vibrio cholerae* FabV defines a new class of enoyl-acyl carrier protein reductase. (2008) *J. Biol. Chem.* 283, 1308-1316.
33. Zhu, L., Lin, J. S., Ma, J. C., Cronan, J. E., and Wang, H. H. Triclosan Resistance of *Pseudomonas aeruginosa* PAO1 Is Due to FabV, a Triclosan-Resistant Enoyl-Acyl Carrier Protein Reductase. (2010) *Antimicrob. Agents Chemother.* 54, 689-698.
34. Marrakchi, H., DeWolf, W. E., Quinn, C., West, J., Polizzi, B. J., So, C. Y., Holmes, D. J., Reed, S. L., Heath, R. J., Payne, D. J., Rock, C. O., and Wallis, N. G. Characterization of *Streptococcus pneumoniae* enoyl-(acyl-carrier protein) reductase (FabK). (2003) *Biochem. J.* 370, 1055-1062.
35. Bergler, H., Fuchsbichler, S., Hogenauer, G., and Turnowsky, F. The enoyl-[acyl-carrier-protein] reductase (FabI) of *Escherichia coli*, which catalyzes a key regulatory step in fatty acid biosynthesis, accepts NADH and NADPH as cofactors and is inhibited by palmitoyl-CoA. (1996) *Eur. J. Biochem.* 242, 689-694.
36. Heath, R. J., and Rock, C. O. Enoyl-Acyl Carrier Protein Reductase (FabI) Plays a Determinant Role in Completing Cycles of Fatty-Acid Elongation in *Escherichia-Coli*. (1995) *J. Biol. Chem.* 270, 26538-26542.

37. Baldock, C., de Boer, G. J., Rafferty, J. B., Stuitje, A. R., and Rice, D. W. Mechanism of action of diazaborines. (1998) *Biochem. Pharmacol.* 55, 1541-1550.
38. Davis, M. C., Franzblau, S. G., and Martin, A. R. Syntheses and evaluation of benzodiazaborine compounds against M-tuberculosis H37RV in vitro. (1998) *Bioorg. Med. Chem. Lett.* 8, 843-846.
39. Grassberger, M. A., Turnowsky, F., and Hildebrandt, J. Preparation and Antibacterial Activities of New 1,2,3-Diazaborine Derivatives and Analogs. (1984) *J. Med. Chem.* 27, 947-953.
40. Pertschy, B., Zisser, G., Schein, H., Koffel, R., Rauch, G., Grillitsch, K., Morgenstern, C., Durchschlag, M., Hoenauer, G., and Bergler, H. Diazaborine treatment of yeast cells inhibits maturation of the 60S ribosomal subunit. (2004) *Mol. Cell. Biol.* 24, 6476-6487.
41. Banerjee, A., Dubnau, E., Quemard, A., Balasubramanian, V., Um, K. S., Wilson, T., Collins, D., Delisle, G., and Jacobs, W. R. InhA, a Gene Encoding a Target for Isoniazid and Ethionamide in Mycobacterium-Tuberculosis. (1994) *Science* 263, 227-230.
42. Zhang, Y., Heym, B., Allen, B., Young, D., and Cole, S. The Catalase Peroxidase Gene and Isoniazid Resistance of Mycobacterium-Tuberculosis. (1992) *Nature* 358, 591-593.
43. Rawat, R., Whitty, A., and Tonge, P. J. The isoniazid-NAD adduct is a slow, tight-binding inhibitor of InhA, the Mycobacterium tuberculosis enoyl reductase:

- Adduct affinity and drug resistance. (2003) *Proc. Natl. Acad. Sci. U. S. A.* 100, 13881-13886.
44. Ramaswamy, S. V., Reich, R., Dou, S. J., Jasperse, L., Pan, X., Wanger, A., Quitugua, T., and Graviss, E. A. Single nucleotide polymorphisms in genes associated with isoniazid resistance in *Mycobacterium tuberculosis*. (2003) *Antimicrob. Agents Chemother.* 47, 1241-1250.
45. Sivaraman, S., Sullivan, T. J., Johnson, F., Novichenok, P., Cui, G. L., Simmerling, C., and Tonge, P. J. Inhibition of the bacterial enoyl reductase FabI by triclosan: A structure-reactivity analysis of FabI inhibition by triclosan analogues. (2004) *J. Med. Chem.* 47, 509-518.
46. Sivaraman, S., Zwahlen, J., Bell, A. F., Hedstrom, L., and Tonge, P. J. Structure-activity studies of the inhibition of FabI, the enoyl reductase from *Escherichia coli*, by triclosan: Kinetic analysis of mutant. (2003) *Biochemistry* 42, 4406-4413.
47. Ward, W. H. J., Holdgate, G. A., Rowsell, S., McLean, E. G., Pauptit, R. A., Clayton, E., Nichols, W. W., Colls, J. G., Minshull, C. A., Jude, D. A., Mistry, A., Timms, D., Camble, R., Hales, N. J., Britton, C. J., and Taylor, I. W. F. Kinetic and structural characteristics of the inhibition of enoyl (acyl carrier protein) reductase by triclosan. (1999) *Biochemistry* 38, 12514-12525.
48. Ende, C. W. A., Knudson, S. E., Liu, N., Childs, J., Sullivan, T. J., Boyne, M., Xu, H., Gegina, Y., Knudson, D. L., Johnson, F., Peloquin, C. A., Slayden, R. A., and Tonge, P. J. Synthesis and in vitro antimycobacterial activity of B-ring modified diaryl ether InhA inhibitors. (2008) *Bioorg. Med. Chem. Lett.* 18, 3029-3033.

49. Luckner, S. R., Liu, N. N., Ende, C. W. A., Tonge, P. J., and Kisker, C. A Slow, Tight Binding Inhibitor of InhA, the Enoyl-Acyl Carrier Protein Reductase from *Mycobacterium tuberculosis*. (2010) *J. Biol. Chem.* **285**, 14330-14337.
50. Sullivan, T. J., Truglio, J. J., Boyne, M. E., Novichenok, P., Zhang, X., Stratton, C. F., Li, H. J., Kaur, T., Amin, A., Johnson, F., Slayden, R. A., Kisker, C., and Tonge, P. J. High affinity InhA inhibitors with activity against drug-resistant strains of *Mycobacterium tuberculosis*. (2006) *ACS Chem. Biol.* **1**, 43-53.
51. Payne, D. J., Miller, W. H., Berry, V., Brosky, J., Burgess, W. J., Chen, E., DeWolf, W. E., Fosberry, A. P., Greenwood, R., Head, M. S., Heerding, D. A., Janson, C. A., Jaworski, D. D., Keller, P. M., Manley, P. J., Moore, T. D., Newlander, K. A., Pearson, S., Polizzi, B. J., Qiu, X. Y., Rittenhouse, S. F., Slater-Radosti, C., Salyers, K. L., Seefeld, M. A., Smyth, M. G., Takata, D. T., Uzinskas, I. N., Vaidya, K., Wallis, N. G., Winram, S. B., Yuan, C. C. K., and Huffman, W. F. Discovery of a novel and potent class of fabI-directed antibacterial agents. (2002) *Antimicrob. Agents Chemother.* **46**, 3118-3124.
52. Heerding, D. A., Chan, G., DeWolf, W. E., Fosberry, A. P., Janson, C. A., Jaworski, D. D., McManus, E., Miller, W. H., Moore, T. D., Payne, D. J., Qiu, X. Y., Rittenhouse, S. F., Slater-Radosti, C., Smith, W., Takata, D. T., Vaidya, K. S., Yuan, C. C. K., and Huffman, W. F. 1,4-disubstituted imidazoles are potential antibacterial agents functioning as inhibitors of enoyl acyl carrier protein reductase (FabI). (2001) *Bioorg. Med. Chem. Lett.* **11**, 2061-2065.
53. Seefeld, M. A., Miller, W. H., Newlander, K. A., Burgess, W. J., Payne, D. J., Rittenhouse, S. F., Moore, T. D., DeWolf, W. E., Keller, P. M., Qiu, X. Y., Janson,

- C. A., Vaidya, K., Fosberry, A. P., Smyth, M. G., Jaworski, D. D., Slater-Radosti, C., and Huffman, W. F. Inhibitors of bacterial enoyl acyl carrier protein reductase (FabI): 2,9-disubstituted 1,2,3,4-tetrahydropyrido[3,4-b]indoles as potential antibacterial agents. (2001) *Bioorg. Med. Chem. Lett.* 11, 2241-2244.
54. Seefeld, M. A., Miller, W. H., Newlander, K. A., Burgess, W. J., DeWolf, W. E., Elkins, P. A., Head, M. S., Jakas, D. R., Janson, C. A., Keller, P. M., Manley, P. J., Moore, T. D., Payne, D. J., Pearson, S., Polizzi, B. J., Qiu, X. Y., Rittenhouse, S. F., Uzinskas, I. N., Wallis, N. G., and Huffmann, W. F. Indole naphthyridinones as inhibitors of bacterial enoyl-ACP reductases FabI and FabK. (2003) *J. Med. Chem.* 46, 1627-1635.
55. Miller, W. H., Seefeld, M. A., Newlander, K. A., Uzinskas, I. N., Burgess, W. J., Heerding, D. A., Yuan, C. C. K., Head, M. S., Payne, D. J., Rittenhouse, S. F., Moore, T. D., Pearson, S. C., Berry, V., DeWolf, W. E., Keller, P. M., Polizzi, B. J., Qiu, X. Y., Janson, C. A., and Huffman, W. F. Discovery of aminopyridine-based inhibitors of bacterial enoyl-ACP reductase (FabI). (2002) *J. Med. Chem.* 45, 3246-3256.
56. Kuo, M. R., Morbidoni, H. R., Alland, D., Sneddon, S. F., Gourlie, B. B., Staveski, M. M., Leonard, M., Gregory, J. S., Janjigian, A. D., Yee, C., Musser, J. M., Kreiswirth, B., Iwamoto, H., Perozzo, R., Jacobs, W. R., Sacchettini, J. C., and Fidock, D. A. Targeting tuberculosis and malaria through inhibition of enoyl reductase. (2003) *J. Biol. Chem.* 278, 20851-20859.

57. He, X., Alian, A., Stroud, R., and de Montellano, P. R. O. Pyrrolidine carboxamides as a novel class of inhibitors of enoyl acyl carrier protein reductase from *Mycobacterium tuberculosis*. (2006) *J. Med. Chem.* **49**, 6308-6323.
58. Ling, L. L., Xian, J., Ali, S., Geng, B. L., Fan, J., Mills, D. M., Arvanites, A. C., Orgueira, H., Ashwell, M. A., Carmel, G., Xiang, Y. B., and Moir, D. T. Identification and characterization of inhibitors of bacterial enoyl-acyl carrier protein reductase. (2004) *Antimicrob. Agents Chemother.* **48**, 1541-1547.
59. Kitagawa, H., Kumura, K., Takahata, S., Iida, M., and Atsumi, K. 4-Pyridone derivatives as new inhibitors of bacterial enoyl-ACP reductase FabI. (2007) *Bioorg. Med. Chem.* **15**, 1106-1116.
60. Yum, J. H., Kim, C. K., Yong, D., Lee, K., Chong, Y., Kim, C. M., Kim, J. M., Ro, S., and Cho, J. M. In vitro activities of CG400549, a novel FabI inhibitor, against recently isolated clinical *Staphylococcal* strains in Korea. (2007) *Antimicrob. Agents Chemother.* **51**, 2591-2593.
61. Zhang, Y. M., and Rock, C. O. Evaluation of epigallocatechin gallate and related plant polyphenols as inhibitors of the FabG and FabI reductases of bacterial type II fatty-acid synthase. (2004) *J. Biol. Chem.* **279**, 30994-31001.
62. Zheng, C. J., Yoo, J. S., Lee, T. G., Cho, H. Y., Kim, Y. H., and Kim, W. G. Fatty acid synthesis is a target for antibacterial activity of unsaturated fatty acids. (2005) *FEBS Lett.* **579**, 5157-5162.
63. Tasdemir, D., Guner, N. D., Perozzo, R., Brun, R., Donmez, A. A., Calis, I., and Ruedi, P. Anti-protozoal and plasmodial FabI enzyme inhibiting metabolites of *Scrophularia lepidota* roots. (2005) *Phytochemistry* **66**, 355-362.



64. Yao, J. J., Zhang, Q. Y., Min, J., He, J., and Yu, Z. N. Novel enoyl-ACP reductase (FabI) potential inhibitors of *Escherichia coli* from Chinese medicine monomers. (2010) *Bioorg. Med. Chem. Lett.* 20, 56-59.
65. Truglio, J. J., Theis, K., Feng, Y. G., Gajda, R., Machutta, C., Tonge, P. J., and Kisker, C. Crystal structure of *Mycobacterium tuberculosis* MenB, a key enzyme in vitamin K-2 biosynthesis. (2003) *J. Biol. Chem.* 278, 42352-42360.
66. Bishop, D. H. L., Pandya, K. P., and King, H. K. Ubiquinone and Vitamin K in Bacteria. (1962) *Biochem. J.* 83, 606-614.
67. Kurosu, M., and Begari, E. Vitamin K2 in Electron Transport System: Are Enzymes Involved in Vitamin K2 Biosynthesis Promising Drug Targets? (2010) *Molecules* 15, 1531-1553.
68. Kindberg, C. G., and Suttie, J. W. Effect of Various Intakes of Phylloquinone on Signs of Vitamin-K Deficiency and Serum and Liver Phylloquinone Concentrations in the Rat. (1989) *J. Nutr.* 119, 175-180.
69. Bentley, R., and Meganathan, R. Biosynthesis of Vitamin-K (Menaquinone) in Bacteria. (1982) *Microbiol. Rev.* 46, 241-280.
70. Meganathan, R., and Bentley, R. Biosynthesis of Ortho-Succinylbenzoic Acid in a Men-*Escherichia-Coli* Mutant Requires Decarboxylation of L-Glutamate at the C-1 Position. (1981) *Biochemistry* 20, 5336-5340.
71. Shineberg, B., and Young, I. G. Biosynthesis of Bacterial Menaquinones - Membrane-Associated 1,4-Dihydroxy-2-Naphthoate Octaprenyltransferase of *Escherichia-Coli*. (1976) *Biochemistry* 15, 2754-2758.

72. Widhalm, J. R., van Oostende, C., Furt, F., and Basset, G. J. C. A dedicated thioesterase of the Hotdog-fold family is required for the biosynthesis of the naphthoquinone ring of vitamin K-1. (2009) *Proc. Natl. Acad. Sci. U. S. A.* 106, 5599-5603.
73. Begley, T. P., Kinsland, C., Taylor, S., Tandon, M., Nicewonger, R., Wu, M., Chiu, H. J., Kelleher, N., Campobasso, N., and Zhang, Y. (1998) in *Biosynthesis: Polyketides and Vitamins, Topics in Current Chemistry*, Vol. 195, 93-142, Springer, Berlin.
74. Meganathan, R. Biosynthesis of menaquinone (vitamin K-2) and ubiquinone (coenzyme Q): A perspective on enzymatic mechanisms. (2001) *Vitam. Horm.* 61, 173-218.
75. Bentley, S. D., Chater, K. F., Cerdeno-Tarraga, A. M., Challis, G. L., Thomson, N. R., James, K. D., Harris, D. E., Quail, M. A., Kieser, H., Harper, D., Bateman, A., Brown, S., Chandra, G., Chen, C. W., Collins, M., Cronin, A., Fraser, A., Goble, A., Hidalgo, J., Hornsby, T., Howarth, S., Huang, C. H., Kieser, T., Larke, L., Murphy, L., Oliver, K., O'Neil, S., Rabinowitsch, E., Rajandream, M. A., Rutherford, K., Rutter, S., Seeger, K., Saunders, D., Sharp, S., Squares, R., Squares, S., Taylor, K., Warren, T., Wietzorrek, A., Woodward, J., Barrell, B. G., Parkhill, J., and Hopwood, D. A. Complete genome sequence of the model actinomycete *Streptomyces coelicolor* A3(2). (2002) *Nature* 417, 141-147.
76. Borodina, I., Krabben, P., and Nielsen, J. Genome-scale analysis of *Streptomyces coelicolor* A3(2) metabolism. (2005) *Genome Res.* 15, 820-829.

77. Collins, M. D., Pirouz, T., Goodfellow, M., and Minnikin, D. E. Distribution of Menaquinones in Actinomycetes and Corynebacteria. (1977) *J. Gen. Microbiol.* 100, 221-230.
78. Tomb, J. F., White, O., Kerlavage, A. R., Clayton, R. A., Sutton, G. G., Fleischmann, R. D., Ketchum, K. A., Klenk, H. P., Gill, S., Dougherty, B. A., Nelson, K., Quackenbush, J., Zhou, L. X., Kirkness, E. F., Peterson, S., Loftus, B., Richardson, D., Dodson, R., Khalak, H. G., Glodek, A., McKenney, K., Fitzgerald, L. M., Lee, N., Adams, M. D., Hickey, E. K., Berg, D. E., Gocayne, J. D., Utterback, T. R., Peterson, J. D., Kelley, J. M., Cotton, M. D., Weldman, J. M., Fujii, C., Bowman, C., Watthey, L., Wallin, E., Hayes, W. S., Weidman, J. M., Fujii, C., Borodovsky, M., Karp, P. D., Smith, H. O., Fraser, C. M., and Venter, J. C. The complete genome sequence of the gastric pathogen *Helicobacter pylori*. (1997) *Nature* 388, 539-547.
79. Parkhill, J., Wren, B. W., Mungall, K., Ketley, J. M., Churcher, C., Basham, D., Chillingworth, T., Davies, R. M., Feltwell, T., Holroyd, S., Jagels, K., Karlyshev, A. V., Moule, S., Pallen, M. J., Penn, C. W., Quail, M. A., Rajandream, M. A., Rutherford, K. M., van Vliet, A. H. M., Whitehead, S., and Barrell, B. G. The genome sequence of the food-borne pathogen *Campylobacter jejuni* reveals hypervariable sequences. (2000) *Nature* 403, 665-668.
80. Marcelli, S. W., Chang, H. T., Chapman, T., Chalk, P. A., Miles, R. J., and Poole, R. K. The respiratory chain of *Helicobacter pylori*: Identification of cytochromes and the effects of oxygen on cytochrome and menaquinone levels. (1996) *FEMS Microbiol. Lett.* 138, 59-64.

81. Moss, C. W., Lambertfair, M. A., Nicholson, M. A., and Guerrant, G. O. Isoprenoid Quinones of *Campylobacter-Cryaerophila*, *C-Cinaedi*, *C-Fennelliae*, *C-Hyointestinalis*, *Campylobacter-Pylori*, and *C-Upsaliensis*. (1990) *J. Clin. Microbiol.* 28, 395-397.
82. Hiratsuka, T., Furihata, K., Ishikawa, J., Yamashita, H., Itoh, N., Seto, H., and Dairi, T. An alternative menaquinone biosynthetic pathway operating in microorganisms. (2008) *Science* 321, 1670-1673.
83. Seto, H., Jinnai, Y., Hiratsuka, T., Fukawa, M., Furihata, K., Itoh, N., and Dairi, T. Studies on a new biosynthetic pathway for menaquinone. (2008) *J. Am. Chem. Soc.* 130, 5614-5615.
84. Collins, M. D., and Jones, D. Distribution of Isoprenoid Quinone Structural Types in Bacteria and Their Taxonomic Implications. (1981) *Microbiol. Rev.* 45, 316-354.
85. Guest, J. R. Menaquinone Biosynthesis - Mutants of *Escherichia-Coli* K-12 Requiring 2-Succinylbenzoate. (1977) *J. Bacteriol.* 130, 1038-1046.
86. Kobayashi, K., Ehrlich, S. D., Albertini, A., Amati, G., Andersen, K. K., Arnaud, M., Asai, K., Ashikaga, S., Aymerich, S., Bessieres, P., Boland, F., Brignell, S. C., Bron, S., Bunai, K., Chapuis, J., Christiansen, L. C., Danchin, A., Debarbouille, M., Dervyn, E., Deuerling, E., Devine, K., Devine, S. K., Dreesen, O., Errington, J., Fillinger, S., Foster, S. J., Fujita, Y., Galizzi, A., Gardan, R., Eschevins, C., Fukushima, T., Haga, K., Harwood, C. R., Hecker, M., Hosoya, D., Hullo, M. F., Kakeshita, H., Karamata, D., Kasahara, Y., Kawamura, F., Koga, K., Koski, P., Kuwana, R., Imamura, D., Ishimaru, M., Ishikawa, S., Ishio, I., Le

- Coq, D., Masson, A., Mauel, C., Meima, R., Mellado, R. P., Moir, A., Moriya, S., Nagakawa, E., Nanamiya, H., Nakai, S., Nygaard, P., Ogura, M., Ohanan, T., O'Reilly, M., O'Rourke, M., Pragai, Z., Pooley, H. M., Rapoport, G., Rawlins, J. P., Rivas, L. A., Rivolta, C., Sadaie, A., Sadaie, Y., Sarvas, M., Sato, T., Saxild, H. H., Scanlan, E., Schumann, W., Seegers, J. F. M. L., Sekiguchi, J., Sekowska, A., Seror, S. J., Simon, M., Stragier, P., Studer, R., Takamatsu, H., Tanaka, T., Takeuchi, M., Thomaidis, H. B., Vagner, V., van Dijk, J. M., Watabe, K., Wipat, A., Yamamoto, H., Yamamoto, M., Yamamoto, Y., Yamane, K., Yata, K., Yoshida, K., Yoshikawa, H., Zuber, U., and Ogasawara, N. Essential *Bacillus subtilis* genes. (2003) *Proc. Natl. Acad. Sci. U.S.A.* 100, 4678-4683.
87. Sassetti, C. M., Boyd, D. H., and Rubin, E. J. Genes required for mycobacterial growth defined by high density mutagenesis. (2003) *Mol. Microbiol.* 48, 77-84.
88. Kurosu, M., Narayanasamy, P., Biswas, K., Dhiman, R., and Crick, D. C. Discovery of 1,4-dihydroxy-2-naphthoate prenyltransferase inhibitors: New drug leads for multidrug-resistant gram-positive pathogens. (2007) *J. Med. Chem.* 50, 5048-5048.
89. Li, X., Zhang, H., and Tonge, P. J. Inhibition of 1,4-dihydroxynaphthoyl-CoA synthase (MenB), an enzyme drug target bacterial menaquinone biosynthesis pathway, (2008), pp 17-21, Philadelphia, PA, USA.
90. Li, X. K., Liu, N. N., Zhang, H. N., Knudson, S. E., Slayden, R. A., and Tonge, P. J. Synthesis and SAR studies of 1,4-benzoxazine MenB inhibitors: Novel antibacterial agents against *Mycobacterium tuberculosis*. (2010) *Bioorg. Med. Chem. Lett.* 20, 6306-6309.

91. Zhang, H., and Tonge, P. J. Enzymatic activity in the crotonase superfamily: The mechanism of the reactions catalyzed by 1,4-dihydroxynaphthoyl-CoA synthase (MenB) and 2-ketocyclohexanecarboxyl-CoA hydrolase (BadI), (2007), pp 19-23, Boston, MA, USA.
92. Xu, H., Graham, M., Karelis, J., Walker, S. G., and Tonge, P. J. Mechanistic studies of MenD, 2-succinyl-5-enoylpyruvyl-6-hydroxy-3-cyclohexene-1-carboxylic acid synthase from *Staphylococcus aureus*, (2009), pp 22-26, Salt Lake City, UT, USA.
93. Fang, M. H., Toogood, R. D., Macova, A., Ho, K., Franzblau, S. G., McNeil, M. R., Sanders, D. A. R., and Palmer, D. R. J. Succinylphosphonate Esters Are Competitive Inhibitors of MenD That Show Active-Site Discrimination between Homologous alpha-Ketoglutarate-Decarboxylating Enzymes. (2010) *Biochemistry* 49, 2672-2679.
94. Lu, X. Q., Zhang, H. N., Tonge, P. J., and Tan, D. S. Mechanism-based inhibitors of MenE, an acyl-CoA synthetase involved in bacterial menaquinone biosynthesis. (2008) *Bioorg. Med. Chem. Lett.* 18, 5963-5966.
95. Tian, Y., Suk, D. H., Cai, F., Crich, D., and Mesecar, A. D. Bacillus anthracis o-Succinylbenzoyl-CoA Synthetase: Reaction Kinetics and a Novel Inhibitor Mimicking Its Reaction Intermediate. (2008) *Biochemistry* 47, 12434-12447.
96. Nakagawa, K., Hirota, Y., Sawada, N., Yuge, N., Watanabe, M., Uchino, Y., Okuda, N., Shimomura, Y., Suhara, Y., and Okano, T. Identification of UBIAD1 as a novel human menaquinone-4 biosynthetic enzyme. (2010) *Nature* 468, 117-121.

97. Suhara, Y., Wada, A., and Okano, T. Elucidation of the mechanism producing menaquinone-4 in osteoblastic cells. (2009) *Bioorg. Med. Chem. Lett.* 19, 1054-1057.
98. WHO (2007) *WHO Report*, WHO, Switzerland.
99. Jain, A., and Mondal, R. Extensively drug-resistant tuberculosis: current challenges and threats. (2008) *FEMS Immunol. Med. Microbiol.* 53, 145-150.
100. Barry, C. E., Lee, R. E., Mdluli, K., Sampson, A. E., Schroeder, B. G., Slayden, R. A., and Yuan, Y. Mycolic acids: Structure, biosynthesis and physiological functions. (1998) *Prog. Lipid Res.* 37, 143-179.
101. Vilcheze, C., Morbidoni, H. R., Weisbrod, T. R., Iwamoto, H., Kuo, M., Sacchettini, J. C., and Jacobs, W. R. Inactivation of the inhA-encoded fatty acid synthase II (FASII) enoyl-acyl carrier protein reductase induces accumulation of the FASII end products and cell lysis of *Mycobacterium smegmatis*. (2000) *J. Bacteriol.* 182, 4059-4067.
102. Heath, R. J., Yu, Y. T., Shapiro, M. A., Olson, E., and Rock, C. O. Broad spectrum antimicrobial biocides target the FabI component of fatty acid synthesis. (1998) *J. Biol. Chem.* 273, 30316-30320.
103. Heath, R. J., White, S. W., and Rock, C. O. Lipid biosynthesis as a target for antibacterial agents. (2001) *Prog. Lipid Res.* 40, 467-497.
104. Surolia, N., and Surolia, A. Triclosan offers protection against blood stages of malaria by inhibiting enoyl-ACP reductase of *Plasmodium falciparum*. (2001) *Nat. Med.* 7, 167-173.

105. Perozzo, R., Kuo, M., Sidhu, A. B. S., Valiyaveetil, J. T., Bittman, R., Jacobs, W. R., Fidock, D. A., and Sacchettini, J. C. Structural elucidation of the specificity of the antibacterial agent triclosan for malarial enoyl acyl carrier protein reductase. (2002) *J. Biol. Chem.* 277, 13106-13114.
106. Freundlich, J. S., Anderson, J. W., Sarantakis, D., Shieh, H. M., Yu, M., Valderramos, J. C., Lucumi, E., Kuo, M., Jacobs, W. R., Fidock, D. A., Schiehser, G. A., Jacobus, D. P., and Sacchettini, J. C. Synthesis, biological activity, and X-ray crystal structural analysis of diaryl ether inhibitors of malarial enoyl acyl carrier protein reductase. Part 1 : 4 '-substituted triclosan derivatives. (2005) *Bioorg. Med. Chem. Lett.* 15, 5247-5252.
107. McMurry, L. M., Oethinger, M., and Levy, S. B. Triclosan targets lipid synthesis. (1998) *Nature* 394, 531-532.
108. Parikh, S. L., Xiao, G. P., and Tonge, P. J. Inhibition of InhA, the enoyl reductase from *Mycobacterium tuberculosis*, by triclosan and isoniazid. (2000) *Biochemistry* 39, 7645-7650.
109. McMurry, L. M., McDermott, P. F., and Levy, S. B. Genetic evidence that InhA of *Mycobacterium smegmatis* is a target for triclosan. (1999) *Antimicrob. Agents Chemother.* 43, 711-713.
110. Freundlich, J. S., Wang, F., Vilcheze, C., Gulten, G., Langley, R., Schiehser, G. A., Jacobus, D. R., Jacobs, W. R., and Sacchettini, J. C. Triclosan Derivatives: Towards Potent Inhibitors of Drug-Sensitive and Drug-Resistant *Mycobacterium tuberculosis*. (2009) *Chem. Med. Chem.* 4, 241-248.



111. Boyne, M. E., Sullivan, T. J., Amende, C. W., Lu, H., Gruppo, V., Heaslip, D., Amin, A. G., Chatterjee, D., Lenaerts, A., Tonge, P. J., and Slayden, R. A. Targeting fatty acid biosynthesis for the development of novel chemotherapeutics against *Mycobacterium tuberculosis*: Evaluation of a-ring-modified diphenyl ethers as high-affinity InhA inhibitors. (2007) *Antimicrob. Agents Chemother.* 51, 3562-3567.
112. Lipinski, C. A., Lombardo, F., Dominy, B. W., and Feeney, P. J. Experimental and computational approaches to estimate solubility and permeability in drug discovery and development settings. (2001) *Adv. Drug Deliv. Rev.* 46, 3-26.
113. O'Shea, R., and Moser, H. E. Physicochemical properties of antibacterial compounds: Implications for drug discovery. (2008) *J. Med. Chem.* 51, 2871-2878.
114. Copeland, R. A., Pompliano, D. L., and Meek, T. D. Opinion - Drug-target residence time and its implications for lead optimization. (2006) *Nat. Rev. Drug Disc.* 5, 730-739.
115. Vilcheze, C., Wang, F., Arai, M., Hazbon, M. H., Colangeli, R., Kremer, L., Weisbrod, T. R., Alland, D., Sacchettini, J. C., and Jacobs, W. R. Transfer of a point mutation in *Mycobacterium tuberculosis* inhA resolves the target of isoniazid. (2006) *Nat. Med.* 12, 1027-1029.
116. Copeland, R. A. (2005) *Evaluation of enzyme inhibitors in drug discovery. A guide for medicinal chemists and pharmacologists*, Wiley, Hoboken, New Jersey.

117. Williams, J. W., Morrison, J. F., and Duggleby, R. G. Methotrexate, a High-Affinity Pseudosubstrate of Dihydrofolate-Reductase. (1979) *Biochemistry* 18, 2567-2573.
118. AbdelMagid, A. F., Carson, K. G., Harris, B. D., Maryanoff, C. A., and Shah, R. D. Reductive amination of aldehydes and ketones with sodium triacetoxyborohydride. Studies on direct and indirect reductive amination procedures. (1996) *J. Org. Chem.* 61, 3849-3862.
119. Collins, L. A., and Franzblau, S. G. Microplate Alamar blue assay versus BACTEC 460 system for high-throughput screening of compounds against *Mycobacterium tuberculosis* and *Mycobacterium avium*. (1997) *Antimicrob. Agents Chemother.* 41, 1004-1009.
120. Lu, H., and Tonge, P. J. Inhibitors of FabI, an enzyme drug target in the bacterial fatty acid biosynthesis pathway. (2008) *Acc. Chem. Res.* 41, 11-20.
121. Rafi, S. B., Cui, G. L., Song, K., Cheng, X. L., Tonge, P. J., and Simmerling, C. Insight through molecular mechanics Poisson-Boltzmann surface area calculations into the binding affinity of triclosan and three analogues for FabI, the *E-coli* enoyl reductase. (2006) *J. Med. Chem.* 49, 4574-4580.
122. Tummino, P. J., and Copeland, R. A. Residence time of receptor-ligand complexes and its effect on biological function. (2008) *Biochemistry* 47, 5481-5492.
123. Lewandowicz, A., Tyler, P. C., Evans, G. B., Furneaux, R. H., and Schramm, V. L. Achieving the ultimate physiological goal in transition state analogue inhibitors for purine nucleoside phosphorylase. (2003) *J. Biol. Chem.* 278, 31465-31468.

124. Heinig, M., and Frishman, D. STRIDE: a web server for secondary structure assignment from known atomic coordinates of proteins. (2004) *Nucleic Acids Res.* 32, W500-W502.
125. Wiersinga, W. J., van der Poll, T., White, N. J., Day, N. P., and Peacock, S. J. Melioidosis: insights into the pathogenicity of *Burkholderia pseudomallei*. (2006) *Nat. Rev. Microbiol.* 4, 272-282.
126. Harding, S. V., Sarkar-Tyson, M., Smither, S. J., Atkins, T. P., Oyston, P. C. F., Brown, K. A., Liu, Y. C., Wait, R., and Titball, R. W. The identification of surface proteins of *Burkholderia pseudomallei*. (2007) *Vaccine* 25, 2664-2672.
127. Cheng, A. C., and Currie, B. J. Melioidosis: Epidemiology, pathophysiology, and management. (2005) *Clin. Microbiol. Rev.* 18, 383-416.
128. Gilad, J., Harary, I., Dushnitsky, T., Schwartz, D., and Amsalem, Y. *Burkholderia mallei* and *Burkholderia pseudomallei* as bioterrorism agents: National aspects of emergency preparedness. (2007) *Isr. Med. Assoc. J.* 9, 499-503.
129. White, N. J. Melioidosis. (2003) *Lancet* 361, 1715-1722.
130. Harland, D. N., Dassa, E., Titball, R. W., Brown, K. A., and Atkins, H. S. ATP-binding cassette systems in *Burkholderia pseudomallei* and *Burkholderia mallei*. (2007) *Bmc Genomics* 8:83.
131. Chan, Y. Y., Ong, Y. M., and Chua, M. L. Synergistic interaction between phenothiazines and antimicrobial agents against *Burkholderia pseudomallei*. (2007) *Antimicrob. Agents Chemother.* 51, 623-630.
132. Webber, M. A., and Piddock, L. J. V. The importance of efflux pumps in bacterial antibiotic resistance. (2003) *J. Antimicrob. Chemother.* 51, 9-11.

133. Van Bambeke, F., Balzi, E., and Tulkens, P. M. Antibiotic efflux pumps - Commentary. (2000) *Biochem. Pharmacol.* 60, 457-470.
134. Poole, K. Multidrug resistance in Gram-negative bacteria. (2001) *Curr. Opin. Microbiol.* 4, 500-508.
135. Moore, R. A., DeShazer, D., Reckseidler, S., Weissman, A., and Woods, D. E. Efflux-mediated aminoglycoside and macrolide resistance in *Burkholderia pseudomallei*. (1999) *Antimicrob. Agents Chemother.* 43, 465-470.
136. Chan, Y. Y., Tan, T. M. C., Ong, Y. A., and Chua, K. L. BpeAB-OpRB, a multidrug efflux pump in *Burkholderia pseudomallei*. (2004) *Antimicrob. Agents Chemother.* 48, 1128-1135.
137. Ma, D., Cook, D. N., Alberti, M., Pon, N. G., Nikaido, H., and Hearst, J. E. Genes *Acra* and *Acrb* Encode a Stress-Induced Efflux System of *Escherichia-Coli*. (1995) *Mol. Microbiol.* 16, 45-55.
138. Poole, K., Krebs, K., McNally, C., and Neshat, S. Multiple Antibiotic-Resistance in *Pseudomonas-Aeruginosa* - Evidence for Involvement of an Efflux Operon. (1993) *J. Bacteriol.* 175, 7363-7372.
139. Brinster, S., Lamberet, G., Staels, B., Trieu-Cuot, P., Gruss, A., and Poyart, C. Type II fatty acid synthesis is not a suitable antibiotic target for Gram-positive pathogens. (2009) *Nature* 458, 83-U85.
140. Balemans, W., Lounis, N., Gilissen, R., Guillemont, J., Simmen, K., Andries, K., and Koul, A. Essentiality of FASII pathway for *Staphylococcus aureus*. (2010) *Nature* 463, E3-E4.

141. Heath, R. J., and Rock, C. O. Fatty acid biosynthesis as a target for novel antibacterials. (2004) *Curr. Opin. Investig. Drugs* 5, 146-153.
142. Tonge, P. J., Kisker, C., and Slayden, R. A. Development of modern InhA inhibitors to combat drug resistant strains of Mycobacterium tuberculosis. (2007) *Curr. Top. Med. Chem.* 7, 489-498.
143. Bergler, H., Wallner, P., Ebeling, A., Leitinger, B., Fuchsbichler, S., Aschauer, H., Kollenz, G., Hogenauer, G., and Turnowsky, F. Protein EnvM Is the NADH-Dependent Enoyl-ACP Reductase (FabI) of Escherichia-Coli. (1994) *J. Biol. Chem.* 269, 5493-5496.
144. Hofstein, H. A., Feng, Y. G., Anderson, V. E., and Tonge, P. J. Role of glutamate 144 and glutamate 164 in the catalytic mechanism of enoyl-CoA hydratase. (1999) *Biochemistry* 38, 9508-9516.
145. Kapoor, M., Reddy, C. C., Krishnasasthy, M. V., Surolia, N., and Surolia, A. Slow-tight-binding inhibition of enoyl-acyl carrier protein reductase from Plasmodium falciparum by triclosan. (2004) *Biochem. J.* 381, 719-724.
146. Thompson, J. D., Higgins, D. G., and Gibson, T. J. Clustal-W - Improving the Sensitivity of Progressive Multiple Sequence Alignment through Sequence Weighting, Position-Specific Gap Penalties and Weight Matrix Choice. (1994) *Nucleic Acids Res.* 22, 4673-4680.
147. Waterhouse, A. M., Procter, J. B., Martin, D. M. A., Clamp, M., and Barton, G. J. Jalview Version 2-a multiple sequence alignment editor and analysis workbench. (2009) *Bioinformatics* 25, 1189-1191.

148. Quemard, A., Sacchettini, J. C., Dessen, A., Vilcheze, C., Bittman, R., Jacobs, W. R., and Blanchard, J. S. Enzymatic Characterization of the Target for Isoniazid in Mycobacterium-Tuberculosis. (1995) *Biochemistry* 34, 8235-8241.
149. Rafi, S., Novichenok, P., Kolappan, S., Zhang, X. J., Stratton, C. F., Rawat, R., Kisker, C., Simmerling, C., and Tonge, P. J. Structure of acyl carrier protein bound to FabI, the FASII enoyl reductase from Escherichia coli. (2006) *J. Biol. Chem.* 281, 39285-39293.
150. Cleland, W. W. Kinetics of Enzyme-Catalyzed Reactions with two or More Substrates or Products .II. Inhibition - Nomenclature and Theory. (1963) *Biochim. Biophys. Acta* 67, 173-187.
151. Segel, I. H. (1975) *Enzyme Kinetics*, Wiley, New York.
152. Jornvall, H., Persson, B., Krook, M., Atrian, S., Gonzalezduarte, R., Jeffery, J., and Ghosh, D. Short-Chain Dehydrogenases Reductases (Sdr). (1995) *Biochemistry* 34, 6003-6013.
153. Holden, M. T. G., Titball, R. W., Peacock, S. J., Cerdeno-Tarraga, A. M., Atkins, T., Crossman, L. C., Pitt, T., Churcher, C., Mungall, K., Bentley, S. D., Sebahia, M., Thomson, N. R., Bason, N., Beacham, I. R., Brooks, K., Brown, K. A., Brown, N. F., Challis, G. L., Cherevach, I., Chillingworth, T., Cronin, A., Crossett, B., Davis, P., DeShazer, D., Feltwell, T., Fraser, A., Hance, Z., Hauser, H., Holroyd, S., Jagels, K., Keith, K. E., Maddison, M., Moule, S., Price, C., Quail, M. A., Rabinowitsch, E., Rutherford, K., Sanders, M., Simmonds, M., Songsivilai, S., Stevens, K., Tumapa, S., Vesaratchavest, M., Whitehead, S., Yeats, C., Barrell, B. G., Oyston, P. C. F., and Parkhill, J. Genomic plasticity of the causative agent

- of melioidosis, *Burkholderia pseudomallei*. (2004) *Proc. Natl. Acad. Sci. U. S. A.* 101, 14240-14245.
154. Swinney, D. C. The role of binding kinetics in therapeutically useful drug action. (2009) *Curr. Opin. Drug Disc.* 12, 31-39.
155. Swinney, D. C. Biochemical mechanisms of drug action: what does it take for success? (2004) *Nat. Rev. Drug Disc.* 3, 801-808.
156. Lu, H., and Tonge, P. J. Drug-target residence time: critical information for lead optimization. (2010) *Curr. Opin. Chem. Biol.* 14, 467-474.
157. Morrison, J. F., and Walsh, C. T. The Behavior and Significance of Slow-Binding Enzyme-Inhibitors. (1988) *Adv. Enzymol. Relat. Areas Mol. Biol.* 61, 201-301.
158. Perry, R. D., and Fetherston, J. D. *Yersinia pestis* - Etiologic agent of plague. (1997) *Clin. Microbiol. Rev.* 10, 35-66.
159. Ayyadurai, S., Sebbane, F., Raoult, D., and Drancourt, M. Body Lice, *Yersinia pestis* Orientalis, and Black Death. (2010) *Emerg. Infect. Dis.* 16, 892-893.
160. Bacot, A. W., and Martin, C. J. LXVII. Observations on the mechanism of the transmission of plague by fleas. (1914) *J. Hyg.* 13, 423-439.
161. Prentice, M. B., and Rahalison, L. Plague. (2007) *Lancet* 369, 1196-1207.
162. Meyer, K. F. Modern Therapy of Plague. (1950) *J. Am. Med. Assoc.* 144, 982-985.
163. Xiao, X. D., Zhu, Z. Y., Dankmeyer, J. L., Wormald, M. M., Fast, R. L., Worsham, P. L., Cote, C. K., Amemiya, K., and Dimitrov, D. S. Human Anti-Plague Monoclonal Antibodies Protect Mice from *Yersinia pestis* in a Bubonic Plague Model. (2010) *Plos One* 5, -.

164. Van Epps, H. L. Rene Dubos: unearthing antibiotics. (2006) *J. Exp. Med.* 203, 259-259.
165. Patrignani, F., Lucci, L., Bellew, N., Gardini, F., Guerzoni, A. E., and Lanciotti, R. Effects of sub-lethal concentrations of hexanal and 2-(E)-hexenal on membrane fatty acid composition and volatile compounds of *Listeria monocytogenes*, *Staphylococcus aureus*, *Salmonella enteritidis* and *Escherichia coli*. (2008) *Int. J. Food Microbiol.* 123, 1-8.
166. Broussy, S., Bernardes-Genisson, V., Quemard, A., Meunier, B., and Bernadou, J. The first chemical synthesis of the core structure of the benzoylhydrazine-NAD adduct, a competitive inhibitor of the *Mycobacterium tuberculosis* enoyl reductase. (2005) *J. Org. Chem.* 70, 10502-10510.
167. Leclercq, A., Guiyole, A., El Lioui, M., Carniel, E., and Decallonne, J. High homogeneity of the *Yersinia pestis* fatty acid composition. (2000) *J. Clin. Microbiol.* 38, 1545-1551.
168. Liu, N., Cummings, J. E., England, K., Slayden, R. A., and Tonge, P. J. Mechanism and Inhibition of the FabI Enoyl-ACP Reductase from *Burkholderia pseudomallei*. (2011) *J. Antimicrob. Chemother.* 66, 564-573.
169. Scheuerbrandt, G., and Bloch, K. Unsaturated Fatty Acids in Microorganisms. (1962) *J. Biol. Chem.* 237, 2064-2068.
170. Demendoza, D., and Cronan, J. E. Thermal Regulation of Membrane Lipid Fluidity in Bacteria. (1983) *Trends Biochem. Sci.* 8, 49-52.



171. Vigh, L., Maresca, B., and Harwood, J. L. Does the membrane's physical state control the expression of heat shock and other genes? (1998) *Trends Biochem. Sci.* 23, 369-374.
172. Cronan, J. E., and Gelmann, E. P. Estimate of Minimum Amount of Unsaturated Fatty-Acid Required for Growth of Escherichia-Coli. (1973) *J. Biol. Chem.* 248, 1188-1195.
173. Mansilla, M. C., Cybulski, L. E., Albanesi, D., and de Mendoza, D. Control of membrane lipid fluidity by molecular thermosensors. (2004) *J. Bacteriol.* 186, 6681-6688.
174. Tocher, D. R., Leaver, M. J., and Hodgson, P. A. Recent advances in the biochemistry and molecular biology of fatty acyl desaturases. (1998) *Progr. Lipid Res.* 37, 73-117.
175. Zhu, K., Choi, K. H., Schweizer, H. P., Rock, C. O., and Zhang, Y. M. Two aerobic pathways for the formation of unsaturated fatty acids in *Pseudomonas aeruginosa*. (2006) *Mol. Microbiol.* 60, 260-273.
176. Sakamoto, T., and Murata, N. Regulation of the desaturation of fatty acids and its role in tolerance to cold and salt stress. (2002) *Curr. Opin. Microbiol.* 5, 206-210.
177. Shanklin, J., and Cahoon, E. B. Desaturation and related modifications of fatty acids. (1998) *Annu. Rev. Plant Physiol. Plant Mol. Biol.* 49, 611-641.
178. Bloomfield, D. K., and Bloch, K. Formation of Delta-9-Unsaturated Fatty Acids. (1960) *J. Biol. Chem.* 235, 337-345.
179. Pasteur, L., Faulkner, F., and Robb, D. C. (1879) *Studies on Fermentation*, Macmillan, London.

180. Aguilar, P. S., Cronan, J. E., and de Mendoza, D. A *Bacillus subtilis* gene induced by cold shock encodes a membrane phospholipid desaturase. (1998) *J. Bacteriol.* *180*, 2194-2200.
181. Grau, R., and Demendoza, D. Regulation of the Synthesis of Unsaturated Fatty-Acids by Growth Temperature in *Bacillus-Subtilis*. (1993) *Mol. Microbiol.* *8*, 535-542.
182. Phetsuksiri, B., Jackson, M., Scherman, H., McNeil, M., Besra, G. S., Baulard, A. R., Slayden, R. A., DeBarber, A. E., Barry, C. E., Baird, M. S., Crick, D. C., and Brennan, P. J. Unique mechanism of action of the thiourea drug isoxyl on *Mycobacterium tuberculosis*. (2003) *J. Biol. Chem.* *278*, 53123-53130.
183. Cronan, J. E. A bacterium that has three pathways to regulate membrane lipid fluidity. (2006) *Mol. Microbiol.* *60*, 256-259.
184. Kass, L. R., and Bloch, K. On Enzymatic Synthesis of Unsaturated Fatty Acids in *Escherichia Coli*. (1967) *Proc. Natl. Acad. Sci. U. S. A.* *58*, 1168-1173.
185. Bloch, K. The biological synthesis of unsaturated fatty acids. (1963) *Biochem. Soc. Symp.* *24*, 1-16.
186. Marrakchi, H., Choi, K. H., and Rock, C. O. A new mechanism for anaerobic unsaturated fatty acid formation in *Streptococcus pneumoniae*. (2002) *J. Biol. Chem.* *277*, 44809-44816.
187. Garwin, J. L., Klages, A. L., and Cronan, J. E. Structural, Enzymatic, and Genetic-Studies of Beta-Ketoacyl-Acyl Carrier Protein Synthases I and II *Escherichia-Coli*. (1980) *J. Biol. Chem.* *255*, 11949-11956.

188. Clark, D. P., DeMaendoza, D., Plolacco, M. L., and Cronan, J. E. beta-Hydroxydecanoyl Thio Ester Dehydrase Does Not Catalyze a Rate-Limiting Step in Escherichia coli Unsaturated Fatty Acid Synthesis. (1983) *Biochemistry* 22, 5897-5902.
189. Garwin, J. L., Klages, A. L., and Cronan, J. E. Beta-Ketoacyl-Acyl Carrier Protein Synthase-I of Escherichia-Coli - Evidence for Function in the Thermal Regulation of Fatty-Acid Synthesis. (1980) *J. Biol. Chem.* 255, 3263-3265.
190. Demendoza, D., Ulrich, A. K., and Cronan, J. E. Thermal Regulation of Membrane Fluidity in Escherichia-Coli - Effects of Overproduction of Beta-Ketoacylacyl Carrier Protein Synthase-I. (1983) *J. Biol. Chem.* 258, 2098-2101.
191. Demendoza, D., Garwin, J. L., and Cronan, J. E. Overproduction of Cis-Vaccenic Acid and Altered Temperature Control of Fatty-Acid Synthesis in a Mutant of Escherichia-Coli. (1982) *J. Bacteriol.* 151, 1608-1611.
192. Hoang, T. T., and Schweizer, H. P. Fatty acid biosynthesis in Pseudomonas aeruginosa: Cloning and characterization of the fabAB operon encoding beta-hydroxyacyl-acyl carrier protein dehydratase (FabA) and beta-ketoacyl-acyl carrier protein synthase I (FabB). (1997) *J. Bacteriol.* 179, 5326-5332.
193. Holden, H. M., Benning, M. M., Haller, T., and Gerlt, J. A. The crotonase superfamily: Divergently related enzymes that catalyze different reactions involving acyl coenzyme A thioesters. (2001) *Acc. Chem. Res.* 34, 145-157.
194. Engel, C. K., Kiema, T. R., Hiltunen, J. K., and Wierenga, R. K. The crystal structure of enoyl-CoA hydratase complexed with octanoyl-CoA reveals the

- structural adaptations required for binding of a long chain fatty acid-CoA molecule. (1998) *J. Med. Biol.* 275, 847-859.
195. Benning, M. M., Haller, T., Gerlt, J. A., and Holden, H. M. New reactions in the crotonase superfamily: Structure of methylmalonyl CoA decarboxylase from *Escherichia coli*. (2000) *Biochemistry* 39, 4630-4639.
196. Benning, M. M., Taylor, K. L., Liu, R. Q., Yang, G., Xiang, H., Wesenberg, G., DunawayMariano, D., and Holden, H. M. Structure of 4-chlorobenzoyl coenzyme A dehalogenase determined to 1.8 angstrom resolution: An enzyme catalyst generated via adaptive mutation. (1996) *Biochemistry* 35, 8103-8109.
197. Crooks, G. P., and Copley, S. D. Purification and Characterization of 4-Chlorobenzoyl Coa Dehalogenase from *Arthrobacter* Sp Strain 4-Cb1. (1994) *Biochemistry* 33, 11645-11649.
198. Gurvitz, A., Mursula, A. M., Firzinger, A., Hamilton, B., Kilpelainen, S. H., Hartig, A., Ruis, H., Hiltunen, J. K., and Rottensteiner, H. Peroxisomal Delta 3-cis-Delta 2-trans-enoyl-CoA isomerase encoded by ECI1 is required for growth of the yeast *Saccharomyces cerevisiae* on unsaturated fatty acids. (1998) *J. Biol. Chem.* 273, 31366-31374.
199. Mursula, A. M., van Aalten, D. M. F., Hiltunen, J. K., and Wierenga, R. K. The crystal structure of Delta(3)-Delta(2)-enoyl-CoA isomerase. (2001) *J. Med. Biol.* 309, 845-853.
200. Chao, J., Wolfaardt, G. M., and Arts, M. T. Characterization of *Pseudomonas aeruginosa* fatty acid profiles in biofilms and batch planktonic cultures. (2010) *Can. J. Microbiol.* 56, 1028-1039.

201. Wallace, P. L., Hollis, D. G., Weaver, R. E., and Moss, C. W. Cellular Fatty-Acid Composition of *Kingella* Species, *Cardiobacterium-Hominis*, and *Eikenella-Corrodens*. (1988) *J. Clin. Microbiol.* 26, 1592-1594.
202. Vasiurenko, Z. P., Sel'nikova, O. P., Polishchuk, E. I., Samygin, V. M., and Ruban, N. M. Cellular fatty acid composition of the *Burkholderia mallei* and *Burkholderia pseudomallei* strains as generic feature of *Burkholderia*. (2006) *Mikrobiol. Z.* 68, 33-40.
203. Thippeswamy, H. S., Sood, S. K., Venkateswarlu, R., and Raj, I. Membranes of five-fold alamethicin-resistant *Staphylococcus aureus*, *Enterococcus faecalis* and *Bacillus cereus* show decreased interactions with alamethicin due to changes in membrane fluidity and surface charge. (2009) *Ann. Microbiol.* 59, 593-601.
204. Jantzen, E., Berdal, B. P., and Omland, T. Cellular Fatty-Acid Composition of *Francisella-Tularensis*. (1979) *J. Clin. Microbiol.* 10, 928-930.
205. Siegel, J. P., Smith, A. R., and Novak, R. J. Comparison of the cellular fatty acid composition of a bacterium isolated from a human and alleged to be *Bacillus sphaericus* with that of *Bacillus sphaericus* isolated from a mosquito larvicide. (1997) *Appl. Environ. Microbiol.* 63, 1006-1010.
206. Aricha, B., Fishov, I., Cohen, Z., Sikron, N., Pesakhov, S., Khozin-Goldberg, I., Dagan, R., and Porat, N. Differences in membrane fluidity and fatty acid composition between phenotypic variants of *Streptococcus pneumoniae*. (2004) *J. Bacteriol.* 186, 4638-4644.
207. Yamamoto, K., Murakami, R., and Takamura, Y. Isoprenoid quinone, cellular fatty acid composition and diaminopimelic acid isomers of newly classified

- thermophilic anaerobic Gram-positive bacteria. (1998) *FEMS Microbiol. Lett.* 161, 351-358.
208. Heath, R. J., Rubin, J. R., Holland, D. R., Zhang, E. L., Snow, M. E., and Rock, C. O. Mechanism of triclosan inhibition of bacterial fatty acid synthesis. (1999) *J. Biol. Chem.* 274, 11110-11114.
209. Byers, D. M., and Gong, H. S. Acyl carrier protein: structure-function relationships in a conserved multifunctional protein family. (2007) *Biochem. Cell Biol.* 85, 649-662.
210. Babbitt, P. C., and Gerlt, J. A. Understanding enzyme superfamilies - Chemistry as the fundamental determinant in the evolution of new catalytic activities. (1997) *J. Biol. Chem.* 272, 30591-30594.
211. Gerlt, J. A., and Babbitt, P. C. Mechanistically diverse enzyme superfamilies: the importance of chemistry in the evolution of catalysis. (1998) *Curr. Opin. Chem. Biol.* 2, 607-612.
212. Glasner, M. E., Gerlt, J. A., and Babbitt, P. C. Evolution of enzyme superfamilies. (2006) *Curr. Opin. Chem. Biol.* 10, 492-497.
213. Gerlt, J. A., and Babbitt, P. C. Divergent evolution of enzymatic function: Mechanistically diverse superfamilies and functionally distinct suprafamilies. (2001) *Annu. Rev. Biochem.* 70, 209-246.
214. Bahnson, B. J., Anderson, V. E., and Petsko, G. A. Structural mechanism of enoyl-CoA hydratase: Three atoms from a single water are added in either an E1cb stepwise or concerted fashion. (2002) *Biochemistry* 41, 2621-2629.

215. Mohrig, J. R., Moerke, K. A., Cloutier, D. L., Lane, B. D., Person, E. C., and Onasch, T. B. Importance of Historical Contingency in the Stereochemistry of Hydratase-Dehydratase Enzymes. (1995) *Science* 269, 527-529.
216. Bell, A. F., Wu, J. Q., Feng, Y. G., and Tonge, P. J. Involvement of glycine 141 in substrate activation by enoyl-CoA hydratase. (2001) *Biochemistry* 40, 1725-1733.
217. Zhang, D. Y., Liang, X. Q., He, X. Y., Alipui, O. D., Yang, S. Y., and Schulz, H. Delta(3,5),Delta(2,4)-dienoyl-CoA isomerase is a multifunctional isomerase - A structural and mechanistic study. (2001) *J Biol Chem* 276, 13622-13627.
218. Leonard, P. M., and Grogan, G. Structure of 6-oxo camphor hydrolase H122A mutant bound to its natural product, (2S,4S)-alpha-campholinic acid - Mutant structure suggests an atypical mode of transition state binding for a crotonase homolog. (2004) *J. Biol. Chem.* 279, 31312-31317.
219. Eberhard, E. D., and Gerlt, J. A. Evolution of function in the crotonase superfamily: The stereochemical course of the reaction catalyzed by 2-ketocyclohexanecarboxyl-CoA hydrolase. (2004) *J. Am. Chem. Soc.* 126, 7188-7189.
220. Heide, L., Arendt, S., and Leistner, E. Enzymatic-Synthesis, Characterization, and Metabolism of the Coenzyme-a Ester of Ortho-Succinylbenzoic Acid, an Intermediate in Menaquinone (Vitamin-K2) Biosynthesis. (1982) *J. Biol. Chem.* 257, 7396-7400.

221. Bryant, R. W., and Bentley, R. Menaquinone Biosynthesis - Conversion of O-Succinylbenzoic Acid to 1,4-Dihydroxy-2-Naphthoic Acid and Menaquinones by Escherichia-Coli Extracts. (1976) *Biochemistry* 15, 4792-4796.
222. Meganathan, R., Bentley, R., and Taber, H. Identification of Bacillus-Subtilis Men Mutants Which Lack Ortho-Succinylbenzoyl-Coenzyme-a Synthetase and Dihydroxynaphthoate Synthase. (1981) *J. Bacteriol.* 145, 328-332.
223. Taber, H. W., Dellers, E. A., and Lombardo, L. R. Menaquinone Biosynthesis in Bacillus-Subtilis - Isolation of Men Mutants and Evidence for Clustering of Men Genes. (1981) *J. Bacteriol.* 145, 321-327.
224. Ramchandra, P., and Sturm, A. W. Expression of the naphthoate synthase gene in Mycobacterium tuberculosis in a self-generated oxygen depleted liquid culture system. (2010) *Anaerobe* 16, 610-613.
225. Jenner, G. Comparative study of physical and chemical activation modes. The case of the synthesis of beta-amino derivatives. (1996) *Tetrahedron* 52, 13557-13568.
226. O'Brien, W. E. Continuous Spectrophotometric Assay for Argininosuccinate Synthetase Based on Pyrophosphate Formation. (1976) *Anal. Biochem.* 76, 423-430.
227. Seitz, L. E., Suling, W. J., and Reynolds, R. C. Synthesis and antimycobacterial activity of pyrazine and quinoxaline derivatives. (2002) *J. Med. Chem.* 45, 5604-5606.



228. Fringuelli, R., Giacche, N., Milanese, L., Cenci, E., Macchiarulo, A., Vecchiarelli, A., Costantino, G., and Schiaffella, F. Bulky 1,4-benzoxazine derivatives with antifungal activity. (2009) *Bioorg. Med. Chem.* 17, 3838-3846.
229. He, W., Myers, M. R., Hanney, B., Spada, A. P., Bilder, G., Galzcinski, H., Amin, D., Needle, S., Page, K., Jayyosi, Z., and Perrone, M. H. Potent quinoxaline-based inhibitors of PDGF receptor tyrosine kinase activity. Part 2: The synthesis and biological activities of RPR127963 an orally bioavailable inhibitor. (2003) *Bioorg. Med. Chem. Lett.* 13, 3097-3100.